FINISHING OF ADVANCED CERAMICS

FINAL PROGRESS REPORT

RANGA KOMANDURI

OCTOBER 30, 2000

U. S. ARMY RESEARCH OFFICE

DAAH04-96-1-0323

OKLAHOMA STATE UNIVERSITY

APPROVED FOR PUBLIC RELEASE

DISTRIBUTION UNLIMITED

REPORT DOCUMENTATION PAGE

Form Approved
OMB NO. 0704-0188

1. AGENCY USE ONLY (Leave Blank)	2. REPORT DATE	3. REPORT TYPE AND DATES COVERED
	October 30, 2000	Final Report 8/01/96 to 7-31/2000

4. TITLE AND SUBTITLE

FINISHING OF ADVANCED CERAMICS

5. FUNDING NUMBERS

Grant No: DAAH04-96-1-0323

6. AUTHOR(S)

RANGA KOMANDURI

7. PERFORMING ORGANIZATION NAME(S) AND ADDRESS(ES)

Mechanical & Aerospace Engineering, Oklahoma State University, 218 Engineering N, Stillwater, OK

8. PERFORMING ORGANIZATION REPORT NUMBER

9. SPONSORING / MONITORING AGENCY NAME(S) AND ADDRESS(ES)

U. S. Army Research Office
P.O. Box 12211
Research Triangle Park, NC 27709-2211

10. SPONSORING / MONITORING AGENCY REPORT NUMBER

ARO 36196.13-RT-DPS

11. SUPPLEMENTARY NOTES

The views, opinions and/or findings contained in this report are those of the author(s) and should not be construed as an official Department of the Army position, policy or decision, unless so designated by other documentation.

12 a. DISTRIBUTION / AVAILABILITY STATEMENT

Approved for public release; distribution unlimited.

12 b. DISTRIBUTION CODE

13. ABSTRACT (Maximum 200 words)

This project deals with both fundamental and applied aspects of finishing of advanced ceramics, such as silicon nitride (Si_3N_4) balls for hybrid bearing applications using the magnetic float polishing (MFP) technology developed under DARPA's Ceramic Bearing Technology Program (CF 33615-92-C-5933). On the fundamental side, an understanding of the material removal mechanisms involving both mechanical and chemo-mechanical polishing (CMP) as well as thermal aspects of polishing were considered. Improvements in the quality of the finished balls in terms of surface finish (Ra 5 nm) and sphericity (0.15-0.25 mm) and the development of prototype equipment for increasing the batch size by almost an order of magnitude (i.e. from about 10 balls of 12 mm diameter per batch with the small apparatus to about 80 balls per batch with a large apparatus) for polishing were investigated on the technology side. The processing time for finishing a batch of balls was about 20 hours.

14. SUBJECT TERMS

Polishing, Ceramic Balls, Magnetic Float Polishing, Hybrid Bearings, Chemo-Mechanical Polishing

15. NUMBER OF PAGES

151

16. PRICE CODE

17. SECURITY CLASSIFICATION OR REPORT	18. SECURITY CLASSIFICATION ON THIS PAGE	19. SECURITY CLASSIFICATION OF ABSTRACT	20. LIMITATION OF ABSTRACT
UNCLASSIFIED	UNCLASSIFIED	UNCLASSIFIED	UL

TABLE OF CONTENTS

LIST OF FIGURE CAPTIONS

LIST OF TABLES

PREFACE

In 1992 DARPA issued an RFP on the Ceramic Bearing Technology. Two principle barriers identified in it for the greater use of ceramic bearings for DoD applications are the high costs and operational reliability. According to it, the high rejection rates at the finished component level can be traced to the inhomogenities in the material, lack of process control for producing rolling element and race blanks, expensive and non-optimum grinding and polishing techniques for ceramic materials, and lack of reliable, non-destructive inspection methods in the prefired green blank, densified blank and finished bearing components stage. Another factor identified is the lack of an apparatus for finishing small batch of balls. With these factors in the background, OSU participated in this program and developed the Magnetic Float Polishing Technology (CF 33615-92-C-5933).

In the current DEPSCoR project on "The Finishing of Advanced Ceramics" (DAAH04-96-1-0323), we addressed both fundamental and applied aspects of finishing of advanced ceramics, such as silicon nitride (Si_3N_4) balls for hybrid bearing applications using the magnetic float polishing (MFP) technology. On the fundamental side, an understanding of the material removal mechanisms involving both mechanical and chemo-mechanical polishing (CMP) as well as thermal aspects of polishing were considered. Improvements in the quality of the finished balls in terms of surface finish and sphericity and the development of prototype equipment for increasing the batch size by almost an order of magnitude (i.e. from about 10 balls of 12 mm diameter per batch with the small apparatus to about 80 balls per batch with a large apparatus) for polishing were investigated on the technology side.

According to the Director of the U.S.Army Research Office (ARO), rapid and wide dissemination of the scientific information developed through its contracts and grants are required. We followed it to the true spirit and have published several technical papers which are included in this report as appendices.

We would like to thank our sponsors and especially Dr. W. Coblenz of DARPA and Dr. K. Mecklenburg of Wright Patterson AFB for their support and encouragement. Thanks are due to Dr. B. M. Kramer of NSF for additional support for this project. We would also like to thank the OSU Board of Regents, MOST Chair for Intelligent Manufacturing, and Dr. Tom Collins of OSU for their interest and support. We also thank Dr. L. L. Fehrenbacher of TA&T Inc. for many valuable discussions. Finally, thanks are due to the ARO for their interest and support of this project.

1. EXECUTIVE SUMMARY

1.1. Introduction

This DoD's DEPSCoR Project on "The Finishing of Advanced Ceramics" (DAAH04-96-1-0323) deals with both fundamental and applied aspects of finishing of advanced ceramics, such as silicon nitride (Si_3N_4) balls for hybrid bearing applications using the magnetic float polishing (MFP) technology developed under DARPA's Ceramic Bearing Technology Program (CF 33615-92-C-5933) [1]. On the fundamental side, an understanding of the material removal mechanisms involving both mechanical and chemo-mechanical polishing (CMP) as well as thermal aspects of polishing were considered. Improvements in the quality of the finished balls in terms of surface finish and sphericity and the development of prototype equipment for increasing the batch size by almost an order of magnitude (i.e. from about 10 balls of 12 mm diameter per batch with the small apparatus to about 80 balls per batch with a large apparatus) for polishing were investigated on the technology side. In the following, these aspects will be briefly summarized.

The conventional method of finishing ceramic balls is basically the same as that used for finishing of steel balls for bearings, namely, by V-groove lapping, except that steel balls are replaced with ceramic balls. The process involves the use of low polishing speeds (50 rpm), high loads (10 N per ball), and diamond abrasive. In practice, it takes considerable time (several weeks depending on the size of the ball, quality required, and the available technology) to finish a batch of ceramic balls. The long processing time and use of expensive diamond abrasives result in high processing costs. Furthermore, the use of diamond abrasive at high loads can result in surface damage, such as deep pits, scratches, and microcracks and subsurface damage, such as large lateral and radial/median cracks. These surface defects can result in catastrophic failure of Si_3N_4 balls in service by the propagation of cracks leading to brittle fracture. This can effect the reliability of parts in service.

To minimize the surface damage, 'gentle'/'flexible' grinding and polishing conditions are required, namely, a low level of load and abrasives not much harder (or preferably even softer) than the workmaterial but can cause chemo-mechanical action. Higher removal rates and shorter polishing cycles can be accomplished by higher polishing speeds. This is accomplished by a new process known as magnetic

float polishing (MFP) [2]. The material removal rate by MFP is ≈ 50 times higher than the conventional groove lapping, owing to higher polishing speed (1,000-10,000 rpm) used in MFP compared to lapping (50 rpm). Furthermore, the resulting surface and subsurface damage can be minimized due to the use of extremely low polishing load (≈ 1 N/ball) and chemo-mechanical polishing.

The magnetic float polishing (MFP) technique is based on the magneto-hydrodynamic behavior of a magnetic fluid that can float a non-magnetic float and an abrasive suspended in it by the magnetic field. The forces applied by the abrasive to the part are extremely small (1N/ball) and highly controllable. The apparatus consists of a series of permanent magnets (Nd-Fe-B) arranged alternate N and S below an aluminum chamber [2]. A non-magnetic polishing float is placed inside an aluminum chamber and filled with the required amount of magnetic fluid and appropriate abrasive (5-10% by volume). The ceramic balls are placed inside the aluminum chamber around the periphery. The polishing shaft was placed on top of the balls and is driven by a high-speed, high-precision air bearing spindle (PI Spindle) with a stepless speed regulation of up to 10,000 rpm. For the balls, a three-point contact is established between the wall of the chamber, the float, and the drive shaft.

1.2. Finishing of Si_3N_4 Balls by Magnetic Float Polishing (MFP)

In order to optimize the finishing conditions for polishing of Si_3N_4 balls by magnetic float polishing (MFP), the Taguchi [3] method was applied [4]. Surface finish parameters, namely, Ra (arithmetic average) and Rt (peak-to-valley height) were considered as criteria for optimization. The three important parameters that can influence the surface quality generated during final mechanical polishing [for a given workmaterial and abrasive (material and grain size)] are identified as (i) the polishing force, (ii) the abrasive concentration; and (iii) the polishing speed. Experimental results indicate that for the surface finish, both Ra and Rt, the polishing force to be the most significant parameters. However, for the surface finish, Ra, the polishing force parameter is the most significant, followed by polishing speed, and then the abrasive concentration; while for the surface finish Rt, the polishing force parameter is the most significant, followed by the abrasive concentration, and then the polishing speed. The experimental results also indicate that within the range of parameters evaluated, a high level of polishing force, a low level of abrasive concentration, and a high level of polishing speed are desirable for

improving both Ra and Rt. A comparison of the results obtained by the Taguchi method with single parameter (i.e. one parameter by one parameter) variation using a fine SiC abrasive (1 μm) yielded similar conclusions regarding optimum conditions. However, Taguchi method can extract information more precisely and more effectively.

A methodology for finishing of HIP'ed Si_3N_4 balls for hybrid bearing applications from the as-received condition using the magnetic float polishing was developed [5]. It involves the mechanical removal of material initially using harder abrasives with respect to the workmaterial (of different materials of progressively lower hardness and finer grain sizes) followed by final chemo-mechanical polishing (CMP) using preferably a softer abrasive for obtaining superior finish with minimal surface or subsurface damage, such as scratches, microcracks, or pits on the Si_3N_4 balls. High material removal rates (1 μm/min) with minimal subsurface damage is obtained with harder abrasives, such as B_4C or SiC (relative to Si_3N_4) due to the use of a flexible support system, small polishing loads (≈ 1 N/ball), and fine abrasives but high polishing speeds (compared to conventional polishing) by rapid accumulation of minute amounts of material removed by microfracture. Final polishing of the Si_3N_4 balls using a softer abrasive, such as CeO_2 (that chemo-mechanically react with the Si_3N_4 workmaterial) results in high quality Si_3N_4 balls of bearing quality with a superior surface finish (R_a < 4 nm, R_t < 0.04 μm) and a damage-free surface. It is found that CMP is very effective for obtaining excellent surface finish (Ra ≈ 4 nm and Rt ≈ 40 nm) on the Si_3N_4 ceramic balls and CeO_2 in particular is one of most suitable abrasive for this application.

1.3. CMP of Si_3N_4 Ceramic Balls With Various Abrasives

Chemo-mechanical polishing (CMP) studies were conducted, using various abrasives (B_4C, SiC, Al_2O_3, Cr_2O_3, ZrO_2, SiO_2, CeO_2, Fe_2O_3, Y_2O_3, CuO, and Mo_2O_3) to investigate their relative effectiveness in the finishing of uniaxially pressed Si_3N_4 ceramic balls by magnetic float polishing (MFP) technique [6]. CMP depends both on the chemical and the mechanical effectiveness of the abrasive and the environment with respect to the workmaterial. Among the abrasives investigated for CMP of Si_3N_4 balls, CeO_2 and ZrO_2 were found to be most effective followed by Fe_2O_3 and Cr_2O_3. Extremely smooth and damage-free Si_3N_4 bearing ball surfaces with a finish R_a of ≈ 4 nm and R_t of ≈ 40 nm were obtained after polishing with either CeO_2 or ZrO_2. Thermodynamic analysis (Gibbs free energy of formation) indicated the

feasibility of the formation of SiO_2 layer on the surface of the Si_3N_4 balls with these abrasives. This is particularly so in a water environment which facilitates the chemo-mechanical interaction between the abrasive and the workmaterial by participating directly in the chemical reaction leading to the formation of a softer SiO_2 layer. Since the hardness of some of the abrasives which were found to be most effective in CMP, namely, CeO_2, ZrO_2, and Fe_2O_3 is closer to that of SiO_2 layer but significantly lower than the hardness of the Si_3N_4 workmaterial, removal of the SiO_2 reaction layer effectively without scratching and/or damaging the Si_3N_4 substrate is facilitated by the subsequent mechanical action of the abrasives. The chemical reaction would proceed on a continuing basis only if the passivating layers are removed continuously by subsequently mechanical action. An oil-based polishing environment was found not to contribute anything towards CMP of Si_3N_4 balls.

Among various abrasives investigated for the chemo-mechanical polishing (CMP) of Si_3N_4 ceramic balls [6], cerium oxide (CeO_2) was found to be the most effective polishing medium (even superior to Cr_2O_3 [2]), yielding an extremely smooth and damage-free surface with a surface finish R_a of $\approx$ 4 nm and R_t of $\approx$ 40 nm. The underlying reasons for the superior finish on Si_3N_4 balls with CeO_2, therefore, were investigated [7].

Various chemical reactions involved in CMP of Si_3N_4 balls with CeO_2 were investigated (Gibbs free energy minimization) and a mechanism for the CMP is developed. The two important functions that CeO_2 performs in the CMP of Si_3N_4 are: 1. It participates directly in the chemical reaction (oxidization-reduction reaction) with Si_3N_4 workmaterial leading to the formation of a thin SiO_2 layer, 2. The hardness of CeO_2 is closer to that of a thin SiO_2 layer likely to form on Si_3N_4 but significantly lower than Si_3N_4 workmaterial ($\approx 1/3$). It can thus remove the brittle SiO_2 reaction product effectively without damaging the Si_3N_4 substrate as no abrasion can take place by CeO_2 on Si_3N_4. The kinetic action, which involves the removal of the reaction products from the interface by subsequent mechanical action of flowing water and CeO_2 is critical to CMP. The chemical reaction could proceed on a continuing basis so long as the passivating layers are removed by the mechanical action at the same time. CeO_2 is found to be very effective in a water environment (hydrolysis) leading to the formation of additional SiO_2 by reacting with Si_3N_4 thereby enhancing the CMP of Si_3N_4. Also, after investigating various

reaction species in the CMP of Si_3N_4 with CeO_2 and Cr_2O_3, the former is found to be much safer from an environmental point of view.

1.4. Thermal Aspects of Magnetic Field Assisted Polishing of Ceramics

1.4. 1. Thermal Model

A thermal model for magnetic field assisted polishing of ceramic balls/rollers was developed [8]. The heat source at the area of contact between the balls and the abrasives where material removal takes place is approximated to a disc. The disc heat source is considered as a combination of a series of concentric circular ring heat sources with different radii. Each ring in turn is considered as a combination of a series of infinitely small arc segments and each arc segment as a point heat source. Jaeger's classical moving heat source theory [9,10] is used in the development of the model starting from an instantaneous point heat source to obtain the general solution (transient and steady-state) of a moving circular ring heat source problem and finally the moving disc heat source problem. Due to the formation of fine scratches during polishing (on the order of a few micrometers long), the conditions are found to be largely transient in nature. Calculation of the minimum flash temperatures and minimum flash times during polishing enables, if adequate temperatures can be generated for chemo-mechanical polishing to take place.

1.4. 2. Application of Thermal Model to Magnetic Float Polishing of Ceramic Balls

The thermal model developed [8] is applied for magnetic float polishing (MFP) of ceramic (Si_3N_4) balls [11]. The general solution for a disk heat source with a parabolic distribution of heat intensity was used for this case. Using this method, the flash temperatures, flash times, and temperature distribution at the interface between the balls and the shaft of the MFP apparatus are calculated. Examination of the polished surfaces (scratch lengths) of the balls showed that the length of most scratches during the final stage of polishing to be < 20 μm. Thus the scratching process appears to be mostly under transient conditions. However, because of the small area of contact and low loads, the results of the calculations under these conditions was found to be very close to quasi-steady state conditions with the differences being rather small. It is, however, not possible to know *a priori* if the conditions are transient or quasi-steady state unless solutions are available for both cases. The minimum flash temperatures and minimum flash times that occur during polishing ensure that adequate temperatures are generated for chemo-

mechanical polishing to take place. Of course, the lengths of the scratches would be much longer and the corresponding flash duration longer during the semifinishing operation than during finishing. The combined temperature and flash duration would determine the extent of chemo-mechanical action under these conditions. The flash temperatures and flash times required for chemo-mechanical action can be used as a basis for optimization of polishing conditions in MFP.

1.4.3. Application of the Thermal Model to the Magnetic Abrasive Finishing (MAF) of Ceramic Rollers

The solution developed for a moving disc heat source with a parabolic distribution of heat intensity [8] is extended to the magnetic abrasive finishing (MAF) process [12]. The minimum flash temperatures and flash times generated at the contact points between the workmaterial (Si_3N_4 roller) and the abrasive (Cr_2O_3) were then determined [13]. Conditions during the final stages of polishing of advanced ceramics by the MAF process are found to be, by and large, transient and hence quasi-steady state solutions for the moving circular heat sources available in the literature is not applicable. The flash temperatures generated were found to be a function of the polishing pressure as well as the rotational speed of the work material. Since chemo-mechanical action between the abrasive, the workmaterial, and the environment depends both on the thermodynamics and kinetics of the process, it is important to determine the flash temperatures as well as flash times during polishing. In this investigation, they were determined at various polishing conditions. Thermodynamic considerations indicate that even the minimum flash temperatures generated under the conditions of lower pressure, lower sliding velocity, and transient state would be adequate to initiate chemo-mechanical action and experimental results confirmed the formation of chemo-mechanical reaction products during polishing [2].

1.5. General Solutions for Moving Heat Source Problems

General solutions for the temperature rise of plane moving heat sources were developed using Jaeger's classical heat source method [14]. An elliptic heat source was used as the basic plane heat source and equations were derived for the temperature rise starting with the moving point heat source solution. This analysis was then extended to other moving plane heat sources, such as circular, square, and rectangular. By considering the major axis of the elliptical heat source to be

equivalent to the minor axis, the equation for the circular heat source is obtained. Similarly, by assuming the width of the moving heat source to be constant, solutions for rectangular ($a \neq b$) or square ($a = b$) heat sources are obtained. In addition, the model developed can be applied in principle for any geometrical shape that can be defined mathematically. Various distributions of the heat sources, namely, uniform, parabolic, and normal distributions were considered to cover a range of manufacturing and tribological problems experienced in practice. This analysis can similarly be extended to other distributions. Thus, the solutions developed here for a single geometry (elliptical shape) as a basis can be extended to solve a wide range of plane moving heat source problems by appropriate substitutions of the boundary conditions. In addition, we have presented for the first time, an analysis for both transient and steady state conditions while almost all analyses to date are for quasi-steady state conditions. The analysis can determine not only the temperature at the surface but also the temperature distribution with depth which again is a very important consideration in most manufacturing applications. It can also calculate both the maximum and average temperatures. Thus, the analysis presented here is more comprehensive than the models developed to date.

1.6. Equipment for Polishing Large Batch of Si_3N_4 Ceramic Balls

Although the principle used in the design of the equipment for finishing large batch of Si_3N_4 ceramic balls is the same as the one for the small apparatus, many design modifications were needed for the large batch apparatus. A 12 in. diameter chamber (instead of 2.5 in. diameter chamber used in the small apparatus) with the magnets located (as integral part) at the base is used in this design. A bank of permanent magnets (Nd-Fe-B) with alternate N and S are arranged into 16 segments at the bottom of the float chamber. Also, while in the small batch apparatus the magnetic field is solely responsible for providing the load on the balls during polishing, in the large batch design, two methods of loading were incorporated. The first one is a dead weight system and the other is the magnetic field system. The former applies the required load/per ball (e.g. 1 N/ball) while the latter acts as a spring load to even out the load during polishing due to differences in the diameter of the balls. In principle, one can use the dead load system alone in which case the float chamber does not contain magnetic fluid but merely water and the abrasive. This apparatus can be used either as a straight polishing apparatus or as a magnetic float polishing (MFP) apparatus. As the chamber is much larger in this equipment,

the spindle can be run at much lower speeds (400 rpm instead of 2000 rpm used with the smaller apparatus).

The polishing shaft is driven by the spindle of a Bridgeport CNC machine tool. The magnetic field is measured by Gauss/Tesla meter. The pH value of polishing environment is measured by pH/Temperature meter. The polishing load is set up by the deadweight. The material removal rates are calculated by the weight reduction in the balls before and after polishing at various stages of testing using a precision balance. The surface finish of the polished balls are characterized using a Form Talysurf 120 L, ZYGO laser interference microscope, and an ABT 32 scanning electron microscope (SEM). The roundness of the balls is measured using TalyRond 250.

Results obtained to date with this equipment are very favorable and better than those obtained with the smaller apparatus. A material removal rate of 1 $\mu m/min$ per ball and a sphericity of < 0.2 μm were obtained. We have finished two batches of of 12 mm diameter balls with a surface finish of 4 nm Ra and a sphericity of ~ 0.15 μm. While this apparatus can finish ~ 100 balls per batch, it can be easily modified to accommodate more balls. For example, instead of one row of balls in the float chamber, several rows can be incorporated. This requires additional magnets at each row of the balls as well as increasing the dead weight to account for the increase in the number of balls. Partitions can be made on the float chamber to separate the rows and the top plate has to be modified appropriately to handle the balls at various diameters.

REFERENCES

1. Komanduri, R.," Final Report on the Ceramic Bearing Technology Program," (C F33615-92-C-5933) Technical Report No. WL-TR-96-4021 dated July 1995. Volume 1. Oklahoma State University, Stillwater, OK.

2. Bhagavatula, S. R. and R. Komanduri,"On Chemo-Mechanical Polishing of Silicon Nitride with Chromium Oxide Abrasive," Philosophical Magazine, A 74 (1996) 1003-1017

3. Taguchi, G.,"Taguchi Methods-Researach and Development," ASI Press, Dearborn, MI (1992)

4. Ming Jiang and R. Komanduri, "Appliction of Taguchi Method for Optimization of Finishing Conditions in Magnetic Float Polishing (MFP)," Wear, 213 (1997) 59-71

5. Ming Jiang and R. Komanduri, "On the Finishing of Si_3N_4 Balls for Bearing Applications," Wear , 215 (1998) 267-278

6. Ming Jiang, Wood, N. O., and R. Komanduri, "On the Chemo-Mechanical Polishing of Si_3N_4 Bearing Balls with Various Abrasives" Wear, 220 (1998) 59-71

7. Ming Jiang, Wood, N. O., and R. Komanduri, "On the Chemo-Mechanical Polishing of Si_3N_4 Bearing Balls with CeO_2," Trans ASME, J of Engineering Materials & Technology, 120, (1998) 304-312

8. Hou, Z. B. and R. Komanduri, "On the Thermal Aspects of the Magnetic Field Assisted Polishing of Ceramics, Part I. Thermal Model," Trans ASME, J of Tribology, 120 (1998) 645-651

9. Jaeger, J. C., "Moving Sources of Heat and the Temperature of Sliding Contacts," Proc. of the Royal Society of NSW, Australia, 71 (1942) 203-224

10. Carslaw, H. S. and J. C. Jaeger, "Conduction of Heat in Solids," Oxford University Press, Oxford, UK (1959)

11. Hou, Z. B. and R. Komanduri, "On the Thermal Aspects of the Magnetic Field Assisted Polishing of Ceramics, Part II. Thermal Aspects of Magnetic Float Polishing (MFP) of Ceramic Balls,"Trans ASME, J of Tribology, 120 (1998) 652-659

12. Fox, M., Agarwal, K, Noori-Khajavi, A., Shinmura, T. and R. Komanduri, "Magnetic Abrasive Finishing of Non-Magnetic Stainless Steel Rods," Annals of CIRP 43/1 (1994) 181-184

13. Hou, Z. B. and R. Komanduri, "On the Thermal Aspects of the Magnetic Field Assisted Polishing of Ceramics; Part III. Thermal Aspects of Magnetic Abrasive Finishing (MAF) of Ceramic Rollers," Trans ASME, J of Tribology 120 (1998) 660-667

14. Hou, Z. B. and R. Komanduri, "General Solutions for Stationary/ Moving the Plane Heat Source Problems in Manufacturing and Tribology, Int. J of Heat & Mass Transfer, 43 (2000) 1679-169

2. FINISHING OF Si_3N_4 BALLS BY MAGNETIC FLOAT POLISHING (MFP)

2.1. Introduction

A critical factor affecting the performance and reliability of ceramics for bearing applications is the quality of the resulting surface by polishing. It is well known that ceramics are extremely sensitive to surface defects resulting from grinding and polishing processes owing to their high hardness and inherent brittleness. Since fatigue failure of ceramics is driven by surface imperfections, it is paramount that the quality and finish of the ceramic bearing elements be as best as possible with minimal defects so that reliability in performance of bearings in service can be achieved.

In order to optimize the finishing conditions for polishing of Si_3N_4 balls by magnetic float polishing (MFP), Taguchi [1] method was used for optimization [2]. Appendix A gives details of the Taguchi method used in this investigation and may be referred to for details. This is followed by the development of a methodology for finishing Si_3N_4 balls by magnetic float polishing (MFP) [3]. Appendix B gives details of the methodology and may be referred to, for details. In the following a brief description of the experimental set-sup, test conditions, and final conclusions are given. Two U.S. Patents were issued in the name of Oklahoma State University, one for the finishing of ceramic workmaterials [4] and the other for finishing of magnetic workmaterials, such as steels and some stainless steels [5]. Two review articles were written on this technology, one for tribology audience [6] and the other for practing manufacturing engineers [7]. Also, an extensive review paper (invited key-note paper) was prepared on the Technological Advanced in Fine Abrasive Processes [8] which discusses this technology as well as several other finishing technologies.

2.2. Experimental Set-Up and Test Conditions

The magnetic float polishing technique is based on the magneto-hydrodynamic behavior of a magnetic fluid that can float non-magnetic float and abrasives suspended in it by a magnetic field [3]. The magnetic fluid is a colloidal dispersion of extremely fine (100 to 150 A) subdomain ferromagnetic particles, usually magnetite (Fe_3O_4), in a carrier fluid, such as water or kerosene. It is made stable against particle agglomeration by coating the particles with an appropriate surfactant. In this investigation a water base (W-40) ferrofluid is used.

The forces applied by the abrasive to the part are extremely small (1N/ball) and highly controllable. Figures 2.1 (a) and (b) are a schematic and a photograph of the magnetic float polishing apparatus for finishing advanced ceramic balls. A bank of permanent magnets (Nd-Fe-B) are arranged alternate N and S below an aluminum chamber. It is filled with the required amount of magnetic fluid and appropriate abrasive (5-10% by volume).

When a magnetic field is applied, the magnetic particles in the magnetic fluid are attracted downward to the area of higher magnetic field and an upward buoyant force is exerted on all non-magnetic materials to push them to the area of lower magnetic field. The abrasive grains, the ceramic balls, and the acrylic float inside the chamber, all being non-magnetic materials, are levitated by the magnetic buoyant force. The drive shaft is fed down to contact with the balls (3-point contact) and presses them down to reach the desired force or height. The balls are polished by the abrasive grains under the action of the magnetic buoyancy levitational force when the spindle rotates. Damage-free surface on ceramic balls are expected by the magnetic float polishing technique because the magnetic buoyant force (1 N/ball) is applied via the flexible float. The function of the acrylic float is to produce more uniform and larger polishing pressure (the larger buoyant force near the magnetic poles can be transmitted to the polishing area by this float). An urethane rubber sheet is glued to the inner guide ring to protect it from wear. The material of the drive shaft is austenitic stainless steel which is non-magnetic.

The polishing shaft was driven by a high-speed, high-precision air bearing spindle (PI Spindle) with a stepless speed regulation up to 10,000 rpm. The magnetic field was measured by Gauss/Tesla meter. pH value of the polishing environment was measured by pH/Temperature meter. The polishing load was set up by measuring the normal force with a Kistler's piezoelectric dynamometer connected to a charge amplifier and a display. To calculate material removal rates, the weight reduction in the balls was measured before and after polishing at every stage of testing using a precision balance. The surface finish of the polished balls was analyzed using a Form Talysurf 120 L (a stylus based instrument), ZYGO laser interference microscope (non-contact), a Digital Nanoscope III atomic force microscope (AFM), and an ABT 32 scanning electron microscope (SEM). The

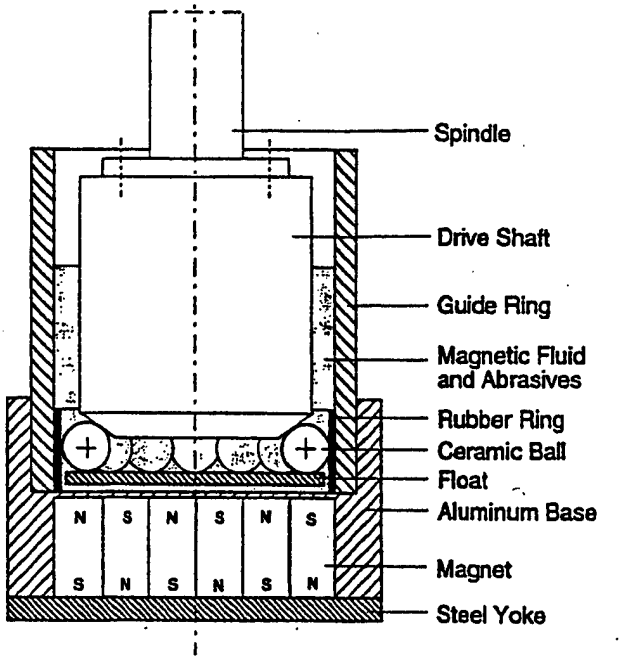

(a)

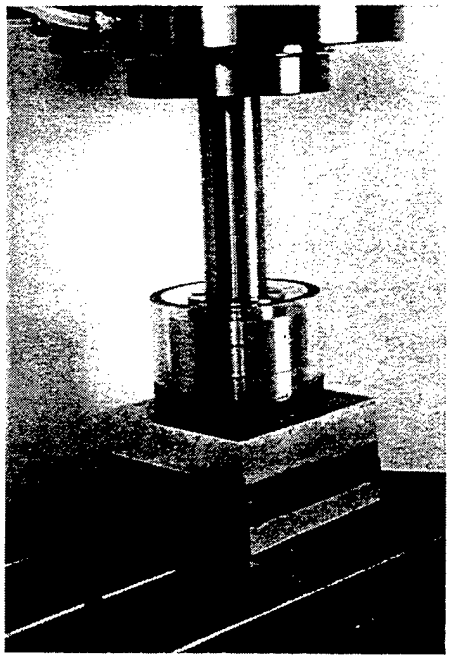

(b)

Figures 2.1 (a) and (b) Schematic and a photograph of the magnetic float polishing (MFP) apparatus for finishing advanced ceramic balls.

sphericity of the balls was measured using TalyRond 250 (a stylus based instrument). The surface chemistry of the finished balls was evaluated using Seimens small angle X-ray diffraction equipment

Appendix B gives details of this investigation and may be referred to for completeness. Tables 2.1 and 2.2 give the chemical composition and the mechanical and thermal properties, respectively of NBD 200 HIP'ed Si_3N_4 balls (supplied by CERBEC) used in this investigation [9]. The sintering aid is ≈ 1 wt.% MgO. Major impurity is Fe_2O_3. Table 2.3 gives the properties of the various abrasive used. Table 2.4 lists the test conditions used for different stages of polishing.

Two coarser, harder abrasives, B_4C (500 grit) and SiC (400 grit) (i.e. compared to Si_3N_4 work material) were used during the initial stages of polishing to reach the desired diameter at high removal rates and at the same time improve the sphericity for proper ball motion. After reaching the diameter close to the desired value, an intermediate (semifinishing) stage is utilized as a transition between the roughing and finishing stages, as the material removal rate is of prime concern in the first stage and surface finish in the final stage. The two harder abrasives with a finer grit size were chosen for this intermediate stage, namely, SiC (1000 grit) and SiC (1200 grit). During this stage, the removal rates are much lower and the finish much superior than roughing but the emphasis during this stage is the improvement of sphericity. In the final stage (prior to CMP), fine SiC abrasive (8000 grit) is used to approach the required diameter and sphericity and remove almost all the deep valleys from the surface. This is followed by final polishing using a softer, chemo-mechanical abrasive, namely, CeO_2 to produce the balls of required diameter, sphericity, and final surface finish which is extremely smooth and almost damage-free by preferentially removing the peaks from the surface. Table 2.5 shows the results of the tests. Based on the detailed methodology developed for finishing Si_3N_4 balls by magnetic float polishing (MFP) (Appendix B), the following conclusions may be reached.

2.3. Conclusions

1. Magnetic float polishing (MFP) process combining mechanical and chemo-mechanical polishing (CMP) is an efficient manufacturing technology for producing high quality Si_3N_4 balls for bearing applications due to high polishing speed, small and controlled polishing force, flexible support, and chemo-mechanical action.

Table 2.1 : Nominal chemical compositions (wt.%) of NBD-200 Si_3N_4 [9]

Al	C	Ca	Fe	Mg	O	Si_3N_4
≤0.5	≤ 0.88	≤ 0.04	≤ 0.17	0.6 - 1.0	2.3 - 3.3	94.11-97.1

Table 2.2 : Mechanical and thermal properties of uniaxially pressed Si_3N_4 [9]

PROPERTY	VALUE
Flexural Strength, MPa	800
Weibull Modulus	9.7
Tensile Strength, MPa	400
Compressive Strength, GPa	3.0
Hertz Compressive Strength, GPa	28
Hardness, Hv (10kg), GPa	16.6
Hardness, Mohs	8.5
Fracture Toughness, K_{1c}, $MPam^{-1/2}$	4.1
Density, g/cm^3	3.16
Elastic Modulus, GPa	320
Poisson's Ratio	0.26
Thermal Expansion Coefficient at 293-1273 K, /K	2.9×10^{-6}
Thermal Conductivity at 373 K, W/m-K	29
Thermal Conductivity at 773 K, W/m-K	21.3
Thermal Conductivity at 1273 K, W/m-K	15.5

Table 2.3 Properties of Various Abrasives

ABRASIVES	DENSITY g/cm^3	HARDNESS	
		Mohs	Knoop kg/mm^2
Diamond	3.52	10	7000
Boron Carbide (B_4C)	2.52	9.3	3200
Silicon Carbide (SiC)	3.22	9.2	2500
Aluminium Oxide (Al_2O_3)	3.98	9	2150
Chromium Oxide (Cr_2O_3)	5.21	8.5	1800
Zirconium Oxide (ZrO_2)	5.85	8	1200
Silicon Oxide (SiO_2)		7	820
Cerium Oxide (CeO_2)	7.13	6	-
Iron Oxide (Fe_2O_3)	5.24	6	-
Yttrium Oxide (Y_2O_3)	5.01	5.5	700
Copper Oxide (CuO)	6.32	3.5	225
Molybdenum Oxide (Mo_2O_3)	4.69	1.5	-

Table 2.4 Test Conditions used for different stages of polishing

Stage	Abrasive			Abrasive (vol.%)	Speed (rpm)	Load (N/ball)	Time (min)	Remarks
	Type	Grit size	Size (μm)					
1	B_4C	500	17	10%	2000	1.0	–	Roughing (high material removal)
	SiC	400	23	10%	2000	1.0	–	
2	SiC	1000	5	10%	2000	1.0	30	Semi-finishing (sphericity and roughness)
	SiC	1200	3	10%	2000	1.0	30	
3	SiC	8000	1	5%	4000	1.2	60	Final finishing (size, sphericity, and finish)
	CeO_2		5	10%	2000	1.2	120	

*All abrasives used, except CeO_2, were obtained from Norton. CeO_2 is obtained from Aldrich Chemicals.

Table 2.5 Average surface finish and material removal rates during various stages of polishing

Stage	Abrasive	Surface finish (average)		MRR (per ball)		Material removal mechanism
		R_a (nm)	R_t (μm)	(mg/min)	(μm/min)	
1	B_4C 500	225	1.95	0.96	1.2	Microfracture
	SiC 400	170	1.40	0.64	0.8	Microfracture
2	SiC 1000	95	0.80	0.30	0.4	Submicrofracture
	SiC 1200	55	0.50	0.20	0.2	Submicrofracture
3	SiC 8000	15	0.15	0.04	–	Submicrofracture
	CeO_2	4	0.03	0.01	–	Tribochemical

2. There are three polishing stages involved in this process, namely, initial stock removal stage where the emphasis is on high material removal rate with minimal surface-subsurface damage or the sphericity, intermediate semi-finishing stage where material removal rate, size, and sphericity have to be closely monitored, and the final finishing stage with emphasis on the required size, sphericity, and finish.

3. High material removal rates (1 μm/min) with minimal subsurface damage are possible using harder abrasives, such as B_4C or SiC due to rapid accumulation of minute amounts of material removed by mechanical microfracture at high polishing speeds and low loads in the MFP process. Although material removal is by brittle fracture, it occurs on a microscale due to low polishing force, flexible float system, and fine abrasives. The cracks generated are localized and suppressed from propagating into microcracks. Consequently, subsurface damage is minimized leading to the higher strength of the workmaterial and reliability of the parts in service.

4. An advantage of the magnetic float polishing (MFP) apparatus used in this investigation is that it is capable of finishing a small batch (10-20 balls) to the finished requirements without the need for sorting them from a large batch of balls or use different equipment for each stage as in conventional lapping. Such an apparatus would be beneficial especially when small batches are needed for specific low volume applications or for the evaluation of materials in the development of new materials for bearing applications.

5. MFP can be a cost effective process for finishing Si_3N_4 balls for bearing applications. The semifinishing and finishing stages can be accomplishing in about 4 hours. The roughing stage depends on the amount of material to be removed from the as-received condition to the final requirements. In any case, a batch of balls can be finished in $\approx$ 16 to 20 hours compared to several weeks by conventional polishing. Also, diamond abrasive is not required for the process. Faster polishing times and use of abrasives other than diamond would significantly reduce the overall costs of manufacture of Si_3N_4 balls for bearing applications. Also, the implementation of this technology would not be very capital intensive as it can be used by modifying the existing equipment.

REFERENCES

1. Taguchi, G., "Taguchi Methods -Researach and Development," ASI Press, Dearborn, MI (1992)

2. Ming Jiang and R. Komanduri, "Appliction of Taguchi Method for Optimization of Finishing Conditions in Magnetic Float Polishing (MFP)," Wear, 213 (1997) 59-71

3. Ming Jiang and R. Komanduri, "On the Finishing of Si_3N_4 Balls for Bearing Applications," Wear , 215 (1998) 267-278

4. Komanduri, R and Ming Jiang, "Magnetic Float Polishing Processes and Materials Therefor," U. S. Patent No. 5,931,718 dated Aug. 3, 1999

5. Komanduri, R and Ming Jiang, "Magnetic Float Polishing Processes of Magnetic Materials," U. S. Patent No. 5,957,753 dated Sept. 28, 1999

6. Komanduri, R. , Hou, Z. B., Umehara, N., Raghunandan, M., Ming Jiang, Bhagavatula, S. R., Noori-Khajavi, A., and N. O. Wood, "A 'Gentle' Method for Finishing Si_3N_4 Balls for Hybrid Bearing Applications," Tribology Letters 7 (1999) 39-49

7. Komanduri, R. and Ming Jiang, "A New Polishing Technology for Finishing Advanced Ceramic Balls for Hybrid Bearings," Abrasives Magazine (Aug./Sept. 1999) 8-20

8. Komanduri, R., Lucca, D. A., and Y. Tani, "Technological Advances in Fine Abrasive Processes," Annals of CIRP 46/2 (1997) 545-596

9. Hah, S. R., Fischer, T. E., and C. Burk, "Ceramic Bearing Development-Tribochemical Finishing of Silicon Nitride, Vol.4, Technical Report No. WL-TR-96-4018, The Materials Directorate, Wright Patterson AFB, OH, March 1995.

3. CHEMO-MECHANICAL POLISHING (CMP) OF Si_3N_4 CERAMIC BALLS WITH VARIOUS ABRASIVES

Chemo-mechanical polishing (CMP) depends on both chemical and mechanical effectiveness of the abrasive relative to the workmaterial and the environment under the conditions of polishing [1]. Since material removal from Si_3N_4 workmaterial by this mechanism would not depend on the hardness of the abrasive but on the chemical potentials and subsequent removal of the reaction layer, it is possible to remove material by abrasives substantially softer than the workmaterial. Chemo-mechanical action is thus very specific in that proper choice of the abrasive and the environment should be made for a given workmaterial. For efficient removal of material, those abrasives that facilitate chemical reactions and efficient mechanical removal would be preferable for CMP. Both thermodynamics and kinetics play an important role on the rates of chemical reactions. Once the reaction products are formed they should be removed from the workmaterial by subsequent mechanical scraping action of the abrasive. Thus the dual role of chemical and mechanical actions in CMP can be delineated.

In the DARPA project [2], we found that Cr_2O_3 is an effective abrasive for chemo-mechanical polishing of Si_3N_4 Balls [3]. However, there are some concerns regarding the suitability of this abrasive from an environmental safety point of view. We, therefore, investigated in this project alternate abrasives to address this problem and find a suitable solution.

3.1. Chemo-Mechanical polishing (CMP) of Si_3N_4 Balls With Various Abrasives

The purpose of this investigation is to determine the most suitable and effective abrasive as well as the environment to finish Si_3N_4 balls with extremely smooth and damage-free surfaces for highly reliable performance in such applications as bearings for aircraft engines and high-speed spindles.

A systematic investigation of the chemo-mechanical polishing (CMP) of a uniaxially pressed Si_3N_4 balls with various abrasives was conducted. Appendix C gives details of this work and may be referred to, for details. The abrasives considered include boron carbide (B_4C), silicon carbide (SiC), aluminum oxide (Al_2O_3), chromium oxide (Cr_2O_3), zirconium oxide (ZrO_2), silicon oxide (SiO_2), cerium oxide (CeO_2),

iron oxide (Fe_2O_3), yttrium oxide (Y_2O_3), copper oxide (CuO), and molybdenum oxide (Mo_2O_3). In Section 2, the chemical composition of the workmaterial and its properties are given in Tables 2.1 and 2.2, respectively and the properties of the abrasives in Table 2.3. They may be referred to, for details. Table 3.1 gives the test conditions used.

The pH value and the conductivity of the polishing fluid (magnetic fluid + abrasive) would influence the surface finish and material removal rate in CMP as the polishing fluid is part of the electrolytic cell. In this investigation, the pH and the conductivity values of the polishing environment were measured using a Cole-Parmer pH/Temperature meter and a TDS-Conductivity/Temperature meter, respectively.

Thermodynamic feasibility of the chemical reactions formed between the abrasive and workmaterial was investigated using the Gibb's free energy change. The flash temperatures and the flash durations at the contact zone of the polishing process were calculated using the thermal models developed by Hou and Komanduri [4,5]. This information was used to determine the feasibility of chemical reactions during CMP. These reactions would proceed on a continuing basis only if the passivating layers are removed by the subsequent mechanical action. The kinetic action, which involves the removal of the reaction products from the interface is thus critical to CMP.

Thermodynamic analysis (Gibb's free energy change, ΔG) was conducted to determine the reaction products that could be formed and to investigate whether such reactions are thermodynamically feasible [6]. It is well known that for a reaction to occur spontaneously at a given temperature and pressure, $\Delta G < 0$. In this investigation, the equilibrium composition and ΔG are calculated using the Outokumpu HSC Chemistry Software package from Finland. Table 3.2 shows the effect of each abrasives on the surface finish. It can be seen from this table that both ZrO_2 and CeO_2 are excellent chemo-mechanical abrasive in polishing Si_3N_4 balls. A discussion of the CMP mechanism for polishing Si_3N_4 with various abrasives is presented in Appendix C [6]. Based on the thermodynamic and kinetic analyses, the following conclusions can be arrived.

1. Chemo-mechanical polishing (CMP) depends not only on the polishing conditions but also on the interactions between the abrasive-workmaterial-

Table3.1 Test Conditions

Workmaterial	Uniaxially Pressed Si_3N_4 balls (CERBEC NBD 200) Initial diameter: 12.7 mm (0.5 inch) Initial Sphericity: 1 μm
Abrasive Concentration	10% by volume
Polishing Load	1.25 N per ball
Polishing Speed	2000 rpm
Magnetic Fluid	Oil based (EMG 40), Water based (W 40)

Table 3.2 Effect of Abrasives on Improving Surface Finish

Abrasive Type	Abrasive Size (μm)	Test Time (min)	Surface Finish		Effectiveness
			Ra (nm)	Rt (μm)	
B_4C 1500	2	45	32	0.280	
Al_2O_3	5	60	46	0.377	FAIL
B_4C 1500	2	45	31	0.295	
CuO	3	60	28	0.241	POOR
CuO	3	90	27	0.240	
B_4C 1500	2	45	31	0.275	
Y_2O_3	20	90	26	0.247	POOR
Y_2O_3	20	60	23	0.244	
B_4C 1500	2	45	30	0.272	
SiO_2	30	90	22	0.236	POOR
SiO_2	30	60	22	0.244	
B_4C 1500	2	45	28	0.270	
Mo_2O_3	20	60	22	0.216	POOR
Mo_2O_3	20	90	18	0.205	
B_4C 1500	2	45	29	0.260	
Cr_2O_3	5	90	14	0.208	GOOD
Cr_2O_3	5	60	12	0.175	
B_4C 1500	2	45	30	0.274	
Fe_2O_3	3	60	13	0.186	GOOD
Fe_2O_3	3	90	9	0.167	
B_4C 1500	2	45	31	0.268	
CeO_2	5	60	16	0.172	EXCELLENT
CeO_2	5	90	8	0.100	
B_4C 1500	2	45	29	0.286	
ZrO_2	5	60	18	0.174	EXCELLENT
ZrO_2	5	90	8	0.126	

environment. Among the various abrasives investigated for CMP of Si_3N_4 bearing balls, CeO_2 and ZrO_2 abrasives were found to be most effective followed by Fe_2O_3 and Cr_2O_3. It is also found that CMP of Si_3N_4 is particularly effective in a water-based fluid environment.

2. Thermodynamic analysis (Gibbs free energy of formation) indicated the feasibility of chemical reactions between CeO_2, ZrO_2, Fe_2O_3, and Cr_2O_3 abrasives and Si_3N_4 workmaterial leading to the formation a SiO_2 layer. Since the hardness of these abrasives is closer to that of SiO_2 layer and lower than Si_3N_4 workmaterial, SiO_2 reaction layer is effectively removed without damaging the Si_3N_4 substrate by the subsequent mechanical action of the abrasives on the workmaterial. The kinetic action, which removes the reaction products from the interface is critical in the CMP process. The chemical reaction will be continued only after the passivating layers are removed continuously by the subsequent mechanical scraping action.

3. CeO_2 and ZrO_2 abrasives are found to be the very effective in the CMP of Si_3N_4 balls yielding an extremely smooth and damage-free surface with a finish R_a of 4 nm and R_t of 40 nm. CeO_2 and ZrO_2 are much softer than Si_3N_4 and could not cause any mechanical damage and scratching on the Si_3N_4 workmaterials. Cr_2O_3 is slightly harder compared to the Si_3N_4 workmaterial. Consequently, while CMP takes place effectively, possibility exists for mechanical abrasion and subsequent microchipping. Further, CeO_2 and ZrO_2 and their various reaction products formed during polishing are much more safer than the compounds formed by the reaction of Cr_2O_3 with Si_3N_4 workmaterial from an environmental point of view.

4. No CMP was found to occur in an oil-based polishing environment. The conductivity and dissolution value of an oil-based polishing fluid is nearly zero. The oil film between the abrasive and the workmaterial prevents the formation of any chemical reaction as well as the removal of the reaction layer formed, if any, thus minimizing CMP. It can be seen that CMP of Si_3N_4 is particularly effective in a water-based environment for water is found to be essential to CMP of Si_3N_4 workmaterial. Water from water-based polishing fluid not only facilitates chemo-mechanical interaction between the abrasive and the workmaterial but also participates directly in the chemical reaction with the Si_3N_4 workmaterial (hydrolysis) leading to the formation of SiO_2 softer layer thereby enhancing the CMP.

5. The Si_3N_4 surface after CMP would consist of an outer SiO_2 layer and an intermediary layer of silicon oxinitride ($Si_xO_yN_z$) on the Si_3N_4 substrate. The layers composed of amorphous and crystalline SiO_2, Si_2N_2O, and $MgSiO_3$/$MgO.SiO_2$ form by the reaction with the sintering aid (1 wt.% MgO). This is not much different from the surface of Si_3N_4 workmaterial which invariably has a natural oxidation layer in air even at room temperature.

3.2. Chemo-Mechanical Polishing of Si3N4 Balls With Water Based CeO_2 Slurry

Since CeO_2 is found to be the very effective in the CMP of Si3N4 balls (even superior to Cr_2O_3 [6]), yielding an extremely smooth and damage-free surface with a finish R_a of 4 nm and R_t of 40 nm, further studies were undertaken with this abrasive [6]. Appendix D gives details of this work. In this investigation, the underlying reasons for the superior finish with CeO_2 were investigated.

Table 3.3 shows the properties of CeO_2 polishing medium and Table 3.4 gives the properties of the SiO_2, a thin layer that is generally formed on the surface of Si_3N_4 during polishing. The Si_3N_4 balls are initially polished with a SiC #8000 (1 μm) abrasive prior to CMP. The polishing conditions used here are listed in Table 3.5. The pH value of polishing solution [a water-based magnetic fluid (W-40) plus 10 vol.% CeO_2 the pH value of the polishing media is ≈ 6.

Various chemical reactions involved in CMP of Si3N4 balls with CeO_2 were investigated (Gibbs free energy minimization) and a mechanism for the CMP is proposed. The two important functions that CeO_2 performs in the CMP of Si3N4 are: i. It participates directly in the chemical reaction (oxidization-reduction reaction) with Si_3N_4 workmaterial leading to the formation of a thin SiO_2 layer, ii. The hardness of CeO_2 is closer to that of the thin SiO_2 layer formed on Si_3N_4 but significantly lower than Si_3N_4 workmaterial (≈ 1/3). It can thus remove the brittle SiO_2 reaction product effectively without damaging the Si_3N_4 substrate as no abrasion can take place by CeO_2 on Si3N4. The kinetic action, which involves the removal of the reaction products from the interface by subsequent mechanical action of flowing water and CeO_2 is critical to CMP. The chemical reaction could proceed on a continuing basis only so long as the passivating layers are removed by the mechanical action at the same time.

Table 3.3 : Properties of CeO_2 polishing medium [9]

PROPERTY	VALUE
Hardness, Mohs	6
Density, g/cm^3	7.13
Elastic Modulus, GPa	165
Poisson's Ratio	0.5
Thermal Conductivity at 373 K, W/m-K	8.4
Thermal Conductivity at 1273 K, W/m-K	0.8

Table 3.4 : Mechanical and thermal properties of SiO_2 [9,10]

PROPERTY	VALUE
Melting point, K	1983
Tensile Strength, MPa	100-120 MN/m2*
Hardness, Hv (100 g), GPa	710-750 kg/mm2
Hardness, Mohs	6.5
Fracture Toughness, K_{1c}, $MPam^{-1/2}$	0.79
Density, g/cm^3	2.2*
Elastic Modulus, GPa	72
Poisson's Ratio	0.17
Thermal Expansion Coefficient at 273-573 K, /K	0.564×10^{-6}
Thermal Conductivity at 273 K, W/m-K	1.45

Table 3.5. Test conditions

Workmaterial	Uniaxially pressed Si_3N_4 balls (CERBEC NBD-200), semifinished Diameter: 12.7 mm (0.5 inch) Initial Sphericity: 1 μm Initial Finish: Ra=20 nm
Abrasive Concentration	10% by volume
Polishing Load	1.2 N per ball
Polishing Speed	2000 rpm
Magnetic Fluid	Water-based (W 40) Saturation Magnetization at 289 K : 400 Gauss Viscosity at 27 °C : 25 Cp

CeO_2 is found to be very effective in a water environment (hydrolysis) leading to the formation of additional SiO_2 by reacting with Si_3N_4 thereby enhancing the CMP of Si_3N_4. Several similarities between polishing of Si_3N_4 and glass (SiO_2) [Cook, 1990], including the polishing environment (CeO_2 plus the magnetic fluid, pH value $\approx$ 6) and the mechanism of polishing were observed. Also, after investigating various reaction species in the CMP of Si_3N_4 with CeO_2 and Cr_2O_3, the former is found to be much safer from an environmental point of view.

Table 3.6 gives various chemical reactions of interest in this investigation as well as the free energy change, ΔG at various temperatures (from 273-1273 K) obtained from the software program used. It is known that Si_3N_4 can readily oxidize in an oxidizing atmosphere [8]. As a result, the surfaces of the as-received HIP'ed Si_3N_4 balls are generally covered with a thin layer of silica (see Eqn. 1 in Table 5.6). However, once this layer is removed, means should be available for the formation of SiO_2 subsequently so that CMP can take place on a continuing basis.

Figure 3.1 shows the variation of the reaction products with temperature for the chemical reaction system consisting of 1 mol of Si_3N_4, 1 mol of CeO_2, and 1 mol of H_2O at equilibrium based on the thermodynamic calculations. This diagram provides an insight on the mechanism of chemo-mechanical polishing of Si_3N_4 with CeO_2 showing various chemical species that can be formed during the process. It shows that while the SiO_2 mole fraction is constant up to about $\approx$ 300 ^oC, it increases with further increase in temperature. A reverse trend can be seen for Si_3N_4, i. e. initially constant followed by a decrease in mole fraction with further increase in temperature, both indicating an increase the material removal rate due to chemo-mechanical action at higher temperatures. It can be seen from the figure that $NH_3(g)$ forms at low temperatures (< 300 ^oC) while $H_2(g)$ and $N_2(g)$ gases form at higher temperatures

CeO_2 thus appears to be the most effective polishing medium for CMP of Si_3N_4 because of the thermodyamic considerations of its reaction with Si_3N_4 as well as its kinetic action of removing the reaction product, namely, SiO_2 from Si_3N_4 workmaterial. More details are given in Appendix D and may be referred to, for details.

Based on the CMP mechanism proposed here and the polishing results, it can be seen that CeO_2 abrasive has two important functions in CMP of Si_3N_4. First, it

Table 3.6 Chemical Reactions between Si_3N_4 , CeO_2 , and the environment along with ΔG at various temperatures

$Si_3N_4 + 3O_2(g) = 3SiO_2 + 2N_2(g)$ (1)								
T(K)	273	373	473	573	673	873	1073	1273
ΔG (kJ)	-1926	-1903	-1882	-1861	-1840	-1800	-1761	-1724
$Si_3N_4 + 6H_2O = 3SiO_2 + 4NH_3(g)$ (2)								
T(K)	273	373	473	573	673	873	1073	1273
ΔG (kJ)	-554.7	-589	-616	-638	-654	-668	-665.8	-612.4
$2NH_3(g) = N_2(g) + 3H_2(g)$ (3)								
T(K)	273	373	473	573	673	873	1073	1273
ΔG (kJ)	37.7	17.89	-3.68	-25.67	-48.2	-94.18	-140.9	-187.9
$NH_3 (g) + H_2O = NH_4OH$ (4)								
T(K)	273	373	473	573	673	873	1073	1273
ΔG (kJ)	31.77	41.38	11.8	49.32	64.37	79.0	22.8	95.3
$SiO2 + 2H_2O = Si(OH)_4$ (a) (5)								
T(K)	273	373	473	573	673	873	1073	1273
ΔG (kJ)	211.9	289.7	356.5	436.4	520.4	701.4	899.1	1114
$Si_3N_4 + 35.294\ CeO_2 = 3SiO_2 + 35.294\ CeO_{1.83} + 2N_2(g)$ (6)								
T(K)	273	373	473	573	673	873	1073	1273
ΔG (kJ)	-199	-257.9	-316.4	-373.7	-434.3	-555.5	-682.2	-815.5
$Si_3N_4 + 21.429\ CeO_2 = 3SiO_2 + 21.429\ CeO_{1.72} + 2N_2(g)$ (7)								
T(K)	273	373	473	573	673	873	1073	1273
ΔG (kJ)	-144.6	-198	-251.2	-303.9	-357	-465	-577.7	-695.6
$Si_3N_4 + 12CeO_2 = 3SiO_2 + 6Ce_2O_3 + 2N_2(g)$ (8)								
T(K)	273	373	473	573	673	873	1073	1273
ΔG (kJ)	148.4	93.2	35.9	-23	-82.76	-206.5	-334.4	-465.7
$2\ Si_3N_4 + 17.647CeO2 = 3\ Si_2N_2O + 17.647\ CeO1.83 + N_2$ (g) (9)								
T(K)	273	373	473	573	673	873	1073	1273
ΔG (kJ)	-285.5	-282.6	-280.9	-279.6	-278	-271.1	-259.6	-240.3
$Si_3N_4 + 1.5H2O = 1.5\ Si_2N_2O + NH_3$ (g) (10)								
T(K)	273	373	473	573	673	873	1073	1273
ΔG (kJ)	-392.9	-399.6	-412.1	-428	-446	-487	-532.5	-582.7

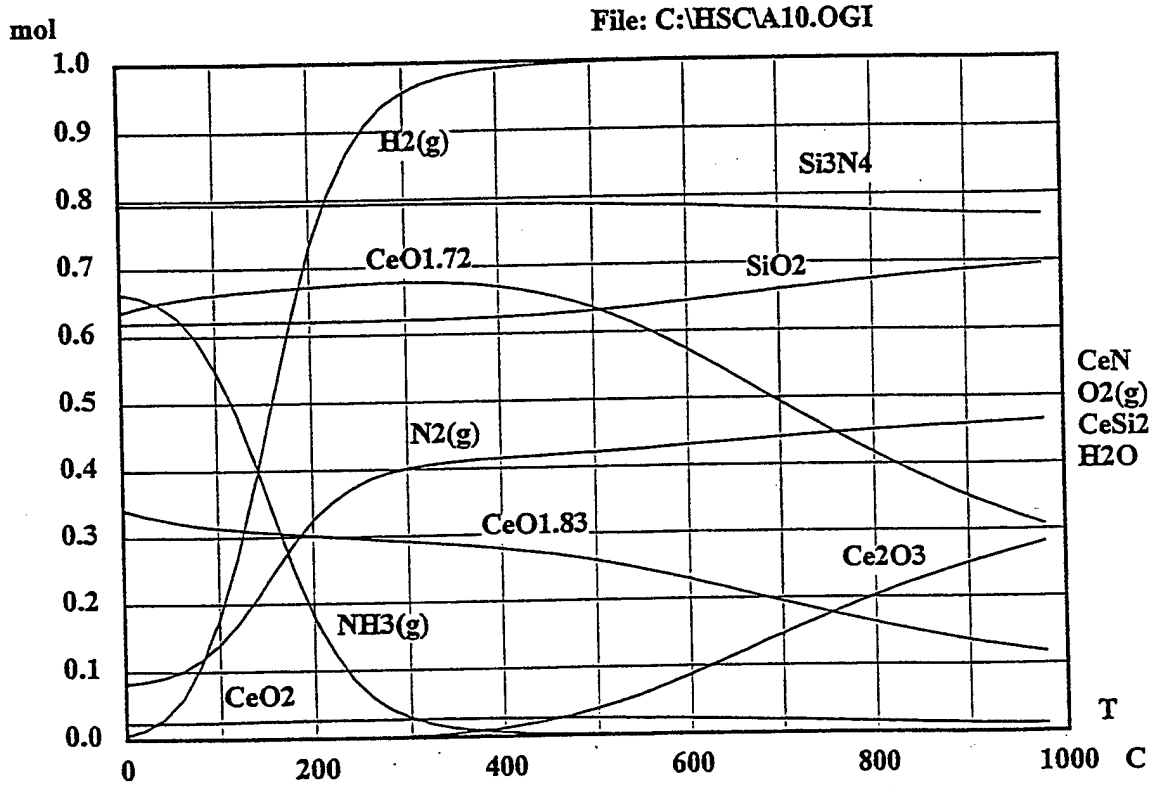

Figure 3.1 Variation of the reaction products with temperature for the chemical reaction system consisting of 1 mol of Si_3N_4, 1 mol of CeO_2, and 1 mol of H_2O at equilibrium based on the thermodynamic calculations.

directly reacts chemically (oxidization-reduction reaction) with Si_3N_4 workmaterial and leads to the formation of SiO_2 layer. Second, the hardness of CeO_2 is close to the SiO_2 layer and significantly lower ($\approx 1/3$) than Si_3N_4 workmaterial. So, the Si_3N_4 substrate can hardly be scratched or damaged by CeO_2 but the SiO_2 layer can be removed under subsequent mechanical action of water and CeO_2 on Si_3N_4 workmaterial. The kinetic action, which removes the reaction products from the interface is critical in the CMP process. The chemical reaction can be continued only after the passivating layers are removed continuously by the mechanical action.

Reaction between Si_3N_4 workmaterial and water (from water-based magnetic fluid) also occurs (hydrolysis) and leads to the formation of SiO_2 layer which is removed from the Si_3N_4 substrate by subsequent mechanical action of water and CeO_2. Thus, the CeO_2 polishing media is particularly effective in a water environment as found in this investigation.

The Si_3N_4 surface after CMP by CeO_2 may consist of an outer SiO_2 layer and an intermediary layer of silicon oxinitride ($Si_xO_yN_z$) on top of Si_3N_4 substrate. This is not much different from the surface of Si_3N_4 workmaterial which has a natural oxidation layer in air even at room temperature.

REFERENCES

1. Komanduri, R., Raghunandan, M., and N. Umehara, "On the Possibility of Chemo-Mechanical Polishing of Silicon Nitride by Magnetic Float Polishing," Trans ASME, J of Tribology , 118 (1996) 721-727

2. Komanduri, R., " Final Report on the Ceramic Bearing Technology Program," Oklahoma State University, Stillwater, OK. Volume 1 (C F33615-92-C-5933) Technical Report No. WL-TR-96-4021 dated July 1995

3. Bhagavatula, S. R. and R. Komanduri, "On Chemo-Mechanical Polishing of Silicon Nitride with Chromium Oxide Abrasive," Philosophical Magazine, A 74 (1996) 1003-1017

4. Zhen Bing Hou and R. Komanduri, "On the Thermal Aspects of the Magnetic Field Assisted Polishing of Ceramics, Part I. Thermal Model," Trans ASME, J of Tribology, 120 (1998) 645-651

5. Zhen Bing Hou and R. Komanduri, "On the Thermal Aspects of the Magnetic Field Assisted Polishing of Ceramics, Part II. Thermal Aspects of Magnetic Float Polishing (MFP) of Ceramic Balls,"Trans ASME, J of Tribology, 120 (1998) 652-659

6. Ming Jiang, Wood, N. O., and R. Komanduri, "On the Chemo-Mechanical Polishing of Si_3N_4 Bearing Balls with Various Abrasives" Wear, 220 (1998) 59-71

7. Ming Jiang, Wood, N. O., and R. Komanduri, "On the Chemo-Mechanical Polishing of Si_3N_4 Bearing Balls with Water Based CeO_2 Slurry," Trans ASME, J of Engineering Materials & Technology, 120, (1998) 304-312

8. Ruhle, M., "Microscopy of Structural Ceramics," Advanced Materials 9 (1) (1997) 195-217

9. Shaffer, P. T. B., "Handbook of High Temperature Materials - Materials Index, Plenum Press, NY (1964

10. Wyatt, O. H., and D. Dew-Hughes, "Metals, Ceramics, and Polymers," Cambridge University Press, Cambridge, U.K. (1974)

4. THERMAL ASPECTS OF MAGNETIC FIELD ASSISTED POLISHING

4.1. Introduction

A thermal model for magnetic field assisted polishing of ceramic balls/rollers was developed (see Appendix E for details) [1]. The heat source at the area of contact between the ceramic balls and the abrasive, where material removal takes place, is approximated to a disc. The disc heat source is considered as a combination of a series of concentric circular ring heat sources of different radii. Each ring, in turn, is considered as a combination of a series of infinitely small arc segments and each arc segment as a point heat source. Jaeger's classical moving heat source theory [2,3] is used in the development of the model starting from an instantaneous point heat source to obtain the general solution (transient and steady-state) of the moving circular ring heat source problem and finally the moving disc heat source problem. Due to the formation of fine scratches during polishing (on the order of a few micrometers long), the conditions are found to be largely transient in nature. Calculation of the minimum flash temperatures and minimum flash times during polishing enables if adequate temperatures can be generated for chemo-mechanical polishing to take place. This model is applied to magnetic float polishing (MFP) of ceramic balls (see Appendix F) [4] and to magnetic abrasive finishing (MAP) of ceramic rollers (see Appendix G) [5].

4.2. Thermal Model of a Moving Disc Heat Source

Figure 4.1 shows schematically the model used for the heat transfer process. It is a moving disc heat source with a radius of r_o and heat generation intensity of q, moving on the ceramic surface with a velocity, v. For convenience, as well as, for the choice of a model closer to practice, a parabolic distribution of heat intensity from the center to the periphery is considered. As a first step, the variation of thermal properties with temperature of the ball and the shaft materials are not considered. The objective of this analysis is to determine the temperature rise at any point and its distribution nearby and at the heat source, including on the surface as well as in the subsurface.

A general solution (both transient and quasi-steady state) for a moving disc heat source with a parabolic distribution of heat intensity was developed. This solution can be used to calculate both flash temperatures generated as well as the flash times

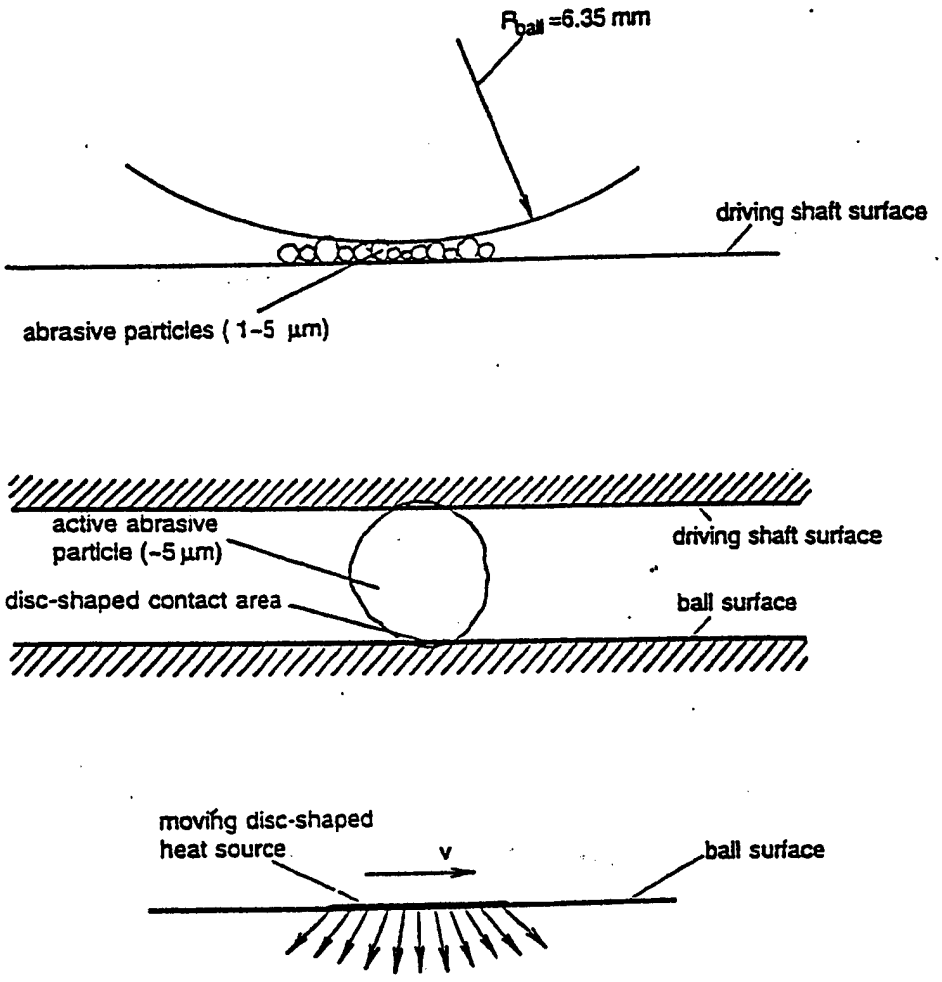

Figure 4.1 Schematic showing the model used for the heat transfer process to simultate magnetic field assisted polishing

at the contact point. This solution was applied to practical cases of magnetic float polishing (MFP) of ceramic balls [4] and for magnetic abrasive finishing (MAF) of ceramic rollers [5].

4.3. Application to magnetic float polishing (MFP) of ceramic balls

The thermal model developed for a disc heat source with a parabolic distribution of heat intensity is applied for magnetic float polishing (MFP) of ceramic (Si_3N_4) balls [4]. Appendix F gives details of this application and may be referred to, for details. Using this method, the flash temperatures, flash times, and temperature distribution at the interface between the balls and the shaft of the MFP apparatus can be calculated. Examination of the polished surfaces (scratch lengths) of the balls showed that the length of most scratches during the final stage of polishing to be only on the order of 0-20 μm. Therefore, the scratching process appears to be mostly under transient conditions. However, because of the small area of contact and low loads, the results of the calculations under these conditions was found to be very close to quasi-steady state conditions with the differences being very small. It is, however, not possible to know *a priori* if the conditions are transient or quasi-steady state unless solutions are available for both cases.

The minimum flash temperature and minimum flash times that occur during polishing ensure that adequate temperatures are generated for chemo-mechanical polishing to take place. Of course, the lengths of the scratches would be much longer and the corresponding flash duration longer during the semifinishing operation than during finishing. The combined temperature and flash duration would determine the extent of chemo-mechanical action under these conditions. The flash temperatures and flash times required for chemo-mechanical action can be used as a basis for the optimization of polishing conditions in MFP.

It is found that depending on the sliding speed, the minimum possible flash temperatures generated under transient conditions even for very short scratch lengths are adequate to activate chemo-mechanical action. For example, even at a low sliding speed of 2 m/sec, the maximum temperature rise is ~ 400 ^{o}C. It increases rapidly with increase in the sliding speed (6 m/sec) to about 1200 ^{o}C. Also, the flash times increase with increase in the scratch length. In the examples shown in Table 4.1, for a sliding velocity of v = 5 m/sec, the flash time is 1.3 - 1.6 μsec for a flash temperature higher than 100 ^{o}C but for a flash temperature of higher than 200 ^{o}C, it

reduces to about 0.7-0.8 μsec. Although the flash times are on the order of a few microseconds, it appears possible to initiate reaction products between the workpiece and the abrasive as evidenced by the X-ray diffraction studies of the wear debris formed in magnetic float polishing [6] .

4.4. Application of Thermal Model to Magnetic Abrasive Finishing (MAF) of Ceramic Rollers

The magnetic abrasive finishing (MAF) is a novel technique for finishing of cylindrical specimens, such as rollers used in ceramic hybrid bearings [7]. Appendix G gives detials of this work and may be referred to, for details. The material removal rate is generally high (1 μm/min) and finish quality is also excellent (Ra ≈ 5 nm). Figures 4.2 (a) and (b) show a schematic and a photograph of the MAF process, respectively. A copper coil, wound in the form of a solenoid, is used for the generation of the magnetic field in the core. The magnetic core material is generally a low carbon steel and in this investigation a 0.16% C steel is used. Magnetic heads are designed such that the magnetic field is concentrated surrounding the air gap with minimum leakage between the magnetic heads and the roller, which in the present case is a non-magnetic ceramic material. A pneumatic air vibrator is used to provide the vibratory motion to the magnetic head so that circumferential grooves that may otherwise form can be eliminated. The MAF equipment is mounted on a 1.5 hp, precision lathe with a continuous speed range of up to 3000 rpm. The function of the magnetic field is to enable the formation of a magnetic brush (iron particles and abrasives) that would remove material from the workmaterial during polishing.

The magnetic abrasive is an agglomerate of ferromagnetic particles (100-400 μm grain size iron power) and fine hard abrasive (1-10 μm grain size). It can be a sintered product or a mechanical mixture. In this investigation the latter type is used. The magnetic abrasive, when charged into the gap between the magnetic poles, forms two magnetic abrasive brushes around the periphery of the roller (Figure 4.3). When a non-magnetic cylindrical workpiece, such as a ceramic roller, is placed in the magnetic field with rotary and vibratory motions (with or without a lubricant), both surface and edge finishing operations can be performed simultaneously by the two magnetic abrasive brushes. The process is highly efficient and the removal rate and finish obtainable depend on the circumferential speed of the roller, magnetic flux intensity, working clearance between the magnetic

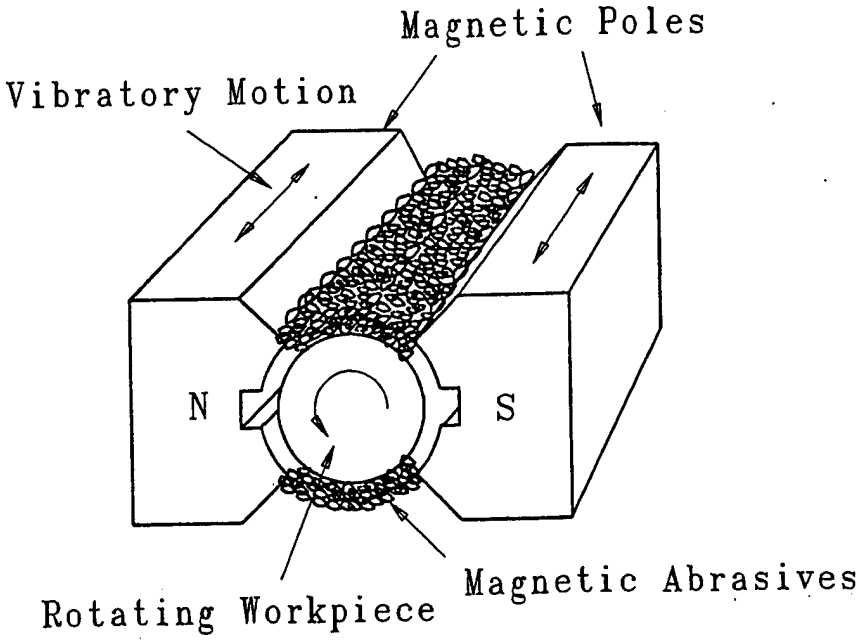

Figures 4.2 (a) Schematic of the magnetic abrasive finishing (MAF) process

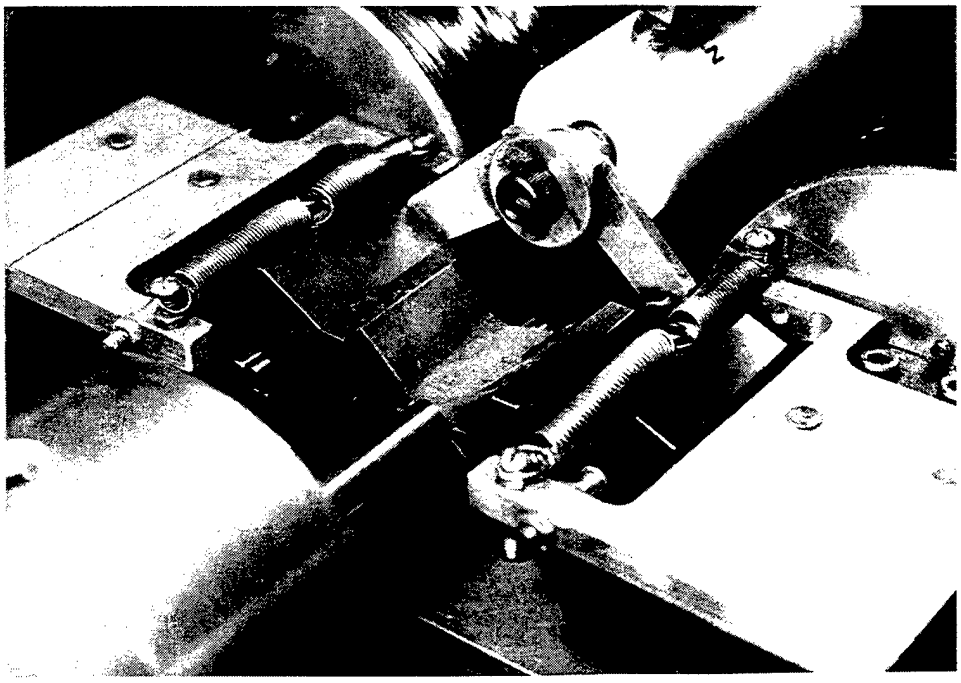

Figures 4. 2. (b) Photograph of the magnetic abrasive finishing (MAF) process

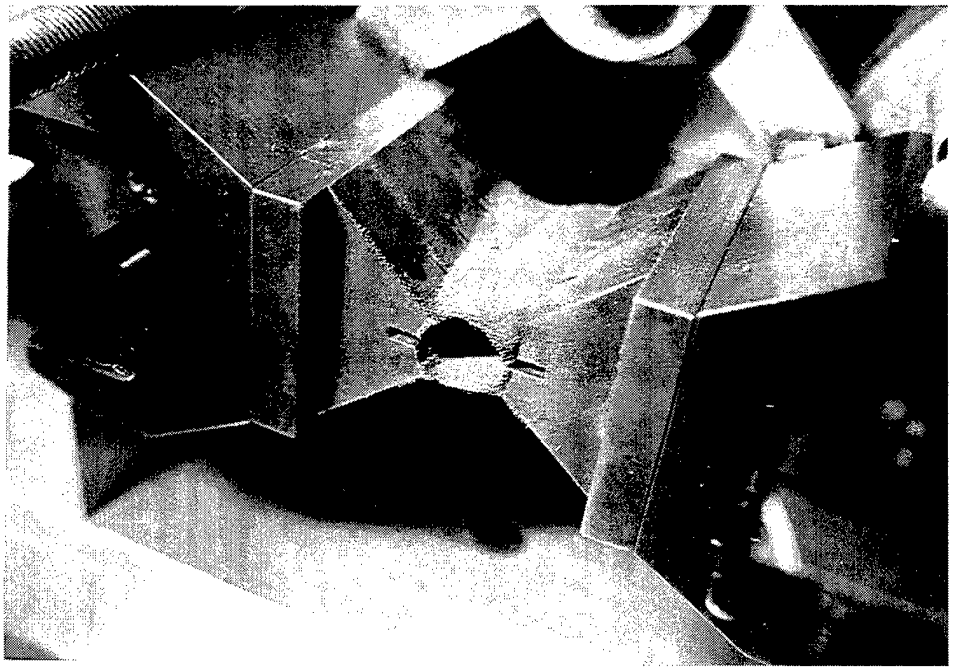

Figure 4.3. Photograph of the magnetic abrasive brush formed between the magnetic heads by the magnetic abrasive

heads and the roller, workpiece material, size of the magnetic abrasive agglomerate, including the type of abrasive used, grain size, and volume fractions of the abrasive and magnetic material in the agglomerate.

In the magnetic abrasive finishing (MAF) process, magnetic field is generated using an electromagnet. Current in the range of 0.5-2 A is passed through the copper coil wound in the form of a solenoid. The magnetic field generated within the magnetic core passes through the magnetic head. Magnetic abrasives are introduced in the gap between the magnetic heads, i. e. between the N and the S poles. Due to the presence of the magnetic field, the abrasives align in the direction of the field. The cylindrical roller to be polished is held in the chuck of a lathe. The roller is given a rotary motion and is positioned in the magnetic field. A small clearance between the magnetic heads and the chuck of the lathe is provided to avoid accidental collision. Vibratory motion is provided to the magnetic heads by means of a pneumatic vibrator to eliminate circumferential grooves that could form otherwise. Typical frequencies of vibration of the head are in the range of 15-20 Hz. The abrasives are stirred periodically at intervals of about 1 minute to achieve uniform wearing of the abrasives.

Detailed examination in the SEM of the polished surfaces of the silicon nitride rollers polished by MAF showed the lengths of the scratches on the work surface to be in the range of ~ 10-50 μm. Consequently, the time required for each contact was found to be on order of ~ 10-50 μsec when the sliding speed, v is ~ 1 m/sec. For higher sliding speeds, say 5 m/sec, the time of contact is less (~ 2-10 μsec). For very short scratch lengths and very short contact times, the conditions of polishing are shown to be transient and quasi-steady state conditions have not been reached.

Conditions during the final stages of polishing of advanced ceramics by magnetic abrasive finishing (MAF) process are found to be, by and large, transient and hence quasi-steady state solutions for the moving circular heat sources available in the literature can not be used. Hence, the general solution developed for a moving disc heat source with a parabolic distribution of heat intensity [1] is applied to determine the minimum flash temperatures and flash times generated at the contact points between the workmaterial (Si_3N_4 roller) and the abrasive (Cr_2O_3) in the magnetic abrasive finishing (MAF) process [5]. The flash temperatures generated were found to be a function of the polishing pressure as well as the rotational speed of the work material. Since chemo-mechanical action between the abrasive, the workmaterial,

and the environment depends both on the thermodynamics and kinetics of the process, it is important to determine the flash temperatures as well as flash times during polishing. In this investigation, they were determined at various polishing conditions. Thermodynamic considerations indicate that even the minimum flash temperatures generated under the conditions of lower pressure, lower sliding velocity, and transient state would be adequate to initiate chemo-mechanical action and experimental results confirmed the formation of chemo-mechanical reaction products during polishing [6].

REFERENCES

1. Hou, Z. B. and R. Komanduri, "On the Thermal Aspects of the Magnetic Field Assisted Polishing of Ceramics, Part I. Thermal Model," Trans ASME, J of Tribology, 120 (1998) 645-651

2. Jaeger, J. C., "Moving Sources of Heat and the Temperature of Sliding Contacts," Proc. of the Royal Society of NSW, Australia 71 (1942) 203-224

3. Carslaw, H. S. and J. C. Jaeger, "Conduction of Heat in Solids," Oxford University Press, Oxford, UK (1959)

4 Hou, Z. B. and R. Komanduri, "On the Thermal Aspects of the Magnetic Field Assisted Polishing of Ceramics, Part II. Thermal Aspects of Magnetic Float Polishing (MFP) of Ceramic Balls,"Trans ASME, J of Tribology, 120 (1998) 652-659

5. Hou, Z. B. and R. Komanduri, "On the Thermal Aspects of the Magnetic Field Assisted Polishing of Ceramics, Part III. Thermal Aspects of Magnetic Abrasive Finishing (MAF) of Ceramic Rollers," Trans ASME, J of Tribology 120 (1998) 660-667

6. Bhagavatula, S. R. and R. Komanduri, "On Chemo-Mechanical Polishing of Silicon Nitride with Chromium Oxide Abrasive," Philosophical Magazine, A 74 (1996) 1003-1017

7. Fox, M., Agarwal, K, Noori-Khajavi, A., Shinmura, T. and R. Komanduri, "Magnetic Abrasive Finishing of Non-Magnetic Stainless Steel Rods," Annals of CIRP 43/1 (1994) 181-184

5. GENERAL SOLUTIONS FOR STATIONARY/MOVING PLANE HEAT SOURCES

Moving heat source problems are commonly encountered in many manufacturing processes including metal cutting, grinding, polishing, welding, heat treatment, cutting (arc, plasma-arc, laser) as well as in many tribological applications, such as meshing of gears, cams, bearings, asperities in sliding contact. Temperature distribution on and near the surface affect the metallurgical microstructure, thermal shrinkage, thermal cracking, hardness distribution, residual stresses, heat affected zone (HAZ), surface integrity, and chemical modifications of the material. Consequently, thermal aspects of manufacturing are very critical in the optimization of the process conditions, quality of the products manufactured as well as their performance and reliability in service. From the mid-1930's to mid-1940's, Rosenthal [1], Blok [2], and Jaeger [3] made seminal contributions in this field which formed the basis for much of the applied research that followed during the past half a century.

Rosenthal [1], in considering the heat transfer and temperature distribution in welding, started with the Fourier's partial differential equation (PDE) of heat conduction in solids and introduced the moving coordinate system for the analysis of the moving heat source problems. He analyzed the moving point and moving line heat source problems and introduced the concept of quasi-stationary state (or steady state conditions) to simplify the equation so that it does not become to quote "too unwieldy for a direct practical application [1]." Actually, even for quasi-steady conditions, one is involved in solving a triple integral that contains a Bessel function or an error function which were tabulated only in certain ranges. Other special functions have to be analyzed and determined numerically (such as Bessel function, trignometric functions, hyperbolic functions) untill the advent of powerful, inexpensive personal computers. Hence, the analysis of necessity was limited to quasi-steady state. Based on the similarity between the differential equation for heat conduction and that encountered in electrical waves, Rosenthal developed a solution to this problem based on analogy.

Jaeger, in his classical paper, on 'Moving Sources of Heat and the Temperature Rise at the Sliding Contacts," published in 1942 [3] introduced the heat source method for solving a range of moving heat source problems for the calculation of

the temperature rise at the sliding contacts (also summarized briefly in Carslaw and Jaeger [4]). He considered a wide range of plane heat sources of different shapes (band, square or rectangular) and developed equations for the temperature rise starting from the instantaneous point heat source. For mathematical simplicity and from practical considerations, both Jaeger [3] and Rosenthal [1] considered the heating time $t = \infty$ in the very early stages of the mathematical derivation, thus limiting the analysis to quasi-steady state conditions. Consequently, time was not a variable and hence the calculations were time independent. Jaeger not only introduced the exact solutions for uniform moving band and moving rectangular heat sources but also gave a series of approximate equations for cases of very high and very low values of L (where L is defined as $vl/2a$ which later on became known as the Peclet number), for calculating the maximum and the average temperatures over the area of the heat source. His reason for choosing the approximate equations is to illustrate the power of the analytical techniques to address some practical, simplified problems. He also chose the average temperature because (a) it is the quantity observed experimentally, (b) it is easily calculable, and (c) it is the single quantity best representative of the temperature distribution.

In this investigation, we considered the problem of an elliptic heat source as a fundamental plane heat source and derive equations for the temperature rise for various moving plane heat sources, including circular, square or rectangular [5]. Appendix H gives details of the solutions to moving/stationary heat source problems. After obtaining this equation, the equation for a circular heat source is obtained by assuming the major axis to be the same as the minor axis. Similarly, the solution for a square or a rectangular heat source is obtained by assuming the width of the moving line heat source to be a constant. As a matter of fact, this model can be used for any geometrical shape that can be defined mathematically. We also considered three distributions of the heat source, namely, normal, uniform, and parabolic distributions. Other distributions can similarly be modeled. Thus, the most interesting result of the theory developed here is the derivation of a single formula capable of solving a wide range of plane moving heat source problems by appropriate substitutions of the boundary conditions. In addition this model can address both transient and steady state conditions and determine not only the temperature at the surface but also the temperature distribution. It can also calculate both the maximum and average temperatures. Thus the model is believed to be more comprehensive than the models developed to date.

This investigation enables the determination of the temperature rise distribution of different shapes of heat sources, such as a square, rectangular, circular, elliptic and with various intensity of heat distributions, such as uniform, normal, parabolic. Thus depending on the thermal problem of interest, solutions can be obtained analytically. It may be noted that in the examples considered here, the heat is given out by one body and is conducted into second body. In other words, no heat partition arises. However, where there is heat partition involved, it can be addressed, using the functional analysis approach for cases of variable heat partition along the length of the heat source, similar to that given in Ref. 6.

REFERENCES

1. Rosenthal, D., "The Theory of Moving Sources of Heat and Its Application to Metal Treatments," Trans ASME, 68 (1946) 849-866.

2. Blok, H., 1937, "Theoretical Study of Temperature Rise at Surface of Actual Contact Under Oiliness Lubricating Conditions," I. Mech. E. Proceedings of General Discussion on Lubrication and Lubricants, 2, (1937) 222-235.

3. Jaeger, J.C., "Moving Sources of Heat and the Temperature of Sliding Contacts," Proc. of the Royal Society of NSW, Australia 71 (1942) 203-224

4. Carslaw, H. S. and J. C. Jaeger, "Conduction of Heat in Solids," Oxford University Press, Oxford, UK (1959)

5. Zhen Bing Hou and R. Komanduri, "General Solutions for Stationary/ Moving the Plane Heat Source Problems in Manufacturing and Tribology , Int. J of Heat & Mass Transfer, 43 (2000) 1679-169

6. Komanduri, R. and Z.B. Hou, "Thermal Modeling of the Metal Cutting Process - Part II: Temperature rise distribution due to frictional heat source at the tool-chip interface," Int. J of Mechanical Sciences, 43 (2001) 57-88

6. LARGE BATCH MAGNETIC FLOAT POLISHING (MFP) EQUIPMENT

Although, the principle used in the design of equipment for finishing large batch of Si_3N_4 caramic balls is the same as the one for the small apparatus, many design modifications were made in the design of large batch apparatus. Reference 1 gives details of this equipment and may be referred to, for details. Figure 6.1 is a schematic of the large batch apparatus for polishing Si_3N_4 balls. A 12 in. diameter chamber (instead of 2.5 in. diameter chamber used in the small batch apparatus) with the magnets located (as integral part) at the base is used in this design. A bank of permanent magnets (Nd-Fe-B) with alternate N and S are arranged into 16 segments at the bottom of the float chamber. Also, while in the smaller apparatus the magnetic field is solely responsible for providing the load on the balls during polishing, in the large batch design, two methods of loading were incorporated. The first one is a dead weight system and the other is the magnetic field system. The former applies the required load/per ball (e.g. 1 N/ball) while the latter acts as a spring load to even out the load during polishing due to differences in the diameter of the balls. In principle, one can use the dead load system alone in which case the float chamber does not contain magnetic fluid but merely water and the abrasive. This apparatus can be used either as a straight polishing apparatus or as a magnetic float polishing apparatus. As the chamber is much larger in this equipment, the spindle can be run at much lower speed (400 rpm instead of 2000 rpm used with the smaller apparatus).

The support base of the apparatus is clamped on to the table of a numerically controlled (N.C.) machine tool (not shown). Four short shafts are mounted on the base plate to hold the carrier table of the magnetic float polishing apparatus. The equipment moves up and down freely in four linear bearings on these shafts. Two clamps were provided one either side of the carrier table, the top of which has two pulleys. A steel wire attached to the carrier plate passes through the pulleys to a deadweight. The total dead weight carried would equal to the polishing load/ball times the number of balls used. The float chamber is located on top of the carrier plate by a three point support at the bottom. Since the primary method of load application is via the deadweights, the magnets need not cover the total base of the float chamber. Instead they can be located around the periphery of the float chamber. In order to reduce the weight at the end the top shaft, an annular ring is used. Four clamps are used to fix the float chamber once it is properly aligned (i.e., the axis of

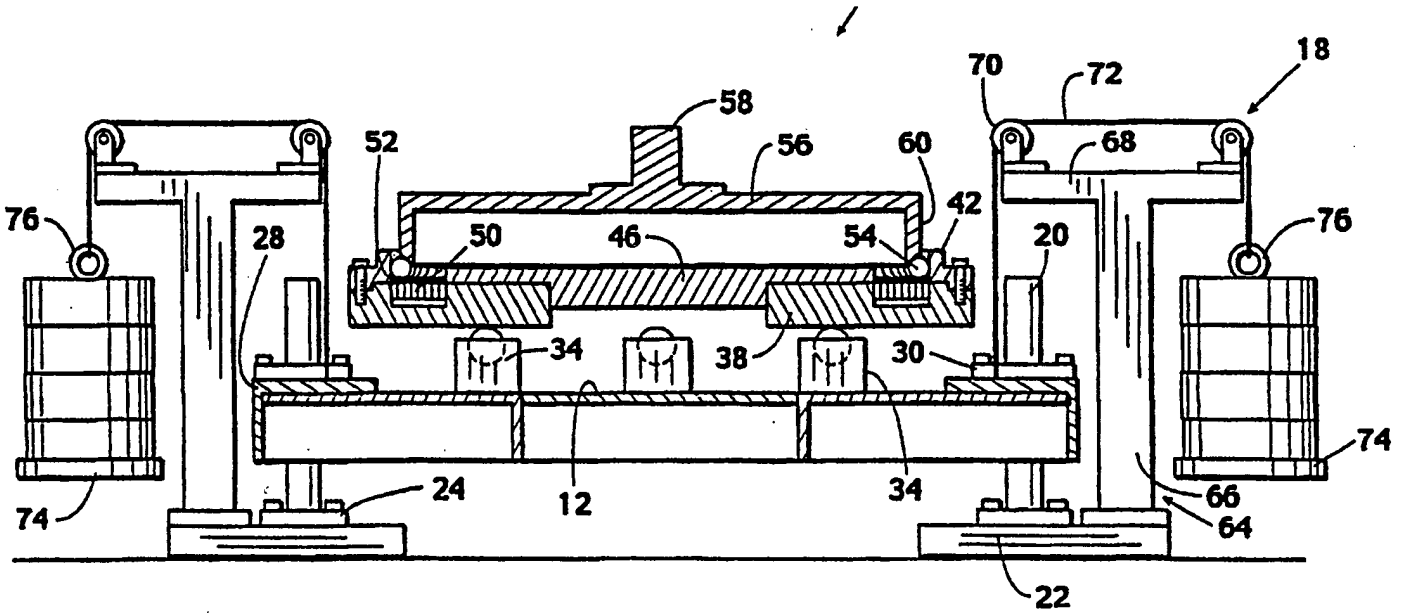

Figure 6.1 Schematic of the large batch magnetic float polishing (MFP) apparatus

the shaft to coincide with the axis of the float chamber. A bore gage is used to ensure proper concentricity of the chamber.

The polishing shaft in the new MFP equipment is driven by the spindle of a Bridgeport CNC machine tool. The magnetic field is measured by Gauss/Tesla meter. The pH value of polishing environment is measured by pH/Temperature meter. The polishing load is set up by the deadweight. The material removal rates are calculated by the weight reduction in the balls before and after polishing at every stage test using a precision balance. The surface finish of the polished balls are characterized using a Form Talysurf 120 L, ZYGO laser interference microscope, and an ABT 32 scanning electron microscope (SEM). The roundness of the balls is measured using TalyRond 250.

Results obtained with this equipment are very favorable and comparable with the results obtained with the smaller apparatus. Table 6.1 show the results of polishing of a large batch of 12.7 mm diameter Si_3N_4 ceramic balls from the as-received condition. During the first stage of polishing with a 400 grit B_4C abrasive, the material removal rate is ~0.8 to 1 μm. The sphericity was brought down from 200 μm to 0.6 μm during this period. During the second stage of polishing, fine SiC abrasive (1200 grit) was used to bring the size close to the actual value as well as bring the sphericity down to 0.3 μm. This was followed by the use of a fine B_4C abrasive (1500 grit) to bring the sphericity further down to 0.2 μm and the size to actual value. During the third stage of polishing, CeO_2 was used for chemo-mechanical polishing. The objective is to improve the surface finish (5 nm Ra) and the sphericity (0.2 μm) without altering the size. It can be seen that a final sphericity of ~ 0.15 μm was accomplished. It may also be noted tfrom Table 6.1 that the actual processing time for this run is only about 17 hours. Of course, the total processing time will be much more as metrology, replacement of magnetic fluid etc. would take some time, which is the non-polishing time.

While this apparatus can finish ~ 100 balls per batch, it can be easily modified to accommodate more balls. For example, instead of one row of balls in the float chamber, several rows can be incorporated. This requires additional magnets at each row of the balls as well as increasing the dead weight to account of the increase in the number of balls. Partitions can be made on the float chamber to separate the rows and the top plate has to be modified appropriately to handle the balls at various diameters.

Table 6.1 Results of polishing of a large batch of 12.7 mm diameter Si_3N_4 ceramic balls from the as-received condition

Abrasive	Time Min	Diameter (mm)		Sphericity (μm)		MRR
		before	after	before	after	(μm/min)
B4C #400	12 x 60	13.1	12.732	200	0.6	0.8-1.0
SiC #1200	2 x 60	12.732	12.706	0.6	0.3	0.2
B4C #1500	1 x 60	12.708	12.702	0.3	0.2	0.1
CeO2	2 x 90	12.702	12.700	0.2	0.15	0.01

REFERENCES

1. Komanduri, R., Umehara, N., Ming Jiang, and P Cao,"Large Batch Magnetic Float Polishing Equipment," International Patent Application No. PCT/US99/05669 dated March 17, 1998

7. LIST OF PUBLICATIONS

1. Ming Jiang and R. Komanduri, "Appliction of Taguchi Method for Optimization of Finishing Conditions in Magnetic Float Polishing (MFP)," Wear, 213 (1997) 59-71

2. Ming Jiang and R. Komanduri, "On the Finishing of Si_3N_4 Balls for Bearing Applications," Wear , 215 (1998) 267-278

3. Ming Jiang, Wood, N. O., and R. Komanduri, "On the Chemo-Mechanical Polishing of Si_3N_4 Bearing Balls with Various Abrasives" Wear, 220 (1998) 59-71

4. Ming Jiang, Wood, N. O., and R. Komanduri, "On the Chemo-Mechanical Polishing of Si_3N_4 Bearing Balls with CeO_2," Trans ASME, J of Engineering Materials & Technology, 120, (1998) 304-312

5. Hou, Z. B. and R. Komanduri, "On the Thermal Aspects of the Magnetic Field Assisted Polishing of Ceramics, Part I. Thermal Model," Trans ASME, J of Tribology, 120 (1998) 645-651

6. Hou, Z. B. and R. Komanduri, "On the Thermal Aspects of the Magnetic Field Assisted Polishing of Ceramics, Part II. Thermal Aspects of Magnetic Float Polishing (MFP) of Ceramic Balls,"Trans ASME, J of Tribology, 120 (1998) 652-659

7. Hou, Z. B. and R. Komanduri, "On the Thermal Aspects of the Magnetic Field Assisted Polishing of Ceramics, Part III. Thermal Aspects of Magnetic Abrasive Finishing (MAF) of Ceramic Rollers," Trans ASME, J of Tribology 120 (1998) 660-667

8. Zhen Bing Hou and R. Komanduri, "General Solutions for Stationary/ Moving the Plane Heat Source Problems in Manufacturing and Tribology , Int. J of Heat & Mass Transfer, 43 (2000) 1679-169

9. Komanduri, R. , Hou, Z. B., Umehara, N., Raghunandan, M., Ming Jiang, Bhagavatula, S. R., Noori-Khajavi, A., and N. O. Wood, "A 'Gentle' Method for Finishing Si_3N_4 Balls for Hybrid Bearing Applications," Tribology Letters 7 (1999) 39-49

10. Komanduri, R. and Ming Jiang, "A New Polishing Technology for Finishing Advanced Ceramic Balls for Hybrid Bearings," Abrasives Magazine (Aug./Sept. 1999) 8-20

11. Komanduri, R., Lucca, D. A., and Y. Tani, "Technological Advances in Fine Abrasive Processes," Annals of CIRP 46/2 (1997) 545-596

8. LIST OF INVENTIONS

1. Komanduri, R and Ming Jiang, "Magnetic Float Polishing Processes and Materials Therefor," U. S. Patent No. 5,931,718 dated Aug. 3, 1999

2. Komanduri, R and Ming Jiang, "Magnetic Float Polishing Processes of Magnetic Materials," U. S. Patent No. 5,957,753 dated Sept. 28, 19991.

3. Komanduri, R., Umehara, N., Ming Jiang, and P Cao,"Large Batch Magnetic Float Polishing Equipment," International Patent Application No. PCT/US99/05669 dated March 17, 1998

4. Conservation of Magnetic Fluid in the Finishing of Balls of Si3N4 and Other Materials (R. Komanduri and Ming Jiang) (disclosure letter)

5. Ultrasonic Assited Magnetic Float Polishing of Ceramic Balls (R. Komanduri, Ming Jiang, and Brian Perry) (disclosure letter)

9. LIST OF PARTICIPANTS

1. Zhen Bing Hou, Visiting Professor, M.S. Mechanical & Aerospace Engineering, Oklahoma State University, Stillwater, OK

2. Dr. Ali Noori-Khajavi, Post Doctoral Fellow, Mechanical & Aerospace Engineering, Oklahoma State University, Stillwater, OK

3. Dr N. Umehara, Visiting Associate Professor, Mechanical & Aerospace Engineering, Oklahoma State University, Stillwater, OK

4. Mr. Brian Perry, M. S. Mechanical & Aerospace Engineering, Oklahoma State University, Stillwater, OK

5. Mr. Cetan Murat, M. S. Mechanical & Aerospace Engineering, Oklahoma State University, Stillwater, OK

6. Mr. Ashok Lakshmanan, M. S. Mechanical & Aerospace Engineering, Oklahoma State University, Stillwater, OK

7. Dr. Ming Jiang, Ph. D., Mechanical & Aerospace Engineering, Oklahoma State University, Stillwater, OK

8. Ashutosh M. Khuperkar, M. S. Mechanical & Aerospace Engineering, Oklahoma State University, Stillwater, OK

9. Mr Srihari Rao, M. S. Mechanical & Aerospace Engineering, Oklahoma State University, Stillwater, OK

10. Mr Peijun Cao, M. S. Oklahoma State University, Stillwater, OK

11. Mr. Satish Ramanadhan, M. S. Mechanical & Aerospace Engineering, Oklahoma State University, Stillwater, OK

APPENDIX A

APPLICTION OF TAGUCHI METHOD FOR OPTIMIZATION OF FINISHING CONDITIONS IN MAGNETIC FLOAT POLISHING (MFP)

Ming Jiang and R. Komanduri

Wear, 213 (1997) 59-71

ELSEVIER

Wear 213 (1997) 59–71

WEAR

Application of Taguchi method for optimization of finishing conditions in magnetic float polishing (MFP)

Ming Jiang, R. Komanduri *

Mechanical and Aerospace Engineering, Oklahoma State University, Stillwater, OK 74078, USA

Received 19 March 1997; accepted 23 July 1997

Abstract

Magnetic float polishing (MFP) technique is used in the finishing of advanced ceramics, namely, silicon nitride (S_3N_4) balls for hybrid bearing applications. In this paper, Taguchi method [Genichi Taguchi, Taguchi Methods—Research and Development, ASI Press, Dearborn, MI (1992); K.E. Dehnad, Quality Control, Robust Design, and the Taguchi Method, Brooks/Cole, CA (1989)] is applied for optimization of the finishing conditions. Surface finish parameters, namely, Ra (arithmetic average) and Rt (peak-to-valley height) are considered as criteria for optimization. Important parameters identified that influence the surface quality generated during final mechanical polishing for a given workmaterial with a given abrasive (material and grain size) are (i) the polishing force; (ii) the abrasive concentration; and (iii) the polishing speed. Experimental results indicate that for the surface finish, both Ra and Rt, the polishing force parameter is the most significant. However, for the surface finish Ra, the polishing force parameter is the most significant, followed by polishing speed and then the abrasive concentration; while for the surface finish Rt, the polishing force parameter is the most significant followed by the abrasive concentration and then the polishing speed. The experimental results also indicate that within the range of parameters evaluated, a high level of polishing force, a low level of abrasive concentration, and a high level of polishing speed are desirable for improving both Ra and Rt. A comparison of the results obtained by the Taguchi method with single parameter (i.e., one parameter by one parameter) variation using a fine SiC abrasive (1 μm) yielded similar conclusions regarding optimum conditions [M. Jiang, Finishing of Advanced Ceramics, PhD thesis (under preparation), Mechanical and Aerospace Engineering, Oklahoma State University (1997)]. However, Taguchi method can extract information more precisely and more effectively. © 1997 Elsevier Science S.A.

Keywords: Polishing; Finishing; Chemo–mechanical polishing; Magnetic float polishing (MFP); Taguchi method; Silicon nitride; Ball bearings

1. Introduction

A critical factor affecting the performance and reliability of ceramics for bearing applications is the quality of the resulting surface by polishing. It is well known that ceramics are extremely sensitive to surface defects resulting from grinding and polishing processes owing to their high hardness and inherent brittleness. Since fatigue failure of ceramics is driven by surface imperfections, it is paramount that the quality and finish of the ceramic bearing elements be as best as possible with minimal defects so that reliability in service and improvements in the performance of the bearings can be achieved.

Conventional polishing of ceramic balls generally uses diamond abrasive, high load, and low polishing speeds (maximum of a few hundred rpm). This is basically the same technology that is used for finishing metal balls extended to the finishing of ceramic and glass balls. This is in spite of the fact that different mechanisms are involved in the material removal processes (from plastic deformation in the case of metals to microfracture and chemo–mechanical polishing (CMP) in the case of ceramics and glasses) due to difference in the material characteristics and their response to polishing conditions. Consequently, considerable time is expended (estimates vary from some 4–6 weeks to 12–16 weeks depending on the size of the balls, the quality requirements, and the manufacturing technology practices) to finish a batch of ceramic balls. The long processing time and the use of expensive diamond abrasive result in high processing costs. Application of diamond abrasive under high loads in conventional polishing can result in deep scratches, pits, and microcracks on the surface of the polished balls. Consequently, performance in service and reliability are major concerns with the conventional polishing of ceramics. To minimize the sur-

* Corresponding author. Mechanical and Aerospace Engineering, Coll. of Eng. Arch. and Tech., Oklahoma State University, 218 Engineering North, Stillwater, OK 74078, USA. Tel.: +1-405-744-5900; Fax: +1-405-744-5720; e-mail: ranga@master.ceat.okstate.edu

PII S0043-1648(97)00180-4

face damage, 'gentle' polishing conditions are required, namely, low level of controlled force and abrasives preferably not much harder (preferably softer) than the workmaterial. This is accomplished by a process known as magnetic float polishing (MFP) originally developed by Umehara and Kato [1], Umehara [2] and subsequently extended by Childs et al. [3–5] in the UK and Raghunandan et al. [6], Komanduri et al. [7], Bhagavatula and Komanduri [8], Jiang and Komanduri [9] in the US. Using this technique, higher removal rate, higher quality finish, and shorter processing times (about 20 h) can be obtained by higher polishing speeds and the use of flexible float. By combining this process with CMP as the last stage of polishing, extremely good surface finish ($\approx$4 nm Ra) can be obtained.

When polishing ball blanks made of advanced ceramics, such as Si_3N_4 by MFP process with a harder abrasive, such as B_4C #500 or SiC #400, high material removal rates (1 μm/min) can be obtained with minimal subsurface damage due to the use of a flexible support system, small, controlled polishing force (1 N/ball), fine abrasives, and high polishing speed compared to conventional polishing [9]. Higher material removal results from the cumulative microfracture of Si_3N_4 at high polishing speeds instead of large radial and circumferential cracks that results in the formation of pits, scratches, and microcracks in conventional polishing with diamond abrasive.

It may be noted that the finish obtained at this stage may not be adequate for bearing applications and further improvements in the surface finish may be required. This can be achieved, for example, by applying CMP technique using CeO_2 abrasive. By this process, a surface finish of Ra $\approx$ 4 nm and Rt $\approx$ 40 nm can be obtained [9]. It may, however, be noted that the surface finish obtainable by CMP during the final stage is influenced by the final mechanical polishing (i.e., semi-finishing stage) using a fine grain B_4C or SiC abrasive. Hence, the surface finish by mechanical polishing by fine, harder abrasive (e.g., B_4C) should be as good as possible prior to CMP to obtain ultimate surface finish.

This investigation focuses on the application of Taguchi method for the optimization of process parameters to obtain the best finish possible with a fine B_4C #1500 abrasive (grain size 1–2 μm) on HIP'ed Si_3N_4 balls using MFP process. The main objective is to determine the effect of process variables (polishing load, polishing speed, and abrasive concentration) on the surface finish obtainable during the final mechanical polishing (semi-finish polishing) prior to CMP.

2. On the design of experiments

Several approaches are available for the design of experiments to investigate the effect of various parameters on the surface finish obtainable in MFP process. They include, simple single-factor by single-factor approach, i.e., only one factor is changed for a given trial run, the traditional factorial and fractional factorial approaches [10], and the highly-fractional factorial experimental design, namely, the Taguchi method [11–15]. Of course, the number of experiments to be conducted decreases rapidly as one chooses from a single-factor by single-factor approach to the factorial design, to the fractional factorial design, to the Taguchi method. This, in turn, will have a significant impact on the time consumed as well as the overall costs.

Compared to the single-factor by single-factor approach, Taguchi method can extract information more precisely and more efficiently. Also, fewer number of tests are needed even when the number of variables is quite large. Although Taguchi's experimental design and analysis are conducted by highly fractional factorial experimental design (Taguchi Orthogonal Arrays) to determine the influence of the factors and their levels and identify the best combination of parameters, it has been shown that this method yields the same or even better results (in terms of precision) as a complete factorial experiment [13–15].

Compared to the traditional factorial and fractional factorial approaches, Taguchi method, as will be shown, overcomes most of their limitations. A full-factorial design of experiments will include all possible combination settings of the factors involved in the study, resulting in a very large number of trial runs and considerable time to accomplish this task. To simplify the experimental effort and reduce the number of tests to a reasonable level, only a small fraction of settings that produces most information from all the possible combinations is selected. This method is known as fractional–factorial design of experiments. Although this shortcut method is well known, its shortcoming is that there are no generally accepted standard guidelines for both the design of experiments and the analysis of the results. Consequently, the experimental design and analysis of the results can be rather complex. Taguchi's method overcomes these limitations by first simplifying and standardizing the fractional factorial designs by developing a set of standard Orthogonal Arrays (OA) which can be used for many experimental situations, and then devising a standard method for the analysis of results. The combination of standard experimental design and analysis techniques used in Taguchi method produces consistency and reproducibility which are not commonly found in other statistical methods. Design of highly fractional factorial experiments, say, for the same problem by two different investigators using Taghuchi method, will yield similar data and conclusions. It is, thus, a standardized experimental design methodology that can easily be applied by investigators having particularly no strong statistical background [13].

The Taguchi experimental design was conceived and developed by Dr. Genichi Taguchi in Japan after World War II. It is considered as a highly effective method for the determination of optimal values for the various parameters involved in a given manufacturing system. The quality of automobiles is particular and various other products in general by the Japanese manufacturers is attributable largely to the widespread application of this method. Since its intro-

duction in the US (first implemented at AT&T Bell Laboratories) in 1980, Taguchi method has been widely applied and broadly discussed. Several industries including AT&T, Xerox, Ford, and ITT have applied this method in various product realization stages [12,15].

3. Magnetic float polishing and test setup

The MFP technique is based on the magneto–hydrodynamic behavior of a magnetic fluid that can float non-magnetic float and the abrasives suspended in the magnetic fluid [16]. The forces applied by the abrasive to the part are extremely low ($\approx$1 N/ball) and highly controllable. Fig. 1(a,b) show a schematic and a photograph of the permanent magnet float polishing apparatus for finishing advanced ceramic balls. A bank of permanent magnets (Nd–Fe–B) with alternate N and S are arranged below an aluminum float chamber. The float chamber is filled with the required amount of magnetic fluid and appropriate abrasive (5–10%). The magnetic fluid is a colloidal dispersion of extremely fine (100 to 150 Å) subdomain ferromagnetic particles, usually magnetite (Fe_3O_4), in a carrier fluid, such as water or kerosene. It is made stable against particle agglomeration by coating the surface of the particles with an appropriate surfactant. In this investigation, a water base magnetic fluid (W-40) is used (see Table 1).

When a magnetic field is applied, the magnetic particles in the magnetic fluid are attracted downward to the area of higher magnetic field and an upward buoyant force is exerted on all non-magnetic materials to push them to the area of lower magnetic field. The abrasive grains, the ceramic balls, and the acrylic float inside the chamber (all being non-magnetic materials) are floated by the magnetic buoyant force. The drive shaft is lowered to make contact with the balls and to press them down to reach the desired level of force or height. The balls are held by three point contact between the float chamber wall, the float, and the drive shaft and polished by the abrasive grains under the action of the magnetic buoyancy when the spindle rotates. Damage-free surface on ceramic balls is accomplished by the magnetic float polishing technique because low and controlled magnetic buoyant force (1 N/ball) is applied via the flexible float. The function of the acrylic float used here is to produce more uniform and larger polishing pressure (the larger buoyant force near the magnetic poles can be transmitted to the polishing area by this float). An urethane rubber sheet is glued on to the inner guide ring to protect it from wear. The material of the drive shaft is non-magnetic, austenitic stainless steel.

Table 1
Test conditions used

Workmaterial	HIP'ed Si_3N_4 balls (CERBEC)
	Diameter: 12.7 mm (0.5 inch)
	Sphericity: 1 μm
Abrasive	Type: B_4C (NORTON)
	Size: #1500 (1–2 μm)
	Concentration: 5%, 10%, 20%
Load, N/ball	0.4, 0.8, and 1.4
Speed, rpm	2000, 4000, and 7000
Test time	45 min/step
Magnetic fluid	Water-based (W-40)
	saturation magnetization at 25°C: 400 Gauss
	Viscosity at 27°C: 25 Cp

Various parameters affect the quality of the ceramic balls finished by the MFP process. They include the magnetic field strength, the workmaterial, the abrasive used (material and grain size), the rotational speed of the shaft, the type of magnetic fluid used (water based or hydrocarbon based), the volume % of the abrasive in the magnetic fluid, and the stiffness of the system. For a given abrasive–workmaterial

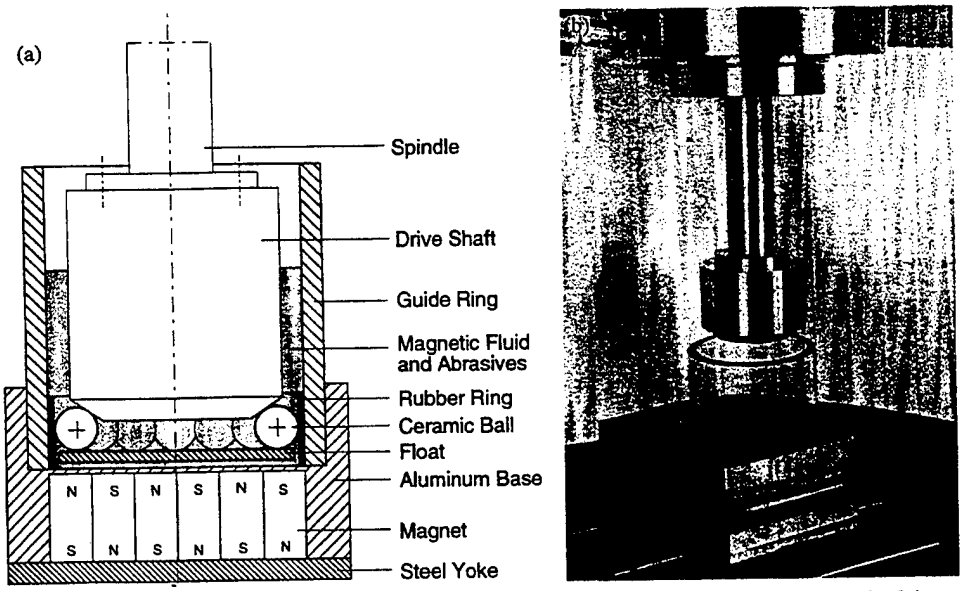

Fig. 1. 223(a) Schematic of the magnetic float polishing (MFP) apparatus used for polishing Si_3N_4 balls. (b) Photograph of the magnetic float polishing (MFP) apparatus used for polishing Si_3N_4 balls.

combination and the MFP system, the following three polishing parameters, namely, (1) the polishing force; (2) the abrasive concentration; and (3) the polishing speed, are considered to have major influence on the surface quality.

A critical factor affecting the roundness of the ceramic balls finished by the MFP process is the set-up accuracy (coaxiality of driving shaft and guiding ring, vertical straightness between the rotation axial of driving shaft and polishing plate) but this would not have much effect on the surface finish obtainable. In this investigation, the best roundness obtained on S_3N_4 balls after finishing with fine B_4C (1–2 μm) was 0.25 μm for 1/2″ balls and 0.20 μm for 3/8″ balls. As the emphasis in this investigation is on the surface finish, fine abrasives and low normal forces are used. Consequently, the material removal rate during this controlled study of necessity is low ($\approx$0.01–0.06 mg/min or μm/min) for it is the objective to improve the surface finish without significant material removal.

Table 1 lists the test conditions used together with the details of the workmaterial, the abrasive, and magnetic fluid used. Fine grain (1–2 μm) B_4C was selected as the abrasive and HIP'ed Si_3N_4 (CERBEC NBD-200 from Norton Advanced Ceramics) as the ball material. The polishing shaft was driven by a high-speed, high-precision air bearing spindle (PI Spindle) with a stepless speed regulation up to 10,000 rpm. The magnetic field was measured using a Gauss/Tesla meter. The pH value of the polishing environment was measured using a pH/Temperature meter. The polishing load was set up by measuring the normal force with a Kistler's piezoelectric dynamometer connected to a charge amplifier and a display. To calculate material removal rates, the weight reduction in the balls was determined by measuring the weight before and after polishing at every stage of the test using a precision balance. The surface finish of the polished balls was measured using a Form Talysurf 120 l (cut-off: 0.8 mm, evaluation length: 6 consecutive cut-off, Filter: ISO 2CR). The roundness of the balls was measured using TalyRond 250 (cut-off: 50 upr, Filter: 2CR).

4. Experimental design and approach

Details on the experimental design and approach are given in the following.

4.1. Selection of the parameters and their levels

The three process parameters identified as the most critical variables in the generation of best surface finish for a given abrasive (material and size)–workmaterial combination during semi-finishing are: (i) the polishing force; (ii) the abrasive concentration; and (iii) the polishing speed. Each factor is investigated at three levels to determine the optimum settings for the polishing process. The smallest, standard 3-level orthogonal array L_9 (3^4) which has four 3-level columns (for a maximum of four parameters that can be tested) available is chosen for this case. The factors and their levels are given in Table 2.

Table 2
Test parameters used and their levels

Level	Parameters		
	A: Load	B: Vol.%	C: Speed
1	0.4 N	5%	2000 rpm
2	0.8 N	10%	4000 rpm
3	1.4 N	20%	7000 rpm

4.2. Orthogonal Array (OA) design

Taguchi method employs standard tables known as Orthogonal Arrays (OA) for constructing the design of experiments [13]. It may be noted that the term 'Orthogonal' is used here to indicate balanced and not to be mixed, or separable. OAs are generalized from Graeco–Latin squares. The mathematical discovery of OA was originally due to the French mathematician, Jacques Hadamard, who developed it in the 1890s but the technique was not explored for use until World War II [15].

The main functions of the Orthogonal Arrays are the following: (1) because of the pairwise balancing property of the orthogonal arrays, any two columns of an OA form a 2-factor complete factorial design. Consequently, whatever is happening of all the other parameters at one level of parameter being studied is also happening in the same way at other levels being studied. The effects of the other parameters on the parameter level being studied can be counteracted (offset) by averaging the responses. That means, the effect of one parameter being studied is separable from the effects of other parameters. So, the contribution and optimum level value of each factor can be determined in the balanced experiment; (2) Orthogonal array experiments also minimize the number of test runs due to pairwise balancing property. With 4 factors and each at three levels, there are 3^4 possible combinations and would require 81 trial runs for a factorial experiment, and with 3 factors and each at three levels, there are 3^3 possible combinations and would require 27 trial runs for the factorial experiment. With the OA technique, there are only 9 runs required for L_9 (3^4). Further, the effects of the experimental errors on the parameter being studied as in the case of factorial design or one factor by one factor design can be eliminated (counteracted and offset) as the analysis of Taguchi method takes care of this factor (by the analysis of averaging the level responses).

An OA L_9 (3^4) for a 3-level factor used in this investigation is shown in Table 3. This array has 9 rows and each row represents a trial condition with factor levels indicated by the numbers in the row. The vertical columns correspond to the factors specified in the study and each column contains three Level 1, three Level 2, and three Level 3 conditions (a total of 9 conditions) for the factor assigned to the column. And

Table 3
$L_9(3^4)$ Orthogonal arrays used

Trial no.	Factors investigated				Test results
	A	B	C	D	
1	1	1	1	1	
2	1	2	2	2	
3	1	3	3	3	
4	2	1	2	3	
5	2	2	3	1	
6	2	3	1	2	
7	3	1	3	2	
8	3	2	1	3	
9	3	3	2	1	

each column (factors) has nine possible combinations: (1,1), (1,2), (1,3), (2,1), (2,2), (2,3), (3,1), (3,2), and (3,3). We note that any two columns of an L_9 (3^4) not only have these possibilities but also have the same number of times of these possible combinations. Thus, all four columns of an L_9 (3^4) are said to be balanced, *orthogonal* or statistically independent of each other.

4.3. Experimental design

Details of the experimental design and approach are given in Table 4. The factors under consideration, namely, load (N), abrasive concentration (vol.%), and speed (rpm) are placed in the first three columns (A, B, C) of the OA L_9 (3^4) leaving the fourth column D open (and is designated for uncontrolled or unknown parameters in this investigation). The outputs, namely, the surface finish (Ra and Rt) values are the test results.

The vertical columns show the levels of polishing parameters specified in the study and each row represents a trial condition. The performance characteristic value from each trial run (discussed in Section 5.1) is then used to compute the statistical performance characteristic (discussed in Section 5.2) which is affected by any one parameter but independent of the others.

Table 4
Experimental design

Trial no.	Factors			Test results	
	Load (N)	Abr. vol.%	Speed (rpm)	Ra (nm)	Rt (nm)
1	0.4	5%	2000		
2	0.4	10%	4000		
3	0.4	20%	7000		
4	0.8	5%	4000		
5	0.8	10%	7000		
6	0.8	20%	2000		
7	1.4	5%	7000		
8	1.4	10%	2000		
9	1.4	20%	4000		

*The fourth column (factor D) is unset and designated as the unknown parameter(s) in this investigation.

5. On the data evaluation and analysis

5.1. Data evaluation

The surface finish of the polished ceramic balls under various trial conditions is evaluated at random in terms of surface finish parameters, Ra and Rt. These repetitive sample data in each trial run (each polishing condition) is further consolidated into an average value or a signal-to-noise ratio (S/N) to interpret each trial run (each polishing condition) into one evaluation value for the optimum setting analysis study.

5.1.1. Evaluation of each trial run by average value

$$\overline{R_i}=\sum_{j=1}^{r}\frac{R_{ij}}{r}=\frac{1}{r}(R_{i1}+R_{i2}+\cdots+R_{ir}) \quad (1)$$

where i is trial number; r is number of regions where surface roughness values are measured in a trial run (sample data). Average value of each trial run can be considered as an average deviation from the target value of zero (Ra and Rt $\rightarrow 0$).

5.1.2. Evaluation of each trial run by S/N dB value η

Taguchi method uses the signal-to-noise (S/N) ratio instead of the average value to interpret the trial result data into a value for the evaluation characteristic in the optimum setting analysis. This is because signal-to-noise ratio (S/N) can reflect both the average (mean) and variation (scatter) of the surface quality under one trial run, namely, one polishing condition.

If the S/N ratio is expressed in dB units, it can be defined by a logarithmic function based on the mean square deviation around the target, smaller-the-better:

$$S/N=-10\log_{10}MSD$$

where MSD is the mean square deviation (MSD) around the target value rather than around the average value. The purpose of using the constant, 10 in the calculation is to magnify the S/N number for easier analysis and the negative sign is used to set signal-to-noise ratio of larger-the-better (a larger signal and a smaller noise) relative to the square deviation of the smaller-the-better. The target value in this study tends to zero (Ra and Rt $\rightarrow 0$) and all random samples are equally important. Therefore, the mean squared deviation (variance) is calculated from the sum of the squares $(R_{ij}-0)^2$ of all the data points. As can be seen in the following, this value reflects both the average, $\bar{R}_i$ and variance, ΔR_{ij} of each trial result data:

$$MSD_i=\sigma_{ij}^2=\frac{1}{r}\sum_{j=1}^{r}(R_{ij})^2=\frac{1}{r}\sum_{j=1}^{r}(\overline{R_i}+\Delta R_{ij})^2$$

$$=\frac{1}{r}\left(\sum_{j=1}^{r}\overline{R_i}^2+2\sum_{j=1}^{r}\overline{R_i}\Delta R_{ij}+\sum_{j=1}^{r}\Delta R_{ij}^2\right)$$

$$=\frac{1}{r}\left(\sum_{j=1}^{r}\overline{R_i}^2+\sum_{j=1}^{r}\Delta R_{ij}^2\right)$$

(ΔR_{ij} are normally distributed, so $2\sum_{j=1}^{r}\overline{R_i}\Delta R_{ij}=0$)

where MSD_i is the square of the deviation around the target value of zero (Ra and Rt $\rightarrow 0$) and reflects the deviation of the trial result from the target value of zero.

$$\therefore S/N_i = -10 \log MSD_i = -10 \log \frac{1}{r}\sum_{j=1}^{r} R_{ij}^2 \quad (2)$$

where i is the number of a trial; MSD_i is the square of the standard deviation of a trial i; σ_i is the standard deviation in a trial i; r is number of regions where surface roughness measurements are made in a trial. It is known that smaller average and smaller variability (smaller MSD) are desirable for the surface finish of the balls. That is, an uneven amount of surface damage is worse than an even amount of surface finish when the average values are the same. This means smaller averages or larger signal-to-noise ratios are better. The evaluation by average value is more a perception while the S/N value is more objective.

The experimental results are to be analyzed to achieve the following three objectives: (1) to establish the optimum conditions for the finishing process; (2) to estimate the contributions of individual parameters; and (3) to predict the response under optimum conditions.

5.2. Level average response analysis

The optimum conditions for the polishing process are identified by investigating the average response of each parameter level in the OA experiments. This is accomplished by analyzing the following.

5.2.1. Level average response analysis using average value of each trial run

The level average analysis is based on combining and averaging the response associated with each level for each factor. It may be noted from Table 3 that the 1st level of factor A occurs, in experiment numbers 1, 2, and 3, all three levels of factors B and C appear once in these three experiments. The 2nd level of factor A occurs in experiment numbers 4, 5, and 6, all three levels of factor B and C also appear once in these three experiments. The 3rd level of factor A occurs in experiment numbers 7, 8, and 9, all three levels of factor B and C also appear once in these three experiments. It means the level conditions of factors B and C with different levels of factor A are the same. Hence, it counteracts the effects of the factors B and C on the response of factor A. Thus, from the average data of each of the three experiments wherein one level of factor A occurs, the optimum value of factor A can be determined. By the same way, the optimum values for factors B and C can be determined.

5.2.2. Level average response analysis using S/N value

The level average S/N analysis actually is similar to the level average analysis except that S/N values are used instead of the average values. The objective of this analysis is to determine the optimum polishing conditions such that the signal-to-noise (S/N) ratio is as large as possible relative to the mean (the target Ra, Rt $\rightarrow 0$) and variation as small as possible. The analysis using the S/N value is more objective but the S/N value is rather abstract and cannot indicate the physical meaning of the quality/parameter response directly.

5.3. Analysis of variance (ANOVA)

Analysis of variance (ANOVA) is used to evaluate the response magnitude (%) of each parameter in the orthogonal experiment here. This method was first developed by Fisher in the 1930s [10]. It is used to identify and quantify the sources of different trial results from different trial runs (i.e., different polishing conditions).

For different trial conditions, the results can be different due to (a) the variations produced by unknown parameters or random interferences (noise factors) (also known as the variations from uncontrolled parameter conditions); and (b) the variations produced by the changing of polishing conditions (also called as the variations from controlled parameter level conditions or testing conditions). Therefore, it is important to identify whether the variations under different trial runs are from the unknown parameters or from different test parameter (control parameters) level settings. This way, the influence of the variations in the control parameter settings (different trial run settings or different polishing conditions tested) can be determined and the percent contribution of each parameters can be evaluated to make a decision on how significant is the effect of each parameter (known and unknown) on the polishing results.

Since standard deviation is not additive, the sum of the squares of the standard deviation, which is additive $\sigma_T^2 = \sigma_A^2 + \sigma_B^2 + \sigma_C^2$, is usually used for the calculation and analysis of the variation or variability from each and all factors (parameters) in ANOVA. The basic property of ANOVA is that the total sums of the squares (total variation) is equal to the sum of the SS (sums of the squares of the deviation) of all the condition parameters and the error components, i.e., adding the variations from each factors, $SS_T = SS_A + SS_B + SS_C + SS_e$.

Values of S/N and $(S/N)^2$ for Ra and Rt, respectively are used in the following calculations for SS_T, SS_A, SS_B, SS_C, and SS_e.

5.3.1. Total variation (SS_T)

The total variation of the experimental results caused by both the controlled (tested) parameter setting variations (i.e., different polishing conditions tested) and uncontrolled (or unknown) parameters can be represented as the sum of squares (SS_T) of the deviation of all the resulting data from the trial runs:

Table 5
Experimental results

Test no.	Surface finish, Ra(nm)							Average (nm)	S/N (dB)
	R_1	R_2	R_3	R_4	R_5	R_6	R_7		
1	32	37	37	35	33	34	36	35	−30.86
2	37	38	36	39	38	42	38	38	−31.67
3	38	35	35	34	36	32	35	35	−30.89
4	33	29	28	28	29	27	27	29	−29.18
5	31	29	28	27	26	26	24	27	−28.74
6	38	35	42	39	42	40	37	39	−31.84
7	23	24	23	20	22	24	25	23	−27.25
8	35	32	31	38	34	32	30	33	−30.43
9	24	26	33	28	30	27	29	28	−29.03
Test no.	Surface finish, Rt (nm)							Average (nm)	S/N (dB)
	R_1	R_2	R_3	R_4	R_5	R_6	R_7		
1	294	324	318	401	326	302	461	347	−50.9
2	327	498	481	411	399	504	529	450	−53.2
3	395	390	363	385	380	298	513	389	−51.9
4	298	260	346	357	268	251	325	301	−49.6
5	274	254	657	334	283	246	207	322	−50.9
6	405	344	547	547	480	434	368	446	−53.1
7	209	180	210	200	221	250	220	213	−46.6
8	303	297	390	371	334	240	274	316	−50.1
9	229	230	384	214	236	278	228	257	−48.4

$$SS_T = \sum_{i=1}^{n}(y_i-\bar{y})^2 = \sum_{i=1}^{n} y_i^2 - \sum_{i=1}^{n} 2y_i\bar{y} + \sum_{i=1}^{n}\bar{y}^2$$

$$= \sum_{i=1}^{n} y_i^2 - 2n\bar{y}^2 + n\bar{y}^2 = \sum_{i=1}^{n} y_i^2 - \frac{G^2}{n}$$

$$\therefore SS_T = \sum_{i=1}^{n}(y_i-\bar{y})^2 = \sum_{i=1}^{n} y_i^2 - \frac{G^2}{n} \quad (3)$$

where $G=\sum y_i$ is the sum of the resulting data of all trial runs; and n is the total number of the trial runs. The total trial variance is: $V_T = SS_T/F_T$, where F_T is the number of degrees of freedom (DOF) of the total variation (i.e., the number of trial runs minus one). For example, in the present case it is, $F_T = 9-1=8$.

5.3.2. The trial variation from the tested parameter setting variation (condition variation) SS_k

The variation caused by each parameter from their different level settings can be reflected by the total sum of the squares (SS) of the deviation from the average of all trial results involving this parameter level:

$$SS_k = \sum_{j=1}^{t} tx(\bar{y}_j-\bar{y})^2 = \sum_{j=1}^{t}\left(\frac{Sy_j^2}{t}\right) - \frac{G^2}{n} \quad (4)$$

where k represents one of the tested parameters; j is level number of this parameter K; $\bar{Y}$ is the average of all trial runs; $\bar{Y}_j$ is the average of each of the level under the parameter k; t is the repetition of each level of the parameter k; Sy_j is sum of all trial results involving this parameter k level j; n is the total number of trial runs.

The variance of each parameter is determined by the sum of the square deviation (SS) of each parameter divided by the degrees of freedom (DOF) of this parameter: $V_k = SS_k/F_k$. The number of degrees of freedom (or independent comparisons), F, for a parameter is equals to the number of levels (number of observations) for this parameter minus one. For example, in the present case it is, $F_k = 3-1=2$.

5.3.3. The trial variation from the random variations in testing or from unknown parameters, SS_e

$$SS_e = SS_T - SS_{load} - SS_{vol.\%} - SS_{speed}$$

Variance $V_e = SS_e/F_e$, where $F_e = 3-1=2$

Actually, the variance of the unknown parameters is equals to the variance of the parameters in column D (uncontrolled parameters) in Tables 3 and 4.

6. Experimental results and analysis

Table 5 summarizes the experimental results showing the variation of the surface finish Ra and Rt for various Trial Runs (Nos. 1 through 9) at three levels of load, abrasive concentration, and speed, respectively, as the experimental design given in Table 4. Based on this information, the average and S/N values can be obtained. Table 6 gives the average response at each level of load, abrasive concentration, and speed. Table 7 gives the level average response analysis using the S/N ratio for Ra and Rt. Table 8 gives the values of S/N and $(S/N)^2$ for Ra and Rt used in the calculation of Tables 9 and 10. Tables 9 and 10 give the ANOVA for Ra and Rt, respectively. In the following, these experimental results are analyzed in the following as outlined in Section 5.

Table 6
Level average response for Ra and Rt

	Analysis test no.	Test Ra (nm)	Rt (nm)	Response average Ra (nm)	Test response average Rt (nm)
Load level					
0.4 N	1	35	347	36	395
	2	38	450		
	3	35	389		
0.8 N	4	29	301	32	356
	5	27	322		
	6	39	446		
1.4 N	7	23	213	28	262
	8	33	316		
	9	28	257		
Abrasive vol.% level					
5%	1	35	347	29	287
	4	29	301		
	7	23	213		
10%	2	38	450	33	363
	5	27	322		
	8	33	316		
20%	3	35	389	34	364
	6	39	446		
	9	28	257		
Speed level					
2000 rpm	1	35	347	36	370
	6	39	446		
	8	33	316		
4000 rpm	2	38	450	32	336
	4	29	301		
	9	28	257		
7000 rpm	3	35	389	28	308
	5	27	322		
	7	23	213		

6.1. Data evaluation

The surface finish of the polished ceramic balls under various trial conditions was evaluated at random for seven samples R_1, R_2, ..., R_7 in terms of surface finish parameters, Ra and Rt, as shown in Table 5. These seven repetitive sample data in each trial run (each finishing condition) is further consolidated into an average value or a signal-to-noise ratio (S/N) to interpret each trial run (each polishing condition) into one evaluation value for the optimum setting analysis study.

6.1.1. Evaluation of each trial run by average value

The average value of each trial run is calculated using Eq. (1) and the results are given in Table 5.

For example, for Trial No.1 (Table 5), using Eq. (1), we get for R_1:

$R_{(Ra)1} = 35$ nm and $R_{(Rt)1} = 347$ nm.

6.1.2. Evaluation of each trial run by S/N (dB) value η

First, the mean standard deviation, MSD_i is calculated for each of the trial run and then the signal to noise ratio, S/N values are obtained using Eq. (2).

For example, in Test No. 1, the S/N value for Ra (see Table 5) is obtained as:

$MSD_{(Ra)1} = 1218$. Hence, $S/N_{(Ra)1} = -30.86$ dB

Similarly, for Rt,

$MSD_{(Rt)1} = 123466$. Hence, $S/N_{(Rt)1} = -50.9$ dB

6.2. Level average response analysis

6.2.1. Level average response analysis using average value of each trial run

To compute the average performance for the factor A at level 1, results for the tests including factor A_1: load (0.4 N) are added and then divided by the number of such tests. For example, in the column for A: load, level 1 occurs in exper-

Table 7
Level average response analysis using S/N ratio for Ra and Rt

	Test no.	Ra S/N (dB)	Sum. of level Sy_j	Ave. of level
Load level				
0.4 N	1	−30.86	−93.42	−31.14
	2	−31.67		
	3	−30.89		
0.8 N	4	−29.18	−89.76	−29.92
	5	−28.74		
	6	−31.84		
1.4 N	7	−27.25	−86.71	−28.9
	8	−30.43		
	9	−29.03		
Abrasive vol.% level				
5%	1	−30.86	−87.29	−29.10
	4	−29.18		
	7	−27.25		
10%	2	−31.67	−90.84	−30.28
	5	−28.74		
	8	−30.43		
20%	3	−30.89	−91.76	−30.59
	6	−31.84		
	9	−29.03		
Speed level				
2000 rpm	1	−30.86	−93.13	−31.04
	6	−31.84		
	8	−30.43		
4000 rpm	2	−31.67	−89.88	−29.96
	4	−29.18		
	9	−29.03		
7000 rpm	3	−30.89	−86.88	−28.96
	5	−28.74		
	7	−27.25		
Load level				
0.4 N	1	−50.9	−156	−52
	2	−53.2		
	3	−51.9		
0.8 N	4	−49.6	−153.6	−51.2
	5	−50.9		
	6	−53.1		
1.4 N	7	−46.6	−145.1	−48.4
	8	−50.1		
	9	−48.4		
Abrasive vol.% level				
5%	1	−50.9	−147.1	−49.1
	4	−49.6		
	7	−46.6		
10%	2	−53.2	−154.2	−51.4
	5	−50.9		
	8	−50.1		
20%	3	−51.9	−153.4	−51.1
	6	−53.1		
	9	−48.4		
Speed level				
2000 rpm	1	−50.9	−154.1	−51.4
	6	−53.1		
	8	−50.1		
4000 rpm	2	−53.2	−151.2	−50.4
	4	−49.6		
	9	−48.4		
7000 rpm	3	−51.9	−149.4	−49.8
	5	−50.9		
	7	−46.6		

iment numbers 1, 2, and 3. The average effect of load (0.4 N) is therefore calculated by adding the results of these three tests and dividing it by 3:

Thus, $R_a(A1) = 36$ nm and $R_t(A1) = 395$ nm.

The average effects of the other two levels are calculated in a similar manner and tabulated in Table 6.

6.2.2. *Level average response analysis using S/N value*

Level average S/N analysis is obtained by combining the average response for each parameter level (see Table 7). In fact, the analysis presented in Table 7 is similar to the level average analysis presented earlier but using the S/N values rather than the average values.

6.3. *Analysis of variance (ANOVA)*

6.3.1. *Total variation*

The total variation of the experimental results (for the total number of trial runs, $n=9$) caused by both the controlled (tested) parameter setting variations (i.e., different polishing conditions tested) and uncontrolled (or unknown) parameters can be represented as the sum of the square (SS) deviation of all the resulting data from the trial runs (Eq. (3) and Table 8). For Ra,

$$\text{For Ra } SS_T = 8112.05 - \frac{(-269.89)^2}{9} = 18.65.$$

Similarly, for Rt,

$$SS_T = 23009.37 - \frac{(-454.7)^2}{9} = 36.92.$$

6.3.2. *The trial variation from the controlled (tested) parameter setting variations (condition variation)*

Values of Sy_j for Ra and Rt are given in Table 7. Using Eq. (4) and Table 8, we get (see Table 9). For Ra,

$$SS_{load} = \frac{(-93.42)^2 + (-89.76)^2 + (-86.71)^2}{3} - \frac{(-269.89)^2}{9} = 7.52.$$

Table 8
Values of S/N and $(S/N)^2$ for Ra and Rt

Test no.	For Ra S/N or y_i	$(S/N)^2$ or y_i^2	For Rt S/N or y_i	$(S/N)^2$ or y_i^2
1	−30.86	952.34	−50.9	2590.81
2	−31.67	1002.99	−53.2	2830.24
3	−30.89	954.19	−51.9	2693.61
4	−29.18	851.47	−49.6	2460.16
5	−28.74	825.99	−50.9	2590.81
6	−31.84	1013.79	−53.1	2819.61
7	−27.25	742.56	−46.6	2171.56
8	−30.43	925.98	−50.1	2510.01
9	−29.03	842.74	−48.4	2342.56
Σ	−269.89	8112.05	−454.7	23009.37

Table 9
Analysis of variance (ANOVA) for Ra

	DOF	SS	SS %
A: Polishing load	2	7.52	40%
B: Abrasive vol.%	2	3.72	20%
C: Polishing speed	2	6.51	35%
D: Unknown	2	0.9	5%
Total	8	18.65	100%

Table 10
Analysis of variance (ANOVA) for Rt

	DOF	SS	SS %
A: Polishing load	2	21.87	59%
B: Abrasive vol.%	2	10.08	27%
C: Polishing speed	2	3.75	10%
D: Unknown	2	1.22	4%
Total	8	36.96	100%

Similarly,

$SS_{vol.\%} = 3.72$; and $SS_{speed} = 6.51$.

For Rt (see Table 10),

$SS_{load} = 21.87$; $SS_{vol.\%} = 10.08$; and $SS_{speed} = 3.75$

6.3.3. The trial variation from the random variations in testing or from unknown parameters

$SS_e = SS_T - SS_{load} - SS_{vol.\%} - SS_{speed}$.

For Ra (see Table 9),

$SS_e = 18.65 - 7.52 - 3.72 - 6.51 = 0.9$

For Rt (see Table 10),

$SS_e = 36.96 - 21.87 - 10.08 - 3.75 = 1.22$.

7. Discussion

The results of this study illustrate that the experimental design based on Taguchi method can be successfully applied to determine the optimum processing conditions (within the range of parameters and levels tested) for improving the surface quality of the ceramic balls by MFP.

From the level average response analysis using the average values of each trial run, the optimum conditions for each of the factors, A, B, and C can be determined. Fig. 2(a,b) show the average effect of each parameter level on the surface finish Ra and Rt, respectively (based on the data from Table 6). The optimum conditions are those that give the best finish. It can be seen from Fig. 2(a,b) that A_3 (load: 1.4 N), B_1 (5 vol.% abrasive) and C_3 (7000 rpm) are the optimum conditions.

Note that the results in Table 6, namely, the surface quality is affected by one parameter only and is independent of the other parameters due to the pairwise balancing property of the orthogonal design used. For the polishing process, smaller surface finish value (Ra and Rt) of the polished surface is desirable. So, $A_3B_3C_1$ is likely to produce the best results for both Ra and Rt and therefore, the optimum conditions are the following: load 1.4 N, vol.% of abrasive 5%, and speed 7000 rpm.

Fig. 3(a,b) are S/N response plots showing the effect of each parameter level on the surface finish Ra and Rt, respectively (using the data from Table 7). In these plots, the levels corresponding to the highest S/N values are chosen for each parameter for they indicate the best quality (both the mean and variation are smallest). Thus, $A_3B_1C_3$ (Table 2) is the optimum condition for a large S/N value in conjunction with a small mean and a small variation of both Ra and Rt. So, within the range of parameters evaluated in this study, a load of 1.4 N, a concentration of 5 vol.%, and a speed of 7000 rpm are considered as the optimum polishing settings. It is coincidental that the conclusions arrived here from an analysis of S/N values are the same as those drawn from the above simple analysis using the average values.

Tables 9 and 10 show the results of the ANOVA for Ra and Rt, respectively under different trial runs. It can be seen from these tables that for the surface finish Ra, the contribution of factor A (polishing load) (40%) is more significant than factor C (polishing speed, rpm) (35%) and both of them are more significant than factor B (abrasive concentration, vol.%) (20%). For the surface finish, Rt, the contribution of factor A (polishing load) (59%) is more significant than factor B (abrasive concentration, vol.%) (27%) and both of them are more significant than factor C (polishing speed) (10%). Further, it can be seen that the relative significance of factors B and C are reversed for Ra and Rt.

8. Conclusions

1. Based on the experimental results, the three important parameters for surface finish identified are the polishing force,

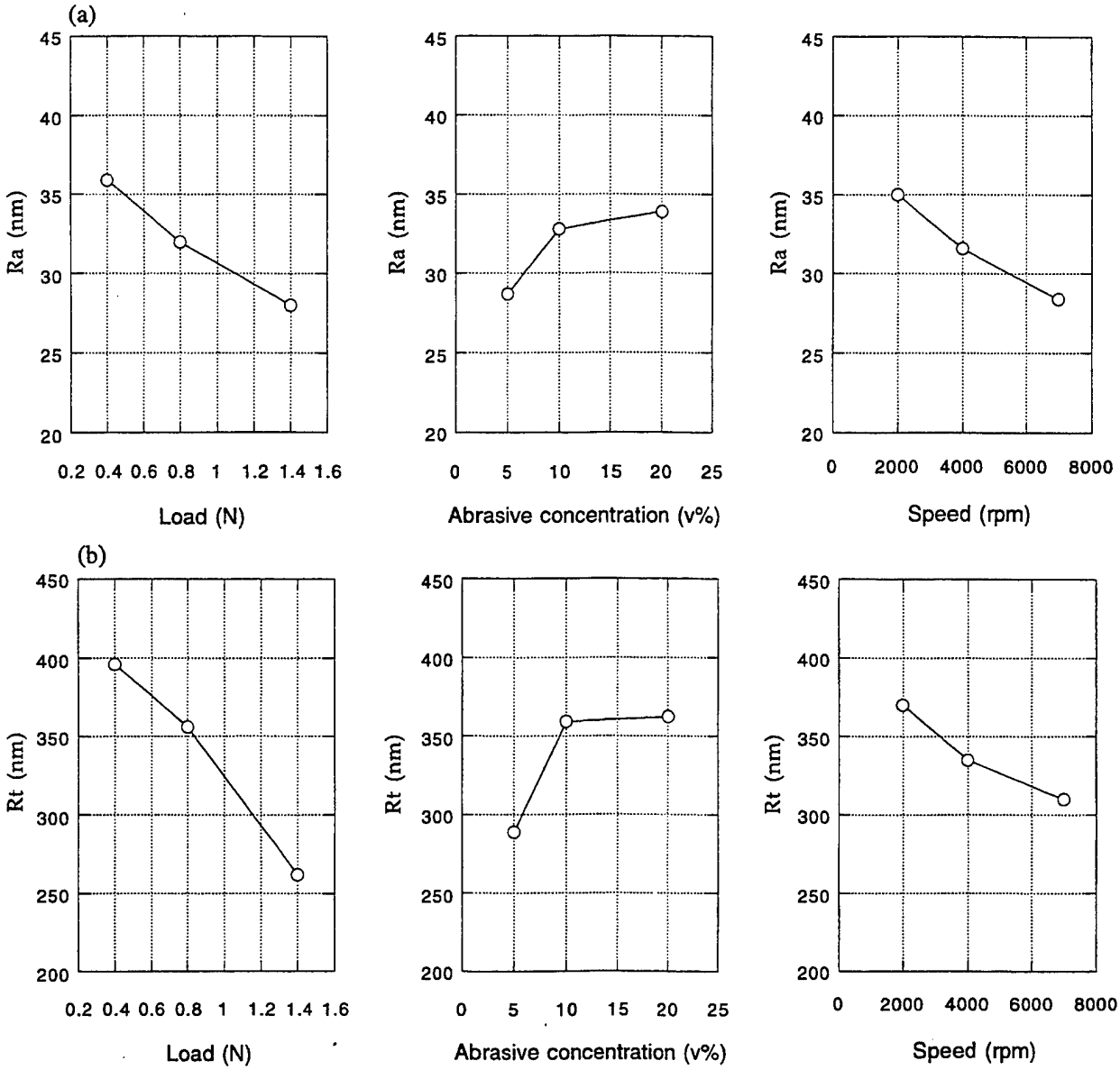

Fig. 2. (a) Plots of the response of each polishing parameter level on the surface finish Ra. (b) Plots of the response of each polishing parameter level on the surface finish Rt.

the abrasive concentration, and the polishing speed for a given abrasive (and its grain size) and final mechanical polishing with workmaterial.

2. Among the three parameters tested, the polishing force parameter is found to be the most significant from the consideration of the overall surface finish, Ra and Rt.

3. For the surface finish Ra, the polishing force parameter is most significant followed by polishing speed and then abrasive concentration while for Rt, the polishing force parameter is most significant followed by the abrasive concentration and then polishing speed.

4. The experimental results also indicate that within the range of parameters evaluated, a high level of polishing force (1.4 N), a low level of abrasive concentration (5%), and a high level polishing speed (7000 rpm) are optimum for improving both Ra and Rt.

5. Using fine B_4C abrasive (grit size 1–2 μm), the best surface finish obtained was ≈20 nm for Ra and ≈200 nm for Rt. To improve the surface finish, further polishing has to be carried out preferably involving CMP where the surface finish was improved using CeO_2 abrasive to ≈4 nm Ra and ≈40 nm Rt [9].

6. A comparison of the results obtained by the Taguchi method with single parameter (i.e., one parameter by one parameter) variation using a fine SiC abrasive (1 μm) [17] yielded similar conclusion for optimum polishing conditions. However, Taguchi method can extract information more precisely and more efficiently.

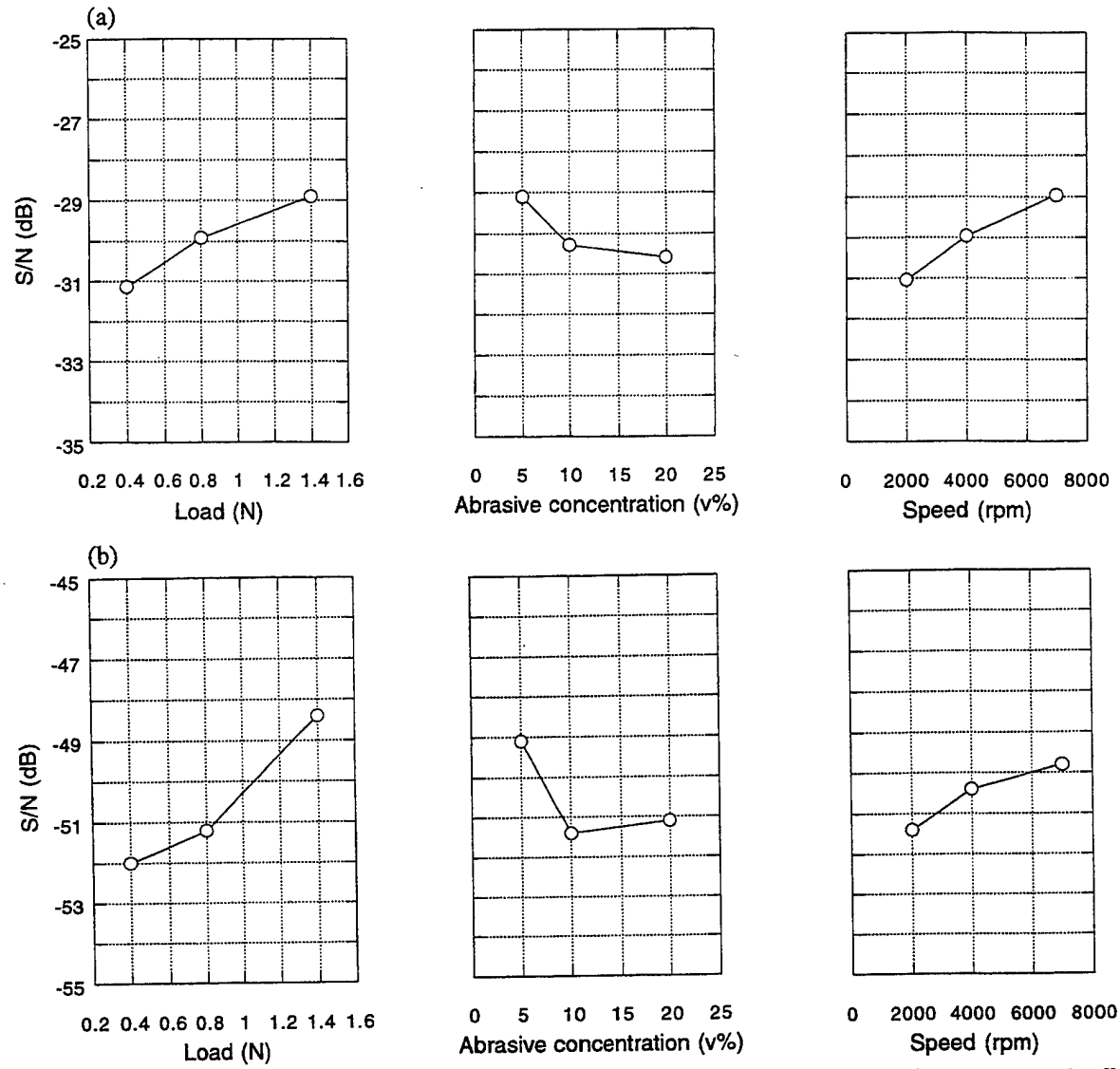

Fig. 3. (a) Plots of the S/N ratios showing the effect of each parameter level on the surface finish Ra. (b) Plots of the S/N ratios showing the effect of each parameter level on the surface finish Rt.

Acknowledgements

This project is sponsored by grants from the National Science Foundation on 'Tribological Interactions in Polishing of Advanced Ceramics and Glasses,' (CMS-94-14610) and 'Design, Construction, and Optimization of Magnetic Field Assisted Polishing,' (DMI-94-02895), and DoD's DEPSCoR Program on 'Finishing of Advanced Ceramics' (DAAH04-96-1-0323). This project was initiated by an ARPA contract on 'Ceramic Bearing Technology Program' (F33615-92-5933). Thanks are due to Drs. J. Larsen Basse, B.M. Kramer, Ming Leu, and J. Lee of NSF and Dr. K.R. Mecklenburg of WPAFB and Dr. W. Coblenz of ARPA for their interest in and support of this work.

References

[1] N. Umehara, K. Kato, Appl. Electromagn. Mat. 1 (1990) 37–43.
[2] N. Umehara, Ann. CIRP 43/1 (1994) 185–188.
[3] T.H.C. Childs, D.A. Jones, S. Mahmood, K. Kato, B. Zhang, N. Umehara, Wear 175 (1994) 189–198.
[4] T.H.C. Childs, S. Mahmood, H.J. Yoon, The Material Removal Mechanism in Magnetic Fluid Grinding of Ceramic Ball Bearings, Proc. of the I. Mech. E. (London), 208/B1 (1994) 47–59.
[5] T.H.C. Childs, S. Mahmood, H.J. Yoon, Tribol. Int. 28/6 (1995) 341–348.
[6] M. Raghunandan, A. Noori-Khajavi, N. Umehara, R. Komanduri, Magnetic Float Polishing of Advanced Ceramics, accepted for publication Trans ASME, J. Eng. Ind. (1996).
[7] R. Komanduri, N. Umehara, M. Raghunandan, Trans ASME, J. Tribol. 118 (1996) 721–727.
[8] S.R. Bhagavatula, R. Komanduri, Phil. Mag. A 74/4 (1996) 1003–1017.
[9] M. Jiang, R. Komanduri, Finishing of Si_3N_4 balls for bearing applications, submitted for publication (1996).
[10] R.S. Fisher, The Design of Experiments, Hafner, NY (1971).
[11] Genichi Taguchi, Taguchi Methods—Research and Development, ASI Press, Dearborn, MI (1992).
[12] K.E. Dehnad, Quality Control, Robust Design, and the Taguchi Method, Brooks/Cole, CA (1989).

[13] R.K. Roy, A primer on the taguchi method, Competitive Manufacturing Series, Van Nostrand Reinhold, NY (1990).
[14] T.B. Barker, Engineering quality by design—interpreting the Taguchi approach, Statistics, Marcel Dekker, 113 (1990).
[15] P.J. Ross, Taguchi Techniques for Quality Engineering, McGraw-Hill, NY (1996).
[16] R.E. Rosensweig, Ferrodynamics, Cambridge Univ. Press, New York (1985).
[17] M. Jiang, Finishing of Advanced Ceramics, PhD thesis (under preparation), Mechanical and Aerospace Engineering, Oklahoma State University (1997).

Biographies

Dr. Komanduri is Professor and MOST Chair in Intelligent Manufacturing in the Mechanical and Aerospace Engineering of Oklahoma State University, Stillwater, OK, USA. He received his B.E. (Mech) and M.E. (Heat Power) from Osmania University, Hyderabad, India and PhD and D. Eng. from Monash University, Melbourne, Australia. He is a Full Member of CIRP and Fellow of ASME and SME. His research interests include machining, grinding, polishing, MD simulation of nanometric cutting, high speed machining, and tribology. He has published over 125 technical papers (several in WEAR) and holds 19 US Patents.

Mr. Ming Jiang is a graduate research assistant in the Mechanical and Aerospace Engineering of Oklahoma State University, Stillwater, OK, USA working towards his PhD. He received his B.S. and M.S from Hua-Qiao University in China.

APPENDIX B

ON THE FINISHING OF Si_3N_4 BALLS FOR BEARING APPLICATIONS

Ming Jiang and R. Komanduri

Wear , 215 (1998) 267-278

ELSEVIER

Wear 215 (1998) 267–278

WEAR

On the finishing of Si_3N_4 balls for bearing applications

Ming Jiang, R. Komanduri *

Mechanical and Aerospace Engineering, Oklahoma State University, Stillwater, OK 74078, USA

Received 8 January 1997; accepted 8 September 1997

Abstract

The conventional method of producing of Si_3N_4 balls for bearing applications by grinding and lapping using diamond abrasive at low speeds (< a few hundred rpm) and higher loads (several tens of N/ball) is generally an expensive and time-consuming operation (several weeks). It also leads to the formation of scratches, microcracks, and pits on the finished balls resulting from large radial and circumferential cracks and dislodgement of grains. Since failure of ceramics initiates from such defects, the reliability of Si_3N_4 balls in service is of prime concern. This paper deals with an alternate technology for finishing Si_3N_4 balls for hybrid bearing applications using magnetic float polishing (MFP) process that overcomes some of these limitations. A methodology for finishing of HIP'ed Si_3N_4 balls from the as-received condition by MFP is presented. It involves the mechanical removal of material initially using harder abrasives with respect to the workmaterial (of different materials of progressively lower hardnesses and finer grain sizes) followed by final chemo–mechanical polishing (CMP) using preferably a softer abrasive for obtaining superior finish with minimal surface or subsurface defects, such as scratches, microcracks, or pits on the Si_3N_4 balls. High material removal rates (1 μm/min) with minimal subsurface damage is obtained with harder abrasives, such as B_4C or SiC (relative to Si_3N_4) due to the use of a flexible support system, small polishing loads ($\approx$ 1 N/ball), and fine abrasives but high polishing speeds (compared to conventional polishing) by rapid accumulation of minute amounts of material removed by microfracture. Final polishing of the Si_3N_4 balls using a softer abrasive, such as CeO_2 (that chemo–mechanically react with the Si_3N_4 workmaterial) results in high quality Si_3N_4 balls of bearing quality with superior surface finish ($R_a < 4$ nm, $R_t < 0.04$ μm) and damage-free surface. It is found that CMP is very effective for obtaining excellent surface finish ($R_a \approx 4$ nm and $R_t \approx 40$ nm) on Si_3N_4 ceramic material and CeO_2 in particular is one of most suitable material for this application.

Keywords: Magnetic float polishing; Finishing of ceramic balls; Silicon nitride; Chemo–mechanical polishing (CMP); Cerium oxide

1. Introduction

A critical factor affecting the performance and reliability of ceramics for bearing applications is the quality of the resulting surface by polishing. It is well known that ceramics are extremely sensitive to surface defects resulting from grinding and polishing processes owing to their high hardness and inherent brittleness. Since fatigue failure of ceramics is driven by surface imperfections, it is paramount that the quality and finish of the ceramic bearing elements be superior with minimal defects so that reliability in performance of bearings in service can be achieved. This investigation focuses on the methodology for obtaining superior finish on Si_3N_4 balls using magnetic float polishing (MFP) process.

Conventional polishing of ceramic balls generally uses low polishing speeds (a few hundred rpm) and diamond abrasive as a polishing medium. In practice, it takes considerable time (some 12–16 weeks) to finish a batch of ceramic balls. The long processing time and use of expensive diamond abrasive result in high processing costs. Also, the use of diamond abrasive at high loads can result in deep pits, scratches, and microcracks. To minimize the surface damage, 'gentle' polishing conditions are required, namely, low level of controlled force and abrasives not much harder than the workmaterial. Further, higher removal rates and shorter polishing cycles can be obtained at high polishing speeds. This is accomplished in this investigation by a process known as magnetic float polishing. This process was originally developed by Tani and Kawata [1] and subsequently improved significantly using the concept of a float by Umehara and Kato [2], Umehara [3], Childs and Yoon [4], Childs et al. [5–7], and Raghunandan et al. [8,9].

When polishing advanced ceramics, such as Si_3N_4 balls by MFP with a harder abrasive, such as B_4C or SiC, high material removal rates (1 μm/min) can be obtained with minimal subsurface damage due to the use of a flexible support system,

* Corresponding author. Oklahoma State University, Mechanical and Aerospace Eng., 218 Engineering North, Stillwater, OK 74078, USA. Tel.: +1-010-1-405-744-5900; fax: +1-010-1-405-744-5720; e-mail: ranga@master.ceat.okstate.edu

0043-1648/98/$19.00
PII S0043-1648(97)00236-6

small polishing force (1 N/ball), fine abrasives but high polishing speed compared to conventional polishing. Higher material removal results from the rapid accumulation of minute amounts of material by microfracture of Si_3N_4 because of high polishing speeds and light loads used instead of large radial and circumferential cracks that results in the formation of pits in conventional polishing. As will be shown, the final polishing of the Si_3N_4 balls with a softer abrasive, such as CeO_2 results in superior surface finish ($R_a < 4$ nm, $R_t < 0.04$ μm) with damage-free surface due to preferential removal of material by chemo-mechanical polishing (CMP). It is found that CMP is very effective in obtaining excellent surface finish on Si_3N_4 workmaterial and that CeO_2 is one of most effective polishing media for this application.

2. Magnetic float polishing and experimental set-up

The magnetic float polishing technique is based on the magneto–hydrodynamic behavior of a magnetic fluid that can float non-magnetic float and abrasives suspended in it by a magnetic field [10]. The forces applied by the abrasive to the part are extremely small (1 N/ball) and highly controllable. Fig. 1a and b are a schematic and a photograph of the magnetic float polishing apparatus for finishing advanced ceramic balls. A bank of permanent magnets (Nd–Fe–B) are arranged alternate N and S below an aluminum chamber which is filled with the required amount of magnetic fluid and appropriate abrasive (5–10% by volume). The magnetic fluid is a colloidal dispersion of extremely fine (100 to 150 Å) subdomain ferromagnetic particles, usually magnetite (Fe_3O_4), in a carrier fluid, such as water or kerosene. It is made stable against particle agglomeration by coating the particles with an appropriate surfactant. In this investigation a water base ferrofluid is used.

When a magnetic field is applied, the magnetic particles in the magnetic fluid are attracted downward to the area of higher magnetic field and an upward buoyant force is exerted on all non-magnetic materials to push them to the area of lower magnetic field. The abrasive grains, the ceramic balls, and the acrylic float inside the chamber, all being non-magnetic materials, are levitated by the magnetic buoyant force. The drive shaft is fed down to contact with the balls (3-point contact) and presses them down to reach the desired force or height. The balls are polished by the abrasive grains under the action of the magnetic buoyancy levitational force when the spindle rotates. Damage-free surface on ceramic balls are expected by the magnetic float polishing technique because the magnetic buoyant force (1 N/ball) is applied via the flexible float. The function of acrylic float here is to produce more uniform and larger polishing pressure (the larger buoyant force near the magnetic poles can be transmitted to the polishing area by this float). An urethane rubber sheet is glued to the inner guide ring to protect it from wear. The material of the drive shaft is austenitic stainless steel which is non-magnetic.

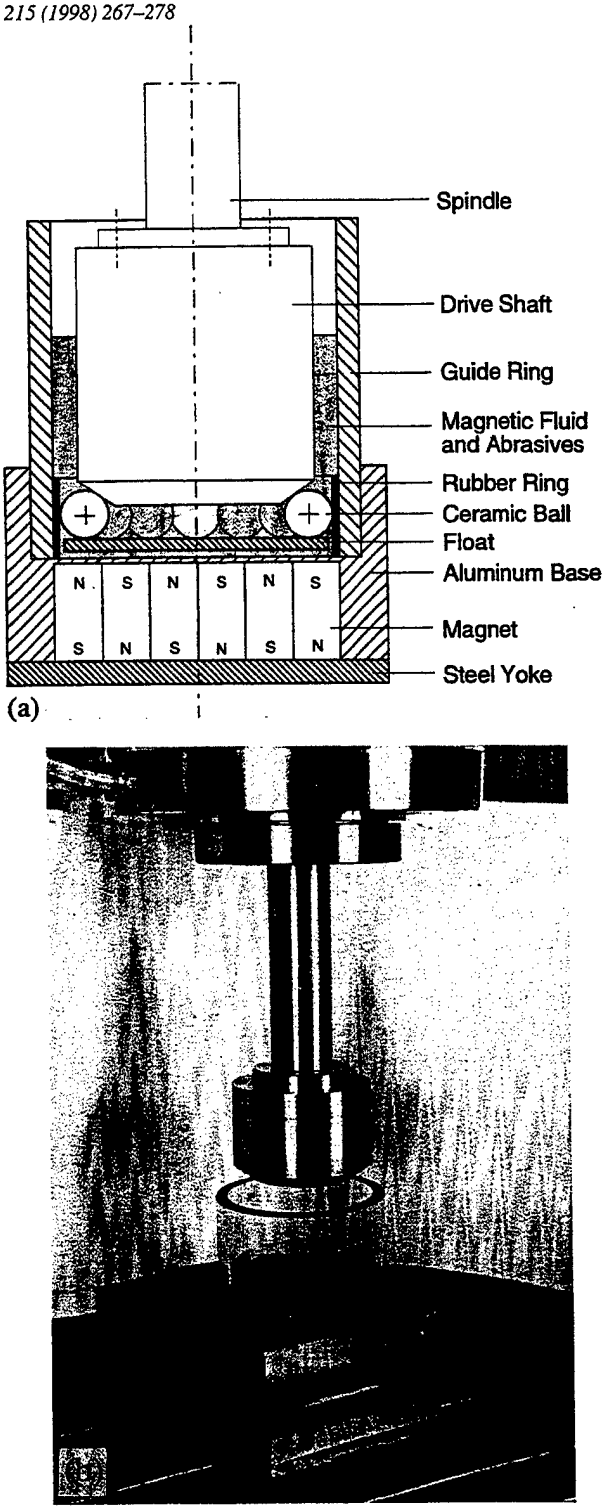

Fig. 1. (a) The schematic plot of the magnetic float polishing (MFP) apparatus used for polishing Si_3N_4 balls. (b) Photograph of the magnetic float polishing (MFP) apparatus used for polishing Si_3N_4 balls.

3. Chemo–mechanical polishing

Chemo–mechanical action depends on the availability for a short duration certain threshold pressure and temperature at the contact zone of the polishing process to enable a chemical reaction layer to be formed by the interaction of the abrasive, workmaterial and the environment [11]. This proc-

ess is considered tribochemical polishing when there is no superimposed mechanical action [12]. Thus, chemo–mechanical action is very specific and proper choice of the abrasive and the environment should be made for a given workmaterial. Both thermodynamics and kinetics play an important role on the rates of chemical reactions. Once the reaction products are formed, it is removed from the workmaterial by subsequent mechanical action by the abrasive. Since material removal by this mechanism does not depend on the hardness but on the chemical potentials, it is possible to remove material by abrasives substantially softer than the workmaterial. Theoretically any abrasive that can react with the workmaterial in a given environment and form a reaction product can be used for CMP. However, some abrasives may be harder than the workmaterial and some mechanical action may occur in addition to the chemo–mechanical action. Material removal by mechanical action may be satisfactory in roughing, or even semi-finishing but in the final finishing operation it is preferable to minimize the mechanical action that can affect the surface integrity. This is the reason why diamond abrasive was not considered in this investigation for finishing Si_3N_4 balls. Similarly, some abrasives react with a given workmaterial much more than others. For efficient removal of material, those with the highest reactions rates would be preferable for chemo–mechanical action. Some idea on this can be obtained by considering the chemical reactions involved using thermodynamic analysis, such as Gibbs free energy of formation.

A review of literature on chemo–mechanical polishing of various materials in general and that of Si_3N_4 in particular has been presented by Komanduri et al. [13] and may be referred to for details. Also, the mechanism of chemo–mechanical polishing of Si_3N_4 with Cr_2O_3 was reported by Bhagavatula and Komanduri [14] in that it was shown conclusively that the role of Cr_2O_3 was more than that of a mere catalyst (as reported in the literature by other researchers) and that Cr_2O_3 does play an active role in the chemical reaction with Si_3N_4 forming chromium silicate and chromium nitride. This was shown by examination of the wear debris in the SEM (both the secondary electron images and the energy dispersion X-ray analysis) as well as X-diffraction of the wear debris using a low-angle X-ray diffraction equipment. In this investigation, this work is extended to investigate the action of CeO_2 abrasive for CMP of Si_3N_4. It is found that CeO_2 to be a superior abrasive than Cr_2O_3 in finishing Si_3N_4 workmaterial, in that the finish obtained by Cr_2O_3 is about 10.7 nm R_a and 0.149 μm R_t (Fig. 4b), while that with CeO_2 is about 3.8 nm R_a and 0.029 μm R_t (Fig. 5f), as reported in this investigation. Also, very few scratch marks, if any, are found on Si_3N_4 surface when polished with CeO_2 even at a magnification of 5000 to 10,000 with the entire surface being smooth without any pits. This is attributed to the use of significantly softer CeO_2 abrasive which will not scratch Si_3N_4 in the final polishing.

4. Why cerium oxide (CEO_2) is abrasive

It is well known that cerium oxide (CeO_2) is an efficient polishing agent for glass. It is also known that the fluid medium in which it is used is also very critical. For example, when polishing glass, CeO_2 is particularly effective in water and in alcohols only when hydroxyl groups are present. Thus, cerium oxide slurry in water is invariably used for polishing. The oxide contains polyvalent cerium atoms, Ce(IV) and Ce(III), which can provide chemical action with the workmaterial. It appears that when $Ce(OH)_4$, i.e., $CeO_2.2H_2O$ is precipitated fresh, i.e., in situ, in the polishing slurry form, a soluble Ce(IV) salt is probably involved in an equilibrium reaction:

$$SiO_2+Ce(OH)_4 \rightarrow CeO_2+Si(OH)_4$$

The breaking and reforming of Si–O bonds is perhaps aided by the transfer of OH groupings to incipient fracture sites by a transport mechanism using the relatively large and mobile coordination sphere around oxophilic cerium atom [15].

Cerium is the most abundant element of the rare earths and ranks around 25th in the listing of abundance in the earth's crust of all the naturally occurring elements. So, Ce is not particularly rare as compared to Ni or Cu. Cerium oxide has a high melting temperature (2750 K) but is a very soft material (Mohs hardness: 5–6) and hence cannot scratch Si_3N_4. Ce ions are present in two stable valence states, namely, the tetravalent Ce^{4+} (Ceric) and the trivalent Ce^{3+} (Cerous). The tetravalent ceric ion is a strong oxidizing agent but can be reduced by ferrous salts, hydrogen peroxide. When associated with oxygen, it is completely stable as CeO_2. Ce_2O_3 is unstable in air, water, and the like and readily converts to CeO_2. Ceria has the CaF_2 structure with 8-coordinate cations and 4-coordinate anions. It can be visualized as a close-packed cubic array of metal atoms with oxygen filling all the tetrahedral holes. Ceria has been tested for acute effects and found to have very low toxicity [15]. Hence, its use is safe from an environmental point of view.

Since CeO_2 can react chemo–mechanically with both Si_3N_4 base material as well as the glassy phase that holds Si_3N_4 particles together, this material is selected in the investigation for final chemo–mechanical polishing.

5. Test procedure, polishing conditions, and ball characterization

The uniaxially pressed-Si_3N_4 balls (CERBEC NBD-200 from Norton Advanced Ceramics) in the as-received condition had a nominal diameter of 13.4 mm. These balls also contained nearly a 200 μm thick × 5 mm wide band of material around the periphery at the parting plane resulting from the uniaxially pressing (HIP) process. These balls have to be finished to a final size of 12.7 mm (0.5 in.), a sphericity of 0.5 μm, and best finish achievable. All the three factors were considered in the finishing of Si_3N_4 balls in this paper with

Table 1
The chemical composition of NBD-200 silicon nitride [16]

Al	C	Ca	Fe	Mg	O	Si_3N_4
≤0.5	≤0.88	≤0.04	≤0.17	0.6–1.0	2.3–3.3	97.1–94.1

Table 2
The mechanical and thermal properties of Si_3N_4 workpiece [16]

Property	Value
Flexural strength (MPa)	800
Weibull modulus	9.7
Tensile strength (MPa)	400
Compressive strength (GPa)	3.0
Hertz compressive strength (GPa)	28
Hardness, Hv (10 kg) (GPa)	16.6
Fracture toughness, K_{Ic}, MN $m^{-3/2}$	4.1
Density (g/cm^3)	3.16
Elastic modulus (GPa)	320
Poisson's ratio	0.26
Thermal expansion coefficient at 20–1000°C (/°C)	2.9×10^{-6}
Thermal conductivity at 100°C (W/m K)	29
Thermal conductivity at 500°C (W/m K)	21.3
Thermal conductivity at 1000°C (W/m K)	15.5

Table 3
The properties of various abrasives

Abrasive	Density (g/cm^2)	Knoop hardness (kg/mm^2)	Elastic modulus (GPa)	Melting point (°C)
B_4C	2.52	2800	450	2450
SiC	3.2	2500	420	2400
CeO_2	7.13	625	165	2500

emphasis on the latter aspect, namely, best finish achievable. The large differences in the diameter between the as-received condition to the final size required is to remove all the reaction material that is formed on and near the surface during the HIP'ing process.

Tables 1 and 2 give the nominal chemical composition and the mechanical properties, respectively of the Si_3N_4 (NBD 200) balls, and Table 3 gives the various properties of the abrasive used in this investigation. As in most finishing operations, there are three stages involved in magnetic float polishing of Si_3N_4 balls, namely: (1) roughing to remove as much material as possible without imparting serious damage to the surface; (2) an intermediate stage of semifinishing where size, sphericity, and surface roughness have to carefully monitored; and (3) final finishing where all three, namely, size, sphericity, and finish have to closely controlled to meet the requirements.

Table 4 lists the test conditions used for different stages of polishing. Two coarser, harder abrasives, B_4C (500 grit) and SiC (400 grit) (i.e., compared to Si_3N_4 work material) were used during the initial stages of polishing to reach the desired diameter at high removal rates and at the same time improve the sphericity for proper ball motion. After reaching the diameter close to the desired diameter, an intermediate (semifinishing) stage is utilized as a transition between the roughing and finishing stages, as the material removal rate is of prime concern in the first stage and surface finish in the final stage. The two harder abrasives with a finer grit size were chosen for this intermediate stage, namely, SiC (1000 grit) and SiC (1200 grit). During this stage, the removal rates are much lower and the finish much better than roughing but the emphasis during this stage is the improvement of sphericity. In the final stage (prior to CMP), fine SiC abrasive (8000 grit) is used to approach the required diameter and sphericity and remove almost all the deep valleys from the surface. This is followed by final polishing using a softer, chemo–mechanical abrasive, namely, CeO_2 to produce the balls of required diameter, sphericity, and final surface finish which is extremely smooth and almost damage-free by preferentially removing the peaks from the surface.

The polishing shaft in MFP apparatus was driven by a high-speed, high-precision air bearing spindle (PI Spindle) with a stepless speed regulation up to 10,000 rpm. The magnetic field was measured by Gauss/Tesla meter. The pH value of polishing environment was measured by pH/temperature meter. The polishing load was set up by measuring the normal force with a Kistler's piezoelectric dynamometer connected to a charge amplifier and a display. To calculate the material removal rates, the weight reduction in the balls was measured by measuring the weight before and after polishing at every

Table 4
Test conditions

Stage	Abrasive			Abrasive (vol.%)	Speed (rpm)	Load (N/ball)	Time (min)	Remarks
	Type	Grit size	Size (μm)					
1	B_4C	500	17	10%	2000	1.0	–	Roughing (high material removal)
	SiC	400	23	10%	2000	1.0	–	
2	SiC	1000	5	10%	2000	1.0	30	Semi-finishing (sphericity and roughness)
	SiC	1200	3	10%	2000	1.0	30	
3	SiC	8000	1	5%	4000	1.2	60	Final finishing (size, sphericity, and finish)
	CeO_2		5	10%	2000	1.2	120	

*All abrasives used, except CeO_2, were obtained from Norton. CeO_2 is obtained from Aldrich Chemicals.

stage of the test using a precision balance. The surface finish of the polished balls was analyzed using a Form TalySurf 120 L, ZYGO laser interference microscope, a Digital Nanoscope III atomic force microscope (AFM), and an ABT 32 scanning electron microscope (SEM). The roundness of the balls was measured using TalyRond 250.

In this study, the finished balls are characterized for roundness using a TalyRond 250 (cut-off: 50 upr, Filter: 2CR), and for surface features using a scanning electron microscope (SEM), a Form TalySurf 120 L (cut-off: 0.25 mm and 0.8 mm, evaluation length: 4–6 consecutive cut-off, Filter: ISO 2CR), and an AFM. Although the latter three instrument measure or illustrate slightly different surface features, they are basically complimentary in nature. Their combined use provides confidence on the data obtained. In this investigation, three randomly selected balls from each batch are traced three times at approximately three orthogonal planes using the TalyRond and Form TalySurf to provide the roundness and surface roughness, respectively. The TalyRond trace measures the maximum departure from a true circle of assumed magnitude and as such it denoted roundness. The sphericity of each ball, according to ABMA, is defined as the maximum value of the roundness measured on three orthogonal planes of the ball. Similarly, the surface finish of each ball is taken as the maximum value of three traces along three orthogonal planes of the ball.

The surface roughness obtained by mechanical polishing generally has approximately a symmetrical profile. However, when the peaks are smoothened preferentially leaving the valleys intact as in CMP of finishing of Si_3N_4 giving a fairly smooth bearing surface, the surface roughness can be unsymmetrical. Many parameters have been proposed to quantify the various surface characteristics. It is necessary to ensure that these values truly represent the surface features of interest. It is generally recognized that only R_a is not enough to evaluate the surface finish and that both R_a and R_t (or R_{max}) may be necessary. The R_a value represents the average roughness is a typical value of the measured surface but information regarding the shape of the irregularities (such as deep surface defects) is averaged out. The R_t value is the vertical distance between the highest and lowest points of the roughness profile. It is not a typical value for the whole surface, but can directly represent the irregular surface defects, such as scratches and pits (deep valleys), which can have a significant effect on the surface quality of advanced ceramic materials ($R_t = R_p + R_v = R_{pv}$) for various applications.

For a stylus instrument, such as TalySurf, the stylus size and shape affect the accuracy of the profile. It would not be possible to trace the complete profile of a deep valley especially the bottom if the size of the valley is smaller than the tip radius. The stylus tip radius of TalySurf 250 used in this study is ≈ 2 μm. However, SEM micrograph can be helpful to identify whether there are surface defects which can be reflected by stylus of TalySulf and whether the value from TalySurf is a reliable for small-damage surface. TalySulf is convenient to use for large area scanning with help by SEM micrograph. We also checked surface finish by ZYGO laser interference microscope which is a non-contact measurement instrument. For the ZYGO laser interference microscope, the focus range is important and should include both peaks and valleys of the polished surface. Otherwise, the surface values from ZYGO are unreliable. The stylus tip radius of AFM is <0.08 μm and can easily be broken and not easy to be operated and used very often. In this study, AFM is used for final high magnification evaluation of some random areas (≈ 12). Based on the evaluation by all of TalySurf, SEM, ZYGO and AFM characterization techniques, one can be more confident that the surface finish value shown are a reliable representation of the true surface quality.

6. Results

Fig. 2a–c are SEM micrograph, a Form TalySurf profile, and an AFM image, respectively of a commercially finished best Si_3N_4 ball surface (considered as a master ball of ABMA Grade 3). From the SEM micrograph (Fig. 2a), it can be seen that while some areas of the surface are extremely smooth, there are many fine scratches and some pits. The AFM image of the polished surface (Fig. 2c) more or less shows the same features with an R_a of ≈ 5 nm and R_{max} of ≈ 220 nm. Even though the TalySurf profile of the smooth region of the polished surface gives an R_a of ≈ 7 nm and R_t of ≈ 70 nm (Fig. 2b) this may not reflect the actual surface roughness as can be seen from the SEM image (Fig. 2a). From the SEM image, several deep pits can be seen the size of such defects at the bottom would be smaller than the stylus tip radius (2 μm) of the TalySulf. As previously pointed out, the values obtained by TalySurf, AFM, and ZYGO would depend on their ability to analyze the data from all the peaks as well as the valleys. If the depth of field is not adequate for a given magnification, the data would be in error on account of this. Consequently, care should be exercised in the quantitative evaluation of the surface finish obtained at these magnifications although relative values and surface topography are helpful in the analysis. Hah et al. [16] recently showed the surface finish of a polished surface of a commercial Si_3N_4 ball (7/16 in diameter) using an AFM, an R_a in the region without defects as 1.8–2.8 nm and the regions including the defects as 11–18 nm (with defect density medium and scratch marks severe). For smaller-sized balls (1/4 in diameter), they reported an R_a of 2.5 to 4 nm in the region without any defects and 35–40 nm including the regions with defects (with defect density large and scratch marks some). However, the R_{max} with defects can be many times this value (at least 10 times). Fig. 3 is an AFM image at higher magnification showing deep pits separated by smooth regions of a commercially finished ball.

Fig. 4a and b are an SEM micrograph and a Form TalySurf profile, respectively, of a Si_3N_4 ball surface finished by Cr_2O_3. From the SEM micrograph (Fig. 4a), it can be seen that while much of the surface is very smooth there are some fine

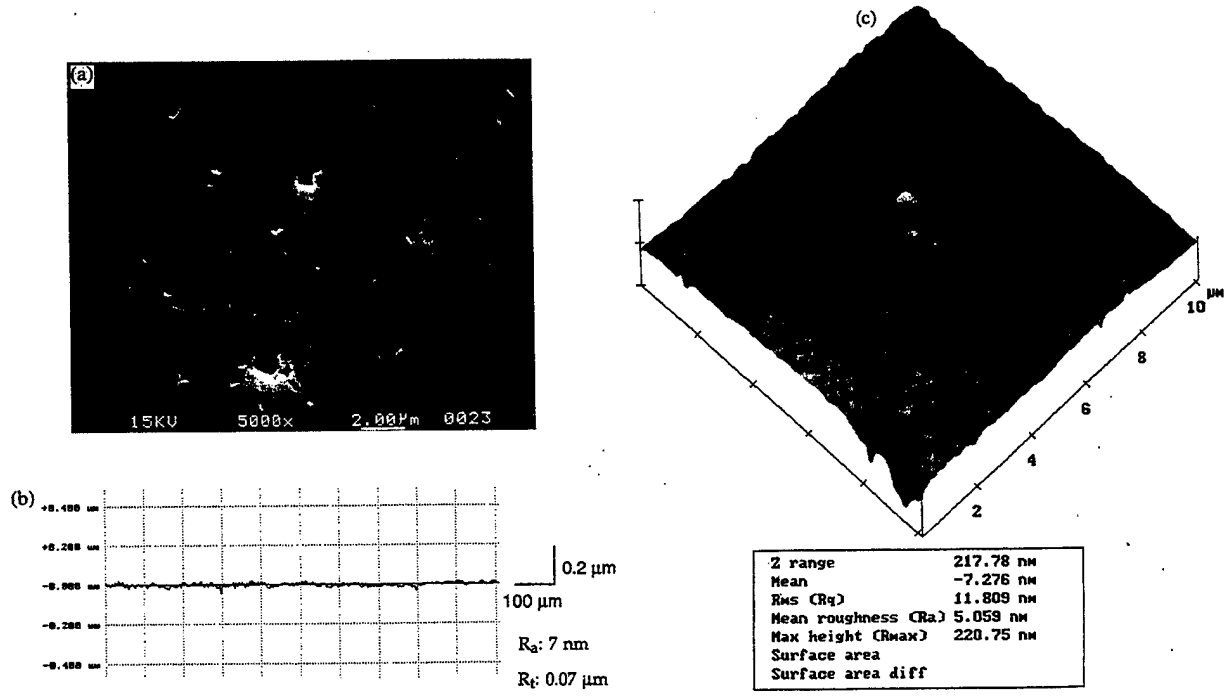

Fig. 2. (a) The SEM micrograph of a commercially finished Si_3N_4 ball surface. (b) The Talysurf surface roughness profile of a commercially finished Si_3N_4 ball surface. (c) The AFM image of a commercially finished Si_3N_4 ball surface.

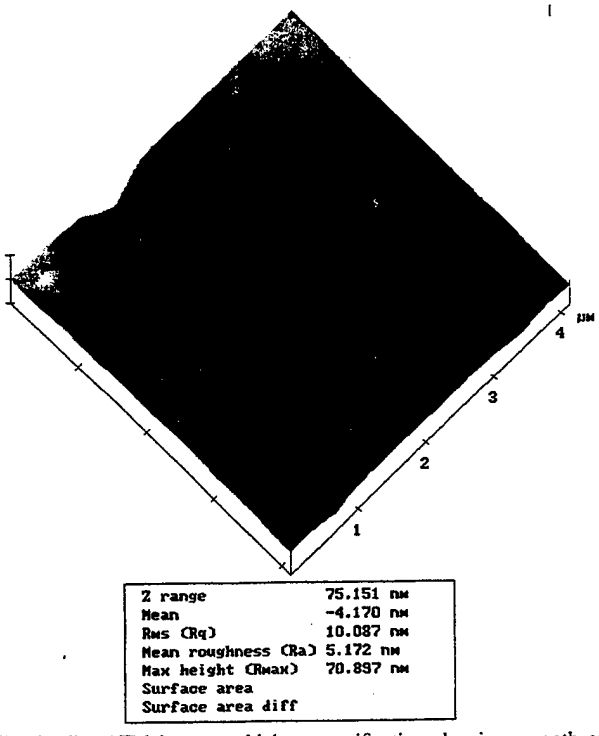

Fig. 3. The AFM image at higher magnification showing smooth area separated by pitting of a commercially finished Si_3N_4 ball surface.

scratches and several small pits. The surface finish values obtained by the Form TalySurf are $R_a \approx 10.7$ nm and $R_t \approx 0.149$ µm. A plausible explanation for the observed roughness with Cr_2O_3 abrasive, in spite of its CMP ability, is its higher hardness (harder than Si_3N_4) and consequent

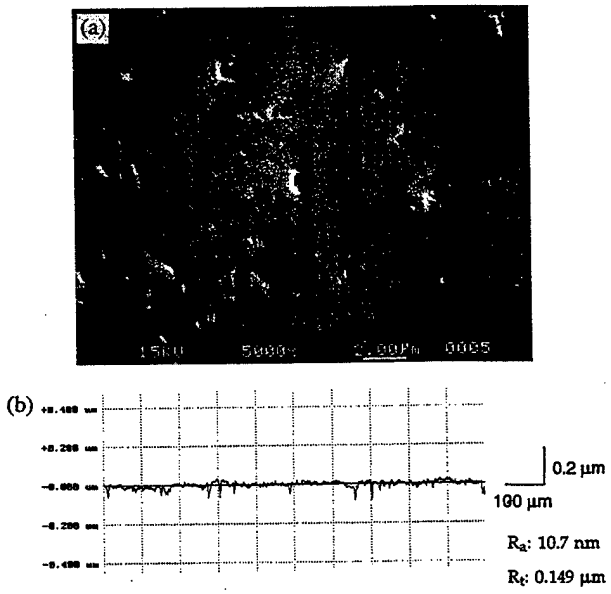

Fig. 4. (a) The SEM micrograph of a Si_3N_4 ball surface finished by Cr_2O_3 abrasive. (b) The Talysurf surface roughness profile of a Si_3N_4 ball surface finished by Cr_2O_3 abrasive.

mechanical abrasion leading to abrasion and pitting. Also, some of the species generated during CMP with Cr_2O_3 may require careful handling from an environmental point of view which is not the case with CeO_2 [17]. Hence, the use of CeO_2 for polishing of Si_3N_4 would be preferable both from CMP and environmental points of view.

Table 5 gives the average surface finish and material removal rates obtained at progressive stages of polishing. The

Table 5
The average surface finish and material removal rates during various stages of polishing

Stage	Abrasive	Surface finish (average)		MRR (per ball)		Material removal mechanism
		R_a (nm)	R_t (μm)	(mg/min)	(μm/min)	
1	B_4C 500	225	1.95	0.96	1.2	Microfracture
	SiC 400	170	1.40	0.64	0.8	Microfracture
2	SiC 1000	95	0.80	0.30	0.4	Submicrofracture
	SiC 1200	55	0.50	0.20	0.2	Submicrofracture
3	SiC 8000	15	0.15	0.04	–	Submicrofracture
	CeO_2	4	0.03	0.01	–	Tribochemical

corresponding TalySurf surface finish profiles are shown in Fig. 5a–f. It can be seen that the surface roughness as well as the material removal rates decease as the hardness and grain size of the abrasive decreases due to a decrease in the size of brittle microfracture. For a harder abrasive with a fine grain size, the material removal is by submicroscopic fracture and therefore results in damage-free subsurface. Further CMP with a softer abrasive, such as CeO_2, as will be shown, will result in an extremely smooth surface.

Fig. 6a and b show the 3-D plot of the surface roughness using the ZYGO non-contacting laser interference microscope and the AFM profile, respectively of the final surface polished by softer CeO_2 abrasive. The surface finish values after the final polishing obtained by Form TalySurf are $R_a \approx 3.8$ nm and $R_t \approx 0.029$ μm, while those obtained by ZYGO are $R_a \approx 3.9$ nm and $R_{tm} \approx 0.021$ μm for the line scan and by AFM are $R_a = 1.4$ nm and $R_{max} = 0.018$ μm for the area scan. The SEM micrographs (Fig. 7b) show essentially smooth surface with practically no surface defects. Both AFM and ZGYO also provide surface finish by averaging over an area. The evaluation of surface topography by all the characterization techniques considered in this investigation, namely, TalySurf, SEM, ZYGO, and AFM, gives confidence that the final surface is damage-free with a finish of $R_a \approx 4$ nm and $R_t \approx 0.04$ μm (cut-off: 0.25 mm, evaluation length: 4–6 consecutive cut-off, Filter: ISO 2CR). If one considers the AFM values, the surface finish R_a would be ≈ 1.4 nm.

Fig. 7a is an SEM micrograph of a Si_3N_4 ball surface obtained after mechanical polishing with a finer SiC abrasive (8000 grit size) indicating that the material removal from the

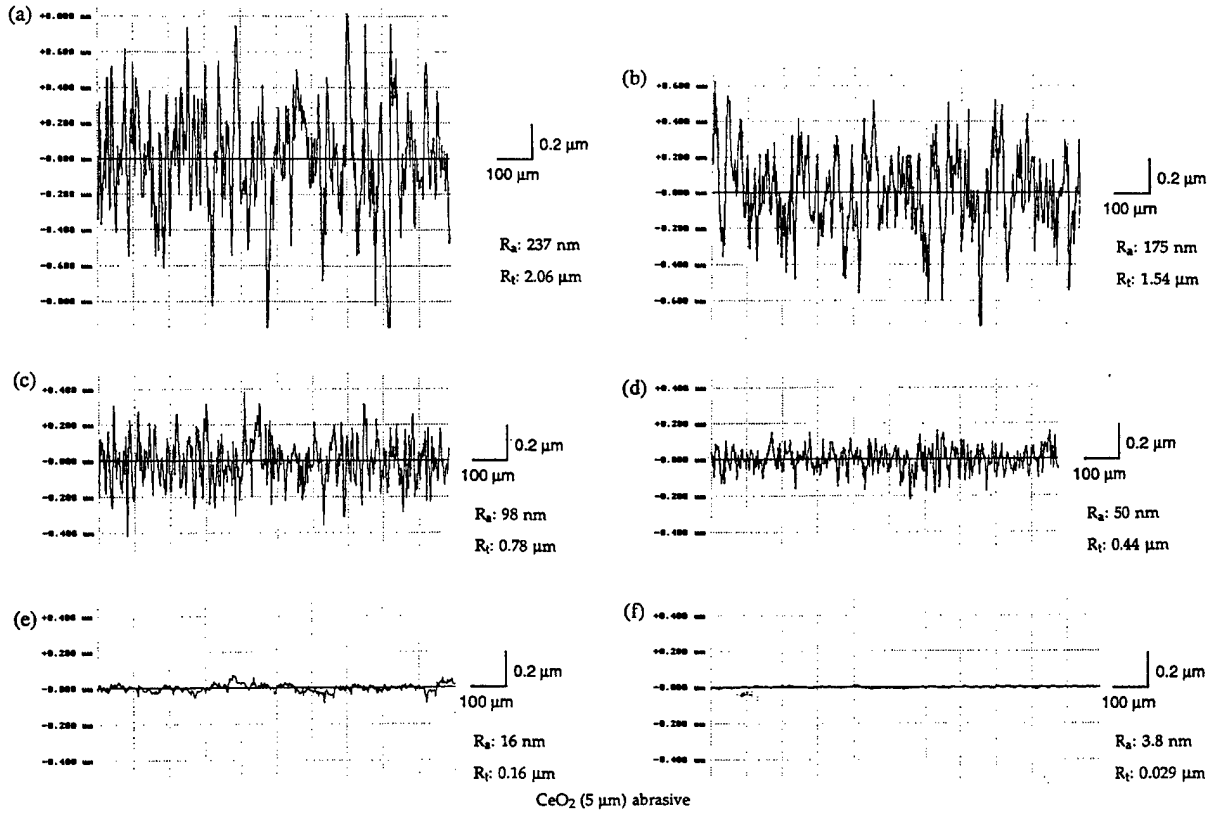

Fig. 5. The TalySurf surface roughness profiles of a Si_3N_4 ball after polishing by: (a) B_4C (500 grit) abrasive, (b) SiC (400 grit) abrasive, (c) SiC (1000 grit) abrasive, (d) SiC (1200 grit) abrasive, (e) SiC (8000 grit) abrasive, and (f) CeO_2 (5 μm) abrasive, respectively.

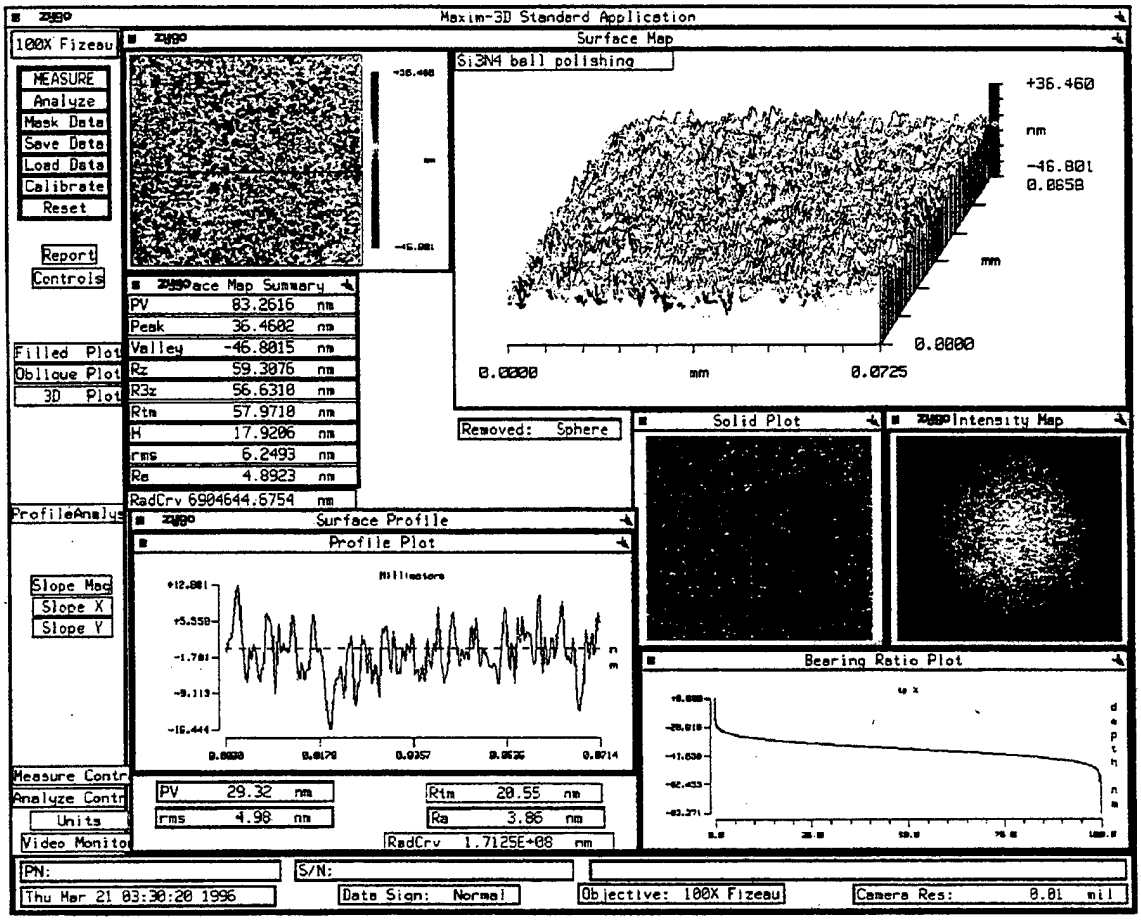

(a)

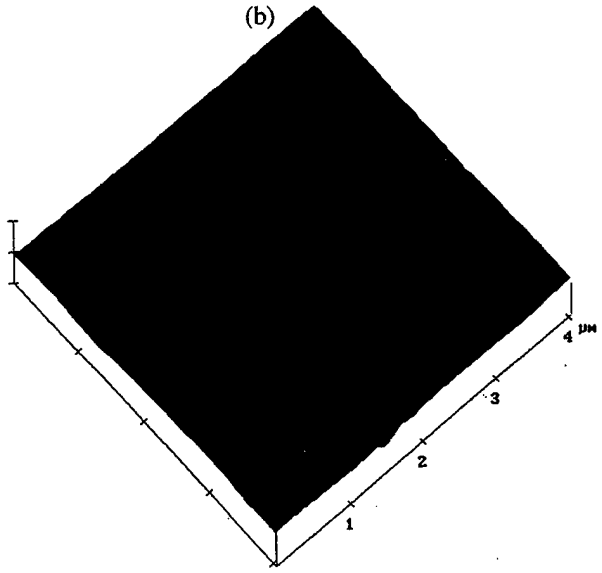

Fig. 6. (a) The ZYGO plot (100×Fizeau) of the surface of a Si_3N_4 ball after finishing by CeO_2 (5 μm) abrasive. (b) The AFM image of the surface of a Si_3N_4 ball after finishing by CeO_2 (5 μm) abrasive.

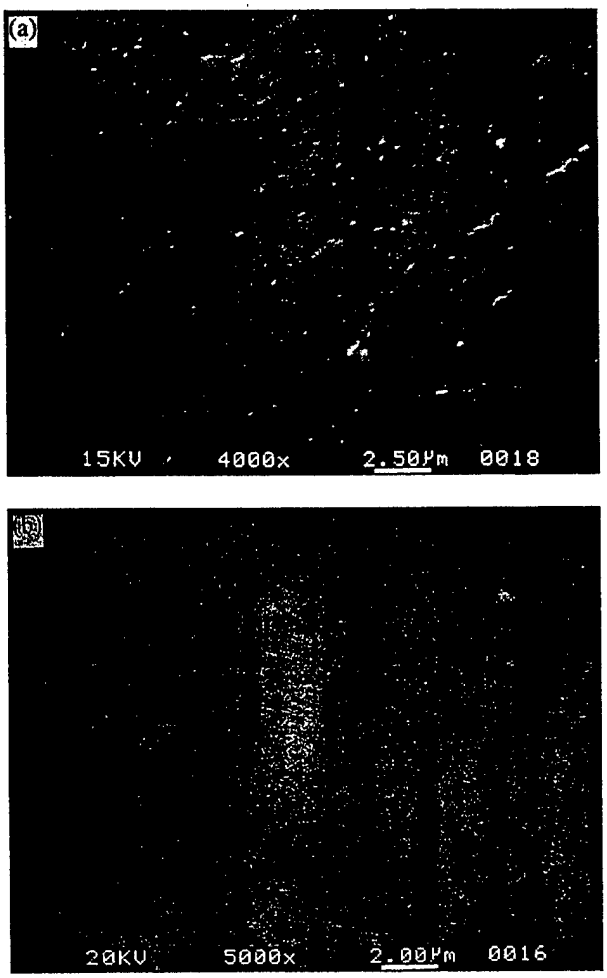

Fig. 7. (a) The SEM micrograph of the surface of a Si_3N_4 ball after polishing by SiC (8000 grit) abrasive. (b) The SEM micrograph of the surface of a Si_3N_4 ball after polishing by CeO_2 (5 μm) abrasive.

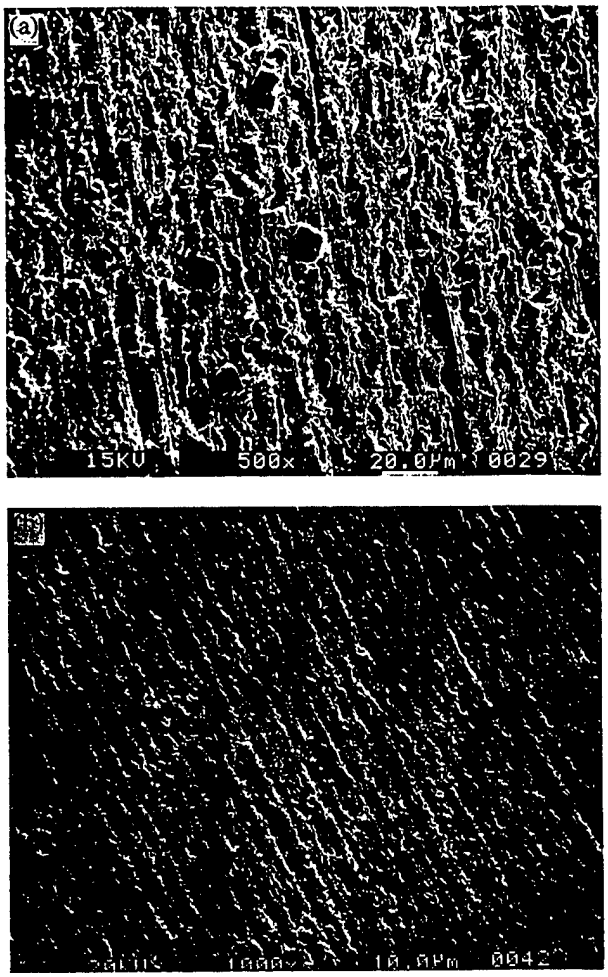

Fig. 8. (a) The SEM micrograph of the stainless steel shaft in contact with Si_3N_4 balls in MFP showing the presence of B_4C (500 grit) particles and abrasion marks on the shaft material. (b) The SEM micrograph of the stainless steel shaft in contact with Si_3N_4 balls in MFP showing the presence of B_4C (1500 grit) particles and abrasion marks on the shaft material.

workmaterial is predominantly by brittle fracture on a submicroscopic scale under the mechanical action of the abrasive. While some polishing scratches can be seen, the surface is relatively free of pits that would normally form using diamond abrasive. Fig. 7b is a representative SEM micrograph of a Si_3N_4 ball surface after the surface has been finished by CMP with a softer abrasive, CeO_2, showing an extremely smooth surface with practically no surface defects, such as pits or scratch marks. Several areas of the Si_3N_4 ball surface were scanned and the micrograph shown in Fig. 7b was found to be a representative of the topography of the surface.

Fig. 8a and b SEM micrographs of the polishing shaft after polishing Si_3N_4 balls with B_4C 500 and B_4C 1500 abrasives. They show that the abrasives are actually not embedded in the shaft as considered by Childs et al. [7] but actually abrade the softer stainless steel polishing shaft. Thus, while the action of the abrasives is one of a two body abrasion (i.e., sliding without rotation) as rightly pointed out by Childs, they are not fixed but move relative to the polishing shaft. The material removal is due to the relative speed between the abrasives and the workmaterials.

Fig. 9a and b show the TalyRond roundness traces of an as-received ball and the finished ball, respectively. It shows that the roundness of the NBD-200 HIP-Si_3N_4 balls was reduced from the as-received condition of $\approx$200 μm to a final value of $\approx$0.25 μm. The sphericity of the balls (i.e., maximum deviation of the roundness of a ball taken in three orthogonal planes) for this batch was found to be in the range of 0.30 μm.

From the work presented here, it can be seen that magnetic float polishing technique can be used for finishing Si_3N_4 balls from the as-received condition to the required diameter, sphericity ($<$0.3 μm), and surface finish ($<$4 nm) without scratches or pits on the surface. The actual polishing process from the as-received condition to the final requirements can be achieved in less than 20 h. This, however, does not take into account the time taken for the characterization of the surfaces by various techniques mentioned in this paper. The methodology developed here incorporates polishing conditions and use of appropriate abrasives (including grain sizes) that are not severe enough at any stage to cause damage, such

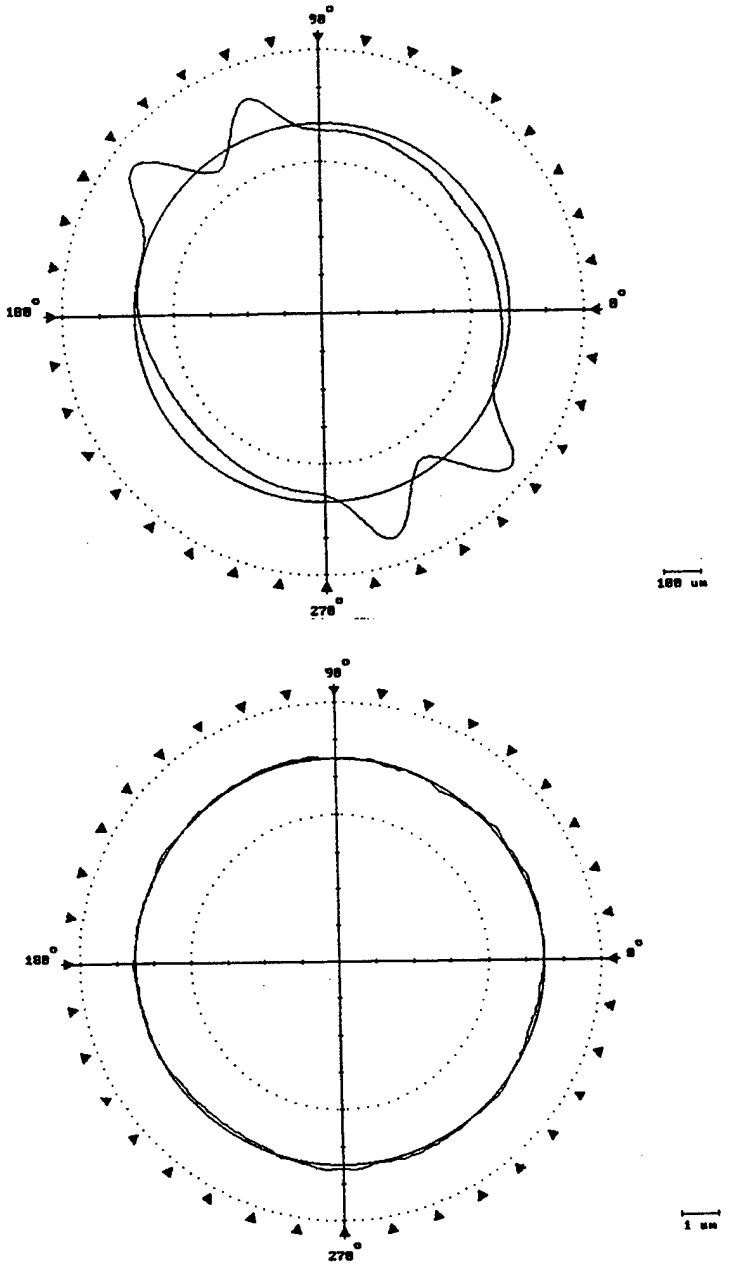

Fig. 9. (a) The TalyRond roundness profile of an as-received Si_3N_4 ball showing a 200 μm × 5 mm band at the parting line due to the uniaxial pressing process (Roundness: 195 μm). (b) The TalyRond roundness profile of a Si_3N_4 ball after the final stage of polishing by CeO_2 (5 μm) abrasive (Roundness: 0.25 μm).

as deep pits and cracks at and near the surface, so that the balls can be finished to the requirements without surface or near surface damage. Of course, whether or not the surface can be finished absolutely smooth also depends on the residual porosity of the uniaxially pressing-Si_3N_4 material.

7. Discussion

7.1. Mechanical polishing

The mechanism of material removal from the Si_3N_4 balls by finer grit, harder abrasives, such as B_4C and SiC in MFP process is by mechanical microfracture because of higher hardness of the abrasive and the inherent hardness of the workmaterial. Under these conditions material removal occurs not by grain pullout, grain fracture, and large fracture but by microfracture by cleavage. While chemo–mechanical action may also occur, its contribution is considered to be much smaller than the mechanical action, namely, microfracture by cleavage.

Childs et al. [7] have shown that in magnetic float polishing, material removal from the balls is accomplished by the action of the abrasives embedded in the shaft due to sliding at the contact area between the drive shaft and the ball. It is unlikely that when fine abrasives are held between the Si_3N_4

balls and the stainless steel shaft that the abrasives will get embedded in the shaft, as in the present case. If this is so, one would never be able to remove material from softer workmaterials with loose abrasives. In an actual situation, the abrasive will abrade the soft stainless steel shaft much more so than the Si_3N_4 workmaterial and it appears unlikely that the abrasives will be embedded as Childs et al. considered but would be moving relative to the polishing shaft forming abrasion marks in the shaft. In fact wear on the stainless steel shaft is as a result of it and may have to be ground periodically to improve sphericity.

For larger-sized abrasives and higher loads, as in conventional polishing with diamond abrasive, the finished surface is effected by the formation of deep pits, grooves and cracks. This will not be the case with finer abrasives and lighter loads. Higher material removal rates without subsurface damage is feasible by magnetic float polishing because of high polishing speeds and very flexible float system used [8]. The low loads used (1 N/ball), while causes microcracking by cleavage, is small enough as to not cause larger cracks, or dislodge grains by grain pullout.

7.2. Chemo–mechanical polishing

The mechanism of material removal in the final stages of polishing by softer cerium oxide is due to CMP. Thermal analysis of flash temperature and flash duration [18] as well as thermodynamic studies of the polishing process strongly suggest the possibility of CMP of Si_3N_4 by CeO_2 [19]. The details of the chemo–mechanical action of the CeO_2 abrasive with the Si_3N_4 balls will be the subject of a subsequent publication. Under the mechanical frictional action during polishing, chemical reactions can be initiated between the Si_3N_4 balls and the CeO_2 abrasive in the presence of water (from the water based magnetic fluid) and the material is removed by the chemical dissolution of material resulting in a reaction product that is subsequently removed by the mechanical action of the abrasive. Since the hardness of CeO_2 abrasive is $\approx 1/3$ of Si_3N_4 workmaterial, it can hardly scratch or damage it and the material is removed by tribological interaction forming a reaction product. Thus, tribochemical action instead of mechanical fracture is credited here for the extremely smooth and damage-free surfaces accomplished on the Si_3N_4 balls.

It has been suggested [7] that magnetic fluid grinding is more likely to replace the roughing stage of finishing than the final polishing stage. We have clearly demonstrated in this investigation that MFP can replace completely (both roughing and finishing) the conventional polishing starting from the as-received balls and completely finish them to the final specifications in the same apparatus. The methodology for finishing Si_3N_4 balls by MFP is presented for the first time in this paper that involves actual finishing time an order or magnitude or more faster than conventional polishing.

8. Conclusions

(1) Magnetic float polishing (MFP) combining mechanical and CMP is an efficient and cost effective manufacturing technology for producing high quality Si_3N_4 balls for bearing applications due to high polishing speed, small and controlled polishing force, flexible support, and chemo–mechanical action.

(2) There are three necessary stages for polishing, namely, initial roughing stage where the emphasis is on high material removal rate with minimal surface–subsurface damage, intermediate semi-finishing stage where material removal rate, sphericity, and surface roughness have to be closely monitored, and final finishing stage with emphasis is on the required size, sphericity, and finish.

(3) High material removal rates (1 μm/min) with minimal subsurface damage are possible using harder abrasives, such as B_4C or SiC due to rapid accumulation of minute amounts of material removed by mechanical microfracture at high polishing speeds and low loads in the MFP process. Although material removal is by brittle fracture, it occurs on a microscale due to low polishing force, flexible float system, and fine abrasives. The cracks generated are localized and suppressed from propagating into microcracks. Consequently, subsurface damage is minimized leading to the higher strength of the workmaterial and reliability of the parts in service.

(4) An advantage of the magnetic float polishing apparatus used in this investigation is that it is capable of finishing a small batch (10–20 balls) to the finished requirements without the need for sorting them from a large batch of balls or use different equipment as in conventional lapping. Such an apparatus would be beneficial especially when small batches are needed for specific low volume applications or for evaluation of materials in the development of new materials for bearing applications.

(5) MFP can be a cost effective process for finishing Si_3N_4 balls for bearing applications. The semifinishing and finishing stages can be accomplishing in about 4 h. The roughing stage depends on the amount of material to be removed from the as-received condition to the final requirements. In any case, a batch of balls can be finished in ≈ 16 to 20 h compared to several weeks by conventional polishing. Also, diamond abrasive is not required for the process. Faster polishing times and use of abrasives other than diamond would significantly reduce the overall costs of manufacture of Si_3N_4 balls for bearing applications. Also, the implementation of this technology would not be very capital intensive as it can be used by modifying the existing equipment. Attempts are currently underway to increase the batch size to finish about a hundred balls per batch with the next generation equipment.

(6) The CMP depends on the polishing conditions used, abrasive–workmaterial combination, and the environment. CeO_2 is found to be the most effective abrasive (superior to even Cr_2O_3) in the CMP of Si_3N_4 balls yielding a damage-free surface with a finish of $R_a < 4$ nm and $R_t < 0.04$ μm.

Also, it is possible that some of the ion species formed with CeO_2 abrasive can be much more safer than those with Cr_2O_3 from an environmental point of view, which will be discussed in more detail in a subsequent publication.

Acknowledgements

This project is sponsored by grants from the National Science Foundation on 'Tribological Interactions in Polishing of Advanced Ceramics and Glasses,' (CMS-9414610), 'Design, Construction, and Optimization of Magnetic Field Assisted Polishing', (DMI-9402895), and DoD's DEPSCoR Program on 'Finishing of Advanced Ceramics' (DAAH04-96-1-0323). This project was initiated by an ARPA contract on 'Ceramic Bearing Technology Program' (F33615-92-5933). Thanks are due to Drs. J. Larsen Basse, B.M. Kramer, Ming Leu, and J. Lee of NSF and Dr. K.R. Mecklenburg of WPAFB and Dr. W. Coblenz of ARPA for their interest and support of this work. Thanks are also due to Dr. M. Raghunandan, a former graduate student at OSU, for his contributions to the research carried out at OSU.

References

[1] Y. Tani, K. Kawata, Development of high-efficient fine finishing process using magnetic fluid, Ann. CIRP 33 (1984) 217–220.
[2] N. Umehara, K. Kato, Principles of magnetic fluid grinding of ceramic balls, Appl. Electromagn. Mater. 1 (1990) 37–43.
[3] N. Umehara, Magnetic fluid grinding—a new technique for finishing advanced ceramics, Ann. CIRP 43 (1) (1994) 185–188.
[4] T.H.C. Childs, H.J. Yoon, Magnetic fluid grinding cell design, Ann. CIRP 41 (1) (1992) 343–346.
[5] T.H.C. Childs, D.A. Jones, S. Mahmood, K. Kato, B. Zhang, N. Umehara, Magnetic fluid grinding mechanics, Wear 175 (1994) 189–198.
[6] T.H.C. Childs, S. Yoon, H.J. Mahmood, The material removal mechanism in magnetic fluid grinding of ceramic ball bearings, Proc. IME (Lon) 208 (B1) (1994) 47–59.
[7] T.H.C. Childs, S. Mahmood, H.J. Yoon, Magnetic fluid grinding of ceramic balls, Tribol. Int. 28 (6) (1995) 341–348.
[8] M. Raghunandan, A. Noori-Khajavi, N. Umehara, R. Komanduri, Magnetic float polishing of advanced ceramics, Trans ASME, J. of Manuf. Sci. + Eng., 119 (1996) 521–528.
[9] N. Umehara, R. Komanduri, Magnetic fluid grinding of HIP-Si_3N_4 rollers, Wear 192 (1996) 85–93.
[10] R.E. Rosensweig, Ferrodynamics, Cambridge Univ. Press, New York, 1985.
[11] N. Yasunaga, N. Tarumi, A. Obara, O. Imanaka, Mechanism and application of the mechanochemical polishing method using softer Powder, in: B.H. Hockey, R.W. Rice (Eds.), Science of Ceramic Machining and Surface Finishing—II, NBS Special Publications No. 562, 1979, p. 171.
[12] T.E. Fischer, Tribochemistry, Ann. Rev. Mater. Sci. 18 (1988) 303–323.
[13] R. Komanduri, N. Umehara, M. Raghunandan, On the possibility of chemo–mechanical action in magnetic float polishing of silicon nitride, Trans. ASME J. Tribol. 118 (1996) 721–727.
[14] S.R. Bhagavatula, R. Komanduri, On chemo–mechanical polishing of silicon nitride with chromium oxide abrasive, Philos. Mag. A 74 (4) (1996) 1003–1017.
[15] B.T. Kilbourn, Cerium—A Guide to Its Role in Chemical Technology, Molycorp, White Plains, NY, 1992.
[16] S.R. Hah, T.E. Fischer, C. Burk, Ceramic bearing development—tribochemical finishing of silicon nitride, Vol. 4, Technical Report No. WL-TR-96-4018, The Materials Directorate, Wright Patterson AFB OH, March 1995.
[17] R.G. Reddy, R. Komanduri, On the nature of chemical species in chemo–mechanical polishing of Si_3N_4 balls with Cr_2O_3 abrasive in magnetic float polishing (MFP), manuscript under preparation, 1997.
[18] Z.B. Hou, R. Komanduri, Magnetic Field Assisted Polishing: Part I. Thermal Model, ASME Trans. J. of Tribology (in press), 1997.
[19] M. Jiang, R. Komanduri, On the Chemo–mechanical Polishing (CMP) of Si_3N_4 Bearing Balls with CeO_2, submitted for publication, 1997.

APPENDIX C

ON THE CHEMO-MECHANICAL POLISHING OF Si_3N_4 BEARING BALLS WITH VARIOUS ABRASIVES

Ming Jiang, N. O. Wood, and R. Komanduri

Wear, 220 (1998) 59-71

ELSEVIER

Wear 220 (1998) 59–71

WEAR

On chemo-mechanical polishing (CMP) of silicon nitride (Si_3N_4) workmaterial with various abrasives

Ming Jiang [a], Nelson O. Wood [b], R. Komanduri [a,*]

[a] *Mechanical and Aerospace Engineering, Oklahoma State University, Stillwater, OK 74078, USA*

[b] *TASC, Midwest City, OK 73130, USA*

Received 17 February 1998; accepted 5 June 1998

Abstract

Chemo-mechanical polishing (CMP) studies were conducted using various abrasives [boron carbide (B_4C), silicon carbide (SiC), aluminium oxide (Al_2O_3), chromium oxide (Cr_2O_3), zirconium oxide (ZrO_2), silicon oxide (SiO_2), cerium oxide (CeO_2), iron oxide (Fe_2O_3), yttrium oxide (Y_2O_3), copper oxide (CuO), and molybdenum oxide (Mo_2O_3)] to investigate their relative effectiveness in the finishing of uniaxially pressed Si_3N_4 bearing balls by magnetic float polishing (MFP) technique. CMP depends both on the chemical and the mechanical effectiveness of the abrasive and the environment with respect to the workmaterial. Among the abrasives investigated for CMP of Si_3N_4 balls, CeO_2 and ZrO_2 were found to be most effective followed by Fe_2O_3 and Cr_2O_3. Extremely smooth and damage-free Si_3N_4 bearing ball surfaces with a finish R_a of ≈ 4 nm and R_t of ≈ 40 nm were obtained after polishing with either CeO_2 or ZrO_2. Thermodynamic analysis (Gibb's free energy of formation) indicated the feasibility of the formation of SiO_2 layer on the surface of the Si_3N_4 balls with these abrasives. This is particularly so in a water environment which facilitates chemo-mechanical interaction between abrasive and workmaterial by participating directly in the chemical reaction leading to the formation of a softer SiO_2 layer. Since the hardness of some of the abrasives which were found to be most effective in CMP, namely, CeO_2, ZrO_2, and Fe_2O_3 is closer to that of SiO_2 layer but significantly lower than the hardness of the Si_3N_4 workmaterial, removal of the SiO_2 reaction layer effectively without scratching and/or damaging the Si_3N_4 substrate is facilitated by the subsequent mechanical action of the abrasives. The chemical reaction would proceed on a continuing basis only if the passivating layers are removed continuously by subsequently mechanical action. It was found that the CMP ability in an oil-based polishing environment to be rather limited. A mechanism similar to the CMP of Si_3N_4 may be applicable to the polishing of silicon wafers, various glasses, and SiC due to similarities in the material removal processes.

Keywords: Chemo-mechanical polishing (CMP); Silicon nitride; Polishing; Magnetic float polishing (MFP); Ceramic bearings

1. Introduction

A critical factor affecting the performance and reliability of ceramics for bearing applications is the quality of the resulting surface after final polishing. It is well known that ceramics are extremely sensitive to surface defects resulting from grinding and polishing processes owing to their high hardness and inherent brittleness. Since fatigue failure of ceramics is driven by surface imperfections, it is paramount that the quality and finish of the ceramic bearing elements be superior with minimal defects so that reliability in performance of bearings in service can be achieved.

When polishing advanced ceramics, such as Si_3N_4 balls by magnetic float polishing (MFP) with harder abrasives, such as B_4C (#500) or SiC (#400) high material removal rates (1 μm/min) can be obtained with minimal subsurface damage due to the use of a flexible support system, small polishing force (~1 N/ball), and fine abrasives but high polishing speed compared to conventional polishing [1,2]. Higher material removal results from the rapid accumulation of minute amounts of material by microfracture of Si_3N_4 workmaterial [1] because of the high polishing speeds and light loads used in MFP. In contrast, in conventional polishing high loads and low polishing speeds lead to large radial and circumferential cracks that results in the formation of pits.

In mechanical polishing, wherein the abrasive is harder than the workmaterial, although the surface defects can be minimized by using very fine grain abrasives, they cannot altogether be eliminated. For example, the best surface finish that was obtained on a uniaxially pressed Si_3N_4 ball by MFP with a finer, harder abrasive, namely, B_4C abrasive (1–2 μm) was ~20 nm R_a and ~200 nm R_t. Similarly, the best surface

* Corresponding author. Tel.: +1-405-744-5900; Fax: +1-405-744-5720; E-mail: ranga@master.ceat.okstate.edu

0043-1648/98/$ - see front matter
PII S0043-1648(98)00245-2

finish obtained using another finer, harder abrasive, namely, SiC abrasive (1 μm) was ~15 nm R_a and ~150 nm R_t [2]. It may be noted that as the hardness differential between the abrasive and the workmaterial decreases, the removal rate decreases but the surface finish (especially R_t) improves. This, of course, depends on the material of the abrasive and its grain size. The R_t value, in general, is an indication of the surface defects such as microchipping on the workmaterial in the case of brittle workmaterials. To produce extremely smooth and damage-free surfaces, further polishing has to be carried out preferably involving chemo-mechanical polishing (CMP). Detailed review of the CMP was covered elsewhere [3] and may be referred to for details. Here some of the salient points will be presented.

CMP can be used to finish hard, brittle workmaterials with extremely smooth and damage-free surfaces [4]. CMP depends on both chemical and mechanical effectiveness of the abrasive and the environment with respect to the workmaterial. This process is considered tribochemical polishing when there is absolutely no mechanical action [5]. In CMP, the selected abrasive is softer or nearly of the same hardness as the workmaterial. Hence, damage due to mechanical action is minimized or eliminated. Chemical reactions are formed between the workmaterial, the abrasive, and the environment under the conditions of polishing. The reaction products so formed are removed from the workmaterial by subsequent mechanical action of the abrasives.

Wang and Hsu [6] concluded that the formation of a thin, soft layer of the reaction product (usually less than 100 Å thick) results in the easy removal of hard workmaterial without directly abrading the surface. High material removal rates (perhaps not as high as in mechanical abrasion but ≈10% of it) and minimal surface damage can be achieved by the formation of softer surface layers. Chemo-mechanical polishing was first demonstrated by Yasunaga et al. [4] for polishing single crystal silicon using a soft abrasive (barium carbonate, $BaCO_3$). Later, Vora et al. [7] and Vora and Stokes [8] reported the feasibility of polishing Si_3N_4 to a high level of finish by CMP with Fe_2O_3 and Fe_3O_4 abrasives. Suga et al. [9] polished Si_3N_4 using $CaCO_3$, MgO, SiO_2, Fe_2O_3 and Fe_3O_4, and Cr_2O_3 abrasives. They concluded that Cr_2O_3 was the most suitable abrasive for the CMP of Si_3N_4. Kikuchi et al. [10,11] also found Cr_2O_3 to be a suitable abrasive for polishing Si_3N_4.

Bhagavatula and Komanduri [12] studied the mechanism of material removal in the finishing Si_3N_4 balls with Cr_2O_3 abrasive by analysing the wear debris generated during polishing using a scanning electron microscope (SEM) with an energy-dispersive X-ray microanalyser (EDXA) and a low-angle X-ray diffraction apparatus. Prior to their investigation, Cr_2O_3 has been identified by other researchers [11] as a catalyst rather than its direct involvement in the chemical reactions with Si_3N_4. Bhagavatula and Komanduri, based on the experimental evidence, showed that the role of Cr_2O_3 was more than that of a mere catalyst as it plays an active role in the chemical reaction with Si_3N_4 forming chromium silicate (Cr_2SiO_4) and chromium nitride (CrN). Till recently, Cr_2O_3 was considered as the most effective abrasive for CMP of Si_3N_4. The best finish reported was 16.6 nm R_a and ~0.54 μm R_t). This is due to some surface damage that can still be seen with this abrasive due to its mechanical action, in spite of its outstanding chemo-mechanical polishing ability. This is because its hardness is nearly the same or slightly more than that of Si_3N_4 [1]. Also, some of the chemical species formed by the reaction of Cr_2O_3 with Si_3N_4 workmaterial during CMP can be environmentally not acceptable and special care may have to be exercised for the disposed of the fluid.

CMP depends on both chemical and mechanical effectiveness of the abrasive in relation to the workmaterial and the environment under the conditions of polishing [13]. Since material removal from Si_3N_4 workmaterial by this mechanism would not depend on the hardness of the abrasive but on the chemical potentials and removal of the reaction layer, it is possible to remove material by abrasives substantially softer than the workmaterial. Chemo-mechanical action is thus very specific in that proper choice of the abrasive and the environment should be made for a given workmaterial. For efficient removal of material, those that facilitate chemical reactions and efficient mechanical removal would be preferable for CMP. Both thermodynamics and kinetics play an important role on the rates of chemical reactions. Once the reaction products are formed they should be removed effectively from the workmaterial by subsequent mechanical action of the abrasive.

This paper presents the results of a systematic investigation of the CMP of a uniaxially pressed Si_3N_4 balls with various abrasives. The abrasives considered include boron carbide (B_4C), silicon carbide (SiC), aluminium oxide (Al_2O_3), chromium oxide (Cr_2O_3), zirconium oxide (ZrO_2), silicon oxide (SiO_2), cerium oxide (CeO_2), iron oxide (Fe_2O_3), yttrium oxide (Y_2O_3), copper oxide (CuO), and molybdenum oxide (Mo_2O_3). The purpose is to determine the most suitable and effective abrasive as well as the environment to finish Si_3N_4 balls with extremely smooth and damage-free surfaces for highly reliable performance in such applications as aircraft engine bearings, high-speed spindle bearings. The surface finish obtained on the Si_3N_4 balls after CMP by various softer abrasives using MFP technique is reported. The dual role of chemical and mechanical actions in CMP are elucidated. Thermodynamic feasibility of the chemical reactions formed between the abrasive and workmaterial are investigated based on Gibb's free energy change. The flash temperature generated and the flash duration at the contact zone of the polishing process was calculated using the models developed by Hou and Komanduri [14,15] to determine the temperatures for the thermodynamic analysis of the chemical reactions during CMP. The chemical reactions would proceed on a continuing basis only if the passivating layers are removed by the subsequent mechanical action. The kinetic action, which involves the removal of the reaction products from the interface is thus critical to CMP. A discussion of

CMP mechanism for polishing Si_3N_4 with various abrasives is presented based on thermodynamic and kinetic analyses.

2. Magnetic float polishing and experimental set-up

Conventional grinding and polishing processes used for finishing ceramic balls (by V-groove lapping) are basically similar to the methods used for making steel balls for bearing applications. The polishing or lapping process uses low polishing speeds (50 rpm), high loads (10 N/ball), and diamond abrasive. In practice, it takes considerable time (some 3–4 months) to finish a batch of ceramic balls depending on the size and accuracy requirements of the balls and the available technology. The long processing time and the use of expensive diamond abrasives result in high processing costs. Furthermore, the use of diamond abrasives at high loads can result in surface damages such as deep pits, scratches, and microcracks and subsurface damages such as the larger lateral and radial/median cracks. These surface defects may bring about catastrophic failure of silicon nitride balls by the propagation of larger brittle fracture. To minimize the surface damage, 'gentle'/'flexible' grinding and polishing conditions are required, namely, a low level of controlled load and abrasives not much harder than the workmaterial. Higher removal rates and shorter polishing cycles are obtained by high polishing speeds. This is accomplished in this study by a new and effective process known as magnetic float polishing (MFP) [16–23]. The material removal rate in magnetic float polishing is ~50 times higher than in conventional V-groove lapping owing to higher polishing speed (1000–10,000 rpm) used in magnetic float polishing compared to lapping (50 rpm). Furthermore, in MFP, the damage on the surface and subsurface on the polished ceramic balls can be minimized by the application of very low polishing loads (1 N/ball), flexible support system, and abrasives other than diamond in the initial mechanical polishing and subsequent chemo-mechanical polishing to obtain the best finish.

The magnetic float polishing technique is based on the magneto-hydrodynamic behavior of a magnetic fluid that can float non-magnetic float and abrasives suspended in it by a magnetic field. The forces applied by the abrasive on the ceramic balls are extremely low (1 N/ball) and highly controllable. A bank of permanent magnets (Nd–Fe–B) are arranged alternate N and S below an aluminum chamber filled with the required amount of magnetic fluid and appropriate abrasive (5–10% by volume). When a magnetic field is applied, the magnetic particles in the magnetic fluid are attracted downward to the area of higher magnetic field and an upward buoyant force is exerted on all non-magnetic materials to push them to the area of lower magnetic field. The abrasive grains and the acrylic float inside the chamber, all being non-magnetic materials, are levitated by the magnetic buoyant force. The ceramic balls are carried by the acrylic float. The drive shaft is fed down to contact with the balls (3-point contact) and presses them down to reach the desired force or height. The balls are polished by the abrasive grains under the action of the magnetic buoyancy levitational force when the spindle rotates. The function of acrylic float is to produce uniform, larger polishing pressure. An urethane rubber sheet is glued to the inner guide ring to protect it from wear. The material of the drive shaft is austenitic stainless steel (a non-magnetic material). The polishing shaft was driven by a high-speed, high-precision air bearing spindle (PI Spindle) with a stepless speed regulation up to 10,000 rpm. Details of the experimental set-up are given elsewhere [1] (Fig. 1).

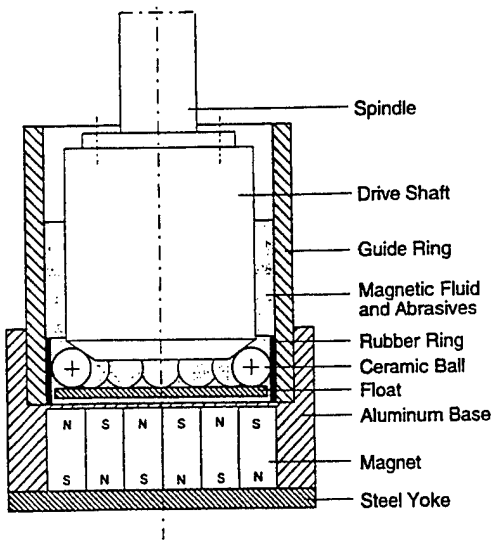

Fig. 1. Schematic of the magnetic float polishing apparatus used for polishing Si_3N_4 balls.

3. Experimental procedure and polishing conditions

Tables 1 and 2 give the chemical composition and the mechanical and thermal properties of the Si_3N_4 workmaterial (NBD-200 uniaxially pressed Si_3N_4 balls: β-Si_3N_4 with ~1 wt.% MgO as a sintering aid) used in this investigation. Table 3 gives the properties of the various abrasives used in this investigation for their relative suitability for chemo-mechanical polishing Si_3N_4 balls for bearing applications. Table 4 lists the polishing conditions used for each test. There are two types of magnetic fluids, one an oil-based (EMG 909) and the other water-based (W 40, saturation magnetization at 25°C is 400 Gauss, viscosity at 27°C is 25 Cp). In this investigation both types are used to compare the effectiveness of the polishing environment. The initial surface finish of the workmaterial for each test was prepared by polishing with B_4C 1500 grit abrasive.

Table 1
Chemical composition of NBD-200 silicon nitride [28]

Al	C	Ca	Fe	Mg	O	Si_3N_4
≤0.5	≤0.88	≤0.04	≤0.17	0.6–1.0	2.3–3.3	97.1–94.1

Table 2
Mechanical and thermal properties of Si_3N_4 workmaterial [28]

Property	Value
Flexural strength (MPa)	800
Weibull modulus	9.7
Tensile strength (MPa)	400
Compressive strength (GPa)	3.0
Hertz compressive strength (GPa)	28
Hardness, Hv (10 kg) (GPa)	16.6
Fracture toughness, K_{1c} (MN $m^{-3/2}$)	4.1
Density (g/cm^2)	3.16
Elastic modulus (GPa)	320
Poisson's ratio	0.26
Thermal expansion coefficient at 20–1000°C ($°C^{-1}$)	2.9×10^{-6}
Thermal conductivity at 100°C (W/m K)	29
Thermal conductivity at 500°C (W/m K)	21.3
Thermal conductivity at 1000°C (W/m K)	15.5

Table 3
Properties of various abrasives

Abrasive	Density (g/cm^3)	Hardness	
		Mohs	Knoop (kg/mm^2)
Boron carbide (B_4C)	2.52	9.3	3200
Silicon carbide (SiC)	3.22	9.2	2500
Aluminium oxide (Al_2O_3)	3.98	9	2150
Chromium oxide (Cr_2O_3)	5.21	8.5	1800
Zirconium oxide (ZrO_2)	5.85	8	1200
Silicon oxide (SiO_2)		7	820
Cerium oxide (CeO_2)	7.13	6	–
Iron oxide (Fe_2O_3)	5.24	6	–
Yttrium oxide (Y_2O_3)	5.01	5.5	700
Copper oxide (CuO)	6.32	3.5	225
Molybdenum oxide (Mo_2O_3)	4.69	1.5	–

Table 4
Test conditions

Workmaterial	Uniaxially pressed Si_3N_4 balls (CERBEC 200) Initial diameter: 12.7 mm (0.5 inch) Initial sphericity: 1 μm
Abrasive concentration	10% by volume
Polishing load	1.25 N/ball
Polishing speed	2000 rpm
Magnetic fluid	Oil-based (EMG 909), water-based (W 40)

As previously pointed out, the CMP depends on the chemo-mechanical interaction of the abrasive, workmaterial, and the environment. The pH value and the conductivity of the polishing fluid (magnetic fluid + abrasive) would influence the surface finish and material removal rate in CMP as the polishing fluid is part of the electrolytic cell. In this investigation, the pH and conductivity values of the polishing environment were measured using Cole-Parmer pH/temperature meter and TDS-conductivity/temperature meter, respectively.

The magnetic field was measured using a Gauss/Tesla meter. The polishing load was set up by measuring the normal force with a Kistler's piezoelectric dynamometer connected to a charge amplifier and a display. To calculate the material removal rates, the weight reduction in the balls was determined by measuring the weight before and after polishing at every stage of the test using a precision balance. The surface finish of the polished balls was measured using a Form TalySurf 120 L (cut-off: 0.8 mm and 0.25 mm, evaluation length: 6 consecutive cut-off, Filter: ISO 2CR). The roundness of the balls was measured using TalyRond 250 (cut-off: 50 upr, Filter: 2CR).

CMP would depend on the availability for a short duration of certain threshold pressure/contact stress and temperature at the contact zone of the polishing process [4]. The flash temperature and the flash duration generated at the contact zone of the polishing process enable chemical reaction products to form by the interaction between the abrasive, workmaterial, and the environment. In this investigation the flash temperatures and the corresponding flash time generated at the contact zone under the conditions of polishing with the most effective abrasive were calculated based on a moving disc heat source model developed by Hou and Komanduri [14,15].

Thermodynamic analysis (Gibb's free energy change, ΔG) was conducted to determine the reaction products that could be formed and whether such reactions are thermodynamically feasible [24]. It is well known that for a reaction to occur spontaneously at a given temperature and pressure, $\Delta G < 0$. Equilibrium composition and ΔG are calculated using the Outokumpu HSC Chemistry Software package developed in Finland. A discussion of the CMP mechanism for polishing Si_3N_4 with various abrasives is presented based on thermodynamic and kinetic analyses.

4. Test results

Table 5 summarizes the average surface finish obtained from polishing Si_3N_4 balls by various abrasives used in this investigation. It may be noted that in each test, the surface of the Si_3N_4 balls is first polishing with B_4C 1500 grit abrasive for 45 min. This is followed by two additional polishings with a given abrasive for a period of time of 60 or 90 min to investigate if surface finish could be further improved. The corresponding TalySurf surface finish profiles are shown in Fig. 2(a)–(j). It can be seen from this data that ZrO_2 and CeO_2 are the most effective abrasives following by Fe_2O_3 and Cr_2O_3. Fig. 3(a) shows SEM micrograph of a Si_3N_4 ball surface after mechanical polishing with a fine B_4C abrasive (2 μm) in which material removal by brittle fractures can be seen clearly and Fig. 3(b) after CMP with CeO_2 abrasive indicating mostly smooth surface with very few shallow pits formed during the previous mechanical polishing by B_4C 1500 grit abrasive. It may thus be noted that the resulting surface finish obtainable by CMP should be affected by the

Table 5
Effect of each abrasive on surface finish

Abrasive type	Abrasive size (μm)	Test time (min)	Surface finish		Effectiveness
			R_a (nm)	R_t (μm)	
1. B_4C 1500	2	45	32	0.280	V. poor
Al_2O_3	5	60	46	0.377	
2. B_4C 1500	2	45	31	0.295	Poor
CuO	3	60	28	0.241	
CuO	3	90	27	0.240	
3. B_4C 1500	2	45	31	0.275	Poor
Y_2O_3	20	90	26	0.247	
Y_2O_3	20	60	23	0.244	
4. B_4C 1500	2	45	30	0.272	Poor
SiO_2	30	90	22	0.236	
SiO_2	30	60	22	0.244	
5. B_4C 1500	2	45	28	0.270	Poor
Mo_2O_3	20	60	22	0.216	
Mo_2O_3	20	90	18	0.205	
6. B_4C 1500	2	45	29	0.260	Good
Cr_2O_3	5	90	14	0.208	
Cr_2O_3	5	60	12	0.175	
7. B_4C 1500	2	45	30	0.274	Good
Fe_2O_3	3	60	13	0.186	
Fe_2O_3	3	90	9	0.167	
8. B_4C 1500	2	45	31	0.268	Excellent
CeO_2	5	60	16	0.172	
CeO_2	5	90	8	0.100	
9. B_4C 1500	2	45	29	0.286	Excellent
ZrO_2	5	60	18	0.174	
ZrO_2	5	90	8	0.126	

previous mechanical polishing. The depth of layers to be removed by CMP for smooth surface finish is at least equivalent to the surface roughness (peak-to-valley height, R_t) of the previous final mechanical polishing surface.

Table 6 gives the average surface finish obtained from polishing Si_3N_4 balls by ZrO_2 and CeO_2 abrasives after mechanical polishing with SiC abrasive (8000 grit). The corresponding TalySurf surface finish profiles are shown in Fig. 4(a)–(c). Surface finish R_a of ~4 nm and R_t of ~40 nm were obtained both for CeO_2 and ZrO_2 abrasives. Fig. 5 is an SEM micrograph of a Si_3N_4 ball surface after mechanical polishing with a fine SiC abrasive (8000 grit) (1 μm) followed by CMP with CeO_2 abrasive indicating extremely smooth surface with practically no surface defects. Since CeO_2 is significantly softer than Si_3N_4 workmaterial, material removal by direct mechanical action would be extremely difficult, if not impossible. Therefore, the mechanism of material removal must be due to chemo-mechanical action between the abrasive, the workmaterial, and the environment. Since material is removed by the tribochemical action instead of mechanical fracture, extremely smooth and damage-free surface can thus be obtained.

Table 7 gives a comparison of the average surface finish obtained from polishing of Si_3N_4 balls by CeO_2 abrasive with oil-based and water-based magnetic fluid. The corresponding TalySurf surface finish profiles are shown in Fig. 6(a)–(c). It may be noted that there is not much improvement between the initial surface finish Fig. 6(a) and the finish after polishing in an oil-based magnetic fluid [Fig. 6(b)] but the surface finish obtained in a water-based magnetic fluid [Fig. 6(c)] shows a significant improvement. It thus appears that water is essential for CMP of Si_3N_4 workmaterial. The electrical conductivity measurements of the water-based polishing environment (water-based magnetic fluid plus CeO_2 abrasive) gave values of specific conductivity of 4.8 mS/cm (S: Siemens or Mho) and the concentration of the total dissolved solids, (TDS) of 2.4 ppt. Both the specific conductivity and the concentration of the total dissolved solids, (TDS) of the oil-based polishing fluid plus CeO_2 abrasive gave zero values. For reference, it may be noted that the specific conductivity of good city water is 50 μS/cm. The oil film between abrasive and workmaterial may have prevented possible chemical reaction between the abrasive and the workmaterial as well as the removal of the reaction layer formed, if any, thus limiting chemo-mechanical polishing.

5. Discussion

CMP is particularly effective in water but in alcohols only when hydroxyl groups are present. During MFP of Si_3N_4 in a water-based magnetic fluid, due to the presence of water environment, NH_3 and SiO_2 are formed. Si_3N_4 can react (hydrolysis) with water from the water-based polishing fluid leading to the formation of SiO_2 and NH_3 (Eq. (2)). At higher temperature (>200°C) dissociation of NH_3 into $N_2(g)$ and $H_2(g)$ may result [Jiang and Komanduri, 1997c]. Kanno et al. [25] identified the formation of NH_3 during grinding of Si_3N_4 powder in water, thus establishing the hydrolysis of Si_3N_4. The thermodynamic analysis presented here strongly suggests the feasibility of this reaction (Eq. (2)). Fischer and Tomizawa [26], Tomizawa and Fischer [27], Hah et al. [28] also showed the formation of SiO_2 and NH_3 in tribochemical polishing of Si_3N_4. But the dissolution of SiO_2 and NH_3 (to silicilic acid $Si(OH)_4$ and ammonium hydroxide NH_4OH) as a second reaction to stimulate the continuation of tribochemical polishing of Si_3N_4 in aqueous solutions does not seem to be thermodynamically feasible from Gibbs free energy analysis [13]. Silica (SiO_2) in the amorphous state is almost insoluble or at best slightly soluble (100–150 ppm of solubility in a neutral solution at room temperature) [29]. The effectiveness of an abrasive for CMP depends on the feasibility of chemical reaction (thermodynamic analysis) with the workmaterial and the kinetic action involving the removal of the reaction product from the workmaterial. The actual material removal in CMP will depend on the kinetic action which removes the reaction products from the interface and the chemical reaction will continue only after the passivating layers are removed.

$$Si_3N_4 + 6H_2O \rightarrow 3SiO_2 + 4NH_3(g) \quad (1)$$

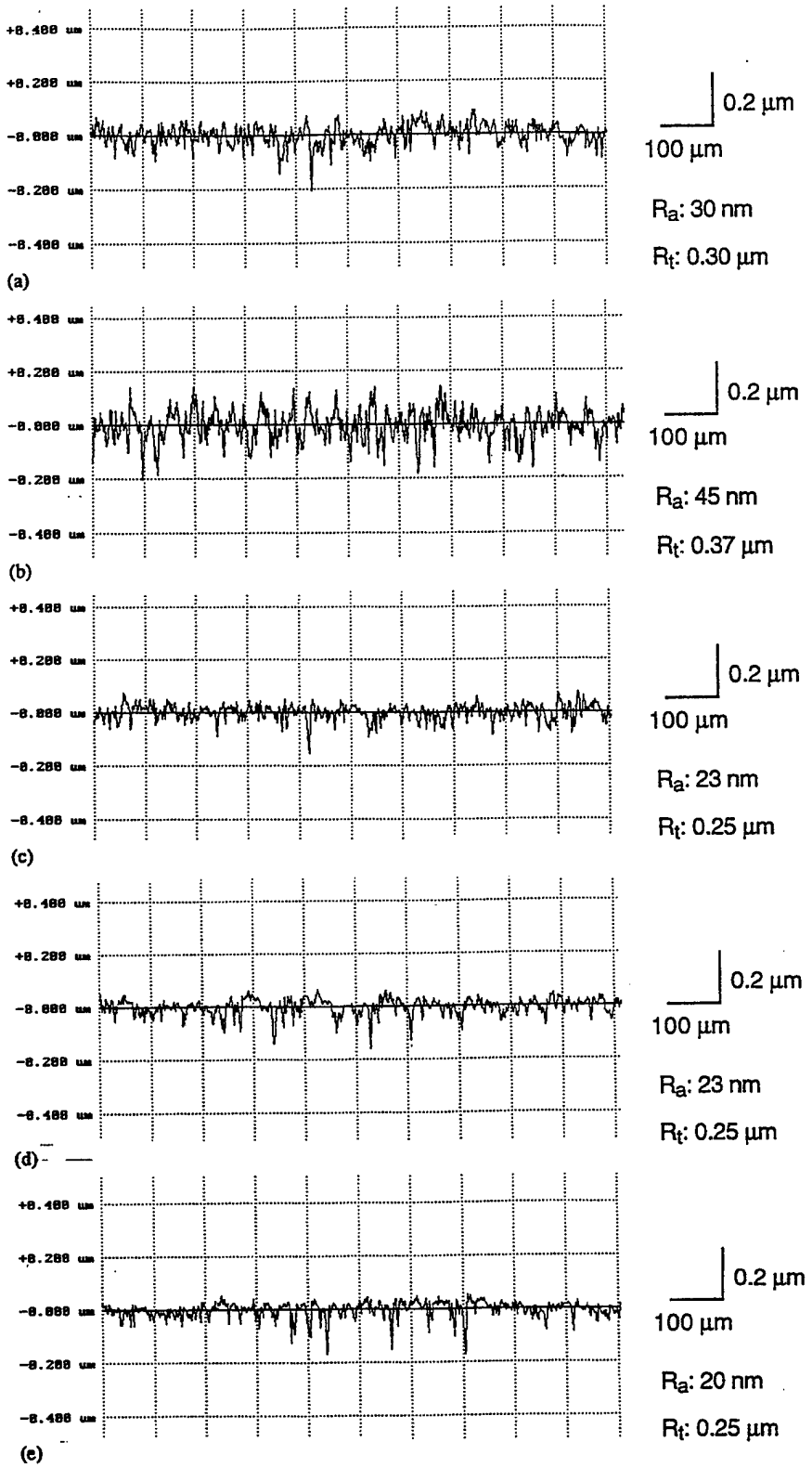

Fig. 2. *(continued)*

$$Si_3N_4+6H_2O\rightarrow 3SiO_2+2N_2(g)+6H_2(g) \quad (2)$$

when $T>200°C$

In CMP, material removal is accomplished by chemical reaction stimulated by frictional heat and the contact pressure at the contact area between the workmaterial and the abrasive.

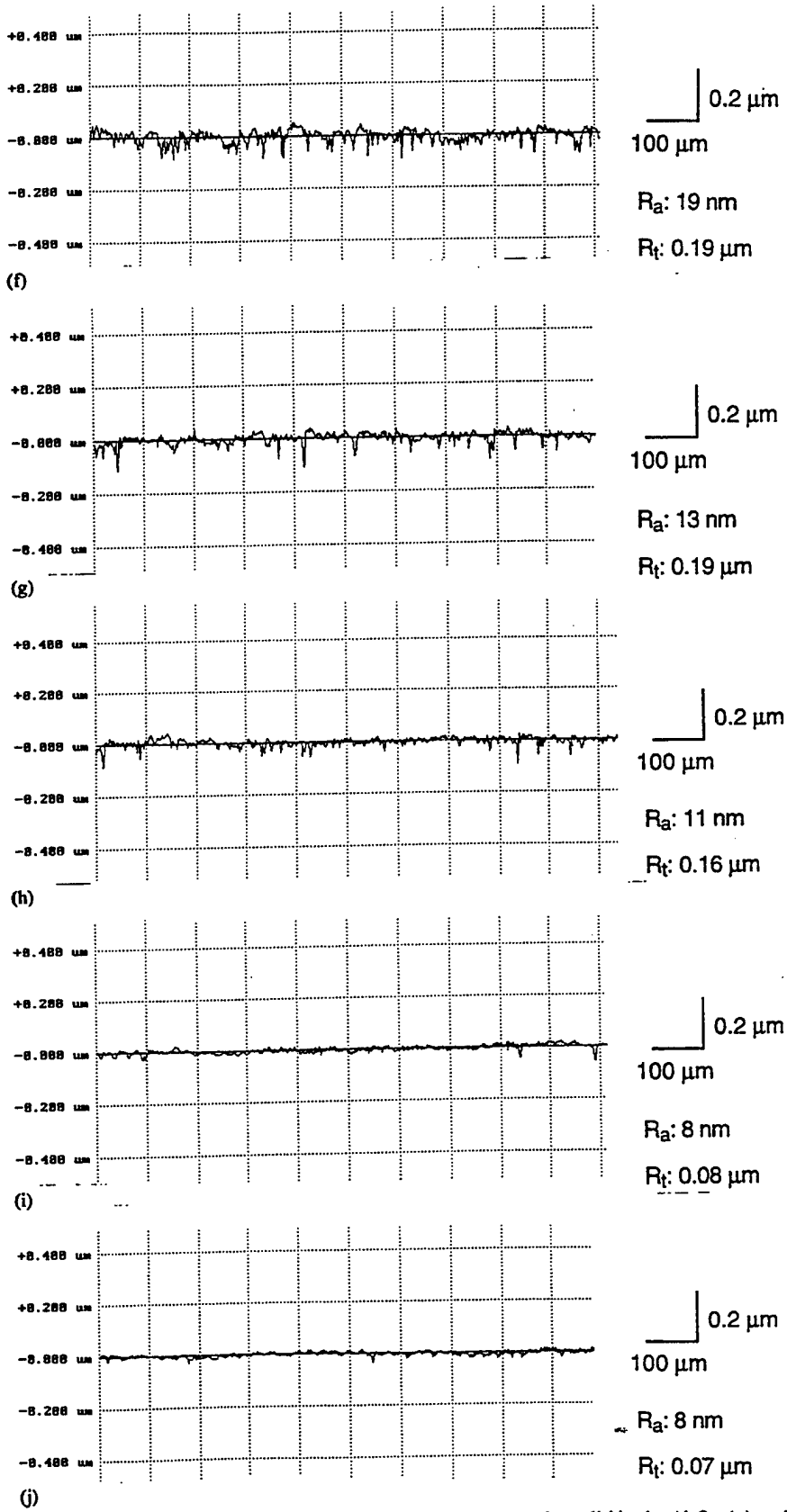

Fig. 2. (a) Initial surface finish prepared by polishing with B_4C (1500 grit), (b) surface finish after polishing by Al_2O_3, (c) surface finish after polishing by CuO, (d) surface finish after polishing by Y_2O_3, (e) surface finish after polishing by SiO_2, (f) surface finish after polishing by Mo_2O_3, (g) surface finish after polishing by Cr_2O_3, (h) surface finish after polishing by Fe_2O_3, (i) surface finish after polishing by CeO_2, (j) surface finish after polishing by ZrO_2.

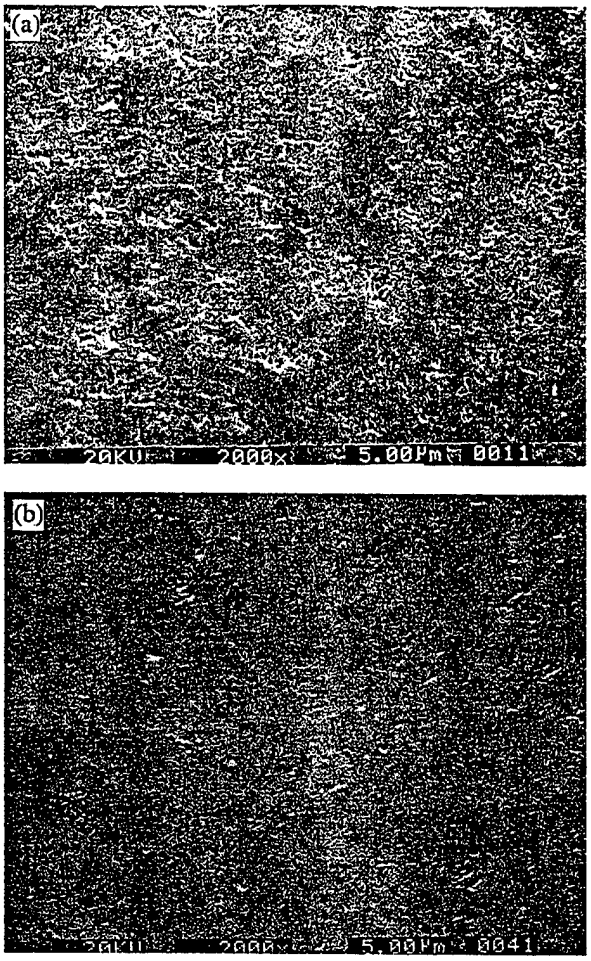

Fig. 3. (a) SEM micrograph of the surface of a Si_3N_4 ball finished by B_4C (1500 grit), (b) SEM micrograph of the surface of a Si_3N_4 ball finished by CeO_2.

Table 6
Surface finish after CMP

Abrasive type	Abrasive size (μm)	Test time (min)	Surface finish		Effectiveness
			R_a (nm)	R_t (μm)	
SiC 8000	1	60	15	0.15	Excellent
ZrO_2	5	120	4	0.04	
SiC 8000	1	60	15	0.15	Excellent
CeO_2	5	120	4	0.03	

The reaction layer is removal by subsequent mechanical action of the abrasive. Vora et al. [7] reported the feasibility of polishing Si_3N_4 to a good finish by CMP with Fe_2O_3 and Fe_3O_4 abrasives. An oxygen rich silicon oxynitride was reported to have been formed on the polished Si_3N_4 samples based on the Auger electron spectroscopy (AES) analysis. They concluded that oxidation is a possible mechanism causing CMP of Si_3N_4. Bhagavatula and Komanduri [12] found that chemical reactions between Cr_2O_3 and Si_3N_4 occur forming chromium silicate (Cr_2SiO_4) and chromium nitride (CrN). This was established by analysing the wear debris collected from polishing using a scanning electron microscope (SEM) with an energy-dispersive X-ray microanalyser (EDXA) and a low-angle X-ray diffraction (XRD) apparatus.

The following reaction products though not balanced here can be shown to be feasible thermodynamically based on the analysis of Gibb's free energy of formation of the chemical reactions between the Si_3N_4 workmaterial and various abrasives, namely, Fe_2O_3, Cr_2O_3, ZrO_2 and CeO_2:

$$Si_3N_4+Fe_2O_3\rightarrow SiO_2+FeO+FeSiO_3/FeO\cdot SiO_2+Fe_4N+N_2(g) \quad (3)$$

$$Si_3N_4+2Cr_2O_3\rightarrow 3SiO_2+4CrN \quad (4)$$

$$Si_3N_4+ZrO_2\rightarrow SiO_2+ZrSiO_4/ZrO_2\cdot SiO_2+ZrN+N_2(g) \quad (5)$$

$$Si_3N_4+CeO_2\rightarrow SiO_2+CeO_{1.72}+CeO_{1.83}+Ce_2O_3+N_2(g) \quad (6)$$

Here, two types of reactions are considered: (1) oxidation–reduction reaction, and (2) exchange reaction (exchange of both cationic and anionic, i.e., silicate, etc.). $Si_3N_4\rightarrow$ Si: SiO_2, SiO_4^{2-} and N: N^{3-}, $N_2(g)$, $NH_3(g)$. Chemical reactions with Si_3N_4 workmaterial are feasible thermodynamically with Fe_2O_3, Cr_2O_3, ZrO_2 and CeO_2 abrasives and water from the water-based magnetic fluid. SiO_2 is the main reaction product leaving the surface of Si_3N_4 workmaterial.

Based on the moving disc heat source model developed by Hou and Komanduri [14,15], the temperature field and flash temperatures generated at the contact zone in MFP with CeO_2 (elastic modulus: 180 GPa, thermal conductivity: 0.02 cal/cm s °C) are calculated as shown in Fig. 7. The related flash times at the area of contact under the polishing conditions are given in Table 8. It can be seen that the minimum possible flash temperatures generated and the corresponding flash times are adequate for the generation of specific reactions, such as oxidation, hydrolysis and exchange as shown in Table 9. It is known that for a reaction to occur spontaneously at a given temperature T, the Gibb's free energy change, ΔG should be negative.

CeO_2 is found to be the most effective abrasive for CMP of Si_3N_4 material and is particularly effective in water but in alcohols only when hydroxyl groups are present. CeO_2 abrasive can directly react chemically with Si_3N_4 workmaterial (oxidization–reduction reaction) leading to the formation of SiO_2 and $N_2(g)$ [Eq. (1)] as shown in Table 9. CeO_2 is stable only at low temperatures and will convert to $CeO_{1.72}$ and $CeO_{1.83}$ as the temperature is increased [30]. Further increase in temperature (>400°C) results in a decrease in the amounts of $CeO_{1.72}$ and $CeO_{1.83}$ and increase in the more stable form, namely, Ce_2O_3 at higher temperatures (>1000°C). The reactions involved in CMP of Si_3N_4 with CeO_2 in a water environment [Eq. (3)] are given in Table

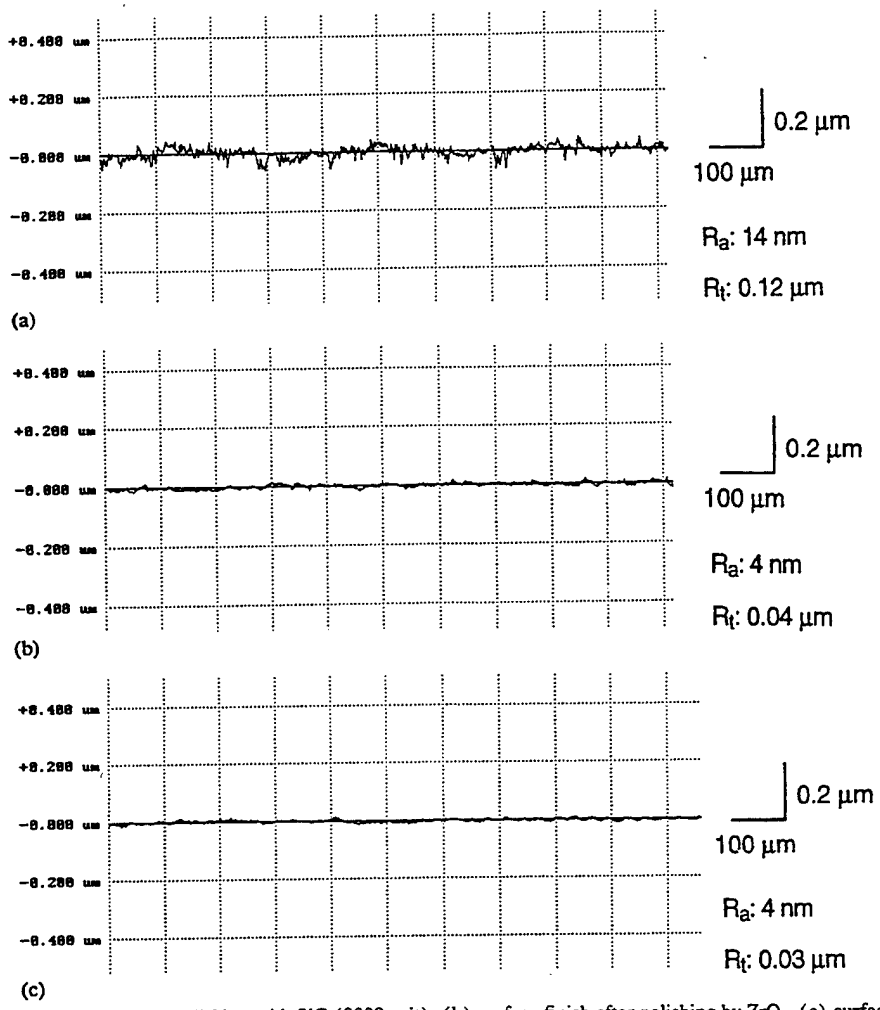

Fig. 4. (a) Initial surface finish prepared by polishing with SiC (8000 grit), (b) surface finish after polishing by ZrO_2, (c) surface finish after polishing by CeO_2.

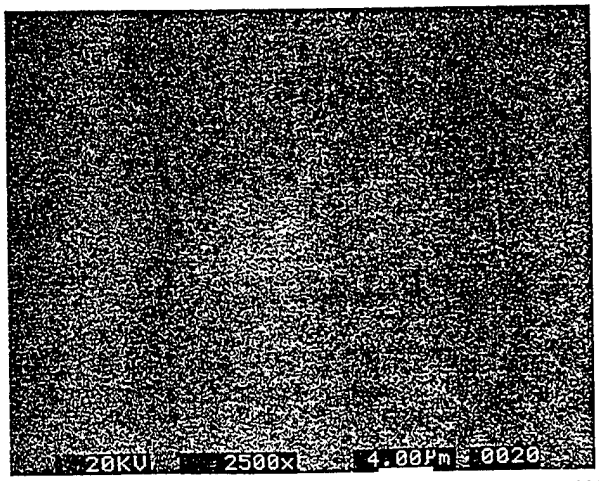

Fig. 5. SEM micrograph of the surface of a Si_3N_4 ball finished by SiC 8000 followed by CeO_2.

9. It has been shown that almost all the material removal is by chemo-mechanical action between the Si_3N_4 workmaterial and the CeO_2 polishing media in the water environment by the formation of SiO_2 reaction layer on Si_3N_4 and its subsequent removal by mechanical action by cerium oxide abrasive [13].

The kinetic action, which removes the reaction products from the interface is also a critical step in the CMP process. The chemical reaction can continue only after the passivating layers are removed by the subsequent mechanical action of the abrasive. It may be noted that the hardness of abrasives that are most suited for CMP of Si_3N_4, namely, Fe_2O_3, Cr_2O_3, ZrO_2 and CeO_2, is close to the SiO_2 layer but significantly lower (i.e., Fe_2O_3, ZrO_2 and CeO_2) than or close (i.e., Cr_2O_3)

Table 7
Surface finish after polishing with water-based and oil-based magnetic fluid

Abrasive type	Magnetic fluid	Test time (min)	Surface finish		Effectiveness
			R_a (nm)	R_t (μm)	
B_4C 1500	W 40	45	30	0.29	Poor
CeO_2 5 μm	EMG 40	60	26	0.24	
B_4C 1500	W 40	45	30	0.29	Excellent
CeO_2 5 μm	W 40	60	14	0.14	

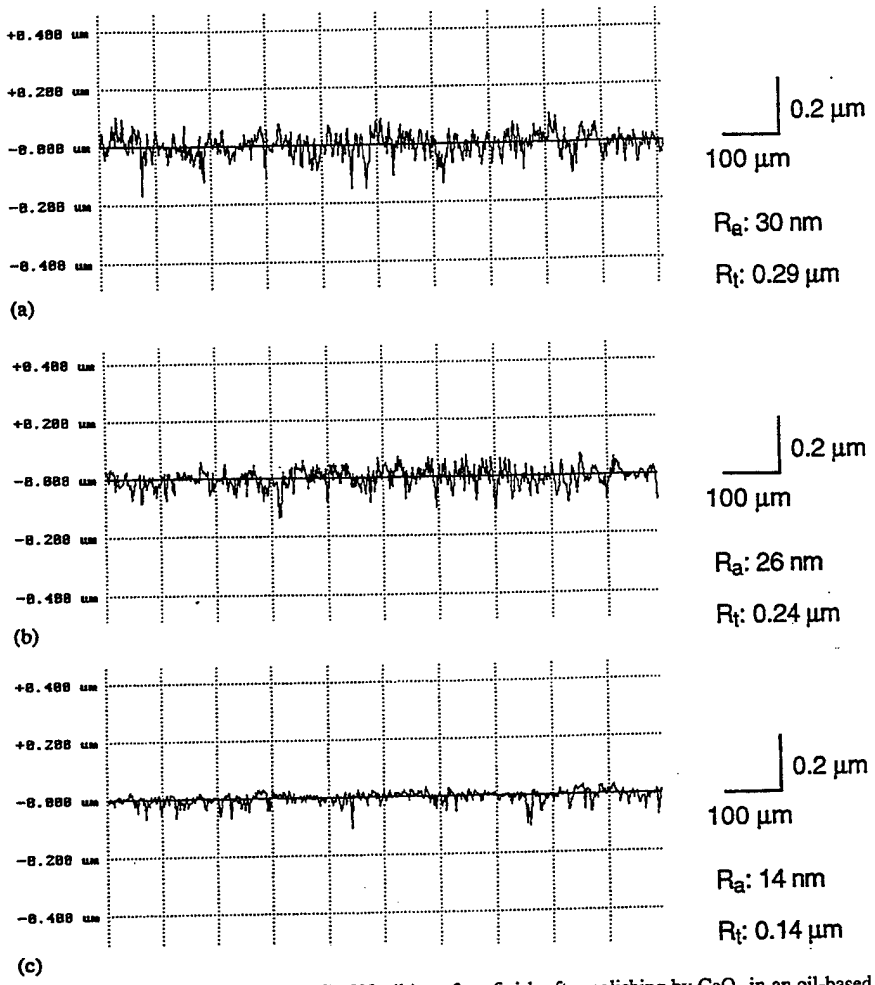

Fig. 6. (a) Initial surface finish prepared by polishing with B_4C 1500, (b) surface finish after polishing by CeO_2 in an oil-based magnetic fluid, (c) surface finish after polishing by CeO_2 in a water-based magnetic fluid.

to Si_3N_4 workmaterial. Thus, the Si_3N_4 workmaterial can hardly be scratched, or damaged by Fe_2O_3, ZrO_2 and CeO_2. Hence, SiO_2 reaction layers formed during chemical action are removed without damaging Si_3N_4 workmaterial by these abrasives.

In general, the hardness for best polishing abrasive for glasses (SiO_2) is ≈ 7 on the Moh's scale, which is very close to the hardness of SiO_2 [31]. The hardness of CeO_2, ZrO_2, and Fe_2O_3 abrasives is also close to this value. Cr_2O_3 (Mohs hardness 8.5) is harder compared to the hardness of the Si_3N_4 workmaterial for CMP. Wallace et al. [32] investigated the CMP of SiO_2 thin films using X-ray reflectivity. They concluded that stress-corrosion mechanism may be responsible whereby the stress induced by the abrasion of abrasive particle in water strains the bonds in the SiO_2 thin films. The polished material shows an increased density in the near-surface region. The compaction of the SiO_2 network leads to enhanced dissolution of SiO_2 into the polishing slurry and an extremely smooth surface.

It can be seen from the above results that the most effective abrasives for polishing Si_3N_4 workmaterial are CeO_2 and ZrO_2 following by Fe_2O_3 and Cr_2O_3. The pH of the polishing slurry used here (abrasives + water-based ferrofluid) ranges from 6 to 6.4 for all the abrasives used; for example, the pH of ZrO_2 + ferrofluid is ~ 6 and for CeO_2 + ferrofluid is ~ 6.2 except for MoO_2 which has a pH of ~ 5. It is found that SiO_2 abrasive has minimal polishing ability for Si_3N_4 in the pH range of 6 [Fig. 2(e)]. Also, the hardness of the most effective abrasives are CeO_2: Mohs 6, ZrO_2: Mohs 8, Fe_2O_3: Mohs 6, and Cr_2O_3: Mohs 8.5. These hardness values are closer to the SiO_2 reaction layer which has a Mohs hardness of ~ 7. It is somewhat coincidental that in general the chemical effectiveness and the mechanical hardness of abrasives for polishing *glass*, is also ≈ 6.5 Mohs which is close to the hardness of glass ($\sim$ Mohs 7).

There are other similarities between polishing Si_3N_4 workmaterial and polishing glass including the role of water. Cook [31] after a careful review and analysis of literature concluded that the best abrasives for polishing glasses are CeO_2 following by ZrO_2, ThO_2, TiO_2 and Fe_2O_3 in the pH range 7–9 and that SiO_2 abrasive has little polishing ability for finishing glasses except at very high pH ($\sim$ 12–14) values. This is not altogether surprising as the material removal mechanism in the case of Si_3N_4 is through the formation of

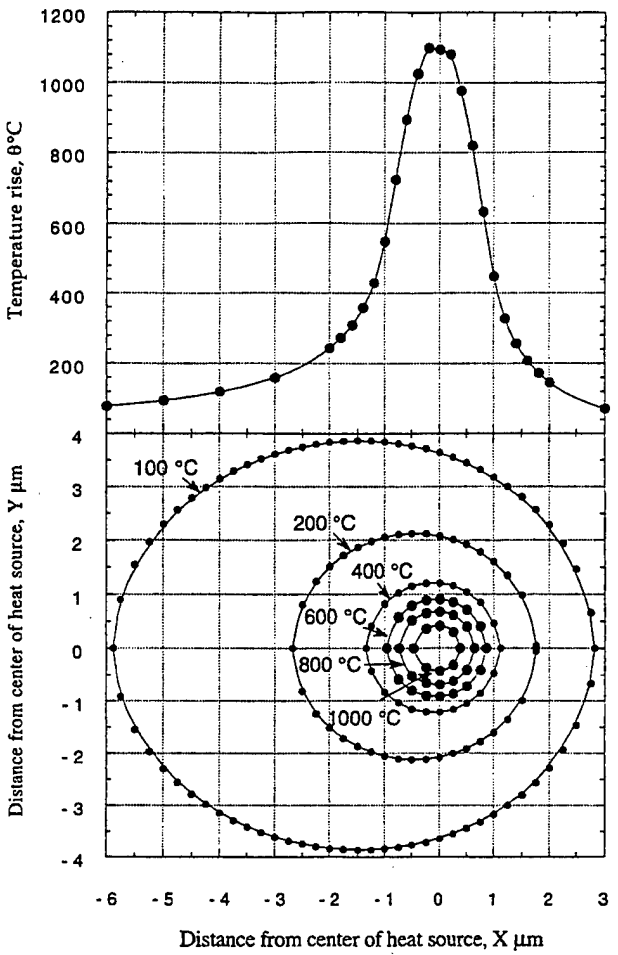

Fig. 7. (a) Calculated temperature rise on the surface along the X-axis, (b) isotherms of temperature on the work surface (W=1.25 N/ball, V=4 m/s).

Table 8
Flash time for different flash temperature (V=4 m/s, W=1.2 N/ball)

Flash temperature (°C)	>100	>200	>300	>400	>600	>800	>1000
Flash time (μs)	2.2	1.1	0.8	0.6	0.4	0.3	0.2

SiO_2 and in the case of glasses it is naturally SiO_2. A similar mechanism may be applicable for the polishing of silicon wafers with CeO_2, ZrO_2, and Fe_2O_3 in a water-based solution which are effective abrasives for polishing Si_3N_4 ceramics and SiO_2 glasses. So, it is not too surprising to note that the first mirror finished silicon wafers used for integrated circuits were polished with CeO_2 and Fe_2O_3 [33]. Currently, the most widely used abrasive for polishing silicon wafers is colloidal silica, i.e., nanocrystalline SiO_2 particles in an alkaline (KOH) solution (pH 10). This combination has an advantage of little or no decomposition on the surface of silicon wafers which has a natural oxidation layer of SiO_2 in air at room temperature. For epitaxial growth, the surface layer and subsurface lattice structure of the semiconducting wafers are

Table 9
Chemical reaction systems in a water-based CMP of Si_3N_4 with CeO_2

T (°C)	0	100	200	300	400	600	800	1000
(1) $Si_3N_4 + 35.294CeO_2 = 3SiO_2 + 35.294CeO_{1.83} + 2N_2(g)$								
ΔG (kcal)	−47.6	−61.7	−75.7	−89.8	−103.9	−132.9	−163.2	−195.1
(2) $Si_3N_4 + 6H_2O \triangleq 3SiO_2 + 4NH_3(g)$								
ΔG (kcal)	−132.7	−140.9	−147.4	−152.6	−156.4	−159.8	−156.9	−146.5
(3) $2Si_3N_4 + 35.294CeO_2 + 6H_2O = 6SiO_2 + 35.294CeO_{1.83} + 4NH3(g) + 2N_2(g)$								
ΔG (kcal)	−180.3	−202.6	−223.1	−242.4	−260.3	−292.7	−320.1	−341.6
(4) $2Si_3N_4 + 17.647CeO2 = 3Si_2N_2O + 17.647CeO1.83 + N_2(g)$								
ΔG (kcal)	−68.3	−67.6	−67.2	−66.9	−66.5	−65.0	−62.1	−57.5
(5) $Si_3N_4 + 1.5H2O = 1.5Si_2N_2O + NH_3(g)$								
ΔG (kcal)	−94.0	−95.6	−98.6	−102.4	−106.7	−116.5	−127.4	−139.4
(6) $Si_3N_4 + SiO_2 = 2Si_2N_2O$								
ΔG (kcal)	−46.8	−43.2	−40.5	−38.4	−36.5	−33.3	−30.5	−27.9
(7) $Si_3N_4 + 3O_2(g) = 3SiO_2 + 2N_2(g)$								
ΔG (kcal)	−460.7	−455.4	−450.3	−445.2	−440.2	−430.6	−421.3	−412.4

required to be free of any chemical change or sub-surface damage in the form of dislocation tangles. This is not the case with glasses and advanced ceramics (Si_3N_4) for optical and mechanical applications. However, SiO_2 layer on a silicon substrate is an excellent insulator and can be used for isolation and passivation purposes which is an advantage for Si for electronic application.

It is possible that an outer layer of SiO_2 and an intermediate silicon oxynitride may form between SiO_2 thin layer and Si_3N_4 substrate according to Eqs. (4)–(6) in the Table 9. The oxide scale on MgO uniaxially pressed Si_3N_4 forms in layers composed of amorphous and crystalline SiO_2, Si_2N_2O, and $MgSiO_3$ ($MgO.SiO_2$, from 1 wt.% MgO sintering additive) [34–36]. It is notable that Si_3N_4 is easily oxidized in an oxygen-containing atmosphere [37]. As a result, the surface of Si_3N_4 is always covered with a thin silica layer as shown by Eq. (6). CMP does not produce a layer that is chemically different from the natural oxidation layer formed in air at room temperature on the Si_3N_4 substrate [13]. It has been shown in this investigation that several not-so-hard oxides, such as CeO_2 and ZrO_2 following by Fe_2O_3 and Cr_2O_3 etc are effective abrasive for CMP of Si_3N_4 material. This is because of the thermodynamic feasibility of chemical reactions between the abrasive and the Si_3N_4 workmaterial but also due to the subsequent kinetic action of removing the reaction products from the Si_3N_4 workmaterial.

6. Conclusions

1. Chemo-mechanical polishing (CMP) depends not only on the polishing conditions but also on the interactions between the abrasive-workmaterial-environment. Among various abrasives investigated for CMP of Si_3N_4 bearing balls with magnetic float polishing (MFP) CeO_2 and ZrO_2 abrasives were found to be most effective followed by Fe_2O_3 and Cr_2O_3. It is also found that CMP of Si_3N_4 is particularly effective in a water-based fluid environment.

2. Thermodynamic analysis (Gibb's free energy of formation) indicated the feasibility of chemical reactions between CeO_2, ZrO_2, Fe_2O_3, and Cr_2O_3 abrasives and Si_3N_4 workmaterial leading to the formation a SiO_2 layer. Since the hardness of these abrasives are closer to that of SiO_2 layer and lower than Si_3N_4 workmaterial, SiO_2 reaction layer is effectively removed without damaging the Si_3N_4 substrate by the subsequent mechanical action by the abrasives on the workmaterial. The kinetic action, which removes the reaction products from the interface is critical in the CMP process. The chemical reaction will be continued only after the passivating layers are removed continuously by the subsequent mechanical action.

3. CeO_2 and ZrO_2 abrasives are found to be the very effective in the CMP of Si_3N_4 balls yielding an extremely smooth and damage-free surface with a finish R_a of 4 nm and R_t of 40 nm. CeO_2 and ZrO_2 are much softer than Si_3N_4 and could not cause any mechanical damage and scratching on the Si_3N_4 workmaterials. Cr_2O_3 is slightly harder compared to the Si_3N_4 workmaterial. Consequently, while CMP with Cr_2O_3 takes place effectively, possibility exists for mechanical abrasion and subsequent microchipping. Further, CeO_2 and ZrO_2 and their various reaction products formed during polishing are much more safer than the compounds formed by the reaction of Cr_2O_3 with Si_3N_4 workmaterial from an environmental point of view.

4. It is found that there is very little, if any, of CMP occurring in an oil-based polishing environment. The conductivity and dissolution value of an oil-based polishing fluid is nearly zero. The oil film between the abrasive and the workmaterial prevents any chemical reactions between them as well as the removal of reaction layer formed, if any, thus minimizing CMP. It can be seen that CMP of Si_3N_4 is particularly effective in a water environment and water is found to be essential for CMP of Si_3N_4 workmaterial. Water from water-based polishing fluid not only facilitates chemo-mechanical interaction between the abrasive and the workmaterial but also participates directly in the chemical reaction with the Si_3N_4 workmaterial (hydrolysis) leading to the formation of SiO_2 softer layer thereby enhancing the CMP.

5. The Si_3N_4 surface after CMP would consist of an outer SiO_2 layer and an intermediary layer of silicon oxynitride ($Si_xO_yN_z$) on the Si_3N_4 substrate. The layers composed of amorphous and crystalline SiO_2, Si_2N_2O, and $MgSiO_3$/$MgO \cdot SiO_2$ form by the reaction with the sintering aid (1 wt.% MgO). This is not much different from the surface of Si_3N_4 workmaterial which invariably has a natural oxidation layer in air even at room temperature.

6. It has been reported that the best abrasives for polishing glasses are CeO_2 and ZrO_2 [31]. There are similarities between polishing glass and polishing Si_3N_4 workmaterial including the role of water, polishing environment pH value 7–9, and abrasive hardness ~ Mohs 7 for effective polishing. It is somewhat coincidental, that in general, chemical effectiveness and mechanical hardness of abrasives for CMP of Si_3N_4 is similar to that for glass. This is not altogether surprising as the material removal mechanism in the case of Si_3N_4 is through the formation of SiO_2 and in the case of glass which is basically SiO_2 (Mohs 6.5). From an analysis of CMP mechanism for Si_3N_4 it appears reasonable to extend this mechanism to the polishing of silicon wafers, SiO_2 glasses, and SiC advanced ceramic. This is based on the similarity of the formation of SiO_2 on the surface and its subsequent removal by mechanical action.

Acknowledgements

This project is sponsored by grants from the National Science Foundation on "Tribological Interactions in Polishing of Advanced Ceramics and Glasses"; (CMS-9414610); "Design, Construction, and Optimization of Magnetic Field Assisted Polishing"; (DMI-9402895); DoD's DEPSCoR Program on "Finishing of Advanced Ceramics" (DAAH04-

)6-1-0323); and CATTS project on Ceramic Bearing Tech-
ıology. This project was initiated by a DARPA contract on
Ceramic Bearing Technology Program' (F33615-92-5933).
Thanks are due to Drs. J. Larsen Basse, B.M. Kramer, Ming
Leu, and Delci Durham of NSF and Dr. K.R. Mecklenburg
of WPAFB and Dr. W. Coblenz of DARPA for their interest
ınd support of this work. Thanks are also due to Prof. Zhen-
Bing Hou for valuable discussions.

References

[1] J. Ming, R. Komanduri, Wear 215 (1998) 267–278.
[2] J. Ming, R. Komanduri, Wear 213 (1997) 59–71.
[3] R. Komanduri, N. Umehara, M. Raghunandan, Trans. ASME J. Tribology 118 (1996) 721–727.
[4] N. Yasunaga, N. Tarumi, A. Obara, O. Imanaka, in: B.H. Hockey, R.W. Rice (Eds.), Mechanism and Application of the Mechano-Chemical Polishing Method Using Softer Powder, Science of Ceramic Machining and Surface Finishing II, NBS Special Publications No. 562, 1979, 171.
[5] T.E. Fischer, Tribochemistry, Ann. Rev. Mater. Sci. 18 (1988) 303–323.
[6] J.C. Wang, S.M. Hsu, J. Tribology 116 (1994) 423–429.
[7] H. Vora, T.W. Orent, R.J. Stokes, J. Am. Ceram. Soc. 65 (9) (1982) C140–C141.
[8] H. Vora, R.J. Stokes, Study of Mechano-Chemical Machining of Ceramics and the Effect on Thin Film Behavior, Rept. No. N00014-80-C-0437-2, 1983.
[9] T. Suga, S. Suzuki, K. Miyazawa, J. JSPE 55 (12) (1989) 2247–2253 (in Japanese).
[10] M. Kikuchi, Y. Takahashi, T. Suga, S. Suzuki, N. Yasunaga, Mechano-Chemical Polishing of Silicon Carbide, Proc. Fall Meeting of JSPE, 1990, 327–328, in Japanese.
[11] M. Kikuchi, Y. Takahashi, T. Suga, S. Suzuki, Y. Bando, J. Am. Ceram. Soc. 75 (1) (1992) 189–195.
[12] S.R. Bhagavatula, R. Komanduri, Philosophical Magazine A 74 (4) (1996) 1003–1017.
[13] J. Ming, R. Komanduri, On the Chemo-Mechanical Polishing (CMP) Si_3N_4 Bearing Balls with CeO_2, accepted for publication, J. Eng. Materials (1998).
[14] Z.B. Hou, R. Komanduri, Magnetic field assisted polishing of ceramics: Part I. Thermal model, ASME J. Tribology, accepted for publication, 1997.
[15] Z.B. Hou, R. Komanduri, Magnetic field assisted polishing of ceramics: Part II. On the thermal aspects of magnetic float polishing (MFP) of ceramic balls, ASME J. Tribology, accepted for publication, 1997.
[16] Y. Tani, K. Kawata, Annals CIRP 33 (1984) 217–220.
[17] N. Umehara, K. Kato, Applied Electromagnetics in Materials 1 (1990) 37–43.
[18] N. Umehara, Annals CIRP 43 (1) (1994) 185–188.
[19] N. Umehara, R. Komanduri, Wear 192 (1996) 85–93.
[20] M. Raghunandan, A. Noori-Khajavi, N. Umehara, R. Komanduri, Trans. ASME J. Manf. Sci. Eng. 119 (1997) 520–528.
[21] T.H.C. Childs, D.A. Jones, S. Mahmood, K. Kato, B. Zhang, N. Umehara, Wear 175 (1994) 189–198.
[22] T.H.C. Childs, S. Mahmood, H.J. Yoon, Proc. I. Mech. E. (London) 208 (B1) (1994) 47–59.
[23] T.H.C. Childs, S. Mahmood, H.J. Yoon, Tribology International 28 (6) (1995) 341–348.
[24] R.C. Oliver, S.E. Stephanou, R.W. Baier, Chem. Engr. (Feb. 1962) 121–128.
[25] Y. Kanno, K. Suzuki, Y. Kuwahara, NH_3 formation caused by the presence of H_2O in the wet grinding of silicon nitride powder, Yog Yo-K Yokai-Shi 91 (1983) 386.
[26] T.E. Fischer, H. Tomizawa, Wear 105 (1985) 29–45.
[27] H. Tomizawa, T.E. Fischer, Trans. ASLE 30 (1) (1986) 41–46.
[28] S.R. Hah, T.E. Fischer, C. Burk, Ceramic Bearing Development—Tribochemical Finishing of Silicon Nitride, Vol. 4, Technical Report No. WL-TR-96-4018, the Materials Directorate, Wright Patterson AFB OH, March 1995.
[29] F. Honda, T. Saito, Applied Surface Science 92 (1996) 651–655.
[30] B.T. Kilbourn, CERIUM—A Guide to Its Role in Chemical Technology, Molycorp, White Plains, NY, 1992.
[31] L.M. Cook, J. Non-Crystalline Solids 120 (1990) 152–171.
[32] T.W. Wallace, W.L. Wu, R.A. Carpio, Thin Solid Films 280 (1996) 37–42.
[33] T. Abe, Precision Engineering 13/4 (1991) 251–255.
[34] N.J. Tighe, Analysis of Oxide and Oxide/Matrix Interfaces in Silicon Nitride, National Bureau of Standards, NBSIR 82-2574, 1982.
[35] S.C. Singhal, J. Materials Science 11 (1976) 500–509.
[36] F.F. Lange, J. Am. Ceram. Soc. 62 (1979) 617.
[37] M. Ruhle, Microscopy of structural ceramics, Adv. Mater. 9 (1) (1997) 195–217.

APPENDIX D

ON THE CHEMO-MECHANICAL POLISHING OF Si_3N_4 BEARING BALLS WITH WATER BASED CeO_2 SLURRY

Ming Jiang, N. O. Wood, and R. Komanduri

Trans ASME, J of Engineering Materials & Technology, 120, (1998) 304-312

On the Chemo-Mechanical Polishing (CMP) of Si_3N_4 Bearing Balls With Water Based CeO_2 Slurry

Ming Jiang
Mechanical and Aerospace Engineering,
Oklahoma State University,
Stillwater, OK 74078

Nelson O. Wood
TASC, Midwest City, OK 73130

R. Komanduri
Mechanical and Aerospace Engineering,
Oklahoma State University,
Stillwater, OK 74078
Fellow ASME

Among various abrasives investigated for the chemo-mechanical polishing (CMP) of Si_3N_4 balls (Jiang, 1998), cerium oxide (CeO_2) was found to be the most effective polishing medium (even superior to Cr_2O_3, Bhagavatula and Komanduri, 1996), yielding an extremely smooth and damage-free surface with a finish R_a of ≈4 nm and R_t of ≈40 nm. In this investigation, the underlying reasons for the superior finish with CeO_2 were investigated. Various chemical reactions involved in CMP of Si_3N_4 balls with CeO_2 were investigated (Gibbs free energy minimization) and a mechanism for the CMP is proposed. The two important functions that CeO_2 performs in the CMP of Si_3N_4 are: 1. It participates directly in the chemical reaction (oxidization-reduction reaction) with Si_3N_4 workmaterial leading to the formation of a thin SiO_2 layer, 2. The hardness of CeO_2 is closer to that of the thin SiO_2 layer formed on Si_3N_4 but significantly lower than Si_3N_4 workmaterial ($\approx\frac{1}{3}$). It can thus remove the brittle SiO_2 reaction product effectively without damaging the Si_3N_4 substrate as no abrasion can take place by CeO_2 on Si_3N_4. The kinetic action, which involves the removal of the reaction products from the interface by subsequent mechanical action of flowing water and CeO_2 is critical to CMP. The chemical reaction could proceed on a continuing basis so long as the passivating layers are removed by the mechanical action at the same time. CeO_2 is found to be very effective in a water environment (hydrolysis) leading to the formation of additional SiO_2 by reacting with Si_3N_4 thereby enhancing the CMP of Si_3N_4. Several similarities between polishing of Si_3N_4 and glass (SiO_2) (Cook, 1990), including the polishing environment (CeO_2 plus the magnetic fluid, pH value ≈6) and the mechanism of polishing were observed. Also, after investigating various reaction species in the CMP of Si_3N_4 with CeO_2 and Cr_2O_3, the former is found to be much safer from an environmental point of view (Reddy and Komanduri, 1998).

1 Introduction

A critical factor affecting the performance and reliability of ceramics for bearing applications is the quality of the resulting surface by polishing. It is well known that ceramics are extremely sensitive to surface defects resulting from grinding and polishing processes owing to their high hardness and inherent brittleness. Since fatigue failure of ceramics is driven by surface imperfections, it is paramount that the quality and finish of the ceramic bearing elements be superior with minimal defects so that reliability in performance of bearings in service can be achieved.

When polishing advanced ceramics, such as Si_3N_4 balls by magnetic float polishing (MFP) (see Bhagavatula and Komanduri, 1996 for a brief description of the process) (Fig. 1) with harder abrasives, such as B_4C or SiC, high material removal rates (1 μm/min) can be obtained with minimal subsurface damage due to the use of a flexible support system, small polishing load (1 N/ball), fine abrasives but high polishing speed compared to conventional polishing. Higher material removal results from the rapid accumulation of minute amounts of material by microfracture of Si_3N_4 because of high polishing speeds (but light loads) used (Jiang and Komanduri, 1997a) instead of large radial and-circumferential cracks that results in the formation of pits in conventional polishing, especially with diamond abrasive.

In mechanical polishing in which the abrasives used are harder than the workmaterial, the surface damage can be minimized but not eliminated altogether even when very fine, hard abrasive is used. For example, the best surface finish obtained with a fine B_4C abrasive (1 μm) (harder abrasive) by magnetic float polishing (MFP) on HIP'ed Si_3N_4 balls was ≈20 nm Ra and ≈200 nm Rt (it may be noted that Ra is the arithmetic average surface roughness and Rt is the peak to valley distance). Similarly, the best surface finish obtained using a fine, SiC abrasive (1 μm) (also a harder abrasive than Si_3N_4) was ≈15 nm for Ra and ≈150 nm for Rt (Jiang and Komanduri, 1997b). To improve the final surface finish and to meet the application requirements as well as reliability in performance of the balls in service, further polishing has to be carried out preferably involving CMP.

An extensive review of literature on the CMP, in general, and that on Si_3N_4 work material in particular, was reported by Komanduri et al. (1996) and may be referred to for details. Based on that analysis, it was concluded that Cr_2O_3 is a candidate abrasive for the CMP of Si_3N_4. Bhagavatula and Komanduri (1996) reported a surface finish Ra ≈ 16.6 nm and Rt ≈ 0.54 μm in CMP of Si_3N_4 balls with Cr_2O_3 abrasive. However, because of the higher hardness of Cr_2O_3 abrasive compared to Si_3N_4, some surface damage due to mechanical action is inevitable, in spite of CMP. This is in contrast to CMP of Si_3N_4 by CeO_2 where abrasion can be ruled out due to the softness

Contributed by the Materials Division for publication in the JOURNAL OF ENGINEERING MATERIALS AND TECHNOLOGY. Manuscript received by the Materials Division October 8, 1997; revised manuscript received June 15, 1998. Associate Technical Editor: H. Sehitoglu.

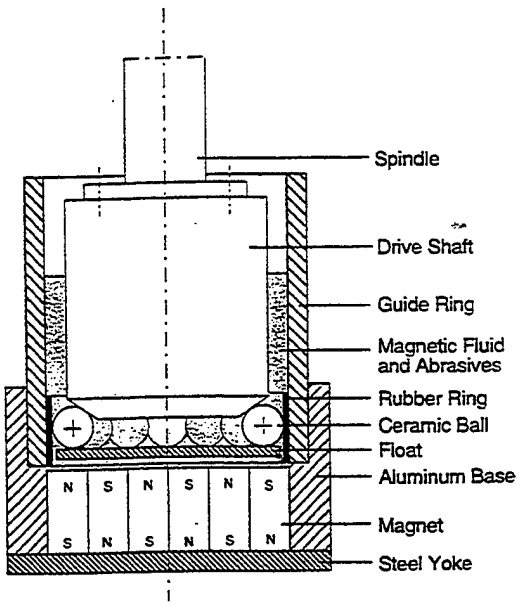

Fig. 1 Schematic of the magnetic float polishing (MFP) apparatus for finishing Si_3N_4 balls

of the abrasive relative to the workmaterial. They also investigated the mechanism of material removal in polishing of Si_3N_4 balls with Cr_2O_3 abrasive and showed that the role of Cr_2O_3 is not one of a mere catalyst as identified by some earlier researchers (Kikuchi et al., 1992) but played an active role in the chemical reaction with Si_3N_4 forming chromium silicate and chromium nitride. This was based on the examination of the wear debris in the SEM with an X-ray microanalysis and in a low angle X-ray diffractometer. Based on the magnetic float polishing (MFP) experiments, Cr_2O_3 abrasive was considered as the most effective for CMP of Si_3N_4. However, some of the chemical species formed with Cr_2O_3 during polishing may not be environmentally acceptable and special care may need to be exercised for the disposal of the magnetic fluid containing the debris (Reddy and Komanduri, 1997). In contrast, the species formed with CeO_2 do not pose any hazard to the environment (Kilbourn, 1992).

After investigating a number of abrasives to assess their effectiveness in CMP of Si_3N_4 balls, CeO_2 was found to be the most effective (yielding a damage-free surface with a finish Ra $\approx$ 4 nm and Rt $\approx$ 40 nm) (Jiang and Komanduri, 1997a). This paper presents the results of an investigation on the chemo-mechanical polishing (CMP) mechanism of Si_3N_4 balls with CeO_2. Specifically, it investigates the various reactions that can take place between the Si_3N_4 balls, the CeO_2 abrasive, and the environment and proposes a mechanism of CMP of Si_3N_4 balls with the CeO_2 abrasive. Experimental results of polishing Si_3N_4 balls with the CeO_2 yielding extremely smooth scratch-free surface are explained in light of the proposed mechanism. Although, polishing of Si_3N_4 balls with Cr_2O_3 abrasive and the CeO_2 abrasive involve chemo-mechanical action, some of the specifies are found to be different interms of reaction products by comparing the results of this investigation with that of Bhagavatula and Komanduri (1996).

2 Magnetic Float Polishing (MFP) and Experimental Setup

The conventional grinding and polishing of ceramic balls uses basically the same method used for making steel balls for bearings, i.e., by V-groove lapping. It involves the use of low polishing speeds (50 rpm), high loads (10 N per ball), and diamond abrasive. In practice, it takes considerable time (some 12–16 weeks depending on the size of the ball, quality required, and the available technology) to finish a batch of ceramic balls. The long processing time and the use of expensive diamond abrasives result in high processing costs. Furthermore, the use of diamond abrasives at high loads can result in surface damage, such as deep pits, scratches, and microcracks and subsurface damages such as large lateral and radial/median cracks. These surface defects can result in catastrophic failure of silicon nitride balls in service by propagation cracks by brittle fracture.

To minimize the surface damage, 'gentle'/'flexible' grinding and polishing conditions are required, namely, a low level of load and abrasives not much harder than the workmaterial and preferably softer but can cause chemo-mechanical action. Higher removal rates and shorter polishing cycles can be accomplished by higher polishing speeds. This is accomplished by a new process known as magnetic float polishing (MFP) (see Bhagavatula and Komanduri, 1996 for details). The material removal rate by MFP is $\approx$50 times higher than the conventional V-groove lapping, owing to higher polishing speed (1000–10,000 rpm) used in MFP compared to lapping (50 rpm). Furthermore, the resulting surface and subsurface damage can be minimized due to the use of extremely low polishing load ($\approx$1 N/ball) and chemo-mechanical polishing.

The magnetic float polishing (MFP) technique is based on the magneto-hydrodynamic behavior of a magnetic fluid that can float nonmagnetic float and abrasives suspended in it by a magnetic field. The forces applied by the abrasive to the part are extremely small (1 N/ball) and highly controllable. Figure 1 is a schematic of the magnetic float polishing apparatus for finishing Si_3N_4 balls. A series of permanent magnets (Nd-Fe-B) are arranged alternate N and S below an aluminum chamber which is filled with the required amount of magnetic fluid and appropriate abrasive (5–10% by volume). The magnetic fluid is a colloidal dispersion of extremely fine (100 to 150 A) subdomain ferromagnetic particles, usually magnetite (Fe_3O_4), in a carrier fluid, such as water or kerosene. It is made stable against particle agglomeration by coating the particles with a suitable surfactant. In this investigation a water base ferrofluid (W-40) was used.

The polishing shaft was driven by a high-speed, high-precision air bearing spindle (PI Spindle) with a stepless speed regulation up to 10,000 rpm. The magnetic field was measured by a Gauss/Tesla meter. pH value of the polishing environment was measured by a pH/Temperature meter. The polishing load was set up by measuring the normal force with a Kistler's piezoelectric dynamometer connected to a charge amplifier and a display. To calculate material removal rates, the weight reduction in the balls was measured before and after polishing at every stage of testing using a precision balance. The surface finish of the polished balls was analyzed using a Form Talysurf 120 L (a stylus based instrument), ZYGO laser interference microscope (non-contact), a Digital Nanoscope III atomic force microscope (AFM), and an ABT 32 scanning electron microscope (SEM). The sphericity of the balls was measured using TalyRond 250 (a stylus based instrument). The surface chemistry of the finished balls was evaluated using Seimens small angle X-ray diffraction equipment.

3 Experimental Procedure and Polishing Conditions

Table 1 and Table 2 give the chemical composition and the mechanical and thermal properties of NBD 200 HIP'ed Si_3N_4 balls (supplied by CERBEC) used in this investigation (Hah et

Table 1 Nominal chemical compositions (wt.%) of NBD-200 Si_3N_4 (Hah et al., 1995)

Al	C	Ca	Fe	Mg	O	Si_3N_4
≤0.5	≤ 0.88	≤ 0.04	≤ 0.17	0.6 - 1.0	2.3 - 3.3	94.11-97.1

Table 2 Mechanical and thermal properties of uniaxially pressed Si_3N_4 (Hah et al., 1995)

PROPERTY	VALUE
Flexural Strength, MPa	800
Weibull Modulus	9.7
Tensile Strength, MPa	400
Compressive Strength, GPa	3.0
Hertz Compressive Strength, GPa	28
Hardness, Hv (10kg), GPa	16.6
Hardness, Mohs	8.5
Fracture Toughness, K_{1c} MPam$^{-1/2}$	4.1
Density, g/cm^3	3.16
Elastic Modulus, GPa	320
Poisson's Ratio	0.26
Thermal Expansion Coefficient at 293-1273 K, /K	2.9×10^{-6}
Thermal Conductivity at 373 K, W/m-K	29
Thermal Conductivity at 773 K, W/m-K	21.3
Thermal Conductivity at 1273 K, W/m-K	15.5

al., 1996). The sintering aid is ≈1 wt.% MgO. Major impurity is Fe_2O_3. Table 3 shows the properties of CeO_2 polishing medium. Table 4 gives the properties of the SiO_2, a thin layer that is formed on the surface of Si_3N_4 during polishing. The Si_3N_4 balls are initially polished with a SiC #8000 (1 μm) abrasive prior to CMP. The polishing conditions are listed in Table 5. The pH value of polishing solution [a water-based magnetic fluid (W-40) plus 10 vol.% CeO_2 the pH value] of the polishing media is ≈6.

Thermodynamic analysis was conducted using the Gibbs free energy minimination program to determine the nature of the reaction products as well as whether such reactions are thermodynamically feasible. For a reaction to occur spontaneously at a given temperature and pressure, the Gibbs free energy change, ΔG should be negative. Equilibrium compositions and ΔG are calculated using the Outokumpu HSC Chemistry Software. Appendix A gives a brief outline of this program. A CMP mechanism for polishing Si_3N_4 balls with CeO_2 is presented based on the thermodynamic and kinetic analyses.

Table 3 Properties of CeO_2 polishing medium (Shaffer, 1964)

PROPERTY	VALUE
Hardness, Mohs	6
Density, g/cm^3	7.13
Elastic Modulus, GPa	165
Poisson's Ratio	0.5
Thermal Conductivity at 373 K, W/m-K	8.4
Thermal Conductivity at 1273 K, W/m-K	0.8

Table 4 Mechanical and thermal properties of SiO_2 (Wyatt and Dew-Hughes, 1974; Shaffer, 1964)

PROPERTY	VALUE
Melting point, K	1983
Tensile Strength, MPa	100-120
Hardness, Hv (100 g), GPa	7-7.4
Hardness, Mohs	6.5
Fracture Toughness, K_{1c} MPam$^{-1/2}$	0.79
Density, g/cm^3	2.2
Elastic Modulus, GPa	72
Poisson's Ratio	0.17
Thermal Expansion Coefficient at 273-573 K, /K	0.564×10^{-6}
Thermal Conductivity at 273 K, W/m-K	1.45

Table 5 Test conditions

Workmaterial	Uniaxially pressed Si_3N_4 balls (CERBEC NBD-200), semifinished Diameter: 12.7 mm (0.5 inch) Initial Sphericity: 1 μm Initial Finish: Ra=20 nm
Abrasive Concentration	10% by volume
Polishing Load	1.2 N per ball
Polishing Speed	2000 rpm
Magnetic Fluid	Water-based (W 40) Saturation Magnetization at 289 K : 400 Gauss Viscosity at 27 °C : 25 Cp

4 Mechanism of CMP of Si_3N_4 With CeO_2

Figure 2(*a*) is an SEM micrograph of a Si_3N_4 ball surface after polishing with CeO_2 (5 μm) showing essentially a smooth surface with no pits, scratches, or cracks. The corresponding Talysurf surface finish profile [Fig. 2(*b*)] shows a surface finish Ra of 4 nm and Rt of 40 nm (ISO: cut-off 0.25 mm, evaluation length 6 × 0.25 mm, ISO 2CR Filter). Figure 2(*c*) is an AFM image (stylus tip radius <0.08 μm) at higher magnification again showing an extremely smooth surface obtained by polishing with CeO_2 without any pitting or scratching.

Table 6 gives the free energy of formation of selected compounds (that are of interest to this investigation) from their constituents and Table 7 gives various chemical reactions of interest [Eqs. (1)–(11)] in this investigation as well as the free energy change, ΔG at various temperatures (from 273–1273 K) obtained from the software program used. It is known that Si_3N_4 can readily oxidize in an oxidizing atmosphere (Ruhle, 1997). As a result, the surfaces of the as-received uniaxially pressed Si_3N_4 balls are generally covered with a thin layer of silica [see Eq. (1) in Table 7]. However, once this layer is removed, means should be available for the formation of SiO_2 subsequently so that CMP of Si_3N_4 can take place on a continuing basis.

The Si_3N_4 balls finished by CeO_2 was examined in a Siemens Low Angle X-ray diffraction apparatus. The diffractometer employs a 3.0 kW sealed-tube X-ray generator, with a 3-circle goniometer for sample positioning, and a radiation safety enclosure. Copper is used as a target for the X-ray source. Graphite is used to monochromatize the Cu radiation from the tube after which the radiation is collimated with pinhole optics. A nickel filter is used to filter the K-β Cu radiation. Samples are mounted on a three circle goniometer and can be precisely positioned in the χ and ω axes. A two-dimensional, position-sensitive area detector is mounted on the 2θ arm of the goniometer, for the measurement of diffracted X-rays. Standard runs were made from 10 to 90 deg of 2θ, with a step size of 0.05 deg. Samples were mounted on the goniometer in a fixture which held the samples at a proper height for the exposure of the beam. The sample is held on the aluminum fixture with wax. Frames of the scattering data from the sample are collected and processed by GADDS software. Figure 3 shows the XRD spectra of the finished ball showing the peaks corresponding to the α and β phases of Si_3N_4. It can be seen that in addition to Si_3N_4, the presence of crystalline form of the silica phase (crystabollite) was also detected, indicating the presence of an extremely thin silica layer on the surface of the finished balls (Mallika and Komanduri, 1998).

During mechanical polishing of Si_3N_4 (i.e., prior to CMP) by a harder abrasive, such as SiC and B_4C, the silica surface layer on the surface of Si_3N_4 along with a portion of Si_3N_4 can be removed by brittle fracture or abrasion, thus exposing the

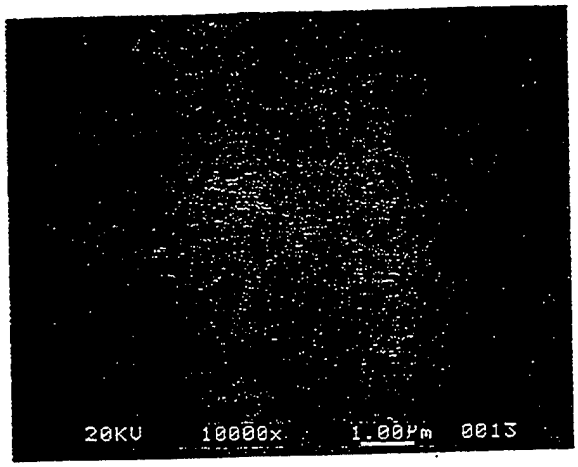

Fig. 2(*a*) SEM micrograph of a Si_3N_4 ball surface after polishing with CeO_2 (5 μm) showing an essentially smooth surface with no pits, or scratches, or cracks

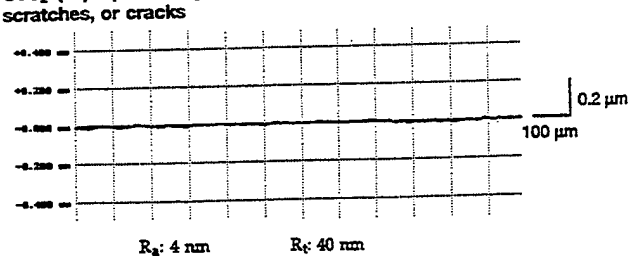

Fig. 2(*b*) Talysurf surface finish profile showing a surface finish Ra of 4 nm and Rt of 40 nm (ISO: cut-off 0.25 mm, evaluation length 6 × 0.25 mm, ISO 2CR filter)

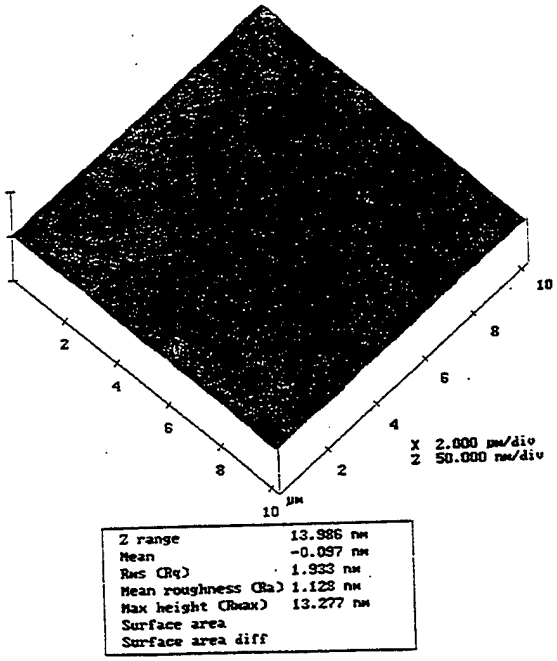

Fig. 2(*c*) AFM image at high magnification showing an extremely smooth surface obtained by polishing with CeO_2 without any pitting or scratching

base Si_3N_4. In subsequent CMP, Si_3N_4 can react with water (hydrolysis) (from the water-based magnetic fluid) leading to the formation of SiO_2 and NH_3 [Eq. (2)]. Figure 4(*a*) shows the variation of the mole fraction of various species with temperature at equilibrium based on the thermodynamic calculations of the chemical reaction system consisting of 1 mol of Si_3N_4 and 1 mol of H_2O. It can be seen from the figure that at low temperatures (<300°C), $NH_3(g)$ formation is promoted while

Table 6 Free energy of formation of selected compounds from their constituents (Wicks and Block, 1963; Reed, 1971)

$2Ce + 1.5O_2(g) = Ce_2O_3$								
T (K)	298	400	500	600	700	800	1000	1200
ΔG (kJ)	-1708	-1686	-1653	-1620	-1588	-1555	-1490	-1423
$Ce + O_2(g) = CeO_2$								
T (K)	298	400	500	600	700	800	1000	1500
ΔG (kJ)	-1028	-1008	-988.5	-969.2	-949.3	-929.9	-891.2	-792
$Si + O_2 = SiO_2$ (Crystobalite)								
T (K)	298	400	500	600	700	800	1000	1200
ΔG (kJ)	-821.8	-803.2	-785	-767.2	-749.5	-731.9	-696.6	-662.3
$3Si + 2N_2 = Si_3N_4$								
T (K)	298	400	500	600	700	800	1000	1200
ΔG (kJ)	-326	-309.3	-292.6	-275.9	-259.2	-242.4	-209	-183.9

at higher temperatures, $H_2(g)$ and $N_2(g)$ gases are evolved. However, the SiO_2 mole fraction as well as Si_3N_4 mole fraction seems to be somewhat independent of temperature indicating minor effect, if any, of the temperature on the material removal rates under these conditions. Figure 4(*b*) shows the variation of various chemical species with temperature for 1 mol of Si_3N_4 and increasing amounts of H_2O. It can be seen that with increase in the mole fraction of H_2O, the amount of SiO_2 increases and the amount of Si_3N_4 correspondingly decreases both accounting for an increase in the material removal due to chemo-mechanical polishing. This shows the beneficial role of H_2O in CMP. In a similar manner, $NH_3(g)$, $H_2(g)$, and $N_2(g)$ gases also increase with increases in the mole content of H_2O, as can be anticipated.

Equation (3) shows that at low temperatures, ΔG is positive indicating the unlikelihood of dissociating $NH_3(g)$ as $N_2(g)$

Table 7 Chemical reactions between Si_3N_4, CeO_2, and the environment along with ΔG at various temperatures

$Si_3N_4 + 3O_2(g) = 3SiO_2 + 2N_2(g)$ (1)								
T(K)	273	373	473	573	673	873	1073	1273
ΔG (kJ)	-1926	-1903	-1882	-1861	-1840	-1800	-1761	-1724
$Si_3N_4 + 6H_2O = 3SiO_2 + 4NH_3(g)$ (2)								
T(K)	273	373	473	573	673	873	1073	1273
ΔG (kJ)	-554.7	-589	-616	-638	-654	-668	-665.8	-612.4
$2NH_3(g) = N_2(g) + 3H_2(g)$ (3)								
T(K)	273	373	473	573	673	873	1073	1273
ΔG (kJ)	37.7	17.89	-3.68	-25.67	-48.2	-94.18	-140.9	-187.9
$NH_3(g) + H_2O = NH_4OH$ (4)								
T(K)	273	373	473	573	673	873	1073	1273
ΔG (kJ)	31.77	41.38	11.8	49.32	64.37	79.0	22.8	95.3
$SiO2 + 2H_2O = Si(OH)_4$ (a) (5)								
T(K)	273	373	473	573	673	873	1073	1273
ΔG (kJ)	211.9	289.7	356.5	436.4	520.4	701.4	899.1	1114
$Si_3N_4 + 35.294\ CeO_2 = 3SiO_2 + 35.294\ CeO_{1.83} + 2N_2(g)$ (6)								
T(K)	273	373	473	573	673	873	1073	1273
ΔG (kJ)	-199	-257.9	-316.4	-375.7	-434.3	-555.5	-682.2	-815.5
$Si_3N_4 + 21.429\ CeO_2 = 3SiO_2 + 21.429\ CeO_{1.72} + 2N_2(g)$ (7)								
T(K)	273	373	473	573	673	873	1073	1273
ΔG (kJ)	-144.6	-198	-251.2	-303.9	-357	-465	-577.7	-695.6
$Si_3N_4 + 12CeO_2 = 3SiO_2 + 6Ce_2O_3 + 2N_2(g)$ (8)								
T(K)	273	373	473	573	673	873	1073	1273
ΔG (kJ)	148.4	93.2	35.9	-23	-82.76	-206.5	-334.4	-465.7
$2\ Si_3N_4 + 17.647CeO2 = 3\ Si_2N_2O + 17.647\ CeO1.83 + N_2(g)$ (9)								
T(K)	273	373	473	573	673	873	1073	1273
ΔG (kJ)	-285.5	-282.6	-280.9	-279.6	-278	-271.1	-259.6	-240.3
$Si_3N_4 + 1.5H2O = 1.5\ Si_2N_2O + NH_3(g)$ (10)								
T(K)	273	373	473	573	673	873	1073	1273
ΔG (kJ)	-392.9	-399.6	-412.1	-428	-446	-487	-532.5	-582.7
$Si_3N_4 + SiO_2 = 2\ Si_2N_2O$ (11)								
T(K)	273	373	473	573	673	873	1073	1273
ΔG (kJ)	-195.6	-180.6	-169.3	-160.5	-152.6	-139.2	-127.5	-106.6

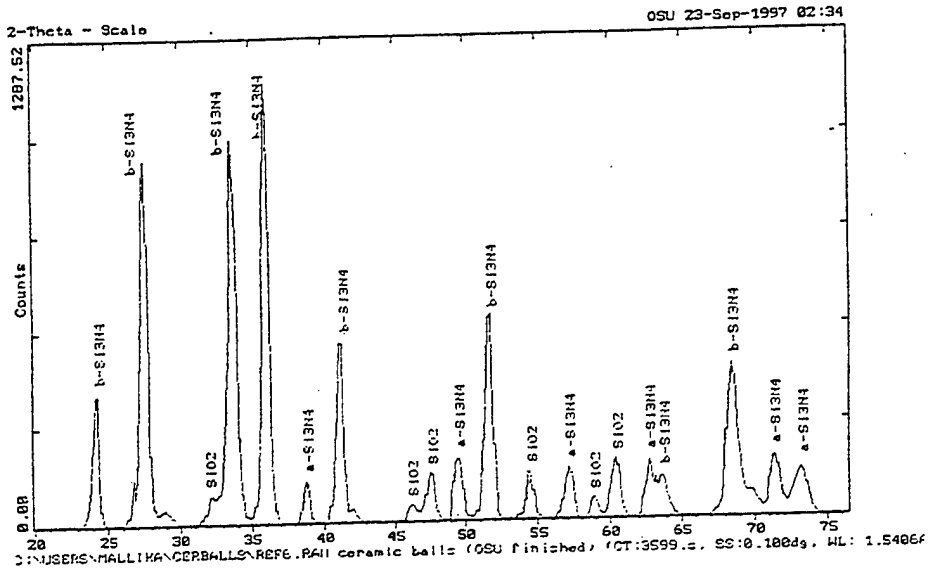

Fig. 3 Low angle X-ray diffraction of a Si_3N_4 ball finished with CeO_2 polishing medium showing the presence of SiO_2 on the surface of the ball

and $H_2(g)$. Thus NH_3 formation is possible in CMP only when the temperature rise at the contact surface is <300°C [Eq. (2) and Fig. 3]. Further increase in temperature may result in the dissociation of NH_3 into $N_2(g)$ and $H_2(g)$ (Eqn. (3) and Fig. 3). This is perhaps the reason why some researchers found $NH_3(g)$ formation while others did not during polishing.

It has been reported in the literature, the formation of $Si(OH)_4$ and NH_4OH as secondary products due to the reaction between $NH_3(g)$ and H_2O, and between SiO_2 and H_2O in the CMP of Si_3N_4 (Hah et al., 1996). It can be seen from Eqs. (4) and (5) that these secondary reactions may not be feasible thermodynamically, as ΔG in all cases is positive.

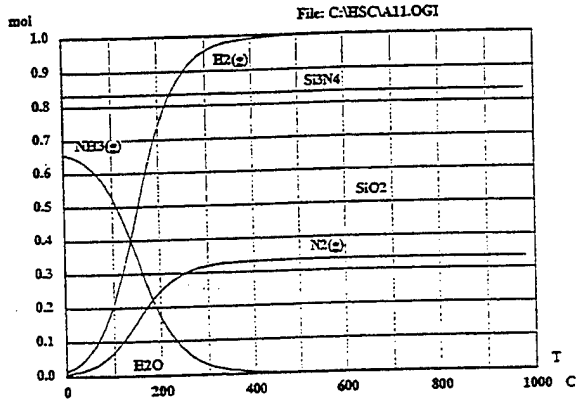

Fig. 4(a) Variation of the mole fractions of various species with temperature of the chemical reaction system consisting of 1 mol of Si_3N_4 and 1 mol of H_2O

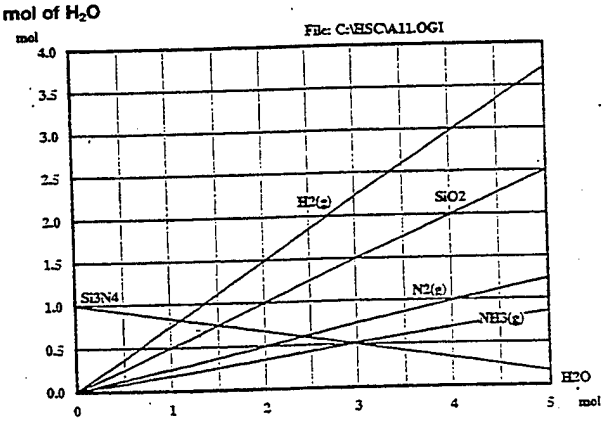

Fig. 4(b) Variation of various chemical species with temperature for 1 mol of Si_3N_4 and increasing amounts of H_2O

CeO_2 can also react directly with Si_3N_4 (oxidation-reduction reaction) forming SiO_2 and N_2 as reaction products. It may be noted that CeO_2 is not stable and will convert to $CeO_{1.72}$ and $CeO_{1.83}$ with increase in temperatures to the more stable form, namely, Ce_2O_3 at much higher temperatures. Figure 5(*a*) shows the variation of the reaction products with temperature at equilibrium based on the thermodynamic calculations of the chemical reaction system consisting of 1 mol of Si_3N_4 and 1 mol of CeO_2 and Fig. 5(*b*) is for 1 mol of Si_3N_4 and with increasing mole fractions of CeO_2. The reactions of Si_3N_4 with CeO_2 yielding $CeO_{1.83}$, $CeO_{1.72}$, and Ce_2O_3 are shown in Eqs. (6)–(8). The reason why fractional numbers, namely, 35.294 moles in Eq. (6), 21.429 moles in Eq. (7), and 17.647 moles in Eq. (9) of CeO_2 are needed is to balance Eqs. (6), (7), and (9). This is because CeO_2 is not stable and will convert to other forms, namely, $CeO_{1.83}$, $CeO_{1.72}$, and Ce_2O_3 with increase in temperature as shown in Fig. 5(*a*). From Fig. 5(*a*) it can be seen that the SiO_2 mole fraction is independent of temperature up to ≈300°C and increases gradually up to 1000°C. Thus temperature does not seem to be as effective as mole fraction of H_2O [compare Figures 5(*a*) with Fig. 4(*a*)]. However, as the mole fraction of CeO_2 is increased, the amount of SiO_2 increases and the amount of Si_3N_4 decreases both accounting for the increase in the material removal rate due to CMP.

Figure 6 shows the variation of the reaction products with temperature for the chemical reaction system consisting of 1 mol of Si_3N_4, 1 mol of CeO_2, and 1 mol of H_2O at equilibrium based on the thermodynamic calculations. This diagram provides an insight on the mechanism of chemo-mechanical polishing of Si_3N_4 with CeO_2 showing various chemical species that can be formed during the process. This figure can be considered as a combination of Figs. 4(*a*) and 5(*a*). It shows that while the SiO_2 mole fraction is constant upto about ≈300°C, it increases with further increase in temperature. A reverse trend can be seen for Si_3N_4, i.e., initially constant followed by a decrease in mole fraction with further increase in temperature, both indicating an increase in the material removal rate due to chemo-mechanical action at higher temperatures. It can be seen from the figure that $NH_3(g)$ forms at low temperatures (<300°C) while $H_2(g)$ and $N_2(g)$ gases form at higher temperatures, similar to Fig. 4(*a*).

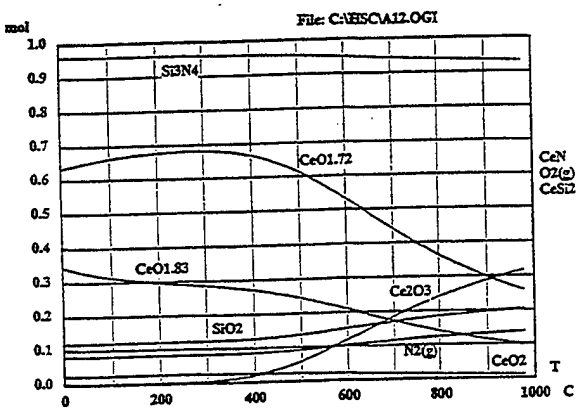

Fig. 5(*a*) Variation of the reaction products with temperature of the chemical reaction system consisting of 1 mol of Si_3N_4 and 1 mol of CeO_2

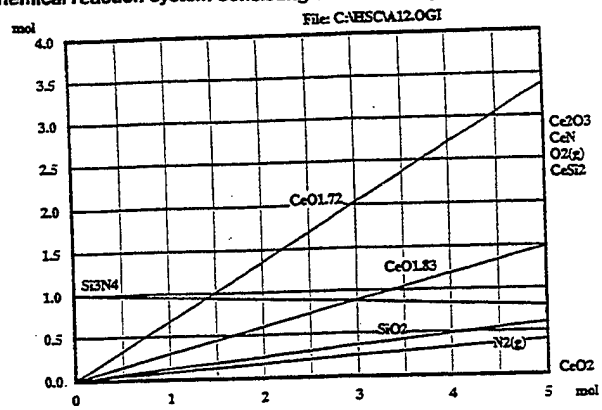

Fig. 5(*b*) Variation of the reaction products with increasing mole fraction of CeO_2

CeO_2 has been reported to be particularly effective in water and in alcohols only when hydroxyl groups are present (Kilbourn, 1992). Thus CeO_2 slurry in water is invariably needed for polishing. The oxide contains polyvalent cerium atoms, Ce(IV) and Ce(III), which can provide chemical action with the workmaterial. It appears that when $Ce(OH)_4$, i.e., $CeO_2 \cdot 2H_2O$ is precipitated fresh, i.e., *in situ*, in the polishing slurry form, a soluble Ce(IV) salt may be involved in an equilibrium reaction:

$$SiO_2 + Ce(OH)_4 \rightarrow CeO_2 + Si(OH)_4$$

It may be noted that silicilic acid, $Si(OH)_4$, is highly soluble in basic aqueous solutions.

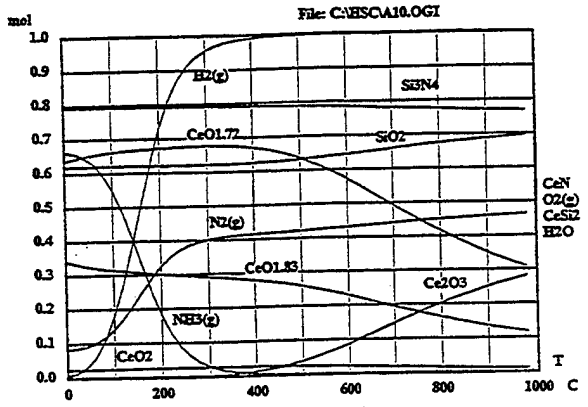

Fig. 6 Variation of the reaction products with temperature for the chemical reaction system of 1 mol of Si_3N_4, 1 mol of CeO_2, and 1 mol of H_2O

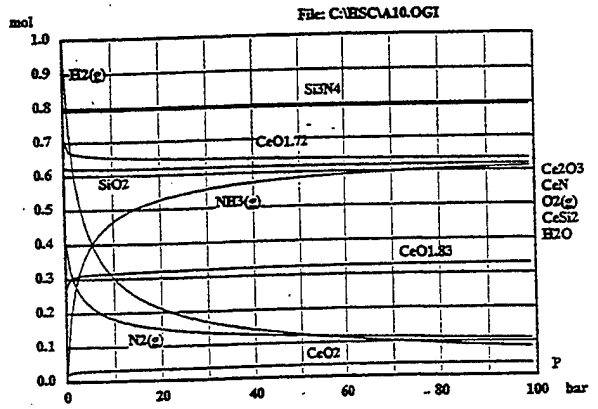

Fig. 7 Variation of the reaction products with pressure for the chemical reaction system of 1 mol of Si_3N_4, 1 mol of CeO_2, and 1 mol of H_2O

CeO_2 appears to be the most effective polishing medium for CMP of Si_3N_4 because of the thermodynamic considerations of its reaction with Si_3N_4 as well as its kinetic action of removing the reaction product, namely, SiO_2 from Si_3N_4 workmaterial.

Figure 7 shows the variation of the reaction products with pressure at equilibrium based on the thermodynamic calculations of the chemical reaction system of 1 mol of Si_3N_4, 1 mol of CeO_2, and 1 mol of H_2O. It can be seen that both Si_3N_4 and SiO_2 more or less remains constant indicating that the formation of SiO_2 due to chemical reaction is independent of the polishing pressure. It may be noted that an increase in the mole fraction of SiO_2 and a corresponding decrease in Si_3N_4 are an indication of the increase in the material transformed by chemical action. However, the actual material removal will depend on the kinetic action involving the removal of the reaction products to enable the chemical reaction to proceed on a continuing basis.

The hardness of CeO_2 is closer to SiO_2 layer but significantly less than Si_3N_4 workmaterial. Thus, the Si_3N_4 workmaterial can hardly be scratched, or damaged by CeO_2. Hence, almost all the material removal by chemo-mechanical action between the Si_3N_4 workmaterial and the CeO_2 polishing media in a water environment is by the formation of SiO_2 reaction layer on Si_3N_4 and its subsequent removal by mechanical action. The chemical reaction can continue only after the passivating layers are removed by the mechanical action. Thus, the kinetic action, which removes the reaction products from the interface is a very important step in the CMP process. It is somewhat coincidental, that in general, the Mohs hardness of best polishing abrasives for glasses (SiO_2) is $\approx$6.5 and that of CeO_2 is $\approx$6. There are other similarities including the role of water and effectiveness of CeO_2 medium for polishing glass. This is not altogether surprising as the material removal mechanism in the case of Si_3N_4 is through the formation of SiO_2 and in the case of glasses it is naturally the SiO_2. A similar mechanism may be applicable for the polishing of silicon wafers with CeO_2 in a water based solution. It is hoped that these and other aspects will be addressed in detail in subsequent publications.

It is possible that in the formation of SiO_2 outer layer, an intermediate oxynitride ($Si_xO_yN_z$) may form between the SiO_2 thin layer and the Si_3N_4 substrate according to Eqns. 9–11 (Table 7). All three equations are thermodynamically feasible at all temperatures upto 1000°C.

5 Discussion

Since CeO_2 is significantly softer than Si_3N_4 workmaterial ($\approx\frac{1}{5}$), material removal by mere mechanical action would be extremely difficult, if not impossible. Therefore, the mechanism of material removal must be due to chemo-mechanical action between the abrasive, the workmaterial and the environment. In CMP, material removal is accomplished by chemical reaction

mulated by friction energy at the contact area and the reaction ıer is removal by subsequent mechanical action of the abra- ıe (Fischer, 1988). Since material is removed by the tribo- emical action instead of mechanical fracture, extremely ıooth and damage-free surface can be obtained as shown in g. 2.

CeO_2 is found to be the most effective abrasive for CMP Si_3N_4 material (both because of its kinetic action to remove e reaction product SiO_2 and thermodynamic feasbility of action with Si_3N_4 workmaterial). CeO_2 abrasive can di- ctly react with Si_3N_4 workmaterial (oxidation-reduction re- ction) to form SiO_2 as shown in Eqs. (6)–(8). Vora et al. 1982) reported the feasibility of polishing Si_3N_4 to a good nish by CMP with Fe_2O_3 and Fe_3O_4 abrasives. An oxygen ich silicon oxynitride was found on the polished Si_3N_4 sam- les based on the analysis using Auger Electron Spectroscopy AES). They concluded that oxidation is a possible mecha- ism causing CMP of Si_3N_4.

Kanno and Suzuki (1983) identified the formation of NH_3 luring grinding of Si_3N_4 powder in water, thus establishing the ıydrolysis of Si_3N_4. The thermodynamic analysis presented ıere suggests the feasibility of this reaction [Eq. (2)]. During nagnetic float polishing (MFP) of Si_3N_4 by CeO_2 due to the presence of water environment (from the water-based magnetic fluid), NH_3 and SiO_2 are formed when the temperature at the contact interface is <300°C. Fischer and Tomizawa (1985), Tomizawa and Fischer (1987), and Hah and Fischer (1995) also showed the formation of SiO_2 and NH_3 in tribochemical polishing of Si_3N_4. But they proposed the dissolution of SiO_2 and NH_3 (to silicilic acid [$Si(OH)_4$] and ammonium hydroxide [NH_4OH]) as a second reaction to stimulate the continuation of tribochemical polishing of Si_3N_4 in aqueous solutions. Fischer (1988) also pointed out that flash temperatures from the frictional heat is important for the tribochemical reaction at the polishing interface. While the hydrolysis reaction shown in Eq. (2) is thermodynamically feasible, the dissolution of SiO_2 and NH_3 [to silicilic acid, $Si(OH)_4$ [Eq. (4)] and ammonium hydroxide (NH_4OH)] [Eq. (5)] as reactants to stimulate the tribochemical polishing does not seem to be feasible thermodynamically as ΔG (kcal) is positive in all cases.

The hardness of CeO_2 is close to the SiO_2 layer but significantly less ($\approx\frac{1}{3}$) than Si_3N_4 workmaterial. Thus, SiO_2 reaction layers formed during chemical action are removed without damaging Si_3N_4 workmaterial by CeO_2. In general, Mohs hardness of best polishing abrasives for glasses (SiO_2) is ≈6.5. Hardness of CeO_2 abrasive is ≈6 on the Moh's scale and the pH of the magnetic fluid plus CeO_2 is ≈6. It may be noted that Cook (1990) after a careful analysis concluded that the best abrasive for polishing glasses is CeO_2 and the best polishing environment is with a pH in the range of 6–7. Wallace et al. (1996) investigated the CMP of SiO_2 thin films using X-ray reflectivity. They concluded that stress-corrosion mechanism may be responsible whereby the stress induced by the abrasion of abrasive particle in water strains the bonds in the SiO_2 thin films. The polished material shows an increased density in the near-surface region. The compaction of the SiO_2 network leads to enhanced dissolution of SiO_2 into the polishing slurry and to an extremely smooth surface. The kinetic action, which removes the reaction products from the interface, is very important in the CMP process. The chemical reaction can continue only after the passivating layers are removed by subsequent mechanical action.

It may be noted that silicon oxynitride ($Si_xO_yN_z$) can form an intermediate layer between the thin SiO_2 layer and Si_3N_4 workmaterial as shown in Eqs. (9–11). The surface after CMP by cerium oxide is reported to be of 0.2–0.5 nm of SiO_2, 1.0–1.5 nm of SiO_xN_y on the Si_3N_4 substrate (Han and Fischer, 1995). The natural oxidation layer of Si_3N_4 at room temperature is no more than 0.25–0.30 nm. Thus, CMP does not produce a layer that is chemically different from the Si_3N_4 which has the natural oxidation layer in air at room temperature.

6 Conclusions

The conclusions outlined in the following are based on the mechanism proposed for the chemo-mechanical polishing of Si_3N_4 balls with CeO_2 abrasive and the experimental results resulting in extremely smooth, scratch-free surface of the balls generated in the magnetic float polishing (MFP) process.

1. A mechanism for the chemo-mechanical polishing (CMP) of Si_3N_4 balls with CeO_2 abrasive is proposed. It depends on the polishing conditions used, abrasive-workmaterial combination, and the environment used. The reaction products formed depend on the flash temperature and flash duration during polishing which in turn depend on the polishing conditions for a given abrasive-workmaterial combination and the environment used. From a comparison of the results obtained in polishing with Cr_2O_3 abrasive in an earlier investigation (Bhagavatula and Komanduri, 1996) and CeO_2 abrasive in the current investigation, it is found that CeO_2 abrasive to be better and perhaps more effective polishing medium in the CMP of Si_3N_4 balls yielding an extremely smooth and damage-free surface with a finish R_a of 4 nm and R_t of 40 nm. It may be noted that in the case of Cr_2O_3 abrasive, even though the R_a value obtained was only slightly higher (16 nm instead of 4 nm), the R_t value was significantly higher (0.54 μm instead of 40 nm). This is mainly because of the mechanical abrasion caused by Cr_2O_3 that could not be eliminated altogether, inspite of its chemo-mechanical polishing ability. This, of course, is not the case with the CeO_2 as it is much softer than Si_3N_4 and could not cause any mechanical damage. Further, CeO_2 and the various reactants formed during polishing is much more safer than Cr_2O_3 from an environmental point of view (Kilbourn, 1992).

2. Based on the CMP mechanism proposed here and the polishing results, it can be seen that CeO_2 abrasive has two important functions in CMP of Si_3N_4. First, it directly reacts chemically (oxidization-reduction reaction) with Si_3N_4 workmaterial and leads to the formation of SiO_2 layer. Second, the hardness of CeO_2 is close to the SiO_2 layer and significantly lower ($\approx\frac{1}{3}$) than Si_3N_4 workmaterial. So, the Si_3N_4 substrate can hardly be scratched or damaged by CeO_2 but the SiO_2 layer can be removed under subsequent mechanical action of water and CeO_2 on Si_3N_4 workmaterial. The kinetic action, which involves the removal of the reaction products from the interface is critical in the CMP process. The chemical reaction can be continued only after the passivating layers are removed continuously by the mechanical action.

3. Moh's hardness of best abrasives for polishing various glasses (SiO_2) is ≈6.5 (Cook, 1990). Similarly, the hardness of the best polishing media used for CMP of Si_3N_4 that chemo-mechanically reacts to form the SiO_2 reaction layer which is removed subsequently by the mechanical action effectively without damaging the Si_3N_4 substrate is ≈6–7, for e.g., the Mohs hardness of CeO_2 is ≈6. The pH value of polishing environment (CeO_2 plus water-based magnetic fluid) is 6, which is also a suitable environment for removing SiO_2 layer by CeO_2. There are other similarities including the effectiveness of water and of CeO_2 medium for polishing glass. This is not altogether surprising as the material removal mechanism in the case of Si_3N_4 is through the formation of SiO_2 and in the case of glasses which is SiO_2 anyway. A similar mechanism may be applicable for the polishing of silicon wafers if CeO_2 is used as a polishing media in a water-based solution. This is based on the similarity of the formation of SiO_2 on the surface and its subsequent removal by mechanical action.

4. Reaction between Si_3N_4 workmaterial and water (from water-based magnetic fluid) also occurs (hydrolysis) and leads to the formation of SiO_2 layer which is removed from

he Si_3N_4 substrate by subsequent mechanical action of water nd CeO_2. Thus, the CeO_2 polishing media is particularly ffective in a water environment as found in this investigation.

5. The Si_3N_4 surface after CMP by cerium oxide may consist of an outer SiO_2 layer and an intermediary layer of silicon oxinitride ($Si_xO_yN_z$) on top of Si_3N_4 substrate. This is not much lifferent from the surface of Si_3N_4 workmaterial which has a atural oxidation layer in air even at room temperature.

Acknowledgments

This project is sponsored by grants from the National Science Foundation (NSF) on "Tribological Interactions in Polishing of Advanced Ceramics and Glasses," (CMS-9414610), and "Design, Construction, and Optimization of Magnetic Field Assisted Polishing," (DMI-9402895) and DoD's DEPSCoR Program on "Finishing of Advanced Ceramics" (DAAH04-96-1-0323) and CATT's program on Finishing Silicon Nitride Balls for Bearing Applications (Contract No. F34601-95-D-0376). This project was initiated by an ARPA contract on "Ceramic Bearing Technology Program" (F33615-92-5933). Thanks are due to Drs. J. Larsen Basse, B. M. Kramer, Ming Leu, and D. Durham of NSF and Dr. K. R. Mecklenburg of WPAFB and Dr. W. Coblenz of ARPA for their interest and support of this work. The authors also thank Dr. T. C. Collins, Vice-President for Research at OSU, for his support of this work. The authors thank Ms. K. Mallika, a graduate student at OSU, for the x-ray work.

References

Bhagavatula, S. R., and Komanduri, R., 1996, "On the Chemo-Mechanical Polishing of Silicon Nitride with Chromium Oxide Abrasive," *Phil. Mag. A*, Vol. 74/4, p. 1003.

Cook, L. M., 1990, "Chemical Processes in Glass Polishing," *J. of Non-Crystalline Solids*, Vol. 120, pp. 152–171.

Fischer, T. E., and Tomizawa, H., 1985, "Interaction of Tribo-chemistry and Microfracture in the Friction and Wear of Silicon Nitride," *Wear*, Vol. 105, p. 29.

Fischer, T. E., 1988, "Tribochemistry," *Ann. Rev. Mater. Sci.*, Vol. 18, p. 303.

Hah, S. R., 1995, "Tribochemical Polishing of Silicon Nitride," Ph.D. thesis, Stevens Institute of Technology, Hoboken, NJ.

Hah, S. R., and Fischer, T. E., 1995, "The Chemistry of Tribochemical Polishing," Chapter 4 in S. R. Hah, Ph.D thesis, Stevens Institute of Technology, Hoboken, NJ.

Hah, S. R., Fischer, T. E., and Burk, C., 1995, "Ceramic Bearing Development-Tribochemical Finishing of Silicon Nitride," Vo. 4, Technical Report No. WL-TR-96-4018, the Materials Directorate, Wright Patterson AFB, OH.

Jiang Ming, "Finishing of Si_3N_4 Balls for Bearing Applications," Ph.D thesis, Mechanical & Aerospace Engineering, Oklahona State University, Stillwater, OK (to be submitted).

Jiang Ming and Komanduri, R., 1997a, "Finishing of Si_3N_4 Balls for Bearing Applications," *Wear*, Vol. 215, pp. 267–278.

Jiang Ming and Komanduri, R., 1997b, "Application of Taguchi Method to Determine Polishing Conditions in Magnetic Float Polishing," *Wear*, Vol. 213, pp. 59–71.

Kanno, Y., Suzuki, K., and Kuwahara, Y., 1983, NH_3 Formation Caused by the presence of H_2O in the Wet Grinding of Silicon Nitride Powder," *Yog Yo-Kyokai-Shi*, Vol. 91, p. 386.

Kikuchi, M., Takahashi Y., Suga, T., Suzuki, S., and Yasunaga, N., 1990, "Mechanochemical Polishing of Silicon Carbide," *Proc. Fall Meeting of JSPE*, Vol. 327 (in Japenese).

Kilbourn, B. T., 1992, "CERIUM—A Guide to Its Role in Chemical Technology," Molycorp, Inc., White Plains, NY.

Komanduri, R., Umehara, N., and Raghunandan, M., 1996, "On the Posibility of Chemo-Mechanical Polishing of Silicon Nitride," ASME Journal of Tribology, Vol. 118, p. 721.

Mallika, K., and Komanduri, R., 1998, "Characterization of Si_3N_4 Balls in the As-received, Semi-Finished, Commercially Finished, and Finished by the MFP Process," paper under preparation.

Reddy, R. G., and Komanduri, R., 1998, "On the Chemical Species in Chemo-Mechanical Polishing of Si_3N_4 with Cr_2O_3," paper under preparation.

Reed, T. B., 1971, *Free Energy of Binary Compounds—An Atlas of Charts for High Temperature Chemical Calculations*, MIT Press, Cambridge, MA.

Ruhle, 1997, "Microscopy of Structural Ceramics," *Adv. Materials*, Vol. 9, No. 3, p. 195.

Shaffer, P. T. B., 1964, *Handbook of High-Temperature Materials—Material Index*, Plenum Press, New York.

Tomizawa, H., and Fischer, T. E., 1987, "Friction and Wear of Silicon Nitride and Silicon Carbide in Water: Hydrodynamic Lubrication at Low Sliding Speed Obtained by Tribochemical Wear," *ASLE Trans.*, Vol. 30, No. 1, pp 41–46.

Vora, H., Orent, T. W., and Stokes, R. J., 1982, "Mechano-Chemical Polishing of Silicon Nitride," *J. Amer. Ceram. Soc.*, Vol. 65, 9, p. C140.

Wang, J. C. and Hsu, S. M., 1994, ASME *J. of Tribology*, Vol. 116, p. 423.

Wallace, T. W., Wu, W. L., and Carpio, R. A., 1996, *Thin Solid Films*, Vol. 280, p. 37.

Wicks, C. E., and Block, F. E., 1963, "Thermodynamic Properties of 65 Elements—Their Oxides, Halides, Carbides, and Nitrides," U. S. Dept. of Interior, Bureau of Mines, Bulletin No. 605.

Wyatt, O. H., and Dew-Hughes, D., 1974, *Metals, Ceramics, and Polymers*, Cambridge University Press, U.K.

Yasunaga, N., Tarumi, N., Obara, A., and Imanaka, O., 1979, "Mechanism and Application of the Mechanochemical Polishing Method Using Soft Powder," *Science od Ceramic Mechining and Surface Finishing II*, B. J. Hockey, and R. W. Rice, eds., NBS Special Publication No. 562, Washington, D.C.; National Bureau of Standards, pp. 171–183.

APPENDIX A

Gibbs Free Energy of Formation Analysis

In this investigation, Outokumpu HSC Chemistry software program developed by the Outokumpu Research Oy Information Service, Finland was used [1]. It is a PC based software which runs on an IBM 486 with a Pentium processor and Microsoft Windows 95. It is used extensively around the world (industry, universities, and national laboratories) by chemists, electrochemists, and mechanical engineers. This program deals with chemical reactions and thermodynamic calculations with extensive thermochemical database (more than 11,000 chemical compounds) collected from references [2–6] and numerous recent articles in various journals. The program can calculate 1. reaction equations, 2. heat and material balances, 3. equilibrium compositions, 4. electrochemical cell equilibira, 5. formula weight, 6. phase stability diagrams, and 7. Eh -pH-diagrams (for studying dissolution and corrosion behavior of different materials). It provides a method and means of studying the effects of different variables of a chemical system at equilibrium. The inputs consist of various components involved in the reaction of any chemical process under consideration and what products to expect. The program will give the amount of products. The equilibrium composition is calculated by the GIBBS or SOLGASMIC program using Gibbs Free Energy Minimization method [7–10]. The user needs to specify the reaction system, with its phases and species, and the amount of raw materials. The program finds the most stable phase combination and seeks the phase compositions where the Gibb free energy of the system reaches its minimum at a fixed mass balance (a constant minimization problem), constant pressure and temperature. It, however, one does not know the substances of the system, one may begin by specifying its elements, i.e., a selection of the system components. Of course, the HSC program does not take into account the kinetics of the chemical reactions and nonideality of solutions. However, it is fast and simple to use for finding the optimum reaction conditions without expensive trial and error chemistry.

References

1 ———, 1998, "HSC Chemistry for Windows—Chemical Reaction and Equilibrium Software with Extensive Thermochemical Database," Outokumpu Research Oy Information Service (97036-ORC-T), Finland, April 30.

2 Barin, I., Knacke, O., and Kubaschewski, 1973, *Thermodynamic Properties of Inorganic Substances*, Spinger-Verlag, Berlin, Supplement 1977.

3 Pankratz, L. B., 1984, "Thermodynamic Properties of Halides," U.S. Dept. of Interior, Bureau of Mines, Bulletin 674.

4 Barner, H. E., and Scheuerman, R. V., 1978, *Handbook of Thermochemical Data for Compounds and Aqueous Species*, Wiley, New York.

5 Pourbaix, M., 1966, *Atlas of Electrochemical Equilibria in Aqueous Solutions*, Oxford University Press, U.K.

6 Schnick, H. L., 1966, *Thermodynamics of Certain Refractory Compounds*, Vols. I and II, Academic Press, NY.

7 Eriksson, G., 1975, "Thermodynamic Studies of High Temperature uilibria XII. SILGASMIX, A Computer Program for Calculation of Equilib- im Compositions in Multiphase Systems," *Chemical Scripta*, Vol. 8, pp. 0–103.
8 Eriksson, G., and Hack, K., 1990, "ChemSage—A Computer Program r the Calculation of Complex Chemical Equilibria, *Metall. Trans.*, Vol. 21(b), . 1013–23.
9 White, W. B., Johnson, S. M., and Dantzib, G. B., 1958, "Chemical Equilibrium in Complex Mixtures," *J. of Chemical Physics*, Vol. 28, pp. 751–755.
10 Lampinen, M. J., and Vuorisalo, J., 1992, "Thermodynamic Analysis of Chemical and Electrochemical Sysgtems with a Computer Program; Basic Theory with Illustrations," *Acta Polytechn., Scand.* Series No. 202, Helsinki.

APPENDIX E

ON THE THERMAL ASPECTS OF THE MAGNETIC FIELD ASSISTED POLISHING OF CERAMICS

Part I. Thermal Model

Zhen Bing Hou and R. Komanduri

Trans ASME, J of Tribology 120 (1998) 645-651

Magnetic Field Assisted Finishing of Ceramics—Part I: Thermal Model

Zhen-Bing Hou

R. Komanduri
Fellow ASME

Mechanical and Aerospace Engineering,
Oklahoma State University,
Stillwater, OK 74078

A thermal model for magnetic field assisted polishing of ceramic balls/rollers is presented. The heat source at the area of contact between the balls and the abrasives where material removal takes place is approximated to a disk. The disk heat source is considered as a combination of a series of concentric circular ring heat sources with different radii. Each ring in turn is considered as a combination of a series of infinitely small arc segments and each arc segment as a point heat source. Jaeger's classical moving heat source theory (Jaeger, 1942; Carslaw and Jaeger, 1959) is used in the development of the model, starting from an instantaneous point heat source, to obtain the general solution (transient and steady-state) of the moving circular ring heat source problem and finally the moving disc heat source problem. Due to the formation of fine scratches during polishing (on the order of a few micrometers long), the conditions are found to be largely transient in nature. Calculation of the minimum flash temperatures and minimum flash times during polishing enables the determination if adequate temperatures can be generated for chemo-mechanical polishing or not. This model is applied in Part II for magnetic float polishing (MFP) of ceramic balls and in Part III for magnetic abrasive finishing (MAP) of ceramic rollers.

1 Introduction

Moving heat source problems are commonly encountered in many manufacturing problems including metal cutting, grinding, polishing, welding, and heat treatment as well as in many tribological applications such as meshing of gears, bearings. The pioneers in this field are Blok (1937), Rosenthal (1941), and Jaeger (1942). For mathematical simplicity and from a practical consideration, both Rosenthal and Jaeger considered the heating time $t = \infty$ in the very early stages of the mathematical derivation, thus considering only the quasi-steady-state conditions. Thus, in their solutions, time is not a variable and hence the calculations are time independent. Other researchers who used quasi-steady state conditions and approximate equations for maximum temperature rise estimation on rubbing surfaces based on continuous plane heat source solutions, include, Archard (1959), Furey (1964), Barber (1967), Francis (1970), Ling (1973), Greenwood (1991), Bos and Moes (1995) and Tian and Kennedy (1994). This investigation is concerned with the determination of the flash temperatures generated at the interface between the abrasive and the workmaterial during finishing of advanced ceramics. It is not known a priori if the conditions during polishing are transient or quasi-steady state. Hence, need exists for the development of a general solution which will take both transient and quasi-steady-state conditions.

Rosenthal (1941, 1946), using a moving coordinate system, analyzed the moving point and moving line heat source problems for quasi-steady-state conditions directly by solving the partial differential equations for heat conduction. At about the same time, Jaeger (1942) (also briefly summarized in Carslaw and Jaeger, 1959), using the heat source method, solved the moving point, the moving line, the moving band, and the moving rectangular heat source problems. Both Rosenthal and Jaeger considered the heating time $t = \infty$ in the very early stages of the mathematical derivation, thus considering only the quasi-steady state conditions to facilitate a solution.

The heat source method developed by Jaeger enables solutions of many complex heat conduction problems including the moving heat source problems. The application of the heat source method also provides better physical interpretation of the process than the use of partial differential equations. The basis for this method is the solution of a simpler problem, namely, instantaneous point heat source. By integrating this equation with respect to appropriate time and spatial variables for a given geometry (in the present case a disc heat source), and a given distribution of heat intensity, moving or stationary, the exact and complete solutions (transient and steady state) can be obtained as will be shown in this paper. A similar analysis can be performed to obtain generalized solutions for different shapes of heat sources (elliptic, circular, square, and rectangular) for instantaneous or continuous or even moving heat source with different heat intensity distributions (e.g., normal, parabolic, uniform) without invoking the assumption of $t = \infty$ during the entire process of mathematical derivation (Hou and Komanduri, 1997). Starting with a moving elliptic heat source, by considering the major axis to be equivalent to the minor axis, the solution for a circular heat source can be developed. Similarly, if the width of the heat source is constant, then solutions for rectangular and square heat sources can be obtained. The advent of powerful, inexpensive computers enables this task to be accomplished efficiently and rapidly.

Tian and Kennedy (1994), using the heat source method of Jaeger, developed a series of quasi-steady-state solutions for moving circular, moving square, and moving elliptical heat sources of uniform and parabolic distribution of heat liberation intensities by integrating the solution of a moving point heat source with appropriate spatial variables. Bos and Moes (1995), also using the heat source method, gave solutions for a moving elliptical heat source with parabolic distribution of heat intensity with consideration for heat partition. They developed a numerical approach to solve the steady-state heat partitioning and the associated flash temperatures for arbitrary shaped contacts by matching the surface temperatures of the two contacting solids

Contributed by the Tribology Division for publication in the JOURNAL OF TRIBOLOGY. Manuscript received by the Tribology Division June 27, 1997; revised manuscript received October 20, 1997. Associate Technical Editor: F. E. Kennedy, Jr.

at all points inside the contact area using relaxation schemes. These functional fits are based on asymptotic solutions covering the entire range of Peclet numbers from small to large. Unfortunately, all these solutions are for quasi-steady-state conditions and may not be applicable for the final stages of polishing where most scratch lengths are extremely short (<15 μm) and consequently, quasi-steady state conditions may not be attained. For consideration of chemo-mechanical action, it is necessary to calculate the minimum possible flash times and flash temperatures under these conditions. Of course, conditions would be more favorable for chemo-mechanical action under quasi-steady state, or longer scratches, or higher polishing speeds as the temperatures and flash times would be much higher.

While quasi-steady-state solutions may be readily available and convenient, one cannot expect or assume that all engineering problems involve quasi-steady-state conditions. Oftentimes, the use of such an assumption can lead to significant errors in many applications. It can be shown that for certain manufacturing operations, such as grinding and polishing, steady state conditions may not be reached in most situations. In fact, these processes are characterized as transient in nature for this very reason. Also, it would be valuable to establish if the conditions are transient or steady state for a given case. It will be shown in this paper that for the case of magnetic float polishing (MFP) of ceramic balls both the load applied as well as the contact area are small. Consequently, the temperature at the interface for both transient and quasi-steady state are nearly the same. In contrast, in the case of magnetic abrasive finishing (MAF) of ceramic rollers, both the loads and contact areas are significantly higher (than MFP) with the result that there is a significant difference in the contact temperatures for the transient and quasi-steady state conditions. The actual case can only be determined by considering the general solution that involves both spatial and time variables. If the conditions are quasi-steady state then one can substitute $t = \infty$ in the solution developed in the present investigation or use for example, Tian and Kennedy (1994) and Bos and Moes (1995) solutions. In this investigation this substitution was made to calculate the temperature rise for the quasi-steady-state conditions and compared with the quasi-steady-state solutions available in the literature (for example, Francis, 1970; Tian and Kennedy, 1994; and Bos and Moes, 1995). The results show good agreement in the temperature rise values for quasi-steady-state conditions. If the conditions are transient, then one can use the general solution developed here.

In this paper, a thermal model of the polishing process is presented for the first time. It includes the development of a heat transfer model of the process by approximating the contact area between the ball/roller and the abrasive to a moving disc source. The temperature field, the expected flash temperatures, and related flash times nearby and at the areas of contact under the polishing conditions for both transient and quasi-steady state can be calculated. The solutions for different Peclet numbers were obtained for the quasi-steady-state conditions and compared qualitatively with the quasi-steady state solutions available in the literature, e.g., Tian and Kennedy's model (1994). This model is then applied for the case of magnetic float polishing (MFP) of ceramic balls in Part II (Hou and Komanduri, 1998a) and for magnetic abrasive finishing (MAF) of rollers in Part III (Hou and Komanduri, 1998b), respectively.

2 Thermal Model of Magnetic Field Assisted Polishing

Figure 1 shows schematically the model used for the heat transfer process during magnetic float polishing (MFP) of ceramic balls. A moving disk heat source with a radius of r_o and heat generation intensity of q, moves on the ceramic surface with a velocity of v. For convenience, as well as, for the choice of a model closer to practice, a parabolic distribution of heat generation from the center to the periphery is considered. In this analysis, as a first step, the variation of thermal properties with temperature of the ball and the shaft materials are not considered. The objective of this analysis is to determine the temperature rise at any point and its distribution nearby and at the heat source, including on the surface as well as in the subsurface.

The disk plane heat source can be considered as a combination of a series of concentric circular ring heat sources with different radii (from $r = 0$ to r_o). Each ring can be regarded as a combination of a series of infinitely small arc segments and each segment as a point heat source. Based on the solution for the instantaneous point heat source, the instantaneous circular ring heat source problem can be solved.

Instantaneous Ring Heat Source Problem. Figure 2 is a schematic of the instantaneous ring heat source problem. The origin of the coordinate system coincides with the center of the instantaneous ring heat source with radius, r_o. Consider a small segment of the ring heat source ($r_o\, d\alpha$) as an instantaneous point heat source. Using the solution for the instantaneous point heat source (Jaeger, 1942; Carslaw and Jaeger, 1959) the temperature rise caused by the ring segment of the heat source at any point M and at any instant τ (the time after the initiation of the instantaneous ring segment heat source) can be calculated as:

$$d\theta_M = \frac{Qrg\,d\alpha}{c\rho(4\pi a\tau)^{3/2}\cdot 2\pi}\cdot\exp\left(-\frac{R^2}{4a\tau}\right)$$

where Qrg is the heat released by the instantaneous ring heat

Nomenclature

a = thermal diffusivity, m^2/s
c = specific heat, J/gr/°C
$I_o(p)$ = modified Bessel function of the first kind, order zero, $\frac{1}{2\pi}\int_o^{2\pi}\exp(p\cos\alpha)d\alpha$
N_{Pe} = Peclet Number ($=r_o\, v/2a$)
q = rate of heat generation J/s
q_{dc} = rate of heat generation by a disk heat source, J/s
q_{rg} = rate of heat generation by a ring heat source, J/s
Q_{rg} = heat generated by an instantaneous ring heat source, J
r_i = radius of one of the concentric differential segmental ring heat sources from the disk heat source, $r_i = 0$ to r_o
r_o = radius of the moving ring or moving disc heat source, m
t = time after the initiation of the moving heat source, s
v = velocity of the moving heat source along X-axis or sliding velocity, in m/s
$V = v/2a$
w = normal load, N/particle
W = normal load, N/ball
x, y, z = coordinates of the point M in the absolute coordinate system
X, y, z = coordinates of the point of interest (point M) in the moving coordinate system
μ = coefficient of friction
θ_M = the temperature rise at any point M
τ = time after the initiation of an instantaneous heat source
λ = thermal conductivity, J/m.s °C
ρ = density, gr/cm^3
ω = a dimensionless number which has its value from 0 to $v^2t/4a$

* Refer to the same Nomenclature for Parts II and III.

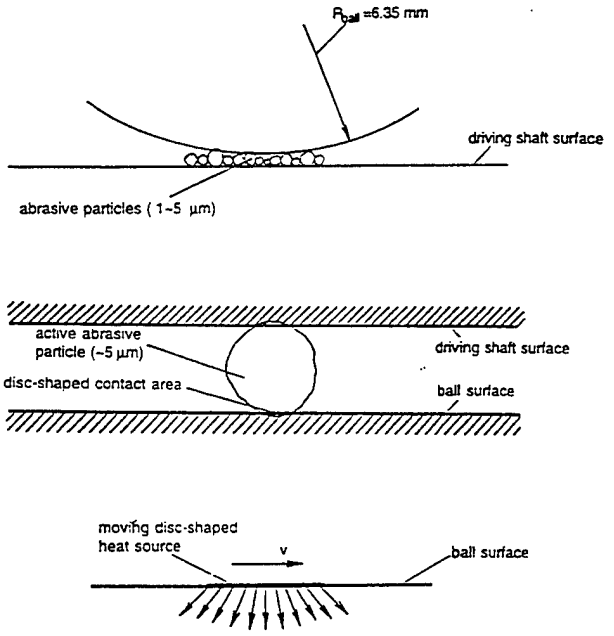

Fig. 1 Schematic showing the model used for simulating the heat transfer process during magnetic float polishing of ceramic balls

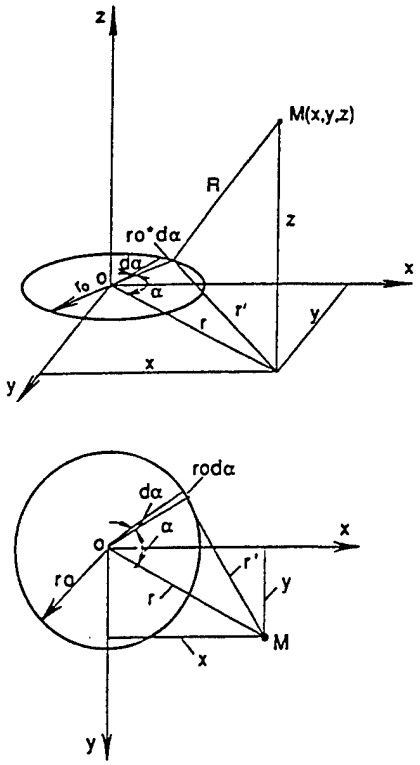

Fig. 2 Illustration of the instantaneous ring heat source problem

source, $Qrg/2\pi r_o$ is the heat released by the ring heat source per unit length, and $Qrgd\alpha/2\pi$ is the heat released by the segment $r_o d\alpha$, where $R^2 = r'^2 + z^2$, r' is the projection of R on the x-o-y plane, $r'^2 = r_o^2 + r^2 - 2rr_o \cos\alpha$, $R^2 = r_o^2 + r^2 + z^2 - 2rr_o \cos\alpha$, and r is the projection of distance vector between the center of the ring heat source o and any point of interest, M on the x-o-y plane.

The total temperature rise at any point M, caused by the instantaneous ring heat source is given by:

$$\theta_M = \frac{Qrg}{c\rho(4\pi a\tau)^{3/2}} \cdot \frac{1}{2\pi} \cdot \exp\left(-\frac{r_o^2 + r^2 + z^2}{4a\tau}\right) \times \int_o^{2\pi} \exp\left(\frac{rr_o}{2a\tau}\cos\alpha\right) d\alpha$$

Here, $(1/2\pi)\int_o^{2\pi} \exp(p\cos\alpha)d\alpha$ is the modified Bessel function of the first kind, order zero and designated as $Io(p)$, where $p = rr_o/2a\tau$.
Hence,

$$\theta_M = \frac{Qrg}{c\rho(4\pi a\tau)^{3/2}} \cdot \exp\left(-\frac{r_o^2 + r^2 + z^2}{4a\tau}\right) \cdot I_o\left(\frac{rr_o}{2a\tau}\right) \quad (1)$$

For the case shown in Fig. 2, Eq. (1) can also be written as:

$$\theta_M = \frac{Qrg}{c\rho(4\pi a\tau)^{3/2}} \cdot \exp\left(-\frac{r_o^2 + x^2 + y^2 + z^2}{4a\tau}\right) \times I_o\left(\frac{r_o}{2a\tau}\sqrt{x^2 + y^2}\right) \quad (2)$$

Figure 3 shows the variation of the function $I_o(p)$ and the approximate exponential function $I'_o(p)$ with p for different ranges of p. The following approximate exponential functions were developed for different regions (I, II, and III in Fig. 3) to fit the curve $I_o(p)$. It can be seen that the fit is very good for values of $p > 1.25$ and the error is <5 percent for values of $p < 1.25$. These exponential functions are used in the later derivations for the moving ring heat source problem for computational ease.

when	$p < 1.6$	$Io(p) \approx 0.935 \cdot \exp(0.352p)$
when	$1.6 \le p \le 3$	$Io(p) \approx 0.529 \cdot \exp(0.735p)$
when	$p > 3$	$Io(p) \approx \exp(p)/(2\pi p)^{0.5}$
when	$p = 0$	$Io(p) = 1$

Moving Ring Heat Source Problem. Figures 4(*a*) and (*b*) illustrate the moving ring heat source problem showing the relationships between the spatial and the temporal parameters. x, y, and z axes are the absolute coordinate system while X, y, z axes are the corresponding moving coordinate system which has its origin coinciding with the center of the moving ring heat source and moves with it with the same velocity along the X-axis. As shown in Fig. 4(*a*), a moving ring heat source continuously liberates heat q_{rg} (J/s) and moves along the X-axis with a velocity v (m/s). It is the objective to determine the temperature rise at any point M (x, y, z) and at any time t after the initiation of the heat source.

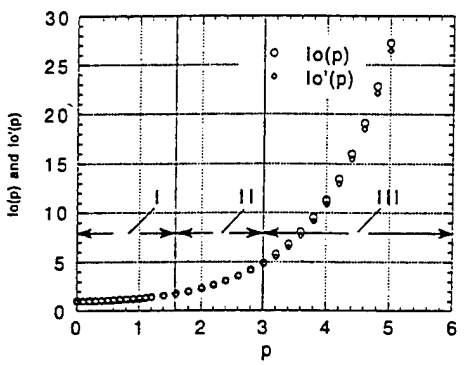

Fig. 3 Variation of *Io*(*p*) and *I'o*(*p*) for various values of *p*

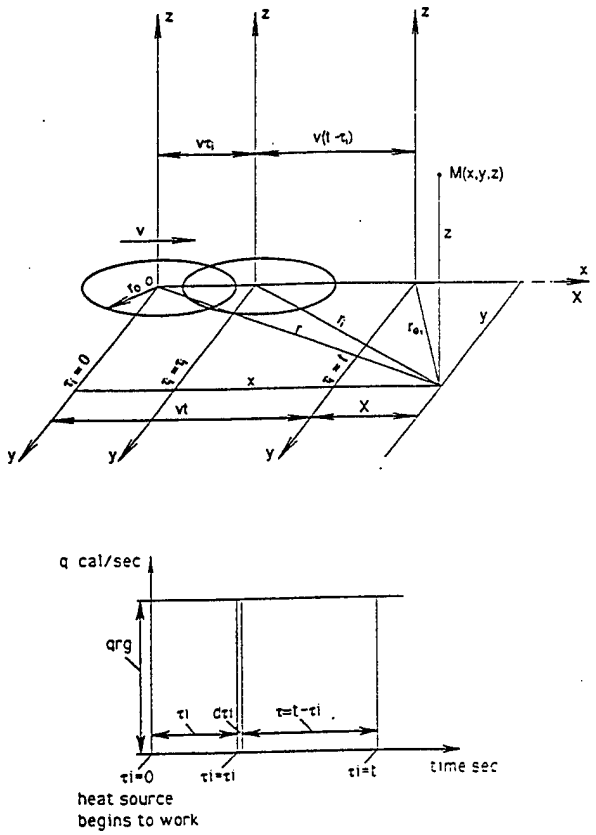

Fig. 4(a)–(b) Schematics of a moving ring heat source in an infinitely large conducting medium showing spacial and time relationships

Consider a small time interval $d\tau_i$ at time τ_i [refer to Fig. 4(*b*)]:

1. In this time interval, the heat liberated by the ring heat source which can be considered as liberated instantaneously is given by $q_{rs} \cdot d\tau_i$, J.
2. At instant τ_i, the ring heat source has moved a distance $v\tau_i$, [see Fig. 4(*a*)]. So, the location of M relative to the heat source center has changed. The projection of the distance vector between the center of the ring heat source and point M on plane x-o-y has changed from r to r_i, where $r_i^2 = (x - v\tau_i)^2 + y^2$
3. At time τ_i, the heat liberated in the small time interval $d\tau_i$ will cause a temperature rise, $d\theta_M$ at point M at time t (using Eq. (2)):

$$d\theta_M = \frac{q_{rs} d\tau_i}{c\rho(4\pi a\tau)^{3/2}} \cdot \exp\left(-\frac{r_o^2 + (x - v\tau_i)^2 + y^2 + z^2}{4a\tau}\right) \times I_o\left[\frac{r_o}{2a\tau}\sqrt{(x - v\tau_i)^2 + y^2}\right] \quad (3)$$

Using the moving coordinate system and the following substitutions, integration of Eq. (3) from $\tau_i = 0$ to $\tau_i = t$, yields the temperature rise at any point M and at any time t caused by the moving ring heat source.

$$X = x - vt;$$

X, x are the coordinates of M in moving and absolute coordinate systems respectively. [in the direction of x-axis see Fig. 4(*a*)]

$$\tau_i = t - \tau, \quad v\tau_i = vt - v\tau,$$

$$x - v\tau_i = x - vt + v\tau = X + v\tau$$

$$\theta_M = \frac{q_{rs}}{c\rho(4\pi a)^{3/2}} \int_{\tau_i=0}^{\tau_i=t} \frac{d\tau_i}{\tau^{3/2}} \times \exp\left(-\frac{r_o^2 + (X + v\tau)^2 + y^2 + z^2}{4a\tau}\right) \times I_o\left[\frac{r_o\sqrt{(X + v\tau)^2 + y^2}}{2a\tau}\right] \quad (4)$$

where $\tau_i = t - \tau$, $d\tau i = -d\tau$

where $\tau_i = 0$, $\tau = t$; when $\tau_i = t$, $\tau = 0$

Here, $(X + v\tau)^2 = X^2 + 2Xv\tau + v^2\tau^2$,

Hence,

$$\exp\left(-\frac{r_o^2 + (X + v\tau)^2 + y^2 + z^2}{4a\tau}\right) = \exp\left(-\frac{r_o^2 + X^2 + y^2 + z^2}{4a\tau}\right) \cdot \exp\left(-\frac{Xv}{2a}\right) \cdot \exp\left(-\frac{v^2\tau}{4a}\right)$$

Thus, Eq. (4) can be written as:

$$\theta_M = \frac{q_{rs}}{c\rho(4\pi a)^{3/2}} \cdot \exp\left(-\frac{Xv}{2a}\right) \int_{\tau=0}^{\tau=t} \frac{d\tau}{\tau^{3/2}} \times \exp\left(-\frac{r_o^2 + X^2 + y^2 + z^2}{4a\tau}\right) \times \exp\left(-\frac{v^2\tau}{4a}\right) \cdot I_o\left[\frac{r_o\sqrt{(X + v\tau)^2 + y^2}}{2a\tau}\right]$$

Let

$$\frac{v^2\tau}{4a} = \omega; \quad R_h^2 = r_o^2 + X^2 + y^2 + z^2;$$

$$\frac{v}{2a} = V; \quad R_hV = u; \quad v\tau = \frac{2\omega}{V}$$

Hence, the solution for the moving ring heat source is given by

$$\theta_M = \frac{q_{rs}v}{16\lambda a\pi^{3/2}} \cdot \exp(-XV) \int_o^{v^2t/4a} \frac{d\omega}{\omega^{3/2}} \cdot \exp\left(-\omega - \frac{u^2}{4\omega}\right) \times I_o\left[\frac{r_oV^2}{2\omega}\sqrt{\left(X + \frac{2\omega}{V}\right)^2 + y^2}\right] \quad (5)$$

It may be noted from Eq. (5) that temperature rise is time dependent. So, it can be used for transient conditions as well. It can also be seen that the function to be integrated in Eq. (5) has in the denominator $\omega^{3/2}$. The lower limit of integration is zero. During numerical integration, when $\omega = 0$, the value of the function becomes infinity. Thus Eq. (5) cannot be used directly for computation on computers. To address the problem, first, the nature of the function being integrated should be investigated. For this purpose, a plot of the variation of the function $f(\omega)$ with ω was made as shown in Fig. 5. The function $f(\omega)$ is given by,

$$f(\omega) = \frac{1}{\omega^{3/2}} \cdot \exp\left(-\omega - \frac{u^2}{4\omega}\right) \times I_o\left[\frac{r_oV^2}{2\omega}\sqrt{\left(X + \frac{2\omega}{V}\right)^2 + y^2}\right]$$

Consider the case of $r_o = 5$ μm. It can be seen that for different values of X, the form of the curves is different but the curves always converge as $\omega \to 0$ and $\omega \to 5$ (Fig. 5). Also note that the function $f(\omega)$ increases initially for $X = 1, 3, 5$ μm (approaching the heat source closer and closer) and then decreases with further increase of X to 7, 9 μm (leaving the heat source farther and farther). When $(v^2t/4a)$ (upper limit of ω) is larger than 5, no matter how large, even ∞, the results of the calculation remain the same. Since, in many cases, the upper limit of integration of Eq. (5) is larger than 5, we may as well consider the upper limit as ∞. Once the integration is from 0 to ∞, the variable ω becomes merely a dimensionless real number. Thus in Eq. (5), the time variable disappears. The temperature rise, therefore, will no longer be time dependent. This means, at all those points in the moving coordinate system, the temperature rise reaches a steady state, i.e., $(d\theta/d\tau) = 0$. This is the so-called quasi-steady state. That means, Eq. (5) can also be used for quasi-steady state. For practical purposes, the upper limit of integration can be taken as 5 instead of ∞ for quasi-steady state. As ω is in the denominator of Eq. (5), the function to be numerically integrated cannot be calculated by a computer when $\omega = 0$. By considering the lower limit not as 0, but a very small but finite value, say 0.0001, it becomes possible to numerically integrate Eq. (5) with negligible error.

Based on above analysis, the time required for establishing the quasi-steady state $t_{\text{steady state}}$ can be calculated as follows:

$$\frac{v^2 t_{\text{steady state}}}{4a} = 5, \quad \text{or} \quad t_{\text{steady state}} = 5 \cdot \frac{4a}{v^2} = \frac{20a}{v^2} \qquad (6)$$

Equation (6) shows that the time required for establishing quasi-steady state is proportional to the thermal diffusivity of the material and inversely proportional to the square of the sliding speed. For a stationary body (the sliding speed relative to the heat source is zero), the t_{steady} is ∞, i.e., the process needs a very long time to establish steady-state conditions.

Using Eq. (5), the temperature rise at any point near and on the moving ring heat source can be calculated. Thus a complete profile of the temperature distribution around the moving ring heat source can be obtained. It may be noted that Eq. (5) is derived for an infinitely large conducting medium. For a semi-infinite conducting medium which is close to the various polishing problems, the temperature rises of those points on the surface and under the surface caused by a moving ring heat source on the surface is given by:

$$\theta_M = \frac{q_{rg} v}{8\lambda a \pi^{3/2}} \cdot \exp(-XV) \times \int_o^{v^2 t/4a} \frac{d\omega}{\omega^{3/2}} \cdot \exp\left(-\omega - \frac{u^2}{4\omega}\right) \cdot Io(p) \qquad (7)$$

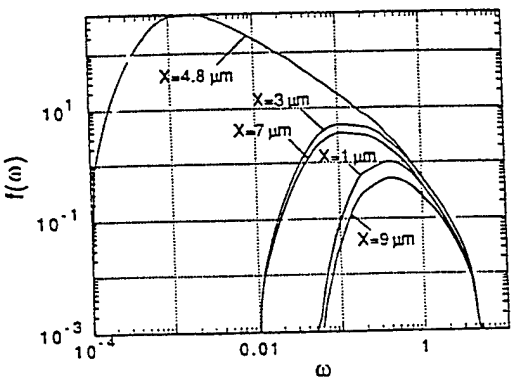

Fig. 5 Variation of $f(\omega)$ with ω for different values of X = 1, 3, 4.8, 7, and 9 μm

where

$$p = \frac{r_o V^2}{2\omega} \sqrt{\left(X + \frac{2\omega}{V}\right)^2 + y^2}$$

Moving Disk Heat Source Problem. The disk heat source of radius r_o can be considered as a combination of a series of concentric ring heat sources with different radii from zero to r_o. Generally the intensity of heat liberation is not uniformly distributed from the center to the periphery. A reasonable assumption would be to consider the distribution as parabolic.

Thus, the heat liberation intensity over the disk heat source is a function of the radius of the differential ring segment r_i ($r_i = 0 \sim r_0$). That is

$$q = 2q_{dc}/\pi r_0^2 \left(1 - \frac{r_i^2}{r_0^2}\right) \quad (\text{J/cm}^2\ \text{s})$$

The rate of heat liberation of the differential ring segment is

$$q_{rg} = 2q_{dc}/\pi r_0^2 \left(1 - \frac{r_i^2}{r_0^2}\right) 2\pi r_i dr_i$$

$$= 4q_{dc} \left(1 - \frac{r_i^2}{r_0^2}\right) r_i dr_i / r_0^2 \quad (\text{J/s})$$

Substituting for q_{rg} in Eq. (7), we get

$$d\theta_M = \frac{q_{dc} v}{2\lambda a \pi^{3/2} r_0^2} \exp(-XV) \left(1 - \frac{r_i^2}{r_0^2}\right) r_i dr_i \times \int_0^{v^2 t/4a} \frac{d\omega}{\omega^{3/2}} \exp\left(-\omega - \frac{u_i^2}{4\omega}\right) I_o(p)$$

Integrating it with respect to r_i from $r_i = 0$ to $r_i = r_0$ the general solution (both for transient and quasi-steady state) for the moving disk heat source for a semi-infinite body, as in the present case, is given by the following equation:

$$\theta_M = \frac{q_{dc} \cdot v}{2\lambda a \pi^{3/2} r_o^2} \cdot \exp(-XV) \int_o^{r_o} \left(1 - \frac{r_i^2}{r_o^2}\right) r_i dr_i \times \int_o^{v^2 t/4a} \frac{d\omega}{\omega^{3/2}} \cdot \exp\left(-\omega - \frac{u_i^2}{4\omega}\right) \cdot I_o(p) \qquad (8)$$

where

$$p = \frac{r_i V^2}{2\omega} \sqrt{\left(X + \frac{2\omega}{V}\right)^2 + y^2}; \quad u_i = R_{hi} \cdot V;$$

$$R_{hi} = r_i^2 + X^2 + y^2 + z^2$$

See Nomenclature for the definition of other parameters.

3 Results

It may be noted that Eq. (8) is for parabolic distribution. It can, however, be modified for uniform distribution simply by substituting $\frac{1}{2}$ for the term $(1 - r_i^2/r_o^2)$. Figures 6 (*a*) to (*b*) show the nondimensional temperature distribution at the contact interface for a uniform disc heat source under quasi-steady-state conditions ($t = \infty$) for various Peclet numbers. X is the distance from the center of the heat source along the sliding direction and r_o is the radius of the moving disk heat source. A comparison of the results of Tian and Kennedy (1994) with these results indicate a close similarity in the general nature of these curves.

For comparing the general equations developed in this investigation for the case of quasi-steady-state conditions ($t = \infty$) with similar equations available in the literature (e.g., Francis,

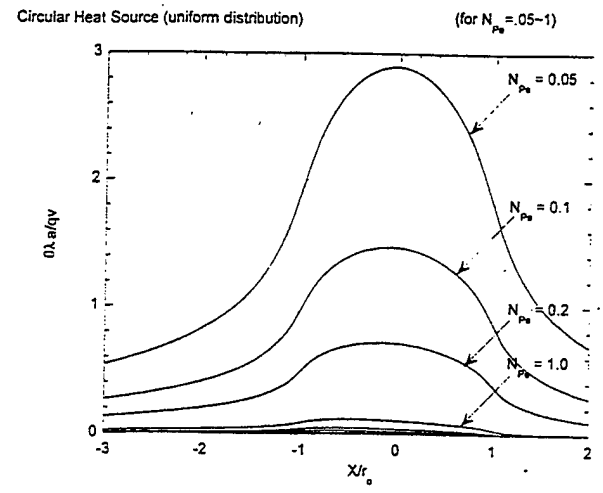

(a)

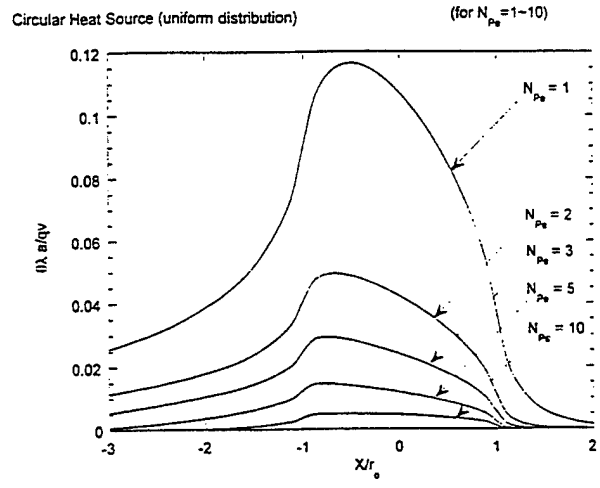

(b)

Fig. 6(*a*)–(*b*) Variation of the temperature distribution [nondimensional temperature ($\lambda a\theta_M/qv$)] at the contact interface for a uniform heat source for quasi-steady-state-conditions using the disk heat source method developed in this paper

1970; Tian and Kennedy, 1994; Bos and Moes, 1995), Eq. (8) was used to calculate the maximum temperature rise for quasi-steady state using typical ball polishing parameter given in the following.

Consider the heat source to be circular with a parabolic distribution. Contact load 1.25/22 N/particle; ball material: Silicon Nitride (λ_1 = 29.3 J/m.s °C; a_1 = 0.139 cm2/s;); Abrasive: Cr_2O_3 (λ_2 = 31.8 J/m.s °C). The maximum temperature rise, θ_M was found to be 400.2°C for a sliding velocity of 2 m/s and 1213.5°C for a sliding velocity of 6 m/s. For the same conditions, the values of θ_M obtained using various equations in the literature are given in Table 1. These values were kindly provided by one of the reviewers to whom the authors are grateful.

Close agreement of the results obtained from the current investigation for the quasi-steady-state conditions with the data generated from the literature validates the model developed.

4 Discussion

In this investigation a thermal model (general solution) for the moving disc shaped heat source was developed starting from the Jaeger's instantaneous point heat source. This model enables the calculation of the flash temperatures, flash times, and temperature distribution at the contact area.

It may be pointed out that many of the earlier models for moving heat sources, some for maximum flash temperature rise estimations, some for exact temperature distribution calculations (Rosenthal, 1946; Archard, 1958/59; Kuhlmann-Wildorf, 1985; Greenwood, 1991; Tian and Kennedy, 1994; Bos and Moes, 1995) all considered for quasi-steady-state conditions. Gecim and Winer (1985) considered the case of transient conditions but only for a stationary heat source. Their solutions would not be applicable for situations such as the transient moving heat source phenomenon in polishing, grinding, and even some frictional sliding contacts. In this paper, exact solutions for both transient and quasi-steady state are considered. The consideration of using disk-shaped moving heat source with a parabolic distribution of the heat liberation intensity is believed to be much closer to the practical cases involved in these manufacturing processes. In the analysis presented here, it is possible to calculate the temperatures over a wide range of sliding speeds. It is also possible to calculate not only the maximum and mean temperatures but also the complete map of the temperature distribution in and around the heat source for both transient and quasi-steady state.

It will be shown in Part II that the results of the temperature rise calculations for the transient and quasi-steady-state cases are quite close (see Part II for details). This is because the load and the contact area are extremely small. In contrast, for those cases with higher loads and larger contact areas as in the case of magnetic abrasive finishing (MAF), the differences in the temperature rise distributions for transient and quasi-steady-state cases will be quite significant (see Part III for details). Consequently, one cannot consider quasi-steady-state conditions for all cases of manufacturing and tribology.

In the assessment of possible chemical reactions that may form during chemomechanical polishing, both flash temperatures (for thermodynamic analysis) and flash times (kinetics) have to be considered. The mathematical analysis presented here enables the calculation of minimum possible flash temperatures and flash times in the transient stage which is not possible with the use of quasi-steady-state solutions mentioned earlier. Also, the mathematical computational analysis presented here imposes no restrictions on the size of the sample while that of using FEM analysis is by necessity limited by the mesh size.

It may also be pointed out that quasi-steady-state equations for flash temperatures were used earlier (Rosenthal, 1946; Jaeger, 1942; and others) basically to reduce the mathematical complexity and consequently the computational time. By considering quasi-steady-state conditions, standard mathematical tables for Bessel functions could be used (Spiegel, 1993) to obtain the solutions which would otherwise be impossible or computationally intensive in those times. However, with the advent of fast computers, use of exact equations, starting from the fundamental equation of Jaeger's instantaneous point heat source (Carslaw and Jaeger, 1959) does not necessarily pose any serious limitations as shown in this paper. The integrals can be solved by numerical methods without the need to resort only to standard mathematical tables. Besides, the results are more accurate. Also, both transient and quasi-steady-state conditions can be addressed with equal ease.

For comparing the general equations developed in this investigation for the case of quasi-steady-state conditions ($t = \infty$) with similar equations available in the literature (e.g., Francis, 1970; Tian and Kennedy, 1994; Bos and Moes, 1995), Eq. (8) was used to calculate the maximum temperature rise for quasi-steady state using typical ball polishing parameters. It was shown in this investigation that by substituting $t = \infty$ in the general solution (Eq. (8)) quasi-steady-state solutions can be obtained. The temperature rise values obtained for different sliding velocities were compared with the values obtainable

Table 1 Maximum temperature rise, θ_M, °C for two different sliding velocities using quasi-steady-state equations from the literature

Sliding velocity, v, m/s	Maximum temperature rise, θ_M, °C			
	Francis (1970)	Tian and Kennedy (1994)	Bos and Moes (1995)	Hou and Komanduri (present work)
2	405	400	385	400.2
6	1220	1175	1100	1213.5

using the quasi-steady-state solutions in the literature. Reasonably good agreement was obtained thus validating the model. However, the model can also be used for transient conditions.

Although a circular disk heat source is considered in this investigation, it is possible to consider other geometries, such as elliptical, square, tear shaped heat sources using a similar approach as presented here starting with the Carslaw and Jaeger's instantaneous point heat source solution (Hou and Komanduri, 1997). This way other manufacturing operations, such as high-energy beam machining, surface coatings, surface heat treatment, and welding as well as tribological problems where moving disk heat source plays an important role can be addressed.

5 Conclusions

1. A general solution (both transient and quasi-steady state) for a moving disk heat source with a parabolic distribution of heat intensity (Eq. (8)) was developed. This solution can be used to calculate both flash temperatures generated as well as the flash times at the contact point. Part II of this three-part series shows the application of this method for magnetic float polishing (MFP) of ceramic balls and Part III shows the application of this method for magnetic abrasive finishing (MAF) of rollers.

2. As the integral part of Eq. (8) cannot be solved directly by analytical methods, it is computed using numerical integration. However, prior to it, the nature of the function, $f(\omega)$ to be integrated has to be investigated rigorously with no arbitrary assumptions as shown in Fig. 5. It can be seen that the function $f(\omega)$ converges when $\omega \to 0$ and $\omega \to 5$. Thus, the integration of the integral part of Eq. (8) from 0 to any value larger than 5 (no matter how large, even ∞) will give the same result as integration from 0 to 5. Or, in other words, for quasi-steady state (when $t = \infty$, i.e., the upper limit of ω is ∞) one can take the upper limit as 5 and conduct the numerical integration as though it should be carried to ∞ without losing any accuracy. Thus, numerical integration from 0 to ∞ becomes possible.

Regarding the lower limit of the function in Eq. (8), it may be noted that it is zero. Therefore, the function actually becomes ∞ at this value and again cannot be solved numerically by the computer. Hence, instead of zero, a small value is given to the lower limit, say, 0.0001 which will then make the value of the function finite with no lose of accuracy. Thus, numerical integration of $f(\omega)$ from 0 to any value becomes possible.

3. In solving the numerical integration of the integral in Eq. (8), for transient conditions, the limits of integration would thus be from 0.0001 to $v^2t/4a$.

4. Comparing the values obtained of the maximum temperatures generated at the interface at different sliding velocities for the quasi-steady-state conditions using the generalized equations developed here with the results obtained from the quasi-steady-state equations available in the literature, good agreement was obtained thus validating the model developed.

Acknowledgments

The material presented in this three-part series on Magnetic Field Assisted Polishing is sponsored by grants from the National Science Foundation on "Tribological Interactions in Polishing of Advanced Ceramics and Glasses," (CMS-9414610), "Design, Construction, and Optimization of Magnetic Field Assisted Polishing," (DMI-9402895), and DoD's DEPSCoR Program on "Finishing of Advanced Ceramics" (DAAH04-96-1-0323). This project was initiated by an ARPA contract on "Ceramic Bearing Technology Program" (F33615-92-5933). Thanks are due to Drs. J. Larsen Basse, B. M. Kramer, Ming Leu, and J. Lee of NSF and Dr. K. R. Mecklenburg of WPAFB and Dr. W. Coblenz of DARPA for their interest and support of this work. Thanks are also due to Dr. M. Raghunandan, a former graduate student at OSU, for his contributions to the research carried out at OSU in this area and to Mr. S. R. Bhagavatula, a former graduate student at OSU for his initial contributions to Part III. The authors would like to thank especially the reviewers and Dr. F. E. Kennedy, Jr. for their thoughtful comments, suggestions, and inputs that enabled significant improvements in the outcome of the paper. This acknowledgement is extended to Parts II and III of this three-part series.

References

Archard, J. F., 1958–59. "The Temperature of Rubbing Surfaces," *Wear*, Vol. 2, pp. 438–455.

Barber, J. R., 1967. "Distribution of Heat Between Sliding Surfaces," *J. of Mech. Eng. Sci.*, Vol. 9, p. 351.

Bos, J. and Moes, H., 1995. "Frictional Heating of Tribological Contacts," ASME JOURNAL OF TRIBOLOGY, Vol. 117, pp. 171–177.

Blok, H., 1937. "Theoretical Study of Temperature Rise at Surface of Actual Contact Under Oiliness Lubricating Conditions," *I. Mech. E. Proceedings of General Discussion on Lubrication and Lubricants*, Vol. 2, pp. 222–235.

Carslaw, H. S., and Jaeger, J. C., 1959, *Conduction of Heat in Solids*, Oxford University Press, 2nd edn.

Francis, H. A., 1970. "Interfacial Temperature Distribution within a Sliding Hertzian Contact," *ASLE Trans.*, Vol. 14, pp. 41–54.

Furey, M. J., 1964. "Surface Temperatures in Sliding Contact," *ASLE Trans.*, Vol. 7, pp. 11.

Gecim, B., and Winer, W. O., 1985. "Transient Temperatures in the Vicinity of an Asperity Contact," ASME JOURNAL OF TRIBOLOGY, Vol. 107, pp. 333–342.

Greenwood, J. A., 1991. "An Interpolation Formula for Flash Temperatures," *Wear*, Vol. 150, pp. 153–158.

Hou, Z. B., and Komanduri, R., 1998a. "Magnetic Field Assisted Finishing of Ceramics—Part II: On Thermal Aspects of Magnetic Float Polishing (MFP) of Ceramic Balls," ASME JOURNAL OF TRIBOLOGY, Vol. 120, pp. 652–659.

Hou, Z. B., and Komanduri, R., 1998b. "Magnetic Field Assisted Finishing of Ceramics, Part III: On Thermal Aspects of the Magnetic Abrasive Finishing (MAF) of Ceramic Rollers," ASME JOURNAL OF TRIBOLOGY, Vol. 120, pp. 660–667.

Hou, Z. B. and Komanduri, R., 1997. "General Solutions for the Temperature Rise in Various Moving Plane Heat Sources with Different Intensities of Heat Distribution," submitted for publication.

Jaeger, J. C., 1942, "Moving Sources of Heat and the Temperature of Sliding Contacts," *Proc. of the Royal Society of NSW*, Vol. 76, pp. 203–224.

Kuhlmann-Wildorf, D., 1985. "Flash Temperatures due to Friction and Joule Heat at Asperity Contacts," *Wear*, Vol. 105, pp. 187–198.

Ling, F. F., 1973. *Surface Mechanics*, Wiley Interscience, New York.

Rosenthal, D., 1941. "Mathematical Theory of Heat Distribution During Welding and Cutting," *Welding Journal*, Vol. 20, Res. Suppl., pp. 220–234.

Rosenthal, D., 1946. "The Theory of Moving Sources of Heat and Its Application to Metal Treatments," *Trans. ASME*, pp. 849–866.

Spiegel, M. R., 1993. *Mathematical Handbook of Formulas and Tables, Schaum's Outline Series*, McGraw-Hill, New York.

Tian, X., and Kennedy, F. E., Jr., 1994. "Maximum and Average Flash Temperatures in Sliding Contact," ASME JOURNAL OF TRIBOLOGY, Vol. 116, pp. 167–174.

APPENDIX F

ON THE THERMAL ASPECTS OF THE MAGNETIC FIELD ASSISTED POLISHING OF CERAMICS

Part II. Thermal Aspects of Magnetic Float Polishing (MFP) of Ceramic Balls

Zhen Bing Hou and R. Komanduri

Trans ASME, J of Tribology 120 (1998) 652-659

Magnetic Field Assisted Finishing of Ceramics—Part II: On the Thermal Aspects of Magnetic Float Polishing (MFP) of Ceramic Balls

Zhen-Bing Hou

R. Komanduri
Fellow ASME

Mechanical and Aerospace Engineering,
Oklahoma State University,
Stillwater, OK 74078

The thermal model developed in Part I of this three-part series is applied in this paper to magnetic float polishing (MFP) of ceramic (Si_3N_4) balls. Using this method, the flash temperatures, flash times, and temperature distribution at the interface between the balls and the shaft of the MFP apparatus are calculated. Examination of the polished surfaces (scratch lengths) of the balls showed that the length of most scratches during the final stage of polishing is <20 μm and most are formed under transient conditions. But because of the small area of contact and low load encountered in MFP, the results of the calculations under these conditions were found to be very close to the quasi-steady-state conditions. However, it is not possible to know a priori if the conditions are transient or quasi-steady state unless solutions are available for each case. The use of the general solution developed in Part I enables this determination. The minimum flash temperatures and minimum flash times that occur during polishing ensure the determination if adequate temperatures are generated for chemo-mechanical polishing to take place. Of course, the lengths of the scratches would be much longer and the corresponding flash duration longer during the semifinishing operation than during finishing. The combined temperature and flash duration would determine the extent of chemo-mechanical action under these conditions. The flash temperatures and flash times required for chemo-mechanical action can be used as a basis for the optimization of polishing conditions in MFP.

1 Introduction

Advanced ceramics, such as silicon nitride (Si_3N_4), alumina (Al_2O_3), zirconia (ZrO_2), silicon carbide (SiC) are difficult to shape and finish materials because of their high hardness and brittleness. They are currently finished using diamond abrasive by conventional grinding followed by polishing or lapping, usually under high load. Consequently, material removal by these processes is mostly by brittle fracture leaving behind several pits, microcracks, and other defects. Since ceramics are sensitive to surface flaws, the performance reliability in service of parts fabricated by this process depends on the quality of the surface (or near surface) generated. Also, conventional polishing takes considerable time, on the order of 3–6 months (depending on the material and size of the balls, quality requirements, and available technology) even with the use of diamond abrasive. Consequently, the process is time consuming and expensive. To overcome some of the problems, a new polishing technique known as Magnetic Fluid Grinding (MFG) was recently introduced (Kato, 1990; Umehara and Kato, 1990). The present authors, however, prefer to use the term Magnetic Float Polishing (MFP) instead of Magnetic Fluid Grinding (MFG) to describe the process, as a float is used to push the balls against the shaft. Also, grinding connotes the use of fixed abrasive (grinding wheel) while MFP process uses loose abrasives. Thus the term "float" in the title of this process seems appropriate. MFP was further developed by Childs et al. (1994a, 1994b, 1995) in the U.K. and in the authors laboratory (Umehara, 1994; Raghunandan et al., 1996; Bhagauatula and Komanduri, 1996; Raghunandan and Komanduri, 1997; Jiang and Komanduri, 1997; Komanduri et al., 1995) in the U.S. More details of the process are given in the next section of the paper.

In MFP, the load on the polishing balls is deliberately kept very low (~1 N/ball) and controlled during the process so that damage due to material removal by brittle fracture is minimal. In addition, by proper choice of the abrasive, polishing conditions, and the environment for a given work material, chemo-mechanical action can be induced where necessary (Yasunaga et al., 1979) to facilitate the material removal other than by brittle fracture. Material removal by chemo-mechanical action involves the formation of the reaction products at the interface and results in an extremely smooth surface with minimal defects. The chemo-mechanical reaction products are subsequently removed in the form of debris by the mechanical action of the abrasive. In addition, the polishing speeds in MFP can be significantly higher (3000–9000 rpm) compared to a few hundred rpm in conventional polishing or lapping. In this way high removal rates can be accomplished without causing damage by brittle fracture of the ceramic workmaterial. Consequently, it is possible to reduce the time required for polishing (from the as received condition of the ball blanks to the finished state) from several weeks to a few days (Raghunandan and Komanduri, 1997; Jiang and Komanduri, 1997).

The chemo-mechanical action, however, depends on the flash temperatures generated at the contact zone of the polishing process as well as the flash duration that enable chemical reaction products to form by the interaction of the abrasive, the work material, and the environment. In addition, the pH value of the magnetic fluid can also influence the removal rate as it is part of the electrolytic cell. Since material removal mecha-

Contributed by the Tribology Division for publication in the JOURNAL OF TRIBOLOGY. Manuscript received by the Tribology Division August 1, 1995; revised manuscript received October 20, 1997. Associate Technical Editor: K. Kato.

nism by chemo-mechanical action depends mainly on the formation of the reaction products, softer abrasives (softer than the work material) can be used. Hence, material removal by abrasion is almost ruled out. This method, thus, is expected to overcome some of the inherent problems associated with surface damage, such as pitting due to brittle fracture, dislodgment of grains, and scratching due to abrasion that are associated with the use of harder abrasives in conventional polishing or lapping. The resulting surface on the ceramic balls is smooth ($Ra \sim 4$ nm and $Rt \sim 40$ nm) and damage-free in terms of pits, microcracks etc. (Jiang and Komanduri, 1997a).

In this paper, thermal aspects of the magnetic float polishing (MFP) are presented for the first time. They include the temperature field calculations, and the calculation of the expected flash temperatures and related flash times at the area of contact under various polishing conditions using the heat transfer model developed in Part I (Hou and Komanduri, 1998a).

2 Magnetic Float Polishing of Ceramic Balls

The magnetic float polishing technique was developed on the principle of the magneto-hydrodynamic behavior of a magnetic fluid that can float nonmagnetic abrasives suspended in it under the action of the magnetic field. The combined function of the magnetic field and the magnetic fluid is to levitate all nonmagnetic materials including the float and the abrasives. The float in the float chamber thus pushes the balls against the shaft and applies a low level of controlled force (1 N/ball or lower) on the balls. While other methods such as springs, or fluid under pressure can be used, the magnetic levitation is considered to be more convenient and highly accurate for the finishing of ceramic balls. The process is considered very effective for finish polishing because a low level levitational force that can be applied to the abrasives in a controlled manner. However, the process is also highly applicable to semi-finishing or finishing the balls from the as-received condition (Raghunandan and Komanduri, 1997). The magnetic fluid is a colloidal dispersion of extremely fine (100 to 150 Å) sub-domain ferromagnetic particles, usually magnetite (Fe_3O_4), in various carrier fluids, such as water or kerosene. In this investigation a water-based magnetic fluid is used. The ferrofluids are made stable against particle agglomeration by coating the particles with a surfactant. When a magnetic fluid is placed in a magnetic field gradient, it is attracted toward the higher magnetic field side. If nonmagnetic substances, such as the abrasives, are mixed in the magnetic fluid, they are discharged toward the lower side of the magnetic field. When a magnetic field gradient is set in the gravitational direction, the nonmagnetic material is made to float on the fluid surface by the action of the magnetic levitational forces. Thus the polishing operation in this process occurs due to the magnetic levitational force applied on the abrasives and the relative sliding motion of the balls.

Figures 1(a) and (b) are a schematic and a photograph of the magnetic float polishing apparatus, respectively, showing permanent magnets located at the base of the apparatus (Umehara, 1994; Raghunandan et al., 1997; Komanduri et al., 1995). The float vessel is placed on top of the magnets with alternate N and S poles. A guide ring is provided on top of the float vessel to contain the magnetic fluid. Magnetic fluid containing fine abrasive particles (5–10% by vol) is filled into the chamber. Ball blanks to be polished are placed around the periphery of the float vessel between the drive shaft and the float. The balls are held in a 3-point contact between the float at the bottom, chamber wall on the side, and the shaft at the top. When a magnetic field is applied, the balls, abrasive grains, and the float of nonmagnetic material are all pushed upwards by the magnetic fluid. The balls are pressed against the drive shaft and are finished by the rotation of the drive shaft. The material of the shaft is selected from an appropriate nonmagnetic material. In this study, a stainless-steel shaft is used. It has been

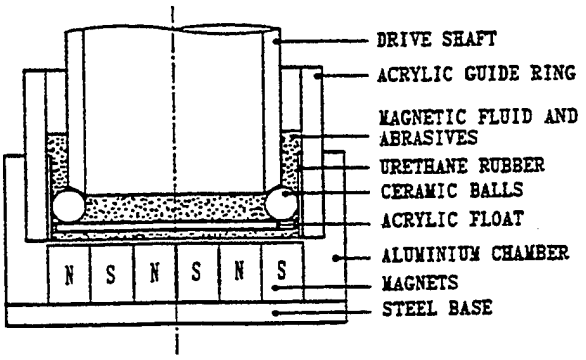

(a)

Fig. 1(*a*)

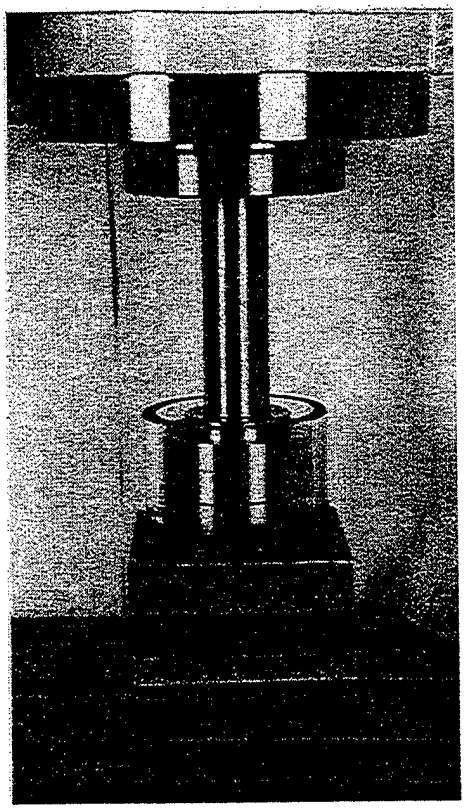

(b)

Fig. 1(*b*)

Fig. 1 Schematic and photograph of the magnetic float polishing apparatus showing permanent magnets located at the base of the apparatus (Komanduri et al., 1995)

reported that sliding of Si_3N_4 on stainless steel in the presence of a water-based magnetic fluid results in the formation of a layer of chemical reaction products (Akazawa et al., 1986) and use of Cr_2O_3 abrasive in polishing Si_3N_4 (Komanduri, Umehara, and Raghunandan, 1995; Bhagavatula, 1995; Bhagavatula and Komanduri, 1996) promotes chemo-mechanical action. These conditions are assumed in the present study.

3 Thermal Aspects of Magnetic Float Polishing

In magnetic float polishing (MFP), Childs et al. (1995) have shown that abrasives can be embedded in the stainless-steel shaft that is in contact with the balls and much of the material

during polishing can be removed by these abrasives. Jiang and Komanduri (1997a) have shown that the abrasives are actually not always embedded in the shaft as reported by Childs et al. (1995b) but actually abrade the softer stainless-steel polishing shaft also. Thus, while the action of the abrasives is one of a two body abrasion (i.e., sliding without rotation) as rightly pointed out by Childs et al., they are not always fixed but sometimes move relative to the polishing shaft. Thus a layer of abrasives with diameter ~1–5 μm is likely to be present between the ball and the shaft in the contact area. When the distance between the surfaces of the ball and the polishing shaft is equal to or less than the diameter of the largest abrasive (say, 5 μm), only a fraction of the larger abrasive particles will be in contact. The load on the ball causes deformation at the contact points between the ball and the abrasives as well as between the shaft and the abrasives. With increase in load, the deformation increases and the distance between the surfaces of the ball and the shaft decreases. Consequently, the number of contacts increases. Or, in other words, the percentage of active particles increases (see Appendix A for details).

During MFP, a typical load of 1.25 N/ball is applied on the Si_3N_4 ceramic balls. It can be shown that the following conditions apply during MFP process (see Appendix A for details):

1. the average deformation at the contacting points is ~0.56 μm
2. the radius of the contact area between the shaft and the ball where the largest particles still have the possibility of contacting with the shaft and the ball is ~84.3 μm
3. the total number of particles in the contact area is ~1588
4. the number of active particles in the contact area is ~22 (~1.4 percent of the total number).

Thus, the average load per abrasive particle, w is given by (1.25/22) or 0.0568 N/particle. The contact area between the abrasive particles and the ball is approximated to a circular disc with radius r_o = 1.03 μm [considering it as a Hertzian contact (Ling, 1973), see Appendix A for details].

The sliding velocity, v between the contacting surfaces of the ball and the polishing shaft in MFP is generally in the range of 2 to 6 m/s. The larger abrasive particles embedded in the softer stainless steel shaft under the load will move at the same velocity (2 to 6 m/s).

Table 1 gives the modulus of elasticity and Poisson's ratio of some related materials of interest in this investigation. Table 2 gives the relevant data for the calculations of the temperature field.

Detailed examination of the polished surfaces of Si_3N_4 balls in the SEM at various magnifications showed that the length of most scratches (denoted as l_{cut}) during the final stages of polishing are <20 μm (an average of 10 μm) (Fig. 2). In this investigation, a normal distribution is assumed for the variation of scratch lengths. Based on the normal distribution curve the probability of occurrence of the scratch lengths in the range of ~5–15 μm can be shown to be ~80 percent. Thus, lengths of cut, l_{cut} of 5 μm and 10 μm are taken as typical examples for the calculation of minimum flash temperature rise and corresponding flash times. If chemo-mechanical action can occur under these conditions, then one can be sure that they would

Table 1 Modulus of elasticity and Poisson's ratio of some materials

Material	Modulus of Elasticity, E, GPa	Poisson's ratio, γ
Silicon Nitride (for bearing balls)	320	0.26
Stainless Steel (shaft)	193	0.28
Cr_2O_3 (abrasive)	320	0.30

Table 2 Representative data for the calculation of the temperature field

Material of the driving shaft:	Stainless steel
Load on the ball (silicon nitride), P:	1.25 N/ball
Sliding speed, v:	2~6 m/s
Thermal properties of silicon nitride:	
Thermal conductivity, λ_1:	29.3 J/m·s·°C
Thermal diffusivity, a:	0.139 cm^2/s
Specific heat, c:	0.65 J/g·°C
Density, ρ:	3.25 g/cm^3
Thermal conductivity of Cr_2O_3 abrasive, λ_2:	31.8 J/m·s·°C

definitely occur under quasi-steady-state conditions and/or longer scratch lengths.

Based on the thermal analysis given in Part I, the time required for establishing the quasi-steady state $t_{\text{steady state}}$ can be calculated as follows:

$$t_{\text{steady state}} = 5 \cdot \frac{4a}{v^2} = \frac{20a}{v^2} \quad (1)$$

Equation (1) shows that the time required for establishing quasi-steady state is proportional to the thermal diffusivity of the material and inversely proportional to the square of the sliding speed. For a stationary body (the sliding speed relative to the heat source is zero) the t_{steady} is ∞, i.e., the process needs a very long time for establishing steady-state conditions. Table 3 shows the values of t_{steady} for different sliding speeds commonly used in the polishing of Si_3N_4 ceramic balls. The thermal diffusivity of Si_3N_4, a is taken here as 0.139 cm^2/s. When the sliding velocity, V_{sliding} during polishing is 2.0 m/s, the time duration for the formation of most scratches (~5–15 μm) was found to be in the range of 2.5–7.5 μs while t_{steady} is 69.5 μs. When the sliding velocity is 6.0 m/s, the time duration of most scratches is in the range of 0.8–2.5 μs, while the t_{steady} is 7.7 μs. These conditions represent the two extremes. Hence, the final stage of polishing is carried out mostly under transient conditions.

Using the following equation (2) (see Part I for details), the temperature rise at any point near and on the moving disk heat source can be calculated. Thus a complete profile of the temperature distribution around the moving disk heat source can be obtained.

$$\theta_M = \frac{q_{dc} \cdot v}{2\lambda a \pi^{3/2} r_o^2} \cdot \exp(-XV) \int_o^{r_o} \left(1 - \frac{r_i^2}{r_o^2}\right) r_i \, dr_i$$

$$\times \int_o^{v^2 t/4a} \frac{d\omega}{\omega^{3/2}} \cdot \exp\left(-\omega - \frac{u_i^2}{4\omega}\right) \cdot I_o(p) \quad (2)$$

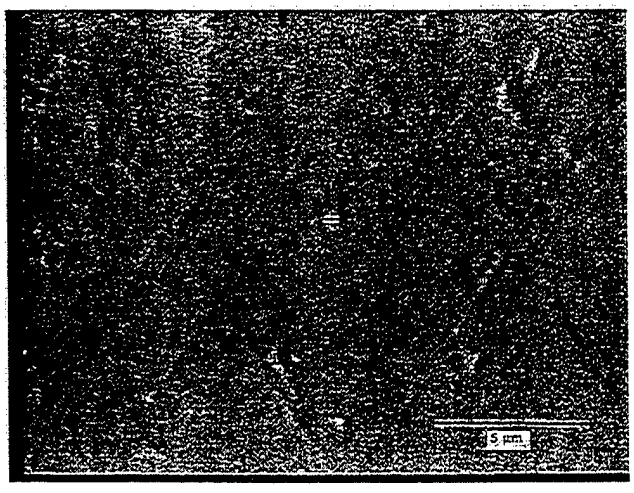

Fig. 2 SEM micrograph of the polished surface of Si3N4 ball showing that most scratch marks are in the range of 5–15 μm

Table 3 Variation of t_{steady} for different sliding speeds in the polishing of Si_3N_4 ceramic balls

Sliding Velocity $V_{sliding}$, m/s	t_{steady} μs
1.0	278.0
2.0	69.5
3.0	30.9
4.0	17.4
5.0	11.1
6.0	7.7

where

$$p = \frac{r_i V^2}{2\omega}\sqrt{\left(X + \frac{2\omega}{V}\right)^2 + y^2};$$

$$u_i = R_{hi} \cdot V; \quad R_{hi} = r_i^2 + X^2 + y^2 + z^2$$

See Nomenclature in Part I for the definition of various parameters.

3 Results

Figures 3(*a*) and (*b*) show the results of temperature rise calculations using Eq. (2) for quasi-steady state and transient conditions, respectively. It shows the distribution of the temperature rise on the surface of the ceramic ball along the *X*-axis ($z = 0$, $y = 0$) for different sliding velocities (v = 2–6 m/s). The radius of the moving disk heat source, r_o is 1.03 μm. Figure 3(*a*) is for quasi-steady state, where the length of scratch l_{cut} > 30 μm (of course, the possibility of the occurrence of such a long cut is very low). Figures 3(*b*) is for a typical transient case, where length of scratch l_{cut} = 5 μm (as the length of most scratches are in the range of 5–10 μm). From Figs. 3(*a*) and (*b*), it can be seen the maximum temperature rise varies from about 400°C to about 1200°C as the sliding speed changes from 2 to 6 m/s. The longer the length of the scratch, the higher is the maximum temperature rise.

Appendix B gives various steps used in the calculation of the flash temperatures as well as the temperature distribution around the contact area. Figure 4 shows the isotherms of temperature on the surface of the ceramic ball for l_{cut} > 30 μm (quasi-steady state), v = 5 m/s and r_o = 1.03 μm as an example. Such plots can be used to calculate the flash times for relevant flash temperatures, as given by the following equation:

$$\text{flash time} = \frac{L}{v}$$

where

L is the length in the *X*-direction of the region enclosed by the isotherm of certain critical temperature
v is the velocity of the moving heat source

The flash times at relevant flash temperatures for various sliding speeds and three scratch lengths, l_{cut} = 5 μm and 10 μm (as typical of transient conditions) and 30 μm (as typical of quasi-steady state) are calculated and shown in Table 5. It can be seen that when the sliding velocity v is 5 m/s, for a flash temperature >100°C, the flash time is 1.3 to 1.6 μs and the flash time for a flash temperature higher than 200°C reduces to 0.7–0.8 μs.

Table 4 Values of q_{total} for different sliding velocities (w = 1.25/22 N/particle and μ = 0.6)

Sliding velocity, v m/s	q_{total} J/s
2	0.0682
3	0.1023
4	0.1364
5	0.1705
6	0.2045

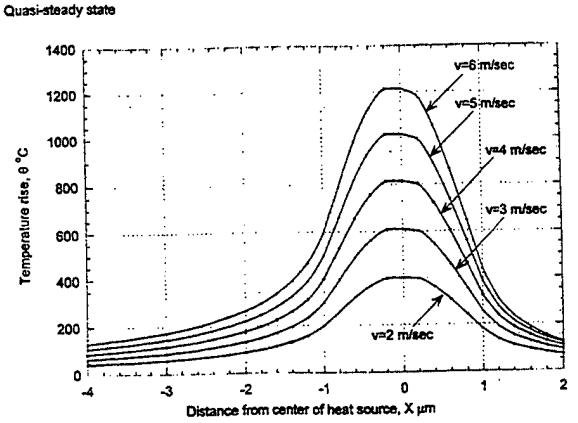

Fig. 3(*a*) Quasi-steady state

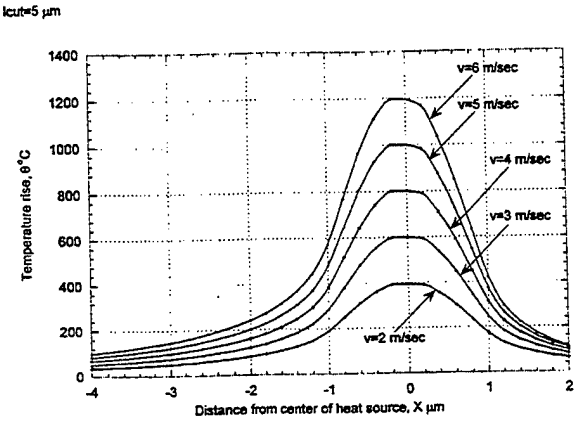

Fig. 3(*b*) 1 cut = 5 μm

Fig. 3 Calculated temperature rise on the surface along the *X*-axis (y = 0 and z = 0) for various velocities (v = 2–6 m/s); radius of the moving disk heat source, r_o = 1.03 μm; location of the center of the moving heat source X = 0 and y = 0

4 Discussion

Comparing Figs. 3(*a*) and (*b*) for the temperature rise on the surface for various velocities for transient and quasi-steady-

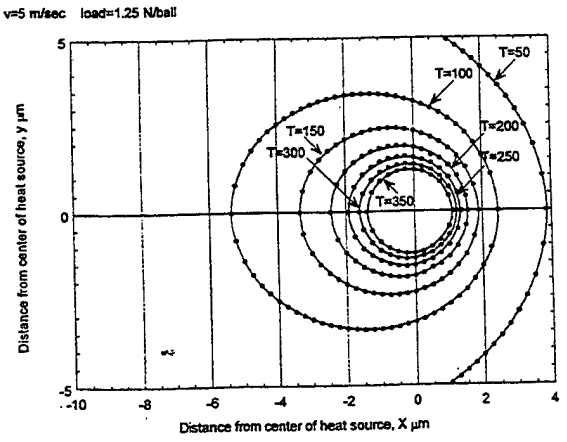

Fig. 4 Isotherms of temperature contour on the work surface radius of the moving disk heat source, r_o = 1.03 μm; N = 1.25 N/ball and v = 5 m/s

Table 5 Flash times in μsec for different flash temperatures (p = 1.25 N/ball)

	Flash temperature, °C														
	100			150			200			250			300		
	I	II_a	II_b	I	II_a	II_b	I	II_a	II_b	I	II_a	II_b	I	II_a	II_b
Sliding Velocity, v m/s															
2.00	2.0	1.9	1.9	1.3	1.3	1.3	1.0	1.0	1.0	0.9	0.9	0.8	0.7	0.7	0.7
3.00	1.8	1.7	1.6	1.2	1.2	1.1	0.9	0.9	0.9	0.8	0.8	0.7	0.7	0.7	0.7
4.00	1.7	1.6	1.4	1.1	1.1	1.0	0.9	0.8	0.8	0.7	0.7	0.7	0.6	0.6	0.6
5.00	1.6	1.4	1.3	1.0	1.0	0.9	0.8	0.8	0.7	0.7	0.6	0.6	0.6	0.6	0.5
6.00	1.5	1.3	1.2	1.0	0.9	0.9	0.8	0.7	0.7	0.6	0.6	0.6	0.5	0.5	0.5

I—quasi-steady state for $l_{cut} \geq 30$ μm.
II_a—transient state for $l_{cut} = 10$ μm.
II_b—transient state for $l_{cut} = 5$ μm.

state conditions, it can be seen that the values of the temperature rise are very close. This is because of the small area of contact and low load encountered in MFP. However, it is not possible to know a priori if the conditions are transient or quasi-steady state unless solutions are available for each case. The use of the general solution developed in Part I enables this determination.

In this investigation the thermal model (general solution) for the moving disc shaped heat source developed in Part I was applied to calculate the minimum flash temperatures and flash times in MFP of Si_3N_4 balls. Using Cr_2O_3 abrasive in MFP of Si_3N_4 balls, at the pressures and sliding speeds used, the minimum possible flash temperatures generated and the corresponding flash times are found to be adequate to generate specific reactions (based on Gibb's Free Energy (ΔG°) calculations), such as oxidation of silicon, and the formation of chromium nitride and chromium silicate compounds (Bhagavatula and Komanduri, 1996; Jiang and Komanduri, 1997b). Singhal (1975) had shown that oxidation of Si_3N_4 in air can take place >167°C. In the presence of water, the Gibbs free energy calculations in the present investigation also indicate that the critical temperature for activating some of the chemo-mechanical reactions is much lower than in air. It can be seen from Fig. 3(b), that at a sliding speed of 2 m/s, even for the transient case of $l_{cut} = 5$ μm, the flash temperature in polishing exceeds the temperature required for the oxidation of Si_3N_4 with sufficiently long duration of time for the reaction products to form even in air. Of course, at the higher speed, namely, 3–6 m/s, the temperature rise is even higher with similarly long duration times. At these conditions chemo-mechanical reactions can be formed between the Si_3N_4 balls and the Cr_2O_3 abrasive in MFP, resulting in the formation of chromium nitride and chromium silicate (Bhagavatula and Komanduri, 1996). Thus chemical reactions can be activated during polishing by proper choice of the abrasive for a given workmaterial, the environment and polishing conditions.

Examination of the wear debris (in the SEM with an X-ray microanalyzer and a low angle X-ray diffraction apparatus) obtained in MFP of Si_3N_4 balls using Cr_2O_3 abrasive showed conclusively that Cr_2O_3 does participate in the chemo-mechanical polishing of Si_3N_4 forming chromium nitride and chromium silicate (Bhagavatula, 1995; Bhagavatula and Komanduri, 1996). This work established the role of Cr_2O_3 not as a mere catalyst as postulated by some earlier researchers but one actively taking part in the chemical reactions during chemo-mechanical polishing. Based on it, phenomenological models were developed for the chemo-mechanical polishing of Si_3N_4 in water (i.e., water based magnetic fluid) and dry with Cr_2O_3 abrasive. These models are based on the formation of such reaction products as chromium silicate and chromium nitride in addition to the formation of silica layer on the surface of Si_3N_4 as well as the gaseous reaction products, such as ammonia (in water) and nitrogen (in air).

5 Conclusions

1 Using Eq. (2) for the moving disk heat source, a contour map of the temperature distribution around the moving disk heat source can be obtained as shown in Figs. 3 and 4. These contour maps enable the calculation of flash times during the polishing process.

2 Examination of the polished surfaces (scratch lengths) of the balls showed that the length of most scratches during the final stage of polishing to be <20 μm and are formed mostly under transient conditions. But, because of the small area of contact and low load encountered in MFP, the results of the calculations under these conditions were found to be very close to the quasi-steady state conditions. However, it is not possible to know a priori if the conditions are transient or quasi-steady state unless solutions are available for each case. The use of the general solution developed in Part I enables this determination.

3 It appears that, depending on the sliding speed, the minimum possible flash temperatures generated under transient conditions even for very short scratch lengths would be adequate to activate chemo-mechanical action. Even though the maximum temperature rise is about 400°C at a low sliding speed of 2 m/s, it increases rapidly with increase in the sliding speed (6 m/s) to about 1200°C. Also, the flash times increase with increase in the scratch length. In the examples shown in Table 5, for a sliding velocity of v = 5 m/s, the flash time is ~1.3–1.6 μs for a flash temperature higher than 100°C but for a flash temperature of higher than 200°C, it reduces to about 0.7–0.8 μs. Although the flash times are on the order of a few microseconds, it appears possible to initiate reaction products between the workpiece and the abrasive as evidenced by the X-ray diffraction studies of the wear debris formed in magnetic float polishing (Bhagavatula, 1995; Bhagavatula and Komanduri, 1996).

4 While flash temperatures can be used as a basis for thermodynamic analysis (Gibb's free energy of formation) for the feasibility of initiating a particular chemical reaction product that can be formed between the workmaterial, abrasive, and the environment, the flash times are needed to investigate the kinetics of the process.

5 The flash temperatures and flash times can be used as basis for the selection of optimum polishing conditions for chemo-mechanical polishing. They will also facilitate in the prediction of various reaction species during Gibbs free energy calculations.

References

Akazawa, M., and K. Kato, 1988, "Wear Properties of Silicon Nitride in Rolling-Sliding Contact," *Wear*, Vol. 124, pp. 123–132.

Akazawa, M., Kato, K., and K. Umeya, 1986, "Wear Properties of Silicon Nitride in Rolling Contact Fatigue," *Wear*, Vol. 110, p. 285.

Bhagavatula, S. R., 1995, "On the Chemo-Mechanical Polishing of Silicon Nitride with Chromium Oxide Abrasive," M.S. thesis, Oklahoma State University, Stillwater, OK.

Bhagavatula, S. R., and R. Komanduri, 1996, "On the Chemo-Mechanical Polishing of Silicon Nitride with Chromium Oxide Abrasive," *Philosophical Magazine,* Vol. 74, No. 4, pp. 1003–10171.

Childs, T. H. C., Jones, D. A., Mahmood, S., Kato, K., Zhang, B., and N. Umehara, 1994a, "Magnetic Fluid Grinding Mechanics," *Wear,* Vol. 175, pp. 189–198.

Childs, T. H. C., Mahmood, S., and H. J. Yoon, 1994b, "The Material Removal Mechanism in Magnetic Fluid Grinding of Ceramic Ball Bearings," *Proc. of the I. Mech. E.,* (London), Vol. 208/B1, pp. 47–59.

Childs, T. H. C., Mahmood, S., and H. J. Yoon, 1995a, "Magnetic Fluid Grinding of Ceramic Balls," *Tribology International,* Vol. 28, No. 6, pp. 341–348.

Hou, Z. B. and R. Komanduri, 1998a, "Magnetic Field Assisted Finishing of Ceramics—Part I: Thermal Model," ASME JOURNAL OF TRIBOLOGY, Vol. 120, pp. 645–651.

Hou, Z. B., and R. Komanduri, 1997c, "Magnetic Field Assisted Finishing of Ceramics—Part III: Thermal Aspects of Magnetic Abrasive Finishing (MAF) of Ceramic Rollers," ASME JOURNAL OF TRIBOLOGY, Vol. 120, pp. 660–667.

Jiang, M., and R. Komanduri, 1997a, "Finishing of Si_3N_4 Balls for Bearing Applications," accepted for publication in *Wear.*

Jiang, M., and R. Komanduri, R., 1997b, "Mechanism of Chemo-Mechanical Polishing of Silicon Nitride with CeO2 abrasive," paper under preparation.

Kato, K., 1990, "Tribology of Ceramics," *Wear,* Vol. 136, 117–133.

Kikuchi, M., Takahashi, Y., Suga, T., Suzuki, S., and Y. Bando, 1992, "Mechano-chemical Polishing of Silicon Carbide Single Crystal with Chromium (III) Oxide Abrasive," *J. Amer. Ceram. Soc.,* Vol. 75, No. 2, pp. 264–270.

Komanduri, R., Umehara, N., and M. Raghunandan, M., 1995, "On the Possibility of Chemo-Mechanical Polishing of Silicon Nitride," ASME JOURNAL OF TRIBOLOGY, Vol. 118, pp. 721–727.

Ling, F. F., 1973, *Surface Mechanics,* Wiley Interscience, New York.

Nagaraj, H. S., Sanborn, D. M., and W. O. Winer, 1978, "Direct Surface Temperature Measurement of Infrared Radiation in Elastohydrodynamic Contacts and the Correlation with the Blok Flash Temperature Theory," *Wear,* Vol. 49, pp. 43–59.

Raghunandan, M., Umehara, N., and Noori-Khajavi, A., and R. Komanduri, 1996, "Magnetic Float Polishing of Advanced Ceramics," ASME *Journal of Manuf. Sci. and Engg.,* Vol. 119, pp. 520–528.

Raghunandan, M., and R. Komanduri, 1997, "Finishing of Silicon Nitride Balls for High-Speed Bearing Applications," accepted for publication T ASME *J. of Manuf. Sci. and Engg.*

Singhal, S. C., 1975, "Effect of Water Vapor on the Oxidation of Hot-Pressed Silicon Nitride and Silicon Carbide," *J. Am. Cer. Soc.,* Vol. 58, p. 17.

Tian, X., and F. E. Kennedy, Jr., 1994, "Maximum and Average Flash Temperatures in Sliding Contacts," ASME JOURNAL OF TRIBOLOGY, Vol. 116, pp. 167–174.

Umehara, N., and K. Kato, 1990, "Principles of Magnetic Fluid Grinding of Ceramic Balls," *Int. J. of Applied Electromagnetics in Materials,* Vol. 1, pp. 37–43.

Umehara, N., 1994, "Magnetic Fluid Grinding—A New Technique for Finishing Advanced Ceramics," *Annals of CIRP,* Vol. 43/1, pp. 185–188.

Yasunaga, N., Tarumi, N., Obara, A., and O. Imanaka, 1979, "Mechanism and Application of the Mechano-Chemical Polishing Method Using Soft Powder," *Science of Ceramic Machining and Surface Finishing II,* B. J. Hockey and R. W. Rice, eds., NBS Special Publication No. 562, p. 171.

APPENDIX A

Estimation of the Number of Active Abrasive Particles

The number of active abrasive particles during magnetic float polishing (MFP) is estimated as follows:

1 Assume the number of active abrasive particles $n_a = 22$. This is obtained by multiplying the total number of abrasive particles in the deforming area by the probability of active abrasive particles (Table AI).

2 Load per particle, w = (load per ball/n_a) = $(1.25/22)N$

3 Calculate the deformations of the two contact points between the stainless steel shaft surface and abrasive particle and between the abrasive and the Si_3N_4 ball

(a) Using Hertzian stress equation (Ling, 1973), calculate the radii of the two contact areas:

$$r_{o1} = 1.135\ \mu\text{m}; \quad r_{o2} = 1.034\ \mu\text{m}$$

(b) the deformation at the contact point Δ (Fig. A1) is given by:

$$\Delta = r_a - \sqrt{r_a^2 - r_o^2}$$

where r_a is the average radius of the abrasive particles under real contact, in this case $r_a = 2.25\ \mu$m, The deformations at the two contacting points are obtained as follows.

$$\Delta_1 = 0.31\ \mu\text{m}; \quad \Delta_2 = 0.25\ \mu\text{m}$$

The total equivalent deformation of the abrasive monolayer (Δ_{total}):

$$\Delta_{\text{total}} = \Delta_1 + \Delta_2 = 0.56\ \mu\text{m}$$

4 Calculation of the possible number of abrasives in the real area of contact

From Fig. A2, it can be seen that from the total equivalent deformation Δ_{total} calculated in the previous section, the contact of abrasives with the ball and the shaft is

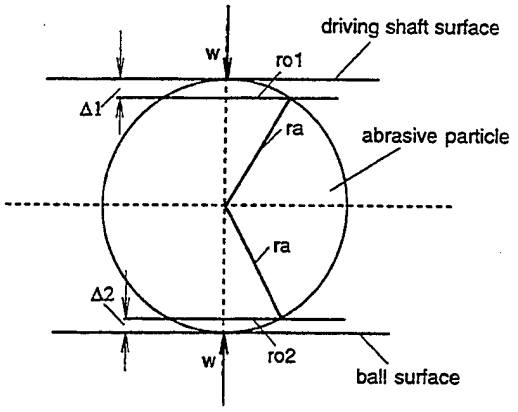

Fig. A1 Schematic showing the relationship between the deformation of the contact between the abrasive and the ball surface (or the abrasive and the drive shaft) and the radius of the Hertzian contact

Table A1 Probability of real contact (range of distribution = 4 μm, for the case discussed in this paper)

Δ_{total} μm	P	Δ_{total} μm	P	Δ_{total} μm	P	Δ_{total} μm	P
2.00	.5000	0.94	.0559	0.68	.0239	0.42	.0089
1.90	.4404	0.92	.0526	0.66	.0222	0.40	.0082
1.80	.3821	0.90	.0495	0.64	.0207	0.38	.0075
1.70	.3264	0.88	.0465	0.62	.0192	0.36	.0069
1.60	.2722	0.86	.0436	0.60	.0179	0.34	.0064
1.50	.2266	0.84	.0409	0.58	.0166	0.32	.0059
1.40	.1841	0.82	.0384	0.56	.0154	0.30	.0054
1.30	.1469	0.80	.0359	0.54	.0143	0.28	.0049
1.20	.1151	0.78	.0336	0.52	.0132	0.26	.0045
1.10	.0885	0.76	.0314	0.50	.0122	0.24	.0041
1.00	.0668	0.74	.0294	0.48	.0113	0.22	.0038
0.98	.0663	0.72	.0274	0.46	.0104	0.20	.0035
0.96	.0594	0.70	.0256	0.94	.0096		

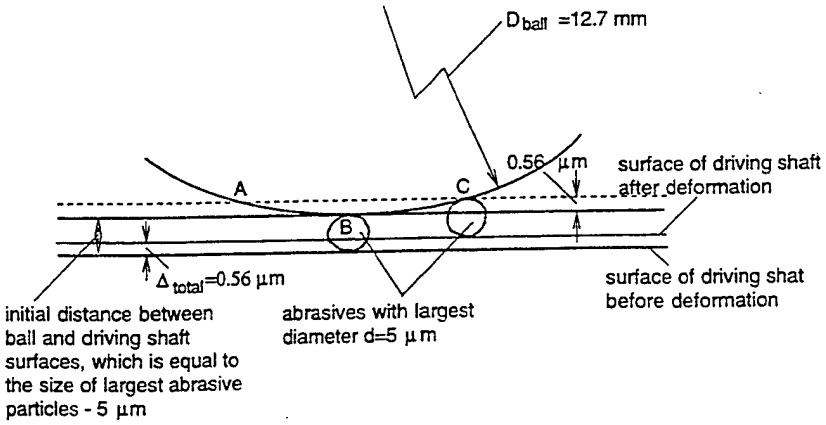

Fig. A2 Schematic showing the area on the ball where the abrasives of largest diameter (d = 5 μm) have the possibility of contact with the ball and the shaft surfaces, respectively

possible only in the region ABC. Outside of it the abrasives do not contact the ball.

Radius of that area, AB (very small compared to the radius of the ball) is:

$$AB \approx \sqrt{\Delta \cdot D_{ball}} = 84.3\mu m$$

Area of that region is: $\pi \times 84.3^2 = 22326\ \mu m^2$

So, the total number of abrasives n_{total} is given by:

$$n_{total} = \frac{\text{Area of region ABC}}{D_a^2}$$

where

D_a is the average diameter of abrasive (here $D_a = 3\ \mu m$)

$$\therefore n_{total} = \frac{22326}{3^2} = 2480$$

Considering that the concentration of this abrasive monolayer cannot be 100 percent, and assuming it to be $0.8 \times 0.8 = 0.64$.

Thus, the possible number of abrasives under the area ABC is:

$$n'_{total} = 2480 \times 0.64 = 1588$$

5 Calculation of the probability of real area of contact

Figure A3 shows the relationships between the deformation of contacts and the probability of real contacts. When the load increases, Δ_{total} increases, the distance between the ball and shaft decreases, the number of contacting (or active) particles increases. The probability of contact is given by the area shaded under the normal distribution curve. The larger the Δ_{total}, the larger the probability of contact. Table A1 shows the numerical relationships between probability of contact and Δ_{total} [converted from the Normal Probability Function (Table A1, Bayer, 1976)].

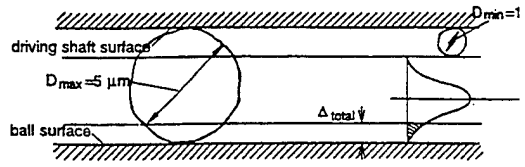

Fig. A3 Schematic showing the relationship between the total deformation under the largest abrasive particles and the probability of other abrasive particles in contact as a consequence

From Step 3 of this Appendix, $\Delta_{total} = 0.56$, $P = .0154$. Thus, the number of active abrasives is:

$$n = 1588 \cdot P = 1588 \cdot .0154 = 24.5$$

That means the assumed n_a is too small. Consider, $n_a = 23$, repeat the procedure for the calculations. It is found that the assumed value is too large. Thus the number of active abrasive particles should be between 22 and 23. In this paper $n_a = 22$ is taken for the sample calculations.

Reference

Beyer, W. H., 1976, *Standard Mathematical Tables*, CRC Press, 24th Ed. p. 478.

APPENDIX B

Temperature Distribution Around the Contact Area

In the following, various steps involved in the calculation of the temperature distribution around the contact area between abrasive and the ceramic ball surface during polishing are given.

1 The contact area between the abrasives and ceramic balls is approximated as disk shaped. Considering the Hertzian contact (Ling, 1973), the radius, r_o of the contact area of the disk is calculated using the following Hertzian stress equation:

$$r_o = (1.5 \cdot w \cdot R'/E')^{1/3}$$

where

w is the load per particle, in N
r_o is the radius of contact area
R' is the equivalent radius of contacting bodies
$R' = 1/[(1/R_{abrasive}) + (1/R_{ball})]$
E' is the equivalent modulus of elasticity of contacting bodies
$E' = 1/[(1 - \nu_1^2)/E_1 + (1 - \nu_2^2)/E_2]$

Since, only the largest abrasive particles are in real contact, the average radius of the larger contacting abrasives is about 2.25 μm. The radius of the ceramic ball is 12.7 mm which is significantly larger than that of the abrasives. Thus, $R' = 2.25$ μm.

Substituting for the values of Poisson's ratio, ν and the modulus of elasticity, E for the relevant materials from Table 1, we get for the contact between the abrasive Cr_2O_3 and Si_3N_4 ceramic ball, E' as:

$$E' = \frac{1}{\frac{1-0.26^2}{320\times10^9}+\frac{1-0.30^2}{320\times10^9}} = 1.7369\times10^{11}\ \text{N/m}^2$$

Thus, the radius of the contact area under a load, $w = (1.25/22)$ N/particle is given by:

$$r_o = \left(\frac{1.5\cdot\frac{1.25}{22}\cdot 2.25\cdot10^{-6}}{1.7369\times10^{11}}\right)^{1/3} = 1.03\ \mu\text{m}$$

2 The total heat liberation rate q_{total} in J/s is given by:

$$q_{\text{total}} = \mu\cdot w\cdot v$$

where w is the load on the abrasive per particle (in this case, it is 1.25/22 N), μ is the coefficient of friction between the abrasive and the Si_3N_4 ball [for MFP it is assumed as 0.6 (Akazawa and Kato, 1988)], and $v = 2$–6 m/s. Table 4 of the paper gives the values of the total liberation rate, q_{total} for the disk heat source for different sliding velocities from 2–6 m/s.

3 The estimation of the heat partition fraction is based on the assumption that during the formation of each scratch in polishing, the heat source at the contact area relative to the abrasive is a stationary heat source. Since, $t_{\text{steady}} = 5\cdot(4a/v^2)$, the time for establishing the quasi-steady state for a stationary heat source ($v \sim 0$) will be rather long. The temperature at the contact area of the abrasive particle increases continuously until quasi-steady state is established. The higher the temperature of the contacting surface on the abrasive particle is, the lower the fraction of the heat flowing into the abrasive particle or the higher the fraction of heat flowing into the ceramic workpiece. The fractions of heat flowing into the two contacting bodies are variable with respect to time until the steady state of the stationary body is established. Using Eq. (1), for a very slow moving body, say $v = 1$ cm/s, the time required for establishing quasi-steady state is 2.78 s. For a stationary body ($v \sim 0$), the time required will be significantly long.

The time required for completing a scratch in MFP will be rather short compared to the time required for establishing quasi-steady-state conditions. For example, it was shown in the body of the paper that when the sliding velocity, V_{sliding} is 2.0 m/s, the duration for the formation of most scratches (~5–15 μm) was ~2.5–7.5 μs while t_{steady} is ~69.5 μs. Thus, it is reasonable to assume that in the process of scratching or rubbing in MFP, the heat partition ratio is nearly constant and equal to the value at the very beginning. In this investigation, we are mainly interested in the initial stages (transient state) when the partition ratio is nearly equal to the value at the beginning of contact. As a first approximation, it can be shown that the heat partition ratio at the very beginning of contact (transient conditions) is proportional to the ratio of the thermal conductivities of contacting bodies for three-dimensional heat flow problems (Jaeger, 1942; Blok, 1937).

Thus, the fraction of the heat that flows into the ball, f_q is:

$$f_q = \frac{\lambda_1}{\lambda_1+\lambda_2}$$

where λ_1 and λ_2 are the thermal conductivities of ball and the abrasive, respectively

$$f_q = \frac{29.3}{29.3+31.8} = 0.479$$

Thus, $q_{dc} = f_q\cdot q_{\text{total}}$

4 Using Eq. (2), the temperature rise at any point nearby the contact can be calculated.

References

Blok, H., 1937, "Theoretical Study of Temperature Rise at Surface of Actual Contact Under Oiliness Lubricating Conditions," *I. Mech. E. Proceedings of General Discussion on Lubrication and Lubricants*, Vol. 2, pp. 222–235.

Jaeger, J. C., 1942, "Moving Sources of Heat and the Temperature of Sliding Contacts," *Proc. of the Royal Society of NSW*, Vol. 76, pp. 203–224.

APPENDIX G

ON THE THERMAL ASPECTS OF THE MAGNETIC FIELD ASSISTED POLISHING OF CERAMICS

Part III. Thermal Aspects of Magnetic Abrasive Finishing (MAF) of Ceramic Rollers

Zhen Bing Hou and R. Komanduri

Trans ASME, J of Tribology 120 (1998) 660-667

Magnetic Field Assisted Finishing of Ceramics—Part III: On the Thermal Aspects of Magnetic Abrasive Finishing (MAF) of Ceramic Rollers

Zhen-Bing Hou

R. Komanduri
Fellow ASME

Mechanical and Aerospace Engineering,
Oklahoma State University,
Stillwater, OK 74078

Conditions during finishing of advanced ceramics by magnetic abrasive finishing (MAF) processes are found to be, by and large, transient. Consequently, the available quasi-steady-state solutions for the moving heat sources are not directly applicable for this case. Hence, the general solution for a moving disk heat source, developed in Part I of this three-part series, is applied to determine the minimum flash temperatures and flash times generated at the contact points between the workmaterial (Si_3N_4 roller) and the abrasive (Cr_2O_3). Since chemo-mechanical action between the abrasive—the workmaterial—the environment depends on both the thermodynamics and kinetics of the process, it is important to determine the flash temperatures as well as flash times during polishing. These were determined as a function of the polishing pressure and the rotational speed of the work material in this investigation. Thermodynamic considerations (not covered in this paper) indicate that even the minimum flash temperatures generated under the conditions of lower pressure, lower sliding velocity, and transient state would be adequate to initiate chemo-mechanical action, and experimental results confirmed the formation of chemo-mechanical reaction products during polishing (Bhagavatula and Komanduri, 1996).

1 Introduction

The interface temperature between a ceramic workmaterial and an abrasive during the finishing process is an important parameter that can determine thermodynamically the possibility of chemical reactions during the removal process. Similarly, the flash times can determine the rate of chemical reaction or kinetics of the process. Together, they determine the feasibility and extent of chemo-mechanical reactions during finishing. However, it is somewhat impractical to measure experimentally the temperatures generated at the points of contact in polishing, although some work was reported in the literature for other applications (e.g., Nagaraj, et al., 1978). Therefore, one has to resort to analytical techniques, such as the general solution for the heat transfer problem developed in Part I (Hou and Komanduri, 1998a) of this three-part series, or, if the conditions are quasi-steady state, use other models available in the literature (Blok, 1937; Rosenthal, 1941, 1946; Archard, 1959; Francis, 1970; Ling, 1973; Kuhlmann-Wildorf, 1985; Greenwood, 1991; Tian and Kennedy, 1994; Bos and Moes, 1995). In this investigation, the flash temperatures and the flash times at the points of contact between the abrasive and the workmaterial during finishing are determined using the moving disk heat source model based on Jaeger's classical solutions (see Part I for details). In the following, a brief description of the magnetic abrasive finishing (MAF) process used for the finishing of ceramic rollers is given first as an introduction to this new technology. This is followed by a brief description of the theoretical model of the moving disk heat source as applied to MAF process. Various steps used in the calculation of the flash temperatures using the moving disk heat source model for MAF process are given in Appendix A.

2 Magnetic Abrasive Finishing

The magnetic abrasive finishing (MAF) process is a novel technique for the finishing of cylindrical specimens such as rollers for use in ceramic hybrid bearings (Fox et al., 1994). The material removal rate is generally high (~1 μm/min) and the finish quality is also excellent (Ra ≈ 5 nm). Figures 1(*a*) and (*b*) are a schematic and a photograph of the MAF process, respectively. A copper coil, wound in the form of a solenoid, is used for the generation of the magnetic field in the core. A low carbon steel (~0.16% C) is used as the magnetic core material. Magnetic heads are designed such that the magnetic field is concentrated surrounding the air gap with minimal leakage between the magnetic heads and the roller, which in the present case is a nonmagnetic, ceramic material. A pneumatic air vibrator is used to provide the vibratory motion to the magnetic head to prevent circumferential grooves that may form otherwise. The MAF equipment is mounted on a 1.5 hp, precision lathe with a continuous speed range of up to 3000 rpm. The function of the magnetic field is to enable the formation of a magnetic brush (iron particles and abrasives) that would remove material from the workmaterial during finishing. Table 1 gives the specifications of the equipment and the finishing conditions used.

The magnetic abrasive is an agglomerate of ferromagnetic particles (100–400 μm grain size iron power) and fine abrasive (1–10 μm grain size). It can be used as a sintered product or a mechanical mixture. In this investigation the latter type is used. The magnetic abrasive, when charged into the gap between the magnetic poles, forms two magnetic abrasive brushes around the periphery of the roller (Fig. 2). When a nonmagnetic cylindrical workpiece, such as a ceramic roller, is placed in the

Contributed by the Tribology Division for publication in the JOURNAL OF TRIBOLOGY. Manuscript received by the Tribology Division October 13, 1995; revised manuscript received October 20, 1997. Associate Technical Editor: K. Kato.

$$r_o = (1.5 \cdot w \cdot R'/E')^{1/3}$$

$$= [(1.5 \cdot 1.44 \cdot 0.192 \cdot 10^{-3})/1.1529 \cdot 10^{11}]^{1/3}$$

$$= 15.33\ \mu\text{m}.$$

(d) Total amount of heat produced during polishing at the disk plane heat source, Q is given by (assuming μ = 0.60),

$$Q = (w \cdot \mu \cdot v) = (1.44 \cdot 0.60 \cdot 2.62) = 2.26\ \text{J/s}.$$

7. The fraction of heat that goes into the workmaterial, x can be obtained as:

$$x = \lambda_{Si_3N_4}/(\lambda_{Si_3N_4} + \lambda_{Cr_2O_3})$$

$$= 29.3/[29.3 + 31.8] = 0.4795$$

Amount of heat that goes into the silicon nitride workmaterial, Q_{wp} is given by,

$$Q_{wp} = Q \cdot x = 2.26 \cdot 0.479 = 1.0837\ \text{J/s}$$

Using Eq. (2), the temperature rise at any point around the contacting area of the roller surface with the magnetic abrasive particles can be calculated. The results of the calculations are shown in Figs. 5–7 of the main text.

8. The flash time (i.e., duration of the expected temperature) is calculated in the following manner: Consider, for example, the flash temperatures are 100, 200, 300, and 400°C.

(i) Calculate from the temperature distribution plots along the X-axis, the total distance in the vicinity of contact where temperature exceeds 100, 200, 300, or 400°C, respectively.

Consider the case where v = 2.62 m/s, P = 34.5 kPa, and l_{cut} = 10 μm, then L_{100} = 35.63 μm, L_{200} = 28.03 μm, L_{300} = 23.06 μm, and L_{400} = 18.6 μm.

(ii) Divide this distance (obtained in Step i) by the sliding velocity to yield the flash time.

The flash times at relevant flash temperatures for the above case are:

$$T_{100} = 13.6\ \mu\text{s}, \quad T_{200} = 10.7\ \mu\text{s},$$

$$T_{300} = 8.8\ \mu\text{s}, \quad \text{and} \quad T_{400} = 7.1\ \mu\text{s}.$$

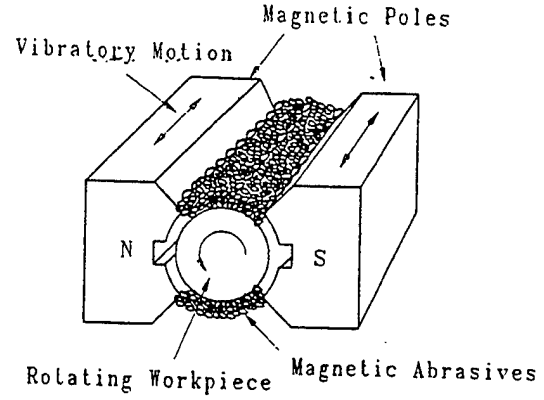

Fig. 1(*a*) Schematic of the magnetic abrasive finishing (MAF) process for polishing of ceramic rollers (Fox et al., 1994)

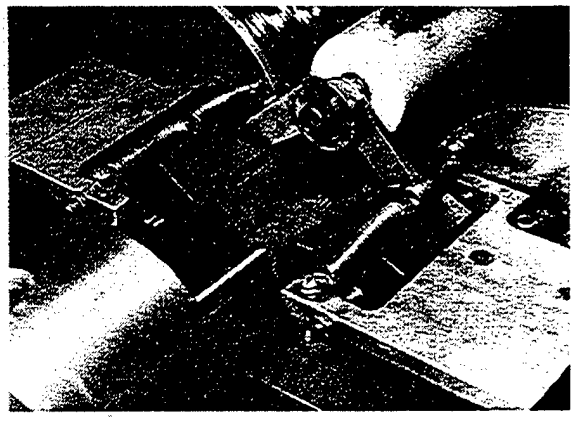

Fig. 1(*b*) Photograph of the magnetic abrasive finishing (MAF) apparatus (Fox et al., 1994)

magnetic field with rotary and vibratory motions (with or without a lubricant), both surface and edge finishing operations can be performed simultaneously by the two magnetic abrasive brushes. The process is highly efficient and the removal rate and finish obtainable depend on the circumferential speed of the roller, magnetic flux intensity, working clearance between the magnetic heads and the roller, workpiece material, the magnetic abrasive agglomerate, including the type, grain size, and volume fractions of the abrasive and magnetic material in the agglomerate.

3 Experimental Procedure

In the magnetic abrasive finishing (MAF) process, magnetic field is generated using an electromagnet. Current in the range of 0.5–2 A is passed through the copper coil wound in the form of a solenoid. The magnetic field generated within the magnetic

Table 1 Specifications of the magnetic abrasive finishing equipment

Machine capacities:	
Machine Tool:	1.5 hp, high precision lathe
Lathe speed:	500–2,500 rpm
Workpiece size cylindrical roller:	5–25 mm diameter × 120 mm long
Max. polishing length:	45 mm
Magnetic field intensity:	0.5–1.2 T
Magnetic pressure:	0–40 kPa
Magnetic core:	0.16% carbon steel
Magnetic abrasives:	a mechanical mixture of Cr_2O_3 abrasive (1–10 μm) and iron particles (100–400 μm)

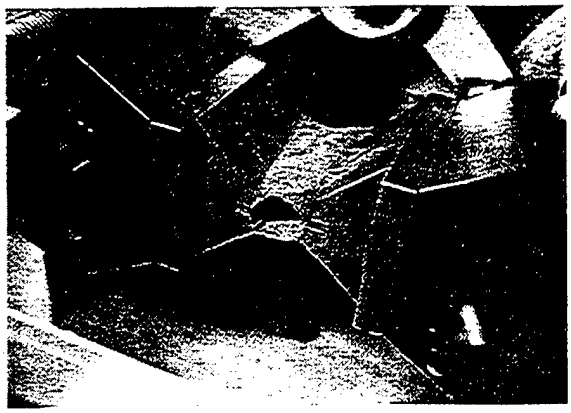

Fig. 2 Photograph of the magnetic abrasive brush formed between the magnetic heads by the magnetic abrasives (Fox et al., 1994)

core passes through the magnetic head. Magnetic abrasive is introduced in the gap between the magnetic heads, i.e., between the N and the S poles. Due to the presence of the magnetic field, the abrasives align in the direction of the field. The cylindrical roller to be polished is held in the chuck of a precision lathe. The roller is given a rotary motion and is positioned in the magnetic field. A small clearance between the magnetic heads and the chuck of the lathe is provided to avoid accidental collision. Vibratory motion is provided to the magnetic heads by means of a pneumatic vibrator to eliminate circumferential grooves that may form otherwise. Typical frequencies of vibration of the head are in the range of 15–20 Hz. The abrasives are stirred periodically at intervals of ~1 minute to ensure uniform wear of the abrasives.

4 Heat Transfer Modeling of the Magnetic Abrasive Finishing (MAF) of Rollers

In the magnetic abrasive finishing (MAF) of ceramic rollers, the pressure applied by the ferromagnetic particles on the cylindrical surface of the roller causes a Hertzian contact, the radius of which can be determined analytically (Ling, 1973). During rotation of the roller, the ferro-magnetic particles carrying hard, fine abrasives interact with the surface of the roller, as shown schematically in Fig. 3, thus removing material. It may be noted that the heat transfer model for both magnetic float polishing (MFP) of the balls and the magnetic abrasive finishing (MAF)

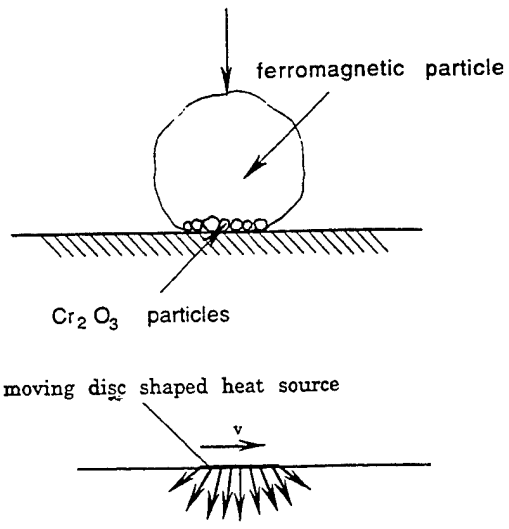

Fig. 3 Schematic of the moving disk heat source problem

of the rollers (Hou and Komanduri, 1998b) uses the same moving disk heat source solution presented in Part I (Hou and Komanduri, 1998a). However, details of the model, as will be shown here, are quite different. For example, in the polishing of ceramic balls by MFP, the magnetic particles in the magnetic fluid are extremely fine, on the order of 10 nm. Hence, in MFP the sliding contacts between the hard abrasives and the ball surface only are considered neglecting the mechanical interactions between the iron oxide particles with the balls. In contrast, in the MAF process, the iron particles used are large (100–400 μm). Hence, in MAF the sliding contacts between the iron particles and the roller surface are considered. As the radius of the roller is much larger than that of the ferromagnetic particles, the real area of contact is assumed to be a disk with a diameter of about ~10–20 μm depending upon the pressure and the mechanical properties of the workmaterial and the ferro-magnetic particles used.

During polishing, the roller rotates with a velocity v and generates heat at the rate of q (J/s) at the real area of contact due to rubbing between the magnetic abrasive and the roller. The rate of heat generation, q is given by,

$$q = w \cdot \mu \cdot v \text{ J/s} \tag{1}$$

The nomenclature used in all the three parts is given once in Part I of this three-part series under Nomenclature and may be referred to for details.

In the final stages of polishing, the material removal by cutting and scratching processes is not continuous for a number of reasons including the following: (a) the interactions of the abrasives with the workmaterial having arbitrary but finite surface roughness, (b) free body motion of the magnetic abrasive particles, and (c) the changing direction of sliding motion of the magnetic abrasive particles with respect to the workmaterial. Detailed examination in the SEM of the polished surfaces of the Si_3N_4 rollers (polished by MAF), showed that most of the scratch lengths on the work surface to be in the range of ~10–20 μm (as shown in Fig. 4). Consequently, the time required for each contact would be on the order of ~10–20μs at a sliding speed, v of ~1 m/s. For higher sliding speeds, say, 5 m/s, the time of contact is even less (~2–4 μs). It is, therefore, necessary to determine the contact times during polishing and investigate if such short times are sufficient to establish quasi-steady-state conditions. Quite likely, a limited number of those contacts would be long enough for the establishment of quasi-steady-state conditions but for the most part this would not be the case. Hence, a general solution that will encompass both transient and quasi-steady-state conditions need to be developed and used. Also, the minimum flash temperatures generated as well as the flash times during the formation of shorter scratches and/or with higher sliding velocities will determine the feasibility of chemo-mechanical action under these conditions. Of course, when the scratch length is longer and/or under quasi-steady-state conditions, the flash temperatures would be much higher and ensure chemo-mechanical action if appropriate abrasive is chosen for a given workmaterial.

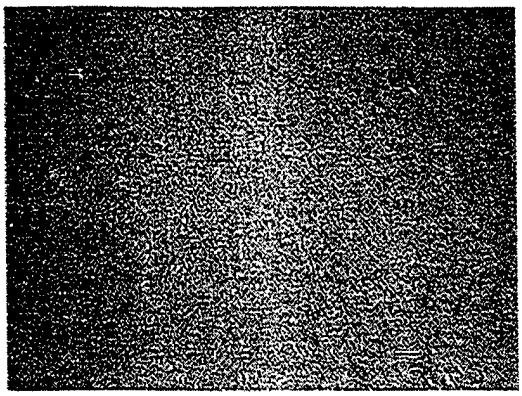

Fig. 4 SEM micrograph of a polished Si_3N_4 roller with a Cr_2O_3 abrasive showing various polishing scratches on the surface

In Part I, a general solution (both transient and steady state) for a moving disk heat source for a semi-infinite body with a parabolic distribution of heat intensity was developed as given by Eq. (2):

$$\theta_M = \frac{q_{dc} \cdot v}{2\lambda a \pi^{3/2} r_o^2} \cdot \exp(-XV) \int_o^{r_o} r_i \cdot \left(1 - \left(\frac{r_i}{r_o}\right)^2\right) \cdot dr_i \times \int_o^{(v^2 t/4a)} \frac{d\omega}{\omega^{3/2}} \cdot \exp\left(-\omega - \frac{u^2}{4\omega}\right) \cdot I_o(p) \tag{2}$$

where

$$p = \frac{r_i V^2}{2\omega} \sqrt{\left(X + \frac{2\omega}{V}\right)^2 + y^2}$$

$$V = \frac{v}{2a}; \quad u = R_i \cdot V; \quad \text{and} \quad R_i^2 = r_i^2 + X^2 + y^2 + z^2$$

Refer to the Nomenclature given in Part I.

It was shown in Part I that the function to be integrated (i.e., the second integration) in Eq. (2) converges to zero as $\omega \to 0$ and $\omega \to 5$. That means, when $(v^2 t/4a) > 5$, no matter how large, even ∞, the integration will always gives the same value. In other words, when the upper limit of integration is >5, it can be considered as infinity. That means, when $(v^2 t/4a) \geq 5$, no matter how large the value of t is, the result of the calculation always remains unchanged, i.e., the calculated temperature rise is time independent and quasi-steady-state conditions have been established.

Thus, it is possible to estimate the time required for establishing quasi-steady-state conditions from the equation, $(v^2 t/4a) = 5$.

$$\text{i.e.,} \quad t_{\text{steady state}} = \frac{5 \cdot 4a}{v^2} = \frac{20a}{v^2} \tag{3}$$

For example, when $a = 0.139$ cm^2/s, $v = 2.62$ m/s, the time required for establishing the quasi-steady-state condition is given by:

$$t_{\text{steady state}} = \frac{20 \cdot 0.139}{262^2} = 40.5 \ \mu\text{s}.$$

In the MAF process, only a fraction of the heat generated at the contact area flows into the workpiece, the remainder flows into the magnetic abrasive particles. The heat partition ratio is not constant until quasi-steady-state conditions are established in both bodies. For the case of scratching or rubbing during polishing, relative to the heat source, the magnetic abrasive particles can be regarded as stationary. The time required for establishing a steady-state condition is inversely proportional to the square of the relative velocity (3). For a stationary body it is infinitely long. But in polishing, the times for each scratch are mostly on the order of only ~3–20 μs.

Bos and Moes (1995) introduced an iterative method for the determination of the heat partition ratio which is valid for cases where steady-state conditions have already been established for both bodies. In this investigation, we are mainly interested in

the initial stage of the transient state, which is nearly equal to the value at the very beginning of contact. At the very beginning, the contact between the two contacting bodies can be considered as an instantaneous heat source. Using the concept of matching the average temperature over the contacting area the heat partition ratio can be determined. For very large contacting area (nearly one-dimensional heat flow) the ratio would be $\lambda_A/\sqrt{a_A}:\lambda_B/\sqrt{a_B}$. For very small contacting area (nearly a point contact, thus three-dimensional heat flow) the ratio would be $\lambda_A:\lambda_B$. As a first approximation, the heat partition ratio at the very beginning of contact (transient conditions) is assumed in this investigation to be equal to the ratio of the thermal conductivities of contacting bodies.

Various steps used in the calculation of the flash temperatures using the moving disk heat source model for MAF process along with a sample calculation are given in Appendix A.

5 Test Results and Discussion

Detailed examination of the polished surfaces of Si_3N_4 rollers in the SEM at various magnifications showed that the lengths of the scratches (denoted as l_{cut}) are in the range of ~0–30 μm (an average of 15 μm) (Fig. 4). In this investigation, normal distribution is assumed for the variation of scratch lengths. Using the normal distribution curve, it can be shown that the probability of occurrence of scratch lengths in the range of ~10–20 μm is about 80 percent. Thus, lengths of cut, l_{cut} of 10 μm and 20 μm are taken as typical examples of transient conditions for the calculation of the flash temperature rise.

Table 2 gives the times required for different cut lengths, l_{cut} at different sliding velocities, $v_{sliding}$. Table 3 gives the times required for establishing quasi-steady-state conditions for different sliding speeds. It can be seen from these tables that a large percentage of scratches are formed under transient conditions. If conditions of minimum flash temperature and flash times are conducive for chemo-mechanical action, then all other conditions would be definitely favorable for the chemo-mechanical action.

Figures 5(*a*) and (*b*) show the variation of the flash temperature rise with distance from the center of the heat source at a sliding velocity of 2.62 m/s and various polishing pressures. Figures 5(*a*) is for a scratch lengths of 10 μm and Fig. 5(*b*) is for quasi-steady state. Figures 6(*a*) and (*b*) show the variation of the temperature rise with distance from the center of the heat source at a polishing pressures of 34.5 kPa and various sliding velocities. Figures 6(*a*) is for a scratch length of 10 μm and Fig. 6(*b*) is for quasi-steady state. It can be seen that as the polishing pressure increases the maximum flash temperature produced also increases. For example, under quasi-steady conditions at a sliding velocity of 2.62 m/s, it is about 1036°C at a polishing pressure of 69.0 kPa and drops to about 720°C at 34.5 kPa. Also, as the sliding speed of the heat source increases, the maximum flash temperature also increases. For example, at a pressure of 34.5 kPa and a velocity of 2.62 m/s, the maximum temperature rise under quasi-steady conditions is about 720°C and increases to over 1150°C at 5.24 m/s. Under transient conditions, at corresponding polishing pressures and sliding velocities, the maximum flash temperatures are lower by about ~10–30 percent. Based on Gibbs Free Energy calculations, it was found that thermodynamically these temperatures are sufficient to initiate chemo-mechanical action between the Si_3N_4 roller and the Cr_2O_3 abrasive. However, the extent of the formation of the chemical compounds also depends upon the kinetics dictated by the flash duration. Hence, some idea on the flash times would be appropriate. In the following, calculations for the flash times are given and it appears that in many cases they may be sufficient to initiate chemo-mechanical action between the abrasive, the workmaterial, and the environment. Bhagavatula and Komanduri (1996) showed by detailed examination in the SEM with an energy dispersive X-ray analysis and a low angle X-ray diffraction, of the wear debris generated during polishing of Si_3N_4 roller with Cr_2O_3 abrasive, the chemo-mechanical products do form during polishing.

Table 2 Times required (μs) for different scratch lengths, l_{cut} and different sliding velocities, $v_{sliding}$

Sliding velocity, $v_{sliding}$ m/s	Scratch length, l_{cut}, μm		
	10	20	30
2.62	3.8	7.6	11.5
3.93	2.5	5.1	7.6
5.24	1.9	3.8	5.7

Table 3 Times required for establishing quasi-steady-state conditions for different sliding speeds, $v_{sliding}$

Sliding velocity, $v_{sliding}$, m/s	2.62	3.93	5.24
$t_{steady\ state}$, μs	40.5	18.0	10.1

Determination of the Flash Times. Flash times for a given flash temperature can be calculated by measuring the length of the region where the temperature is higher than the given flash

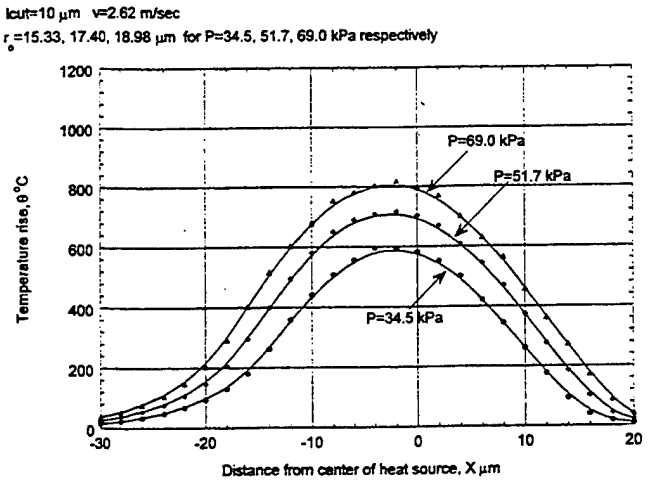

Fig. 5(*a*) Scratch length of 10 μm

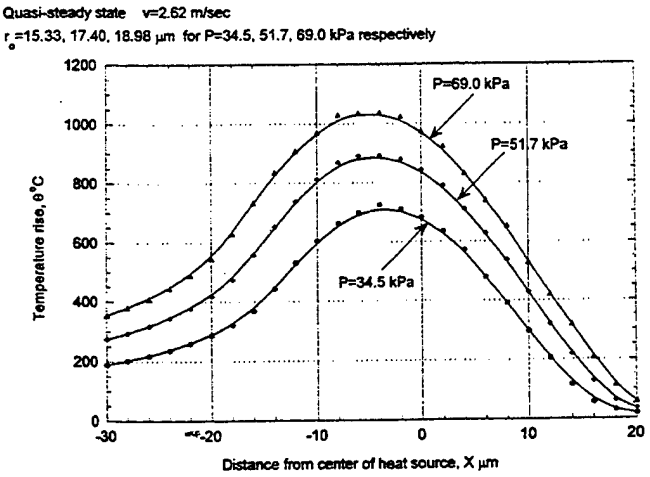

Fig. 5(*b*) Quasi-steady-state conditions

Fig. 5 Variation of the temperature rise with distance from the center of the heat source at a sliding velocity of 2.62 m/s and various polishing pressures

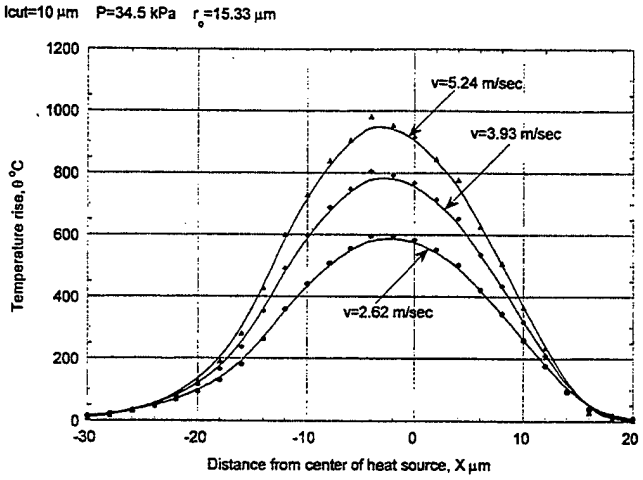

Fig. 6(*a*) Scratch length of 10 μm

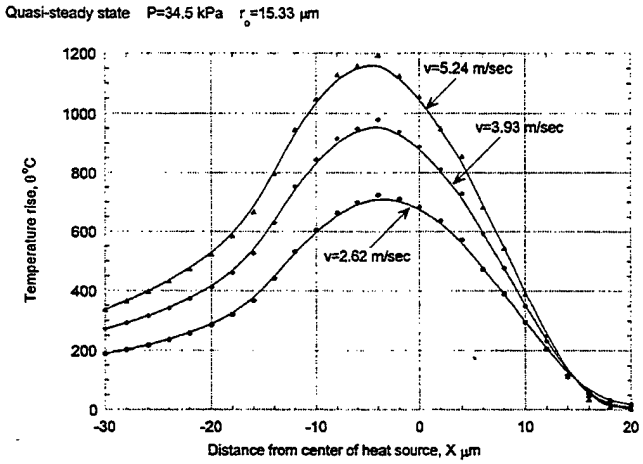

Fig. 6(*b*) Quasi-steady-state conditions

Fig. 6 Variation of the temperature rise with distance from the center of the heat source at a polishing pressure of 34.5 kPa and various sliding velocities

temperature on the temperature distribution plot and dividing it by the velocity of the moving heat source. The total flash time (T_1) is defined as the time from the beginning of the temperature rise to the time when it drops to the room temperature. If this time is more than the time taken (say, T_2), for the next abrasive to reach this present location, then there would be a cumulative effect on the rise of flash temperatures on the roller. Otherwise, there would be no cumulative effect.

Taking the temperature rise plot of Fig. 5 or 6 as an example, the flash time can be calculated using the following equation:

$$\text{Flash time, } T = \frac{L}{v}$$

where

L is the length of the region where the temperature is higher than a certain expected critical temperature.
v is the velocity of the moving heat source.

Table 4 gives the flash times at various flash temperatures for different combinations of the polishing pressure, the sliding speed, and scratch lengths. At a flash temperature of 200°C, it can be seen from Table 4 that depending on the pressure, the sliding velocity, and the length of the scratch, the flash times can range from 5.9 to 28.0 μs for most cases.

(a) Referring to Fig. 7, the total flash time T_1 is given by,

$$T_1 = 270/2.62 = 103.1\ \mu\text{s}.$$

(b) The time taken by the next abrasive to travel through the center to center distance between the abrasives, T_2 is given by (in this case, the minimum possible center to center distance is 400 μm, which is the diameter of the largest abrasive used)

$$T_2 = 400/2.62 = 152.7\ \mu\text{s}.$$

Since, $T_1 < T_2$, there would be no cumulative effect on the flash temperature rise of the roller.

It has been shown that based on Gibb's Free Energy ($\Delta G°$) calculations, the oxidation of Si_3N_4 in air can take place ≥167°C (Shingal, 1975). It can be seen from Table 4, that even at a relatively low pressure (34.48 kPa) and a low sliding speed (2.62 m/s), the flash temperature in polishing exceeds the temperature required for the oxidation of Si_3N_4 with certain duration of time for the reaction products to form.

Detailed examination of the wear debris (in the SEM with an X-ray microanalyzer and a low angle X-ray diffraction apparatus) obtained in MAF of Si_3N_4 rollers using Cr_2O_3 abrasive showed conclusively that Cr_2O_3 does participate in the chemo-mechanical polishing of Si_3N_4 forming chromium nitride and chromium silicate (Bhagavatula and Komanduri, 1996). This work established the role of Cr_2O_3 not as a mere catalyst as considered by earlier researchers (Kikuchi et al., 1992) but one actively taking part in the chemical reactions during chemo-mechanical polishing. Based on the experimental evidence, chemo-mechanical reaction models were developed for the chemo-mechanical polishing of Si_3N_4 in air and in water with Cr_2O_3 abrasive. These models are based on the formation of such reaction products as chromium silicate and chromium nitride in addition to the formation of silica layer on the surface of Si_3N_4 as well as the gaseous reaction products, such as ammonia (in water) and nitrogen (in air). Thus chemical reactions can be activated during polishing by proper choice of the abrasive and polishing conditions for a given workmaterial.

6 Conclusions

1 A moving disk heat source model with a parabolic distribution of heat intensity was applied to magnetic abrasive finishing (MAF) process to determine the flash temperatures and flash times. The workmaterial considered is Si_3N_4 and the abrasive is Cr_2O_3.

2 The flash temperatures were determined as a function of the polishing pressure, sliding speed, and the scratch length made by the abrasives on the worksurface during polishing.

3 Examination in the SEM of the polished surfaces of the Si_3N_4 rollers polished by MAF showed the lengths of most scratches on the work surface to be < 30 μm. Consequently, the time required for each contact was found to be on order of 30 μs or less when the sliding speed, v is ~1 m/s. For higher sliding speeds, say 5 m/s, the time of contact is even less (6 μs or less). For very short scratch lengths and very short contact times, the conditions of polishing are shown to be transient and quasi-steady state conditions have not been reached.

4 As the polishing pressure increases, the maximum flash temperature rise produced also increases. For example, considering the case of a scratch of length of 10 μm even under transient conditions at a sliding velocity of 2.62 m/s, it is about 600°C at a pressure of 34.5 kPa, and increases to 810°C with increase in polishing pressure to 69.0 kPa [Fig. 5(a)]. Similarly, as the sliding velocity of the abrasives on the work surface increases, the maximum flash temperature rise also increases. For example, considering the case of a scratch of length of 10 μm even under transient conditions at a pressure 34.5 kPa and a velocity of 2.62 m/s, the maximum temperature rise is 600°C. With increase in the sliding speed, say 5.24 m/s, the temperature

Table 4 Flash times (μs) for different flash temperatures, length of scratches, contact pressures, and sliding velocities

	Estimated flash temperature, °C											
	100			200			300			400		
	I	II_a	II_b	I	II_a	II_b	I	II_a	II_b	I	II_a	II_b
P = 34.5 kPa												
v = 2.62 m/s	30.8	16.8	13.6	16.8	12.5	10.7	11.8	10.0	8.8	9.1	8.2	7.1
v = 3.93 m/s	20.8	11.6	9.3	14.2	9.3	7.7	10.3	7.8	6.6	7.9	6.6	5.7
v = 5.24 m/s	14.2	8.8	7.0	11.1	7.3	5.9	8.8	6.3	5.2	7.1	5.5	4.7
P = 51.7 kPa												
v = 2.62 m/s	38.4	19.0	15.5	22.9	15.0	12.6	16.1	12.4	10.8	12.5	10.6	9.3
v = 3.93 m/s	23.5	13.0	10.5	17.8	10.7	8.9	13.7	9.3	7.8	10.9	8.1	7.0
v = 5.24 m/s	15.6	9.8	7.9	12.9	8.4	6.8	10.9	7.4	6.1	9.2	6.6	5.5
P = 69.0 kPa												
v = 2.62 m/s	43.2	20.6	16.8	28.0	16.7	14.0	20.0	14.2	12.3	15.6	12.3	10.7
v = 3.93 m/s	25.3	13.9	11.4	20.1	11.8	9.7	16.3	10.4	8.8	13.4	9.3	7.9
v = 5.24 m/s	16.5	10.5	8.5	14.0	9.1	7.5	12.2	8.2	6.8	10.7	7.4	6.3

I—quasi-steady state.
II_a—transient state for l_{cut} = 20 μm.
II_b—transient state for l_{cut} = 10 μm.

rise increased to about 980°C [Fig. 6(*a*)]. Of course, under quasi-steady-state conditions and/or longer scratch lengths, these temperatures would be even higher as shown in Figs. 5(*b*) and 6(*b*).

5 The flash temperatures generated in magnetic float polishing (MFP) are found to be (see Part II for details), in general, lower than in magnetic abrasive finishing (MAF) reported in this paper under similar polishing conditions. Also, the difference in the temperatures between the transient and quasi-steady-state conditions were small in MFP mainly due to lower loads and smaller contact area.

6 The flash temperatures and corresponding flash times can be used to conduct thermodynamic and kinetic analyses to determine if chemo-mechanical action between the abrasive (Cr_2O_3) and the workmaterial (Si_3N_4) under the conditions of polishing can take place or not. It is also possible to investigate possible chemical reaction species at different flash temperatures during Gibbs free energy analysis. Experimental study of the wear debris presented elsewhere (Bhagavatula and Komanduri 1996) showed the feasibility of chemo-mechanical action (formation of chromium nitride and chromium silicate) by the polishing process.

7 Based on the total flash time calculation, no cumulative effect of the abrasive on the flash temperature rise of the roller was found. Thus the average temperature rise of the bulk material of the roller would be low.

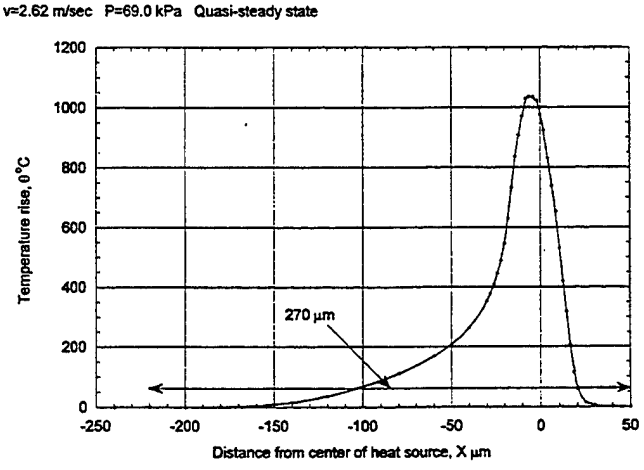

Fig. 7 Total flash temperature rise with distance from the center of contact

8 Flash temperatures and flash times at different polishing conditions can be used as a basis for the selection of optimum polishing conditions.

References

Archard, J. F., 1958/59, "The Temperature of Rubbing Surfaces," *Wear*, Vol. 2, pp. 438–455.

Bhagavatula, S. R., 1995, "On the Chemo-Mechanical Polishing of Silicon Nitride with Chromium Oxide Abrasive," M.S. thesis, Oklahoma State University, Stillwater, OK.

Bhagavatula, S. R., and R. Komanduri, 1996, "On the Chemo-Mechanical Polishing of Silicon Nitride with Chromium Oxide Abrasive," *Philosophical Magazine*, Vol. 74, No. 4, pp. 1003–10171.

Bos. J., and H. Moes, 1995, "Frictional Heating of Tribological Contacts," ASME JOURNAL OF TRIBOLOGY, Vol. 117, pp. 171–177.

Blok, H., 1937, "Theoretical Study of Temperature Rise at Surface of Actual Contact Under Oiliness Lubricating Conditions," *I. Mech. E. Proceedings of General Discussion on Lubrication and Lubricants*, Vol. 2, pp. 222–235.

Carslaw, H. S., and J. C. Jaeger, 1959, *Conduction of Heat in Solids*, Oxford University Press, 2nd Edn.

Francis, H. A., 1970, "Interfacial Temperature Distribution within a Sliding Hertzian Contact," *ASLE Trans*, Vol. 14, pp. 41–54.

Fox, M., Agrawal, K., Shinmura, T., and R. Komanduri, 1994, "Magnetic Abrasive Finishing of Rollers," *Annals of CIRP*, Vol. 43/1, pp. 181–184.

Greenwood, J. A., 1991, "An Interpolation Formula for Flash Temperatures," *Wear*, Vol. 150, pp. 153–158.

Hou, Z. B., and R. Komanduri, 1998a, "Magnetic Field Assisted Finishing of Ceramics—Part I: Thermal Model," ASME JOURNAL OF TRIBOLOGY, Vol. 120, pp. 645–651.

Hou, Z. B., and R. Komanduri, 1998b, "Magnetic Field Assisted Finishing of Ceramics—Part II: On Thermal Aspects of Magnetic Float Polishing (MFP) of Ceramic Balls," ASME JOURNAL OF TRIBOLOGY, Vol. 120, pp. 652–659.

Jaeger, J. C., 1943, "Moving Sources of Heat and the Temperature of Sliding Contacts," *Proc. of the Royal Society of NSW*, Vol. 76, pp. 203–224.

Kikuchi, M., Takahashi, Y., Suga, T., Suzuki, S., and Y. Bando, 1992, "Mechno-chemical Polishing of Silicon Carbide Single Crystal with Chromium (III) Oxide Abrasive," *J. Amer. Ceram. Soc.*, Vol. 75, 2, pp. 264–270.

Komanduri, R., Umehara, N., and M. Raghunandan, M., 1995, "On the Possibility of Chemo-Mechanical Polishing of Silicon Nitride," ASME JOURNAL OF TRIBOLOGY, Vol. 118, pp. 721–727.

Kuhlmann-Wildorf, D., 1985, "Flash Temperatures due to Friction and Joule Heat at Asperity Contacts," *Wear*, Vol. 105, pp. 187–198.

Ling, F. F., 1973, *Surface Mechanics*, Wiley Interscience, New York.

Nagaraj, H. S., Sanborn, D. M., and W. O. Winer, 1978, "Direct Surface Temperature Measurement of Infrared Radiation in Elastohydrodynamic Contacts and the Correlation with the Blok Flash Temperature Theory," *Wear*, Vol. 49, pp. 43–59.

Rosenthal, D., 1941, "Mathematical Theory of Heat Distribution During Welding and Cutting," *Welding Journal*, Vol. 20 res. suppl., pp. 220–234.

Rosenthal, D., 1946, "The Theory of Moving Sources of Heat and Its Application to Metal Treatments," *Trans ASME*, pp. 849–866.

Singhal, S. C., 1975, "Effect of Water Vapor on the Oxidation of Hot-Pressed Silicon Nitride and Silicon Carbide," *J. Am. Cer. Soc.*, Vol. 58, p. 17.

Tian, X., and F. E. Kennedy, Jr., 1994, "Maximum and Average Flash Temperatures in Sliding Contact," ASME JOURNAL OF TRIBOLOGY, Vol. 116, pp. 167–174.

APPENDIX A

Specimen Calculations for the Flash Temperatures and Flash Times Using the Moving Disk Heat Source Model

Table A1 gives the polishing conditions used and Table A2 gives the relevant material properties of the workmaterial and the abrasive used in this investigation.

1. The relative velocity between the abrasive and work piece, V is determined as the resultant of the rotational velocity of the roller, V_1 and the oscillational velocity of the magnetic head, V_2., i.e.,

$$V = [V_1^2 + V_2^2]^{1/2}$$

Consider, for example, the rotational speed of the rod to be 2000 rpm,

$$V_1 = \pi DN/60 = 3.14 \cdot 25 \cdot 10^{-3} \cdot 2000/60 = 2.618 \text{ m/s}$$

$$V_2 = 2 \cdot A \cdot f/100 = 2 \cdot 0.25 \cdot 25/100 = 0.125 \text{ m/s}$$

Hence, $V = 2.621$ m/s.

2. Number of magnetic abrasives in the monolayer $= \pi \cdot 0.5 \cdot D \cdot L/(\text{abr. size})^2 = 3.14 \cdot 0.5 \cdot 25 \cdot 10/(250 \cdot 250 \cdot 10^{-6}) = 6283$

3. Referring to Fig. A1, it can be seen that initially only a few particles which are of the maximum height of the asperities are under contact. With the application of polishing pressure by means of the magnetic field, the contact points of those particles will undergo some deformation. Consequently, the work surface approaches closer to the magnetic brush as shown in Fig. A1.

With a load of about 1–2.5 N/magnetic particle, the deformation of the contact points can be estimated based on the results of a series of test calculations assuming different possible numbers of real contact points to be in the range of 1.0 to 2.5 μm. The total range of distribution of the heights of different particles is around 300 μm (assuming normal distribution). Due to deformation of the initial contact points, the number of particles with actual contact (number of active particles) increases. The deformation is very small (1.0–2.5 μm) compared to the total range of distribution (300 μm). The probability of the heights of asperities falling into this small range (1.0–2.5 μm) is very low. The probability calculations give the following:

when $P = 34.5$ kPa % of active particles is 0.1496%
when $P = 51.7$ kPa % of active particles is 0.1536%
when $P = 69.0$ kPa % of active particles is 0.1575%

Figure A1 shows the relationship between the deformation of contact point and the probability of real contact.

4. Effective Young's modulus, E' is given by,

$$E' = \frac{1}{\frac{1-\nu_1^2}{E_1} + \frac{1-\nu_2^2}{E_2}}$$

Table A1 Polishing conditions used

Polishing pressure p:	34.5, 51.7, 69.0 kPa
Diameter of the silicon nitride rod D:	25 mm
Rotational speed of the rod N:	2000, 3000, 4000 rpm
Oscillational frequency of the magnetic head, f:	25 Hz
Amplitude of oscillation of the magnetic head A:	0.25 cm
Width of the magnetic head L:	1.0 cm
Size of the ferromagnetic particles: (means diameter = 250 μm)	100–400 μm
Volume fraction of Iron powder Fv:	60%

Table A2 Material properties of the workmaterial and the abrasive

Thermal conductivity of Si_3N_4, λ_1:	0.293 J/cm·s°C
Thermal conductivity of Cr_2O_3, λ_2:	0.3182 J/cm·s°C
Thermal conductivity of iron powder:	0.7285 J/cm·s°C
Thermal diffusivity of Si_3N_4, a:	0.139 cm^2/s
Heat capacity of silicon nitride, C:	0.65 J/gm·°K
Density of Si_3N_4, ρ:	3.3 gm/cm^3
Elastic modulus of Si_3N_4, E_1:	320 GPa
Elastic modulus of ferromagnetic particles, iron, E_2:	160 GPa
Poisson's ratio of Si_3N_4, ν_1:	0.26
Poisson's ratio of iron particles, ν_2:	0.28

Consider the contact between the magnetic abrasive particle and the work surface as an example.

$$E' = \frac{1}{\frac{1-0.28^2}{160 \times 10^9} + \frac{1-0.26^2}{320 \times 10^9}} = 1.1529 \cdot 10^{11}$$

5. Effective radius of contact, R' is given by,

$$R' = \frac{1}{\frac{1}{R_1} + \frac{1}{R_2}}$$

where R_1 is the radius of the ferromagnetic particle (only larger particles are in contact, their average radius is about 195 μm), and R_2 is the radius of the roller at the point of contact.

$$R' = \frac{1}{\frac{1}{195 \times 10^{-3}} + \frac{1}{12.5}} = 0.192 \text{ mm.}$$

6 When $P = 34.5$ kPa

(a) Total load on the rod, W = polishing pressure·0.5·π·(rod. dia)·(width of the magnetic head) = $3.45 \cdot 0.5 \cdot \pi \cdot 2.5 \cdot 1.0 = 13.54$ N.

(b) Load per magnetic particle, w = Total load/No. of particles under contact = $13.54/(6283 \cdot 0.001496) = 1.44$ N/particle

(c) Radius of contact between the magnetic abrasive particle and the work surface,

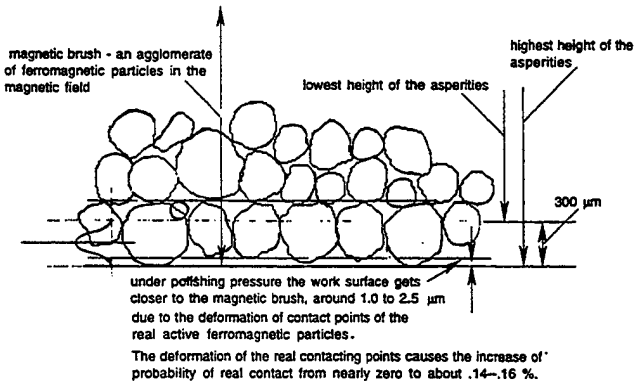

Fig. A1 Coefficient of probability of the real contact in MAF

APPENDIX H

GENERAL SOLUTIONS FOR STATIONARY/MOVING THE PLANE HEAT SOURCE PROBLEMS IN MANUFACTURING AND TRIBOLOGY

Zhen Bing Hou and R. Komanduri

Int. J of Heat & Mass Transfer, 43 (2000) 1679-169

PERGAMON

International Journal of Heat and Mass Transfer 43 (2000) 1679–1698

International Journal of HEAT and MASS TRANSFER

www.elsevier.com/locate/ijhmt

General solutions for stationary/moving plane heat source problems in manufacturing and tribology

Z.B. Hou, R. Komanduri*

Mechanical and Aerospace Engineering, Oklahoma State University, Stillwater, OK 74078, USA

Received 20 April 1999; received in revised form 23 August 1999

Abstract

General solutions (both *transient* and *steady state*) for the temperature rise at any point due to stationary/moving plane heat sources of different shapes (*elliptical*, *circular*, *rectangular*, and *square*) and heat intensity distributions (*uniform*, *parabolic*, and *normal*) are presented using the Jaeger's classical *heat source method* (J.C. Jaeger, Moving sources of heat and the temperature at sliding contacts, Proc. Royal Society of NSW 76 (1942) 203–224). Starting from an instantaneous point heat source solution, an *elliptical moving heat source* with different heat intensity distributions, namely, uniform, parabolic and normal, was used as the *basic plane heat source* and its solution for the temperature rise at any point was derived. This analysis was then extended to other plane heat sources, such as circular, rectangular, and square heat sources to cover a range of manufacturing processes and tribological problems experienced in engineering practice. In addition, the analysis presented here is valid for *both transient and steady state conditions* while most analyses to date are strictly for quasi-steady state conditions. The solutions for the stationary heat sources are obtained from the moving heat source solution by simply equating the velocity of sliding to zero. Further, the analysis can be used to determine the *temperature distribution not only at the surface* but also *with respective to the depth* which again is a very important consideration in most manufacturing and tribological applications since it effects the subsurface deformation, metallurgical changes, hardness variation, and residual stresses. It can also be used to determine the *maximum and average temperatures* within the area of the heat source. Thus, the analysis presented here is believed to be comprehensive.

1. Introduction

Plane heat source problems (both stationary and moving) are frequently encountered in numerous manufacturing processes, such as metal cutting (shear plane heat source and frictional heat source at the chip-tool interface), grinding, and polishing; spot welding (conventional and nonconventional) and cutting (gas-arc, plasma-arc, laser); surface heat treatment using laser irradiation; and EDM machining of openings of various shapes (relative to the EDM tools) as well as in many tribological applications, such as meshing of gears, cams, bearings, asperities in sliding contact. The relevant thermal analysis for these applications begins with the solution of a plane heat source of appropriate shape and heat intensity distribution. Temperature distribution and the rate of cooling at and near the surface can affect the metallurgical microstructure, thermal shrinkage, thermal cracking, hardness distribution, residual stresses, heat affected zone (HAZ), and chemical modifications of the material.

* Corresponding author. Tel.: +1-405-744-5900; fax: +1-405-744-7873.

E-mail address: ranga@ceat.okstate.edu (R. Komanduri).

0017-9310/00/$ - see front matter
PII: S0017-9310(99)00271-9

Nomenclature

a_o, b_o	semi-major and semi-minor axes of an elliptical heat source or half the side of a rectangular heat source. When $a_o = b_o$ radius of a circular heat source or half the side of a square heat source
a	thermal diffusivity of the medium (cm^2/s)
$A_{pl}, A_{ell}, A_c, A_{rec}, A_{sq}$	area of a plane, elliptical ($=\pi a_o b_o$), circular ($=\pi r_o^2$), rectangular ($=4a_o b_o$), and square ($=4a_o^2$) heat sources, respectively (cm^2)
c	specific heat (J/g·°C)
l, L	semi-width and width of the heat source along the direction of motion
l_{y_i}	half length of a differential stripe with a distance from the center of the elliptical source y_i (cm)
m, n	x_i/a_o (or X_i/a_o) and y_i/b_o, respectively
Q_{pt}	amount of heat liberated by the instantaneous point heat source (J)
q_{pt}	heat liberation rate of a stationary point heat source (J/s)
$q_{pl}, q_{ell}, q_c, q_{rec}, q_{sq}$	heat liberation rate of stationary/moving plane, elliptic, circular, rectangular, and square heat sources, respectively (J/s)
q_o	heat liberation intensity of a plane heat source ($J/cm^2 \cdot s$)
R	distance between the stationary/moving point heat source and the point where the temperature rise at time t is concerned (cm)
R_i	distance between the differential segmental heat source and the point where the temperature rise at time t is concerned (cm)
τ	the time after the initiation of an instantaneous heat source (s)
t	time of observation or the time after the initiation of a continuous heat source (s)
x_i, y_i	coordinates of a differential segmental element from the plane heat source of various shapes
x, y, z	coordinates of the point M where the temperature rise is concerned
X_i, y_i	coordinates of a differential segmental element from the plane heat source of various shapes in a moving coordinate system
X, y, z	coordinates of the point M where the temperature rise is concerned, in a moving coordinate system
λ	thermal conductivity of the medium (J/cm·s·°C)
θ	temperature rise at any point at any time t (°C)
θ_M	temperature rise at any point M at any time t (°C)
ρ	density of the medium (g/cm^3)
$K_m(u_i)$	$= \int_0^{v^2 t/4a} \frac{d\omega}{\omega^{3/2}} e^{-\omega - u_i^2/4\omega}$ where $u_i = \frac{R_i v}{2a}$
erf $c(p)$	complementary error function ($1 - \text{erf}(p) = 1 - \frac{2}{\sqrt{\pi}} \int_p^\infty e^{-u^2}\, du$)

These effects are collectively termed as *surface integrity* problems. Consequently, thermal aspects of manufacturing are critical in the optimization of the process parameters and quality of the products produced as well as their performance and reliability in service.

It may be noted that solutions of plane heat source problems (both stationary and moving) of various shapes and heat intensity distributions using the partial differential equations (PDE) method directly may not be simple and straightforward for they encounter boundaries where the temperatures are unknown and only the heat fluxes are known (either a constant value or a known function). Thus, to define and express it mathematically may not be simple. Even if so, it is still not certain whether it would be possible to determine the relevant unknown coefficients in the solutions of the relevant PDE's of heat conduction. For example, in solving the stationary, continuous point heat source problem using the PDE method, the boundary condition at the heat source is not possible to process mathematically while it is one of the simplest stationary heat source problems. Carslaw and Jaeger [2] termed problems of this type as cases of *variable temperature* and introduced an ingenious approach named the heat source method for solving such problems. It will be shown that this method can be used to solve a variety of complicated heat transfer problems in manufacturing processes and tribology with the boundary conditions where the heat fluxes are known (either a constant or a known function) but the temperatures are unknown.

The basis for the *heat source method* is the solution for the instantaneous point heat source, i.e.,

$$\theta = \frac{Q_{pt}}{c\rho(4\pi a\tau)^{3/2}} e^{-R^2/4a\tau} \tag{1}$$

Refer to the **Nomenclature** for the definition of the various parameters. Using Eq. (1) and integrating it with respect to the appropriate spatial and time variables, the solutions for an instantaneous line, plane, ring, circular disc, cylindrical surface, and spherical surface heat source as well as for continuous stationary point, line, plane, ring, and other heat sources can be obtained. A more appropriate term to describe this technique would be the *method of superposition of temperature field of individual heat sources* although for simplicity it is called the *heat source method.*

Jaeger [1] and Carslaw and Jaeger [2] presented solutions for uniform moving band and rectangular heat sources and uniform stationary heat source using the *heat source method.* In the following, a brief consideration of some representative cases of plane heat sources (both stationary and moving) in some manufacturing and tribological applications are given. For details, the readers are referred to the references cited as well as other critical reviews available in the literature.

In the manufacturing processes area, the pioneering works of Trigger and Chao [3] and Chao and Trigger [4] on the analytical evaluation of the metal cutting temperature are significant. They calculated the average tool–chip interface temperature using Jaeger's solutions for a moving band heat source (Eq. (2)), and a stationary rectangular (modified from Jaeger's solution for a stationary square) (Eqs. (2) and (3)) heat source (Eq. (3)): thus

$$\theta_M = \frac{q}{\lambda\pi}\int_{-l}^{+l} e^{-v(X-X_i)/2a} K_0\left[\frac{v}{2a}\sqrt{(X-X_i)^2+z^2}\right] dx_i$$

$$\theta_M = \frac{q}{\lambda\pi}\int_0^l dx_i \int_0^m \frac{dy_i}{\sqrt{(x-x_i)^2+(y-y_i)^2+z^2}} \qquad (3)$$

They solved Eq. (3) analytically resulting in the nondimensional temperature rise at any point at the contacting interface, θ_{xy}. The average temperature rise over the area of the chip–tool sliding contact is given by

$$\theta_{avg} = \frac{1}{lm}\int_0^l \int_0^m \theta_{xy}\, dx\, dy$$

This equation was simplified for orthogonal (two-dimensional) cutting as: $\theta_{avg} = \frac{4ql}{\pi\lambda}$*(shape factor).

Loewen and Shaw [5] (also Shaw [6]) extended Chao and Trigger's work [4] by determining the heat partition ratio for the shear plane heat source between the chip and the workmaterial as well as that for the frictional heat source between the chip and the cutting tool taking into account material properties instead of constant heat partition as used by Trigger and Chao [3]. They also developed a similar equation for the stationary rectangular heat source. However, these equations are valid only for steady state stationary heat sources of uniform heat intensity distribution, square or rectangular in shape.

In the field of tribology, Bowden and Thomas [7], Barber [8], and others (Cameron et al. [9], Gecim and Winer [10], Kuhlmann-Wildorf [11]) used similar approximate equations based on Jaeger's solution for a stationary heat source to estimate the sliding contact temperatures. Ling [12] (also, Ling and Ng [13], Ling [14]) based on the Jaeger's solution of a stationary point heat source under steady state conditions, $q_{pt}/2\pi\lambda R$, used the *heat source method* to develop a solution for a stationary rectangular heat source whose intensity varies spatially: thus

$$\theta_{(x,y,z)} = \frac{1}{2\pi\lambda}\int_{-l}^{l}\int_{-b}^{b} q_1(\xi,\eta)\frac{d\xi\, d\eta}{R}$$

where $R = \sqrt{(x-\xi)^2+(y-\eta)^2+z^2}$. This equation offers the possibility of solving the heat source problems of various distributions of heat intensities. Francis [15] using a similar method, derived two equations for the stationary circular plane heat source — one for a uniform distribution and the other for an elliptical distribution of heat intensity.

From the late 1930's to the mid-1940's, Rosenthal [16–19], Blok [20,21], and Jaeger [1] made seminal contributions to the analysis of moving heat source problems which formed the basis for much of the applied research that followed. Because of the mathematical complexity, various moving heat source problems in manufacturing and tribology were simplified either to a moving point or a moving line heat source (Rosenthal [19]), or uniformly distributed moving band or rectangular heat source (Jaeger [13]). Also, for mathematical simplicity much of the analysis to date was limited to quasi-steady state conditions.

Rosenthal first applied the theory of heat flow due to a moving point and a moving line heat source to welding [16,17]. Based on the similarity between the differential equation of heat conduction and that in electro-magnetic waves, Rosenthal [19] considered the final solution to be a product of two separate functions — one, an exponential function $e^{-vX/2a}$, which is a asymmetric function along the X-axis, and the second, $\varphi(X, y, z)$, which is a symmetric function and solved it using the moving coordinate system. The final solution is an unsymmetric function along the X-axis which is close to practice. However, for mathematical simplicity, Rosenthal considered quasi-stationary state. Mahla et al. [27] considered the method of instantaneous heat sources which is applicable to nonquasi-steady states to a particular case of welding. Rosenthal pointed out that while the solutions of Mahla et al.

does not differ significantly from that obtained on the assumption of quasi-steady state, the solutions in most cases become too unwieldy for a direct practical application.

Jaeger [1] in 1942 introduced the *heat source method* (also covered briefly in Carslaw and Jaeger [2]) for solving a wide range of moving heat source problems. He developed solutions for the temperature rise for plane heat sources of different shapes (band, square, or rectangular) starting from the solution of an instantaneous line heat source. For mathematical simplicity Jaeger considered the heating time, $t = \infty$ in the very early stages of the derivation thus limiting the analysis to quasi-steady state conditions. Jaeger not only introduced the exact solutions for uniform moving band and moving rectangular heat sources but also gave a series of approximate equations for very high and very low values of L where $L = vl/2a$ which later on became known as the Peclet number for calculating the maximum and the average temperatures over the area of the heat source. His reasons for choosing the approximate equations was to illustrate the power of the analytical techniques to address some simplified engineering problems.

Exact solutions for the moving plane heat sources problems of various shapes and heat intensity distributions were attempted only recently. Tian and Kennedy [22] using Jaeger's heat source method, developed a series of quasi-steady state solutions for moving circular, moving square, and moving elliptical heat sources of uniform and parabolic distribution of heat liberation intensity by integrating the solution of a moving point heat source with respect to appropriate spatial variables. They used polar coordinates for the circular heat source and cartesian for the rectangular heat source. Thus, their equations for the circular, square, and elliptical heat sources all seem different though mathematically correct. It also appears that the emphasis of Tian and Kennedy's work was to develop approximate solutions that would be close to the exact solutions. Bos and Moes [23], also using the heat source method, gave solutions for a moving elliptical heat source with uniform and semi-ellipsoidal distribution of heat intensity. They also developed a numerical approach to solve the steady state heat partitioning problem.

In this paper, using the *heat source method*, solutions for stationary/moving plane heat sources of various shapes (*elliptical*, *circular*, *rectangular*, and *square*) and heat intensity distributions (*uniform*, *parabolic*, and *normal*), for both *transient* and *steady state conditions* are presented. An elliptic moving heat source of various heat intensity distributions is considered as the basis and its solution is first determined. By considering the major axis of the elliptical heat source to be equivalent to the minor axis, the equation for the temperature rise for a circular heat source is obtained. Similarly, by assuming the width of the heat source to be constant, solutions for rectangular ($a_o \neq b_o$), and square ($a_o = b_o$) heat sources are obtained. Considering the velocity of the heat source, $v = 0$, the solutions for various stationary plane heat sources are obtained. It may be noted that the model developed can be applied in principle for any *geometrical* shape that can be *defined mathematically*. This analysis can similarly be extended to other distributions. Thus, the solution developed here for a single geometry (elliptical) as a basis can be extended to develop general solutions which then can be used to solve a wide range of stationary/moving plane heat source problems by merely substituting the appropriate integration limits and appropriate coefficients. Thus the analysis is considered to be comprehensive.

2. Solution for a moving point heat source

The commonly used solution of a moving point heat source [1,2]

$$\theta = \frac{q_{\mathrm{pt}}}{4\pi\lambda R} e^{-(R+X)v/2a} \tag{4}$$

is applicable only for quasi-steady state conditions. Hence, to develop a general solution (for both transient and quasi-steady state) an alternate approach is needed. Fig. 1 is a schematic of the moving point heat source problem. x, y, and z form the absolute coordinate system and X, y, and z the moving coordinate system which moves along with the moving point heat source with the same velocity (along x-axis). It is required to determine the temperature rise at any point $M(x, y, z)$ and time t caused by the moving point heat source of heat intensity q_{pt} (J/s). At time τ_i, the moving point heat source had moved a distance $v\tau_i$. Thus, the distance between the heat source and the point M is given by $\sqrt{(x - v\tau_i)^2 + y^2 + z^2}$. The temperature rise, $\mathrm{d}\theta_M$ at point M at time t caused by the heat liberated in this differential infinitesimally small time interval at time τ_i (using the solution for an instantaneous point heat source Eq. (1)) is given by

$$\mathrm{d}\theta_M = \frac{q_{\mathrm{pt}}\,\mathrm{d}\tau_i}{c\rho(4\pi a\tau)^{3/2}} \exp\left[-\frac{(x - v\tau_i)^2 + y^2 + z^2}{4a\tau}\right] \tag{5}$$

The total temperature rise caused by the moving point heat source can be obtained by integrating the above equation from $\tau_i = 0$ to t, where $x - v\tau_i = x - v(t - \tau) = x - vt + v\tau$. It can be noted that $(x - vt)$ is the coordinate of the point M in the moving coordinate system in the X-direction at time t. So, it can be substituted by X. Thus, $x - v\tau_i = X + v\tau$. Set $\tau = t - \tau_i$, then

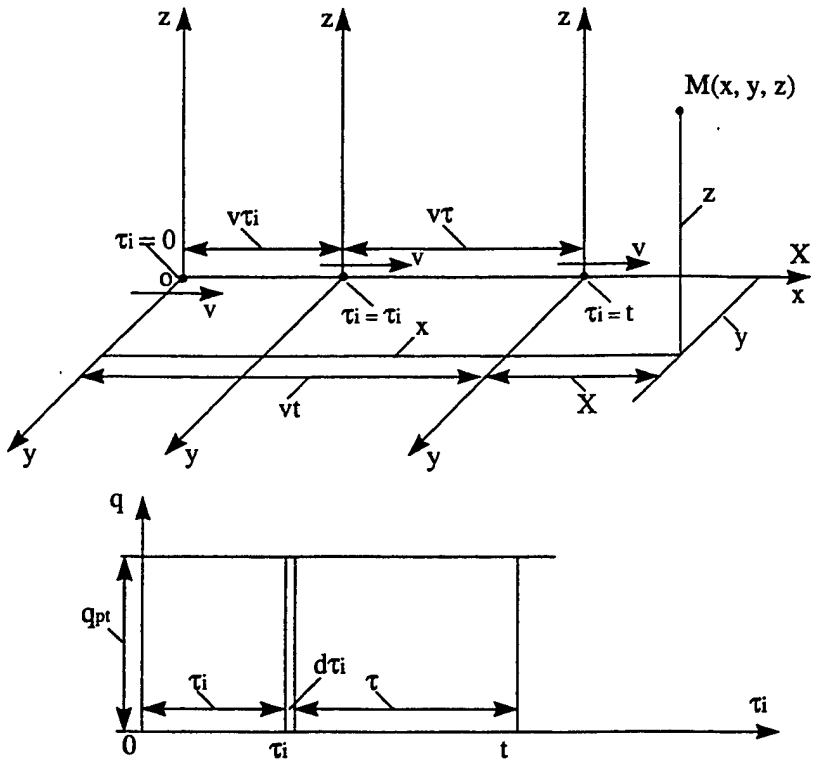

Fig. 1. Schematic showing a moving point heat source problem.

$d\tau_i = -d\tau$; when $\tau_i = 0$, $\tau = t$; when $\tau_i = t$, $\tau = 0$. It can be shown that

$$\theta_M = \frac{q_{pt}}{c\rho(4\pi a)^{3/2}} \int_{\tau=0}^{t} \frac{d\tau}{\tau^{3/2}} \exp\left[- \frac{(X+v\tau)^2+y^2+z^2}{4a\tau} \right] \text{or}$$

$$\theta_M = \frac{q_{pt}}{c\rho(4\pi a)^{3/2}} \exp\left(- \frac{Xv}{2a} \right) \int_{\tau=0}^{t} \frac{d\tau}{\tau^{3/2}} \exp\left[- \frac{X^2+y^2+z^2}{4a\tau} \right] \exp\left[- \frac{v^2\tau}{4a} \right] \tag{6}$$

To express the integral part of Eq. (6) in a non-dimensional form, it is necessary to substitute an appropriate non-dimensional term instead of variable τ. There are two possibilities: (1) $(X^2+y^2+z^2)/4a\tau = \xi$; and (2) $v^2\tau/4a = \omega$. Here, both ξ and ω are non-dimensional variables. Jaeger [1] used the first substitution, namely, $(X^2+y^2+z^2)/4a\tau = \xi$ and assumed $t = \infty$ to obtain the solution (Eq. (4)). Since this solution is time independent, it can be applied only for quasi-steady state conditions. All subsequent solutions derived based on this equation for other applications are also time independent and can be used only for quasi-steady state conditions (e.g. [22] or [23]). The use of the second substitution, namely, $v^2\tau/4a = \omega$, results in an alternate solution (Eq. (7)): thus

$$\theta_M = \frac{q_{pt} \cdot v}{16\lambda a\pi^{3/2}} \exp\left(- \frac{Xv}{2a} \right) \int_0^{\frac{v^2 t}{4a}} \frac{d\omega}{\omega^{3/2}} \exp\left[- \omega - \left(\frac{u^2}{4\omega} \right) \right] \tag{7}$$

where $u = Rv/2a$, $R = X^2+y^2+z^2$, R is the distance between the moving point heat source and point M where the temperature rise is of interest in the moving coordinate system at time t.

The integral part of Eq. (7) is very similar to the modified Bessel function of the second kind, order zero,

$$K_o = \frac{1}{2} \int_0^{\infty} \frac{d\omega}{\omega} \exp\left[- \omega - (u^2/4\omega) \right]$$

Eq. (7) is the solution for a moving point heat source which contains the time variable t in the upper limit of integration. The integral part of Eq. (7) is a non-dimensional coefficient. The longer the heating time t, the larger the coefficient, and higher the temperature rise at any point M. Temperature rise, therefore, is time dependent. Hence, Eq. (7) can be applied for transient conditions. This integral part has no analytical solution but can be solved numerically.

For the quasi-steady state, theoretically the heating time should be ∞ but it can be shown that for all practical purposes this value can be finite and determinable. By investigating the nature of $f(\omega)$ in Eq. (7)

for various values of u, it was found that $f(\omega)$ converges when $\omega \to 0$ and $\omega \to 5$ [24]. That is, when $\omega > 5$, no matter how large (even ∞) the results of integration are almost the same. Thus, it can be assumed that quasi-steady state condition has been established when $\omega \geq 5$, i.e. the upper limit of integration can be considered as 5, instead of ∞ for quasi-steady state. This relationship can also be used to estimate the time required for establishing the quasi-steady state conditions:

$$t_{\text{quasi-steady}} = 5\frac{4a}{v^2} = \frac{20a}{v^2}$$

As the function to be integrated also converges when $\omega \to 0$, it is necessary to consider a very small value, say 0.00001 as the lower limit of integration instead of zero. This will result in insignificant error in the final result. In this paper, Eq. (7) is used as the basis for the derivation of the general solution for moving plane heat sources of various shapes and heat intensity distributions for both transient and quasi-steady state conditions.

3. Heat liberation intensity of heat sources of various distributions

Fig. 2 is a comparison of the three heat intensity distributions, namely uniform, parabolic, and normal distributions. It shows that with the same rate of heat liberation q_{pl}, J/s, the uniform distribution has the highest uniformity, and hence the lowest maximum value of heat intensity q_0, J/cm^2·s. The normal distribution has the least uniformity and the highest maximum value of heat intensity. The parabolic distribution is in between the uniform and the normal distributions.

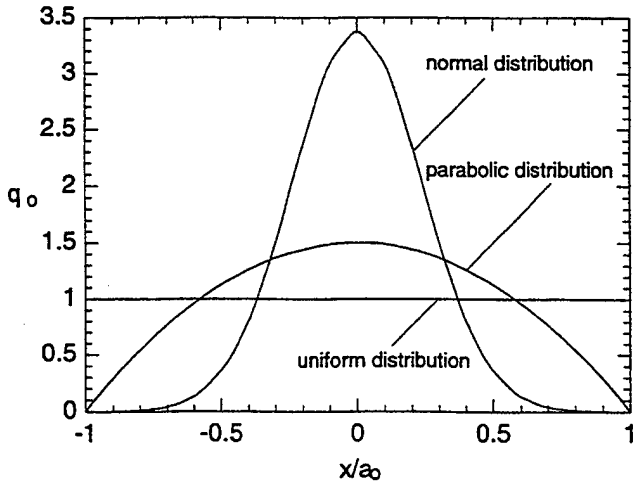

Fig. 2. Variation of the three heat intensity distributions, namely, uniform, normal, and parabolic with x_i/a_o from -1 to $+1$.

3.1. Uniform distribution

The heat intensity for various heat sources with uniform distribution is constant and given by

$$q_o = \frac{q_{\text{pl}}}{A_{\text{pl}}}$$

3.2. Parabolic distribution

Fig. 3(a) shows the variation of (2-dimensional) the heat liberation intensity of an elliptic heat source with a parabolic heat distribution. The relationship between the heat liberation intensity q_o and the distances x_i and y_i from the center is given by

$$q_o = C\left(1 - y_i^2/b_o^2\right)\left(1 - x_i^2/l_{y_i}^2\right)$$

The heat liberation rate from the differential area $\mathrm{d}x_i\,\mathrm{d}y_i$ is given by

$$\mathrm{d}q_{\text{ell}} = q_o\,\mathrm{d}x_i\,\mathrm{d}y_i$$

After appropriate substitutions and integration, it can be shown [25] that the heat intensity for an *elliptical heat source with a parabolic distribution* is given by

$$q_o = \frac{q_{\text{ell}}}{0.5A_{\text{ell}}}(1-n^2)\left[1 - m^2/(1-n^2)\right]$$

Similarly, the heat intensity for a *circular disc heat source* ($a_o = b_o$) *with a parabolic distribution* is given by

$$q_o = \frac{q_{\text{c}}}{0.5A_{\text{c}}}(1-n^2)\left[1 - m^2/(1-n^2)\right]$$

For a rectangular heat source with a parabolic distribution (refer to Fig. 3(b)), the relationship between the heat liberation intensity q_o and the distances x_i and y_i from the center is given by

$$q_o = C\left(1 - y_i^2/b_o^2\right)\left(1 - x_i^2/a_o^2\right)$$

It can be shown that the heat intensity for a *rectangular heat source with a parabolic distribution* is given by

$$q_o = \frac{q_{\text{rec}}}{4/9A_{\text{rec}}}(1-n^2)(1-m^2)$$

Similarly, the heat intensity for a *square heat source with a parabolic distribution* is given by

$$q_o = \frac{q_{sq}}{4/9A_{sq}}(1-n^2)(1-m^2)$$

3.3. Normal distribution

Fig. 4(a) shows the variation (2-dimensional) of the heat liberation intensity of an elliptic heat source with a normal heat distribution. The relationship between the heat liberation intensity q_o and the distances x_i and y_i from the center is given by

$$q_o = C\exp\left[-(3y_i/b_o)^2\right]\exp\left[-(3x_i/l_{y_i})^2\right]$$

It can be shown that the heat intensity for an *elliptical heat source with normal distribution* is given by

$$q_o = \frac{q_{ell}}{0.1079A_{ell}}\exp-(3n)^2\exp\left[-\left(3m/\sqrt{1-n^2}\right)^2\right]$$

Substituting, $a_o = b_o = r_o$, the heat intensity for a *circular disc heat source with normal distribution* is given by

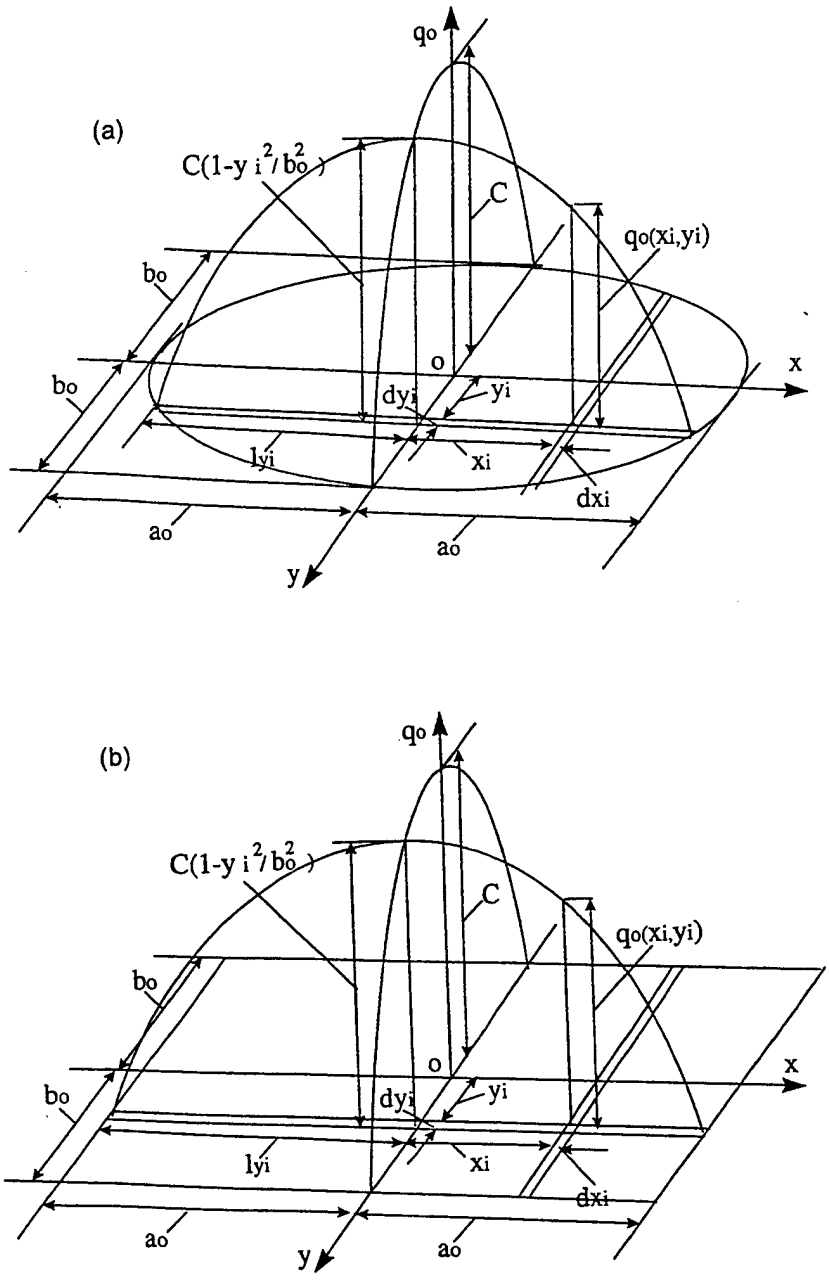

Fig. 3. (a) Variation of the heat liberation intensity of an elliptical heat source with a parabolic heat distribution. (b) Variation of the heat liberation intensity of a rectangular heat source with a parabolic heat distribution.

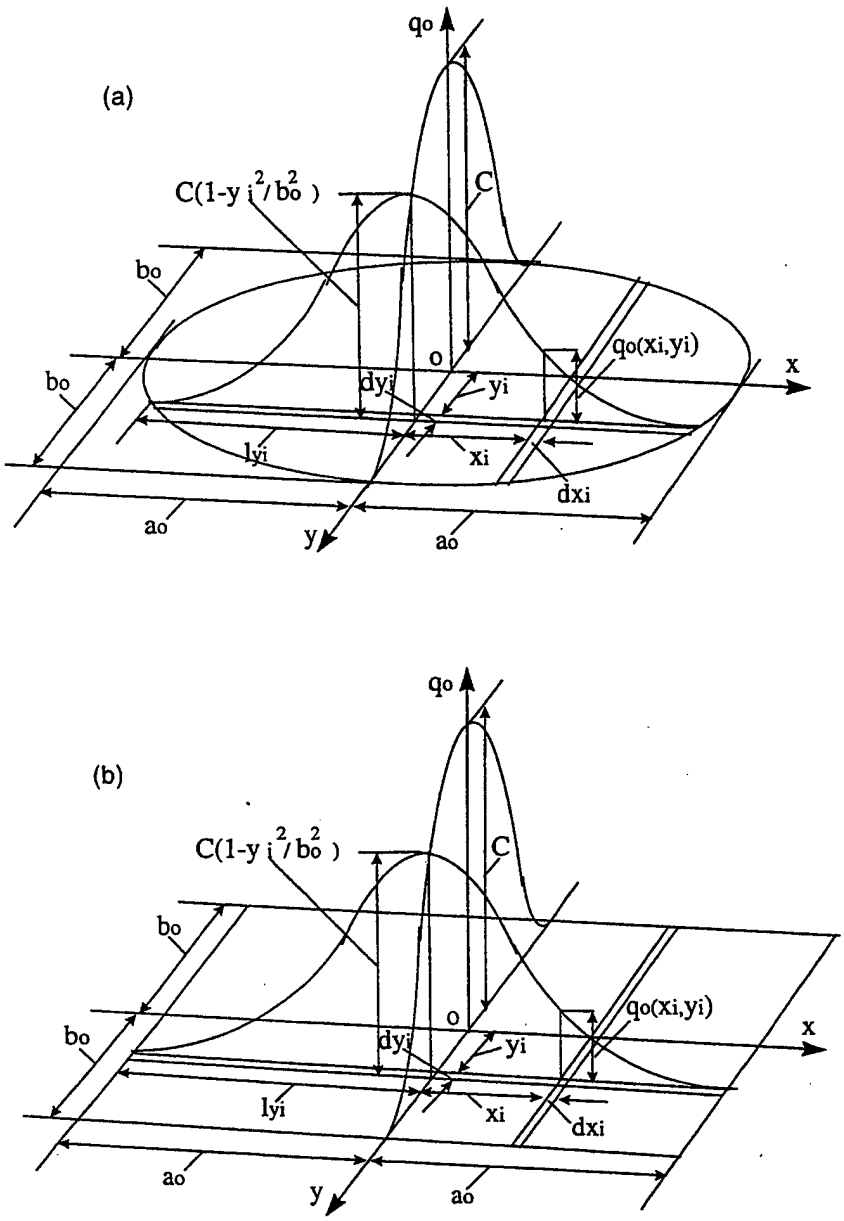

Fig. 4. (a) Variation of the heat liberation intensity of an elliptic heat source with a normal heat distribution. (b) Variation of the heat liberation intensity of a rectangular heat source with a normal heat distribution.

$$q_o = \frac{q_c}{0.1079A_c}\exp[-(3n)^2]\exp\left[-\left(3m/\sqrt{1-n^2}\right)^2\right]$$

For a rectangular heat source with a normal distribution (refer to Fig. 4(b)), the relationship between the heat liberation intensity q_o and the distances x_i and y_i from the center is given by

$$q_o = C\exp[-(3n)^2]\exp[-(3m)^2]$$

After appropriate substitutions and integration, it can be shown that the heat liberation intensity, q_o (J/cm^2·s) for a *rectangular heat source with a normal distribution* is given by

$$q_o = \frac{q_{rec}}{\pi/36A_{rec}}\exp[-(3n)^2]\exp[-(3m)^2]$$

By substituting $a_o = b_o$, we get the heat intensity for a *square heat source with a normal distribution* as

$$q_o = \frac{q_{sq}}{\pi/36A_{sq}}\exp[-(3n)^2]\exp[-(3m)^2]$$

Based on a comparison of the equations for various plane heat sources of different heat intensity distributions (Eq. (4)), a general equation for q_o can be expressed as

$$q_o = \frac{q_{pl}}{E\cdot A_{pl}}\cdot F\cdot G \qquad (8)$$

Table 1
Coefficients E, F, G, and area A_{pl} for the general solution for various heat intensity distributions and various shapes of the heat sources

Shape of heat source	Distribution of intensity	E	F	G	A_{pl}
Elliptical (or circular disc)	Uniform	1	1	1	$\pi a_o b_o$ (or πr_o^2)
	Parabolic	0.5	$(1-n^2)$	$(1-\frac{m^2}{1-n^2})$	
	Normal	0.1079	$\exp[-(3n)^2]$	$\exp[-(\frac{3m}{\sqrt{1-n^2}})^2]$	
Rectangular (or square)	Uniform	1	1	1	$4a_o b_o$ (or $4a_o^2$)
	Parabolic	4/9	$(1-n^2)$	$(1-m^2)$	
	Normal	$\pi/36$	$\exp[-(3n)^2]$	$\exp[-(3m)^2]$	

The non-dimensional parameter E (a constant) and non-dimensional terms F and G for various heat intensity distributions are given in Table 1. For the uniform distribution E, F, and G are all equal to one.

4. General solution for moving plane heat sources

Consider the case of a moving elliptical heat source of various distributions of heat liberation intensities (Fig. 5). The rate of heat liberation of an elliptical heat source is q_{ell}, J/s. By considering the total elliptical area as a combination of stripes of different lengths of width dy_i, each stripe as a combination of numerous segments of length dX_i, and each of it as a moving point heat source, the solution of the moving point heat source, Eq. (7) can be used to calculate the temperature rise at any point M at time t caused by each of the differential segment, $dX_i dy_i$. The rate of heat liberation of this differential segment q_{pt} is given by $q_{pt} = q_o \cdot dX_i\, dy_i$, where q_o is the heat intensity of that segment of the elliptical area of the plane heat source in J/cm^2·s (refer to Figs. 3 and 5).

The area of the elliptical heat source is denoted as A_{ell}. The rate of heat liberation of this differential infinitesimal small segment $dX_i\, dy_i$ is given by

$$\frac{q_{ell}}{E \cdot A_{ell}} \cdot F \cdot G \cdot dX_i\, dy_i \quad \text{J/s}$$

The half length of the differential stripe for the elliptical heat source is a function of y_i, i.e.

$$l_{y_i} = a_o\sqrt{1-(y_i/b_o)^2} = a_o\sqrt{1-n^2} \tag{a}$$

The temperature rise, $d\theta_M$ at any point M at time t caused by each of the differential small segments $dX_i\, dy_i$ (using Eq. (7)) is given by

$$d\theta_M = \frac{q_{ell} \cdot F \cdot G \cdot dX_i\, dy_i \cdot v}{E \cdot 16\lambda a \pi^{3/2} A_{ell}} \exp\left[-\frac{(X-X_i)v}{2a}\right] \int_0^{v^2 t/4a} \frac{d\omega}{\omega^{3/2}} \exp\left(-\omega - \frac{u_i^2}{4\omega}\right) \tag{b}$$

where $u_i = R_i v/(2a)$; $R_i = \sqrt{R'^2 + z^2} = \sqrt{(X-X_i)^2 + (y-y_i)^2 + z^2}$; R_i is the distance between the differential segmental heat source $dX_i\, dy_i$ and the point M where the temperature rise is concerned.

Substituting $X_i/a_o = m$, $y_i/b_o = n$, and denoting the third integral of Eq. (6) as

$$K_m(u_i) = \int_0^{v^2 t/4a} \frac{d\omega}{\omega^{3/2}} \exp(-\omega - u_i^2/4\omega)$$

the temperature rise at any point M at time t caused by the total *elliptical moving heat source* is given by

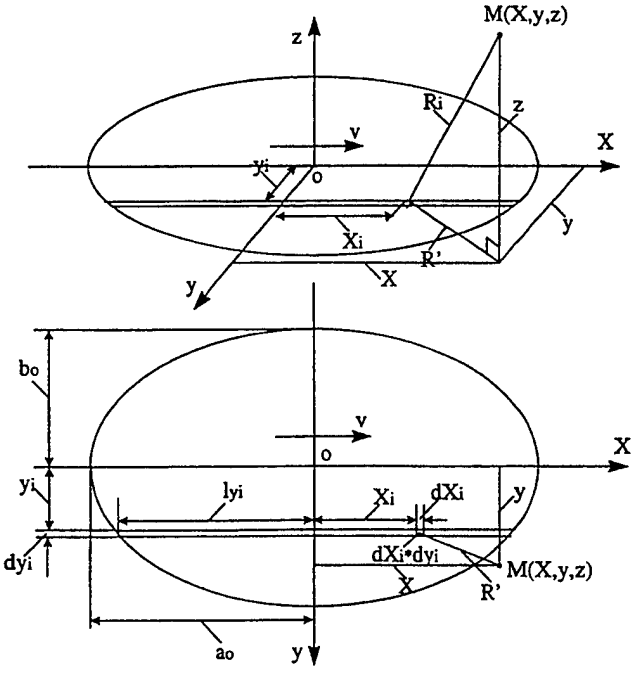

Fig. 5. Schematic showing the moving elliptic heat source problem.

$$\theta_M = \frac{q_{ell} v}{E \cdot 16\lambda a \pi^{3/2} A_{ell}} \int_{y_i=-b_o}^{+b_o} F \cdot dy_i \int_{x_i=-a_o\sqrt{1-n^2}}^{+a_o\sqrt{1-n^2}} dX_i \cdot G \cdot \exp\left[-\frac{(X-X_i)v}{2a} \right] K_m(u_i) \quad (9)$$

Eq. (9) is the general solution of a moving *elliptical heat source* of various distributions of heat intensity. A *circular disc heat source* can be considered as a special case of an elliptic heat source where $a_o = b_o = r_o$, where r_o is the radius of the circular disc. For a *rectangular heat source*, the lengths of the differential stripes are constant and equal to a_o (refer to Fig. 3(b)). A *square heat source* can be considered as a special case of a rectangular heat source, where $a_o = b_o$. It can be shown that for a moving plane heat source of various shapes, their solutions for various heat intensity distributions have the same form but differ only in the relevant limits of integration for different shapes. So, *the general solution for moving plane heat sources of various shapes and various heat intensity distributions* can be expressed as

$$\theta_M = \frac{q_{pl} v}{E \cdot 16\lambda a \pi^{3/2} A_{pl}} \int_{y_i=-j}^{+j} F \cdot dy_i \int_{x_i=-k}^{+k} dX_i \cdot G \cdot \exp\left[-\frac{(X-X_i)v}{2a} \right] K_m(u_i) \quad (10)$$

The relevant integration limits j and k for various shapes are given in Table 2.

5. The general solution for stationary plane heat sources

The stationary heat source problem can be considered as a special case of appropriate moving heat source problem when the velocity of the moving heat source v is zero (refer to Fig. 1). Consequently, $v\tau_i = 0$, $vt = 0$, thus $X = x$ and it is no longer necessary to consider the moving coordinate system. At any time τ_i the distance between the heat source and the point M (where the temperature rise is constant) is given by $\sqrt{x^2+y^2+z^2}$. The amount of heat liberated in the subsequent time interval $d\tau_i$ is $q_{pt} d\tau_i$. This amount of heat generated can be considered as if it is liberated instantaneously, for $d\tau_i$ is infinitesimally small. Thus the temperature rise at any point M near by the heat source caused by this amount of heat from the point heat source can be calculated using the solution of an instantaneous point heat source as follows:

$$d\theta_M = \frac{q_{pt}\, d\tau_i}{c\rho(4\pi a\tau)^{3/2}} \exp\left(-\frac{x^2+y^2+z^2}{4a\tau} \right)$$

The total temperature rise at point M caused by the stationary point heat source from $\tau_i = 0$ to $\tau_i = t$ is then given by

$$\theta_M = \frac{q_{pt}}{c\rho(4\pi a)^{3/2}} \int_{\tau_i=0}^{\tau_i=t} \frac{d\tau_i}{\tau^{3/2}} \exp\left(-\frac{x^2+y^2+z^2}{4a\tau} \right)$$

For $\tau_i = t - \tau$, $d\tau_i = -d\tau$, and when $\tau_i = 0$, $\tau = t$; when $\tau_i = t$, $\tau = 0$: thus

$$\theta_M = \frac{q_{pt}}{c\rho(4\pi a)^{3/2}} \int_{\tau=0}^{\tau=t} \frac{d\tau}{\tau^{3/2}} \exp\left(-\frac{x^2+y^2+z^2}{4a\tau} \right) \quad (11)$$

Eq. (11) is the solution of a continuous stationary point heat source. Referring to the solution of a moving point heat source (Eq. (6)), it can be seen that when $v = 0$, the terms $\exp(-Xv/2a)$ and $\exp(-v^2\tau/4a)$ are each equal to one, and Eq. (6) becomes identically the same as Eq. (11). So, Eq. (11) is a special case of Eq. (6) when $v = 0$. The integral part of Eq. (11) cannot be solved analytically but can be calculated by numerical integration. Usually, it would be preferable to express it in non-dimensional form so that it can be used conveniently for various conditions. The integral part of Eq. (11) can be transformed into a non-dimensional form by the following substitutions. Let

$$\frac{R}{\sqrt{4a\tau}} = u \quad \text{where} \quad R = \sqrt{x^2+y^2+z^2}$$

then

$$\frac{du}{d\tau} = -\frac{1}{2} R \cdot (4a\tau)^{-3/2}$$

$$4a = -2aR(4a\tau)^{-3/2}, \quad d\tau = -\frac{(4a\tau)^{3/2}}{2aR}\, du;$$

$$\frac{d\tau}{\tau^{3/2}} = -\frac{(4a)^{3/2}}{2aR}\, du = -\frac{4\sqrt{a}}{R}\, du$$

when $\tau = 0$, $u = \infty$; when $\tau = t$, $u = \frac{R}{\sqrt{4a\tau}}$.

Then, Eq. (11) can be written as

Table 2
Integration limits j and k, heat liberation rates q_{pl}, and areas for various shapes A_{pl} in the general solution

Shape	Elliptical	Circular	Rectangular	Square
j	b_o	r_o	b_o	a_o
k	$a_o\sqrt{1-(y_i/b_o)^2}$	$\sqrt{r_o^2-y_i^2}$	a_o	a_o
q_{pl} (J/s)	q_{ell}	q_c	q_{rec}	q_{sq}
A_{pl} (cm^2)	$\pi a_o b_o$	πr^2	$4a_o b_o$	$4a_o^2$

$$\theta = \frac{q_{pt}}{c\rho(4\pi a)^{3/2}} \frac{4\sqrt{a}}{R} \int_{u=R/\sqrt{4at}}^{u=\infty} e^{-u^2} du$$

$$= \frac{q_{pt}}{2ac\rho R\pi^{3/2}} \int_{u=R/\sqrt{4at}}^{u=\infty} e^{-u^2} du \quad (12)$$

For $\frac{2}{\sqrt{\pi}} \int_0^p e^{-u^2} du$, defined as an error function, $\mathrm{erf}(p) = \frac{2}{\sqrt{\pi}} \int_0^p e^{-u^2} du$ (see Ref. [26]).

It can be shown [27] that when $p = \infty$, $\mathrm{erf}(p) = 1$. Similarly, it can be shown [27] that

$$\int_0^{u=\infty} e^{-u^2} du = \frac{\sqrt{\pi}}{2}, \text{ and}$$

$$\int_0^{u=R/\sqrt{4at}} e^{-u^2} du = \frac{\sqrt{\pi}}{2} \mathrm{erf}\left(R/\sqrt{4at}\right)$$

Since $ac\rho = \lambda$, Eq. (12) can be written as follows, which is the solution for a stationary point heat source:

$$\theta = \frac{q_{pt}}{4\pi\lambda R}\left[1 - \mathrm{erf}\left(\frac{R}{\sqrt{4at}}\right)\right] \text{ or}$$

$$\theta = \frac{q_{pt}}{4\pi\lambda R} \cdot \mathrm{erf}\, c\left(\frac{R}{\sqrt{4at}}\right) \quad (13)$$

The general solutions for stationary plane heat sources of various shapes and heat intensity distributions can be derived starting from Eq. (13) using a method similar to the one described for the moving plane heat sources.

Substituting $q_o\, dx_i\, dy_i$ (or $\frac{q_{pl} \cdot F \cdot G}{E \cdot A_{pl}} dx_i\, dy_i$) for q_{pt} in Eq. (13), the temperature rise at any point M at any time t caused by the differential segment $dx_i\, dy_i$ (see Fig. 5) is given by

$$d\theta_M = \frac{q_{pl} \cdot F \cdot G \cdot dx_i\, dy_i}{E \cdot A_{pl} \cdot 4\pi\lambda R_i} \mathrm{erf}\, c\left(R_i/\sqrt{4at}\right).$$

Thus, the general solution for a stationary plane heat source of various shapes and heat intensity distributions is given by

$$\theta_M = \frac{q_{pl}}{E \cdot 4\pi\lambda A_{pl}} \int_{y_i=-j}^{y_i=+j} F \cdot dy_i \int_{x_i=-k}^{x_i=+k} G \frac{1}{R_i} \mathrm{erf}\, c\left(\frac{R_i}{\sqrt{4at}}\right) dx_i \quad (14)$$

where values of E, F, G, j, and k can be obtained from Tables 1 and 2.

It should be noted that Eqs. (10) and (14) are for the case of an infinite conduction medium. In most practical cases when the conduction medium is a *semi-infinite body* and the heat source is moving or remaining stationary on its boundary surface, the results of calculation using Eqs (10) and (14) should be doubled for a *semi-infinite body*. Thus, the general solution for a moving plane heat source in a semi-infinite body is given by

$$\theta_M = \frac{q_{pl} v}{E \cdot 8\lambda a\pi^{3/2} A_{pl}} \int_{y_i=-j}^{+j} F \cdot dy_i \int_{x_i=-k}^{+k} dX_i \cdot G \cdot \exp\left[-\frac{(X - X_i)v}{2a}\right] K_m(u_i) \quad (15)$$

The general solution of a *stationary plane heat source* in a *semi-infinite body* is given by

$$\theta_M = \frac{q_{pl}}{E \cdot 2\pi\lambda A_{pl}} \int_{y_i=-j}^{y_i=+j} F \cdot dy_i \int_{x_i=-k}^{x_i=+k} G \frac{1}{R_i} \mathrm{erf}\, c\left(\frac{R_i}{\sqrt{4at}}\right) dx_i \quad (16)$$

6. Results and discussion

6.1. Surface temperature rise distribution, flash temperatures, and flash durations due to a moving plane heat source

There are different critical temperatures and corresponding flash durations that should be considered in the optimization of various advanced manufacturing processing technologies, such as the critical temperatures for certain in situ chemical reactions to take place as in chemo-mechanical polishing of advanced ceramics, or for the diffusion of certain species for improving corrosion resistance, or for certain phase transformation to take place for improving the hardness or toughness, etc. The flash temperatures and relevant flash durations can be predicted using the surface temperature rise distribution plots which in turn are calculated using the general solution for moving plane heat sources in a semi-infinite medium, Eq. (15).

Fig. 6(a)–(f) show the variation of the non-dimensional temperature rise $T(= \theta_M \lambda a/q_{pl} v)$ distributions on the surface of a semi-infinite conduction body along the direction of motion, X, and through the center of the heat source ($y = 0$) for an *elliptic heat source* of various heat intensity distributions and different Peclet numbers, $N_{Pe}[N_{Pe} = va_o/2a$, where v is the moving velocity of the heat source, m/s, a_o is the semi-length of the heat source along the direction of motion, cm, and a is the thermal diffusivity, $cm^2/s]$. Similar distributions can be obtained for heat sources of different shapes, such as circular, rectangular, and square. Peclet number, N_{Pe} is a convenient non-dimensional expression

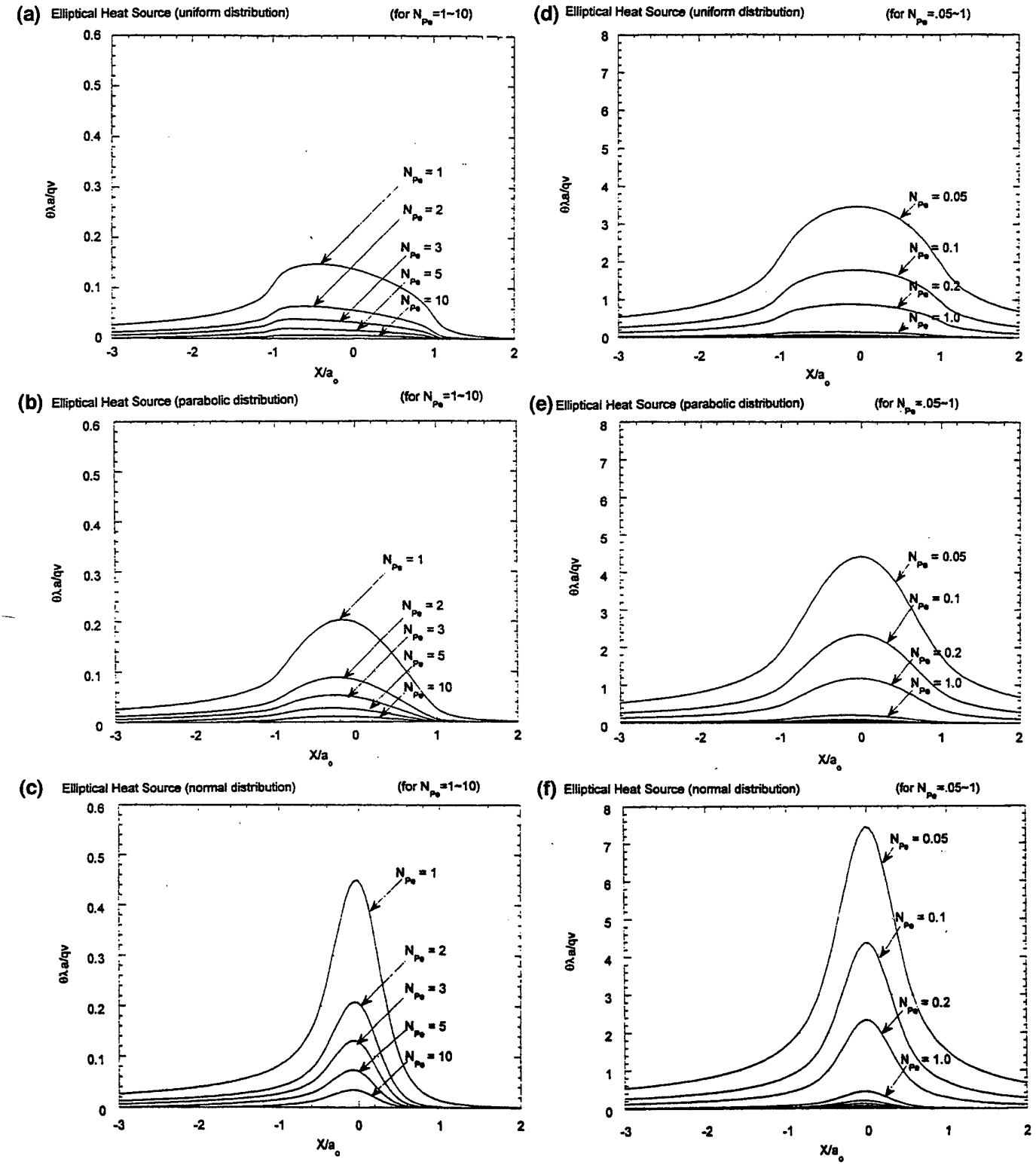

Fig. 6. (a)–(f) Variation of the non-dimensional temperature rise distribution ($\theta\lambda a/qv$) along the direction of motion (X) and through the center ($y = 0$) of an *elliptic heat source* with uniform, parabolic, and normal distributions of heat intensity, respectively, with X/a_o for Peclet numbers of 1–10 and 0.05–1.

for the relative velocity of motion of the heat source considering the thermal properties of the conduction medium which determines the speed of dissipation of heat in the medium. Peclet numbers in the range of 0–10 are generally encountered in most manufacturing and tribological problems. However, since in this range the values of T (non-dimensional temperature rise) can vary significantly, two sets of plots are made here for clarity, i.e., $N_{Pe} = 0.05$–1, and $N_{Pe} = 1$–10. It can be seen that the symmetry of the non-dimensional temperature rise distribution increases with decrease in the Peclet number. Also, the maximum temperature rise is near the rear edge when the Peclet number is large and moves towards the center with decrease in the Peclet number. Also, the maximum temperature rise is closer to the center of the heat source towards the rear edge for the normal distribution and moves further away towards the rear edge for the parabolic, followed by the uniform distribution. The similarity in the nature of the curves for a given heat distribution (uniform, parabolic, and normal) can be clearly seen. It can be seen from Fig. 6, the location of maximum temperature rise is different for different Peclet numbers and different heat intensity distributions. When N_{Pe} is very

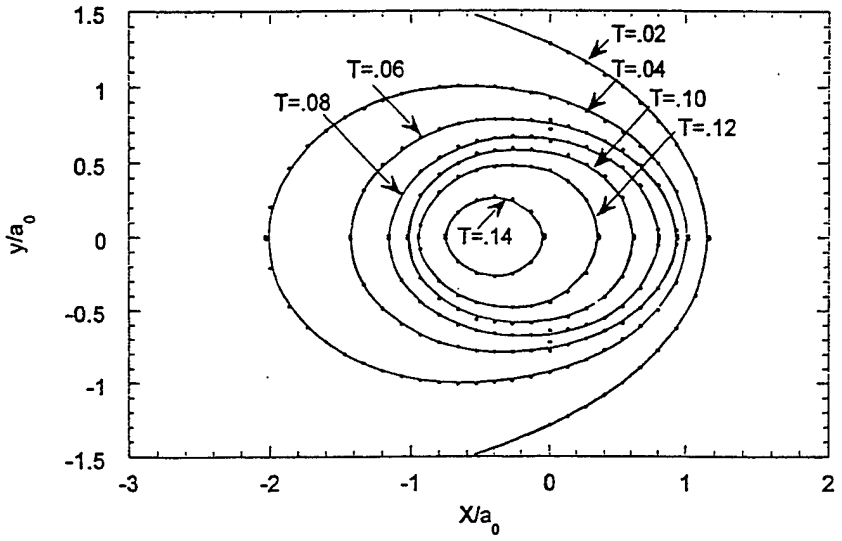

(a) Uniform distribution

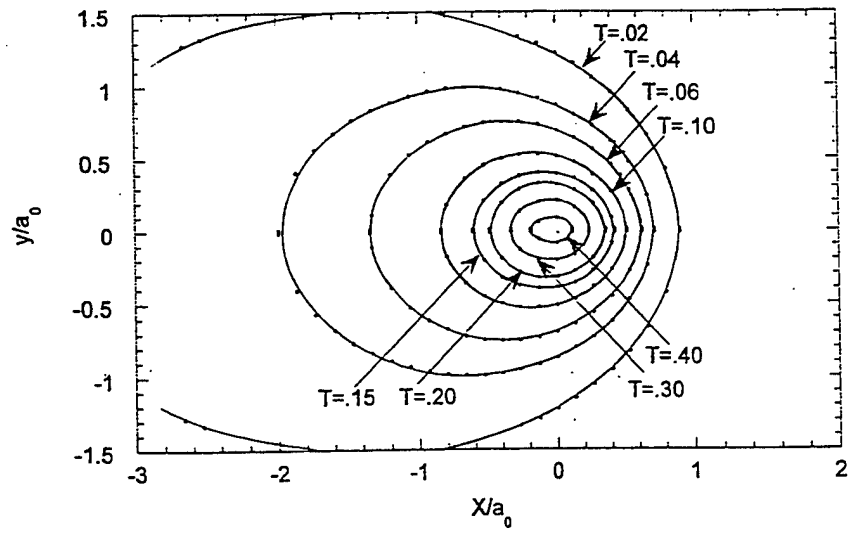

(b) Normal distribution

Fig. 7. (a)–(b) Non-dimensional temperature rise isotherms on the surface for an elliptical heat source with uniform and normal heat intensity distributions, respectively for $N_{pe} = 1$. The non-dimensional temperature rise, $T = \theta\lambda a/qv$.

large (say $N_{Pe} = 10$), for a uniform distribution, the location of the maximum temperature rise is $\sim 0.78(X/a_o)$ towards the trailing edge of the moving heat source. For parabolic distribution, it is $\sim 0.3(X/a_o)$ and for the normal distribution it is ~ 0.1, or, very near the center of the moving heat source.

Fig. 7(a) and (b) show the non-dimensional temperature rise, T $(= \theta_M \lambda a/q_{pl}v)$ isotherms on the surface for an *elliptical* heat source with *uniform* and *normal* distributions for $N_{Pe} = 1$. It can be seen that the peak temperature rise for the case of normal distribution is near the center of the heat source while that for a uniform distribution is between the center and the rear edge of the heat source. Together with Fig. 6, they show the temperature distributions on the surface based on the results of the temperature rise calculations using the general solution of the moving plane heat sources for a semi-infinite medium (Eq. (15)). Such information is extremely valuable for the determination of the expected flash temperatures and corresponding flash durations.

Rosenthal [2] used moving point and moving line heat source models in determining the temperature distribution in welding. Actually the heat source in welding is a moving plane heat source. To approximate it to a point or a line source, the temperature rise calculated for those points near the heat source will always be higher than actual. The closer the point to the source, the larger the error. Of course, for the point at the center of the heat source it would be infinity. Rosenthal plotted the temperature distribution contours using his analysis and compared it experimentally. He pointed out that only the points beyond a distance of 6–8 mm from the heat source gave satisfactory agreement with the experimental results and cautioned regarding the accuracy of values closer to the heat source. Consequently, such an approximation leads to a loss of significant information at and near the heat source. The general solutions for various moving plane heat sources developed in this investigation enable calculations of the temperatures very close to the plane heat source or even at the center of it with sufficiently high accuracy.

6.2. Surface temperature rise distribution due to stationary plane heat sources

Fig. 8 shows isotherms of the temperature rise distribution on the surface of a body due to an *elliptical stationary heat source with a normal, parabolic, and uniform distribution of heat intensity*, respectively. It can be seen that for the uniform distribution, the change of temperature rise from the periphery to the center of the heat source ($x/a_0 = \pm 1$ to 0) is not large and varies from ~ 0.7 to 1.17. For the normal distribution, it varies from ~ 0.5 to 2.97 accompanied by a high temperature peak of ~ 1.8 to 2.97 in the near central region ($x/a_0 = -0.3$ to $+0.3$). For the parabolic distribution, the value is somewhere in between. This means the distribution of temperature rise for a uniform elliptical heat source is comparatively flat while that for the normal elliptical heat source it is rather steep near the center region. For the parabolic elliptical heat source it is somewhere in between.

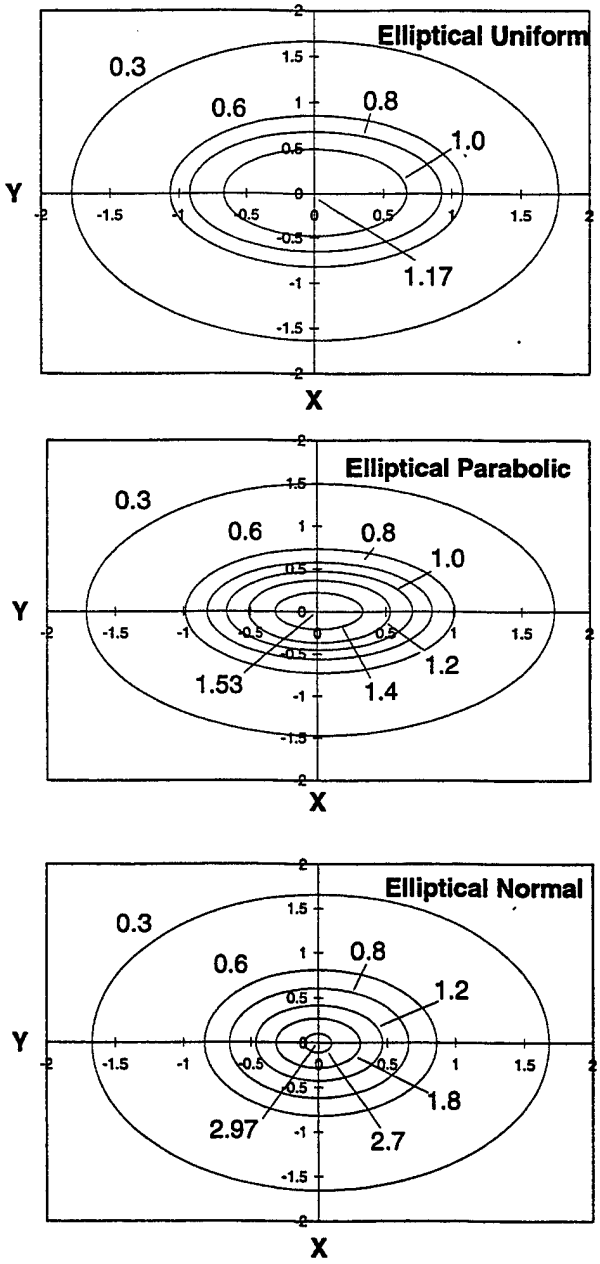

Fig. 8. (a)–(c) Isotherms of the non-dimensional temperature rise distribution on the surface of a body due to an elliptical heat source with (a) uniform, (b) parabolic, and (c) normal distributions of heat intensity, respectively.

6.3. On the estimation of the time required for establishing the steady state conditions for stationary plane heat sources

Fig. 9(a)–(c) show the variation of the non-dimensional temperature rise distribution on the surface using the general equation for a semi-infinite medium (Eq. (16)) for a *stationary elliptical heat source* of various heat intensity distributions, namely, *uniform*, *parabolic*, and *normal*, respectively. Each figure contains a set of temperature distribution curves for different heating times ($t = 1$, 10 and 100 μs, 1 and 10 ms as well as for the steady state). It can be seen from Fig. 9(a), that when $t \geq 10$ ms, the temperature rise caused by the stationary heat sources is very close to the values for the steady state. From a practical consideration, it is, therefore, not necessary to consider $t = \infty$ for reaching the steady state conditions but a finite value instead. However, this involves the acceptance of a small error. Depending on the allowable error, the time required for establishing the steady state may not be very long. Practically, when the radius of the area of concern is ~1–2.5 times that of the heat source and the allowable error is about 1%, the time required for reaching the steady state is usually finite and on the order of ~0.1–1 s.

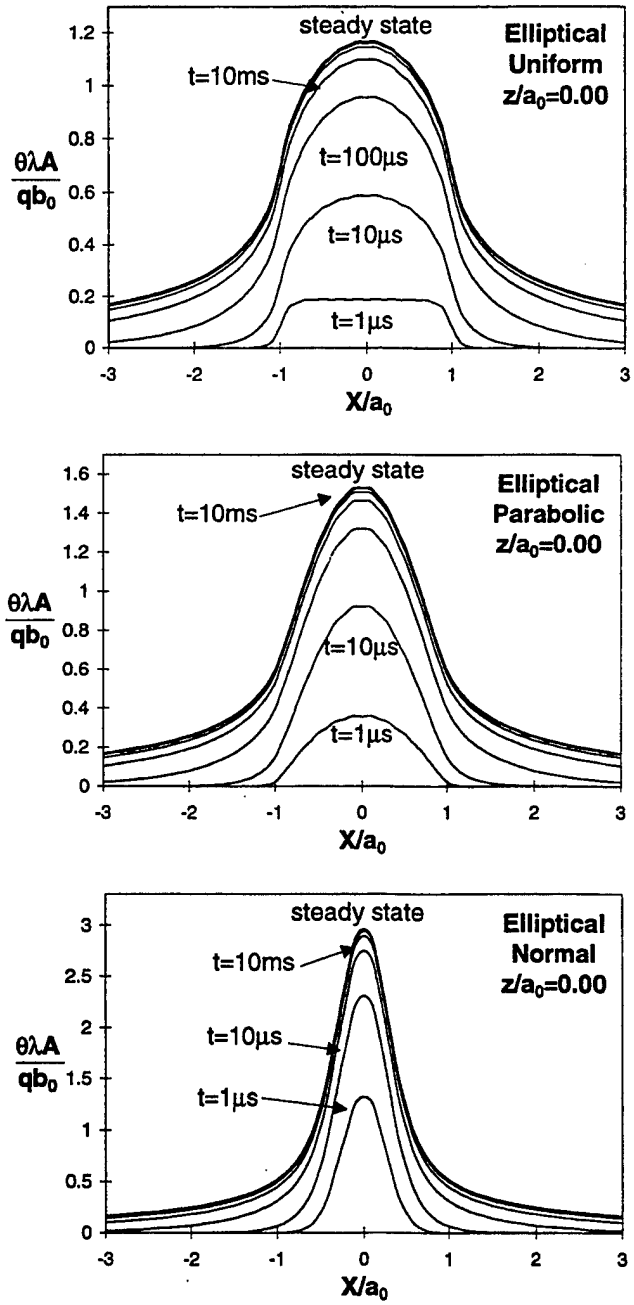

Fig. 9. (a)–(c) Variation of the non-dimensional temperature rise on the surface with x_i/a_o from −3 to +3 due to an elliptical heat source with (a) uniform, (b) parabolic, and (c) normal distributions of heat intensity, respectively.

6.4. Temperature distribution under the surface

Temperature distribution under the surface is very important in many manufacturing applications. For example, surface integrity including metallurgical changes at and near the surface, and the residual stresses are affected by the temperature gradients from the surface into the interior. Hence, it is desirable to know not only the temperature at the surface but also the distribution of the temperature under the surface. Fig. 10(a) and (b) show the variation of the non-dimensional temperature distribution under the surface of a body along the X-axis in the X–o–z plane of the moving coordinate system due to an elliptical moving heat source of *uniform* and *normal* distributions, respectively for different Peclet numbers (1, 5, and 10), where the origin of the moving coordinate system coincides with the center of the heat source. X/a_o and z/a_o are non-dimensional distances from the center of the heat source and the depth, respectively. Fig. 10(a) and (b) show that the temperature gradient is rather steep initially followed by a gradual change with increasing depth. Also, the temperature gradient is much steeper at higher values of Peclet numbers.

Based on the variation of the temperature rise in the heat conduction body under the point where the maximum temperature rise takes place with depth, the following approximate equations for the calculation of the non-dimensional temperature distribution under the surface at the point of maximum surface temperature at different depths are obtained.

$\theta = 0.14578 N_{Pe}^{-1.15} e^{-(0.56742+0.6796 N_{Pe})z/a_o}$ (for an elliptical *uniform* heat source)

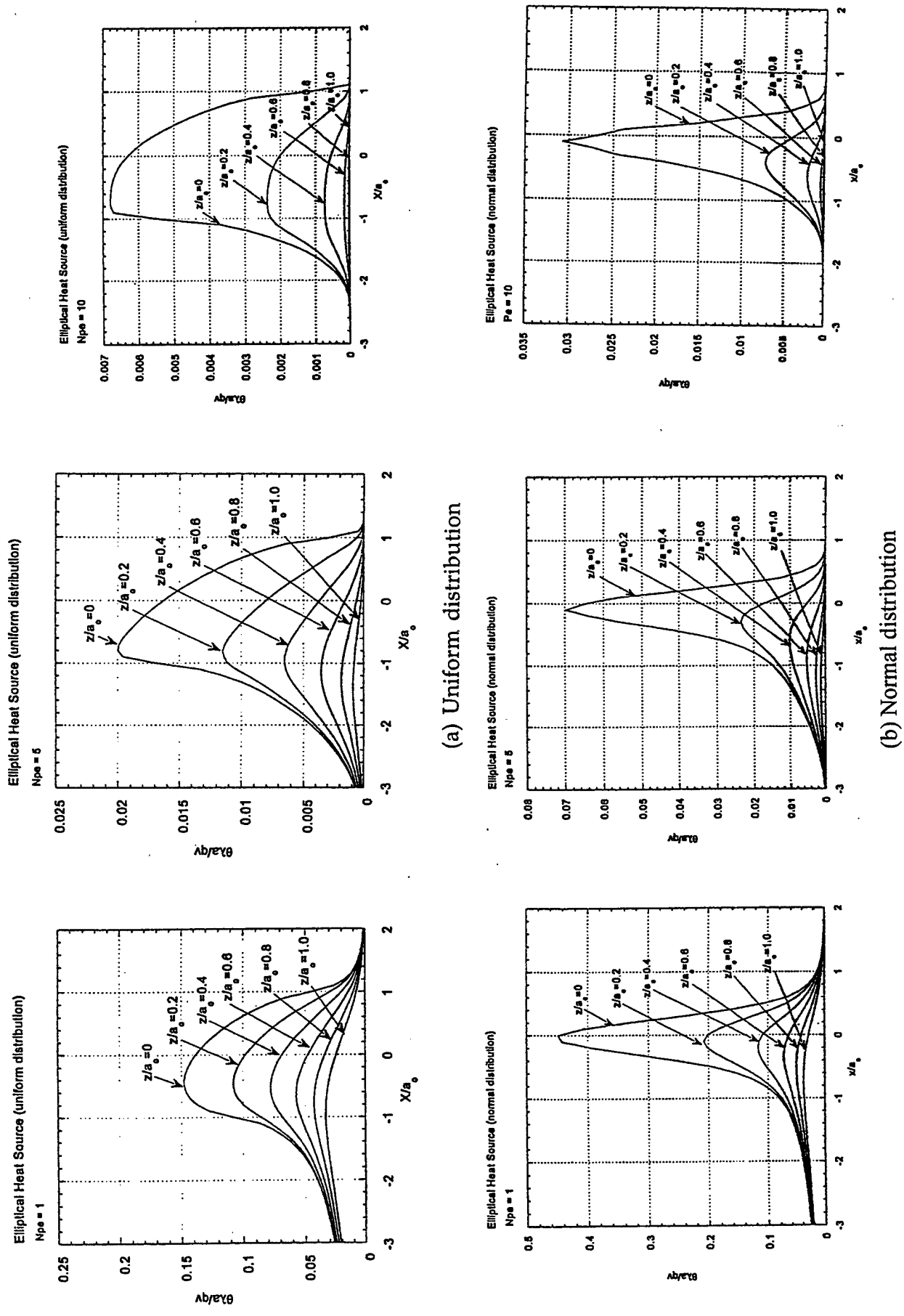

Fig. 10. (a)–(b) Variation of the non-dimensional temperature rise under the surface, along the X-axis, in the X–o–z plane of the moving coordinate system X–y–z (where the origin coincides with the center of the heat source for an elliptical heat source) of uniform and normal distributions, respectively, for different Peclet numbers (1, 5, and 10).

$$\theta = 0.36271 N_{Pe}^{-0.98862} e^{-(1.8388+0.82371 N_{Pe})z/a_o}$$

(for an elliptical *normal* heat source)

Fig. 11(a) and (b) show the variation of the temperature rise under the maximum surface temperature point on the surface with depth for an elliptical heat source with uniform and normal heat distributions, respectively, for values of Peclet numbers in the range of 0.1–10. Here, the logarithmic scale is adopted for the non-dimensional temperature rise axis as these values are distributed over a very wide range (from 6×10^{-6} to 5). They show that higher the Peclet number, the steeper the temperature gradient which is an important factor in determining the residual stresses and subsurface damage in such manufacturing processes as grinding. It can also be seen that the gradient of the temperature drop from the surface to a given depth, say $z/a_o = 0.2$ or 0.3, for a normal elliptical heat source is higher than for a uniform elliptical heat source.

Using the general solution for the stationary plane

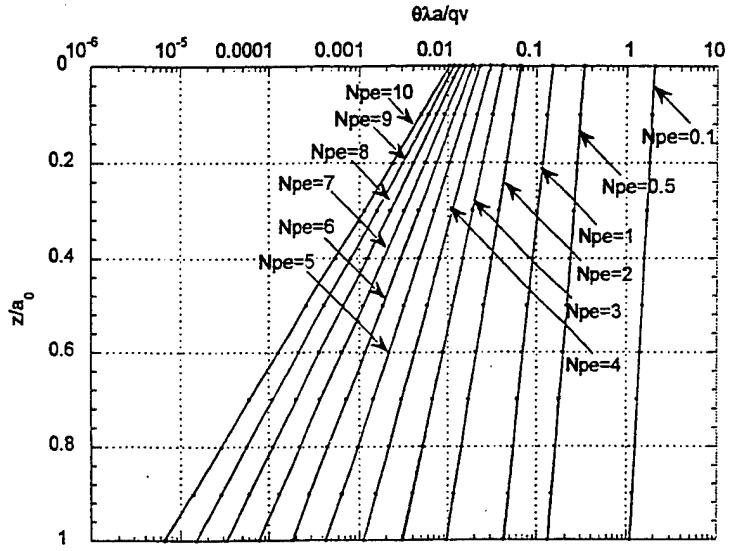

(a) Uniform distribution

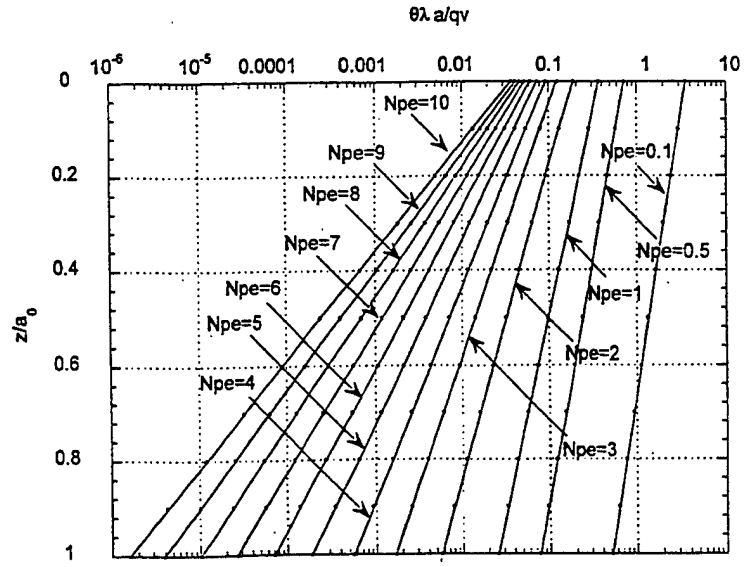

(b) Normal distribution

Fig. 11. (a)–(b) Variation of the non-dimensional temperature rise distribution ($\theta\lambda a/qv$) under the maximum temperature point on the surface with z/a_o for an elliptic heat source for various Peclet numbers with uniform and normal distributions, respectively, using the approximate equations.

heat sources for a semi-infinite medium (Eq. (16)), the temperature rise distributions under the surface caused by the stationary plane heat source can be calculated. Fig. 12 shows the distribution of the steady state temperature rise at different depths under the surface of the body and Fig. 13 shows the steady state distribution of the temperature rise along the z-axis under the point of maximum surface temperature. It can be seen from Fig. 13 that for the cases of stationary heat sources the temperature gradient is low for a uniform heat source, much higher for a parabolic heat source, and even higher for the normal heat source.

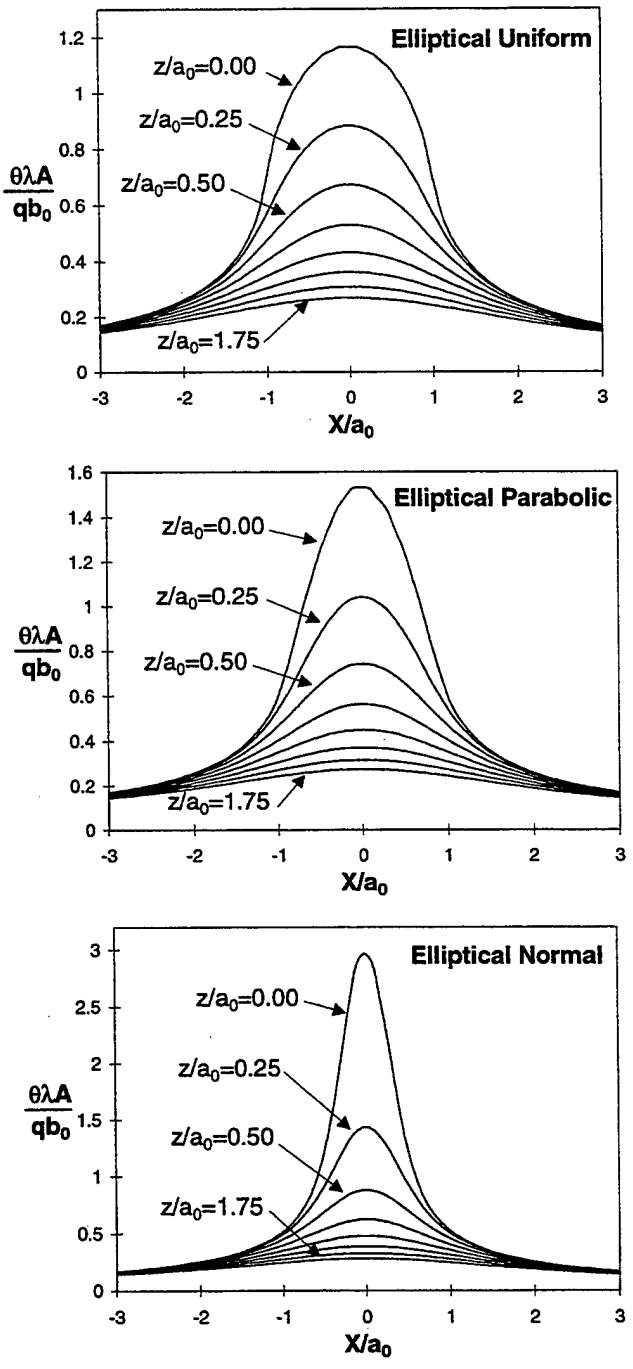

Fig. 12. (a)–(c) Variation of the non-dimensional temperature rise at different depths under the surface of a body with x_i/a_o from -3 to $+3$ due to an elliptical heat source of (a) uniform, (b) parabolic, and (c) normal distributions of heat intensity.

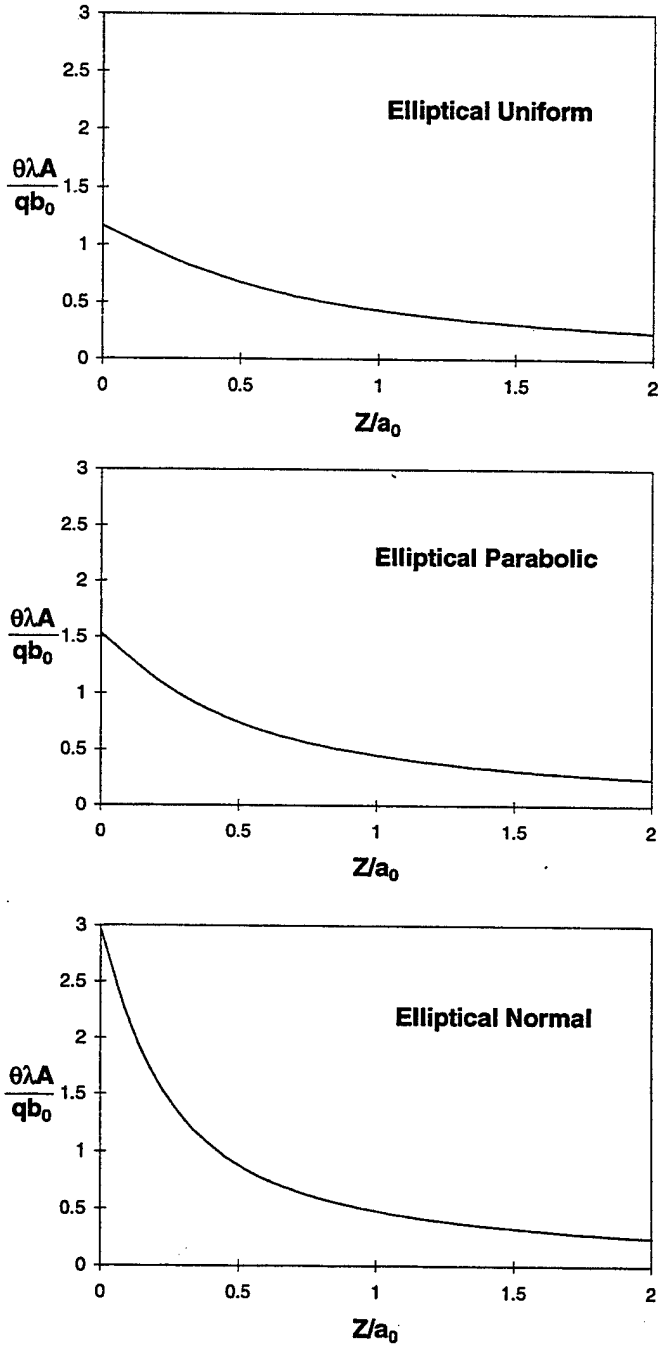

Fig. 13. (a)–(c) Variation of the maximum non-dimensional temperature rise under the surface of a body with z/a_o from 0 to $+2$ due to an elliptical heat source of (a) uniform, (b) parabolic, and (c) normal distributions of heat intensity, respectively.

7. Conclusions

1. The *general solutions* for the temperature rise at any point (Eq. (15)) for various moving heat sources and (Eq. (16)) for various stationary heat sources caused by various stationary and moving plane heat sources of different shapes (*elliptical*, *circular*, *rectangular*, and *square*) and heat intensity distributions (*uniform*, *parabolic*, and *normal*) were developed based on Jaeger's classical *heat source method*. These equations can be used for both *transient* and *steady state* conditions. They can also be used for determining the *temperature distribution on the surface* as well as *with respect to the depth*. Only one program is sufficient for computation which is very convenient for addressing a range of manufacturing and tribological problems.
2. The *general solution* for moving plane heat sources can be used for transient conditions when $v^2t/4a < 5$ and for quasi-steady state conditions when $v^2t/4a = 5$. This relationship can also be used to estimate the time required for establishing the quasi-steady state conditions, namely, $t_{\text{quasi-steady}} = 5[4a/v^2]$.
3. Using the general solution for the temperature rise at any point due to various moving heat sources, the temperature rise (non-dimensional or dimensional) isotherms on the surface can be plotted. This information is valuable for the determination of the flash temperatures and the corresponding flash durations which play an important role in the optimization of various advanced manufacturing technologies for improving the quality, productivity, and cost.
4. For moving heat sources, the location of the point of maximum temperature rise is shown to be different for different Peclet numbers and heat intensity distributions. When N_{Pe} is very large (say $N_{Pe} = 10$), for a uniform distribution, it is $\sim 0.78(X/a_o)$ towards the trailing edge of the moving heat source. For parabolic distribution, it is $\sim 0.3(X/a_o)$ and for the normal distribution it is about 0.1 or very near the center of the moving heat source.
5. For moving heat source problems, the magnitude of the temperature rise as well as its distribution around the heat source depends on several factors, including the heat intensity and its distribution, the shape and size of the heat source, the thermal properties, and the velocity of sliding (usually the non-dimensional Peclet number is used to express the relative sliding velocity considering the thermal properties and the size of heat source). It was shown that the symmetry of the non-dimensional temperature rise distribution increases with decrease in the Peclet number.
6. Temperature rise distribution under the surface can also be calculated using the general solution developed in this investigation. Temperature gradients from the surface into the interior play a very important role in many manufacturing applications and affect the surface integrity including metallurgical changes at and near the surface and the residual stresses. The results obtained show that the temperature gradient is steep initially followed by a gradual change with increasing depth. The temperature gradient is much steeper at higher values of the Peclet numbers. It is also different for different heat intensity distributions — steeper for normal, less steeper for parabolic, and even less steeper for uniform distribution.

Acknowledgements

This project is sponsored by grants from the National Science Foundation on "Tribological Interactions in Polishing of Advanced Ceramics and Glasses," (CMS-94-14610) and "Design, Construction, and Optimization of Magnetic Field Assisted Polishing," (DMI-94-02895), and DoD's DEPSCoR Program on "Finishing of Advanced Ceramics," (DAAH 04-96-1-0323). This project was initiated by an ARPA contract on "Ceramic Bearing Technology Program," (F33615-92-5933) and an NSF U.S.–China cooperative research project on the Thermal Aspects of Manufacturing. Thanks are due to Drs. J. Larsen Basse, B.M. Kramer, Ming Leu, Delci Durhan, and A. Hogan of NSF and Dr. K.R. Mecklenburg of WPAFB and Dr. W. Coblenz of DARPA for their interest in and support of this work.

References

[1] J.C. Jaeger, Moving sources of heat and the temperature at sliding contacts, Proc. Roy. Soc. NSW 76 (1942) 203–224.
[2] H.S. Carslaw, J.C. Jaeger, Conduction of Heat in Solids, 2nd ed., Oxford University Press, Oxford, 1959.
[3] K.J. Trigger, B.T. Chao, An analytical evaluation of metal-cutting temperatures, Trans. ASME 73 (1951) 55–68.
[4] B.T. Chao, K.J. Trigger, Cutting temperatures and metal cutting phenomena, Trans. ASME 73 (1951) 777–787.
[5] E.G. Loewen, M.C. Shaw, On the analysis of cutting tool temperatures, Trans. ASME 76 (1954) 217–231.
[6] M.C. Shaw, Metal Cutting Principles, Oxford University Press, Oxford, 1984.

[7] F.P. Bowden, P.H. Thomas, Surface temperatures of sliding solids, Proc. Roy. Soc. A 223 (1953) 29–39.
[8] J.R. Barber, Distribution of heat between sliding surfaces, J. Mech. Eng. Sci 9 (1967) 351–354.
[9] A. Cameron, A.N. Gordon, G.T. Symm, Contact temperatures in rolling/sliding surfaces, Proc. Roy. Soc. (1964) 45–61.
[10] B. Gecim, W.O. Winer, Transient temperatures in the vicinity of an asperity contact, Trans. ASME, J. Tribology 107 (1985) 333–342.
[11] D. Kuhlmann-Wildorf, Flash temperatures due to friction and Joule heat at asperity contacts, Wear 105 (1985) 187–198.
[12] F.F. Ling, A quasi-Iterative method for computing interface temperature distributions, Zeitschrift fur Angewandte Mathematik X (1959) 461–474.
[13] F.F. Ling, C.W. Ng, On temperatures at the interfaces of bodies in sliding contact, in: Proc. of Fourth U.S. Nat. Congr. of Appl. Mech., ASME, New York, vol. 4, 1962, pp. 1343–1349.
[14] F.F. Ling, Surface Mechanics, Wiley/Interscience, New York, 1973.
[15] H.A. Francis, Interfacial temperature distribution within a sliding hertzian contact, ASLE Trans. 14 (1970) 41–54.
[16] D. Rosenthal, Theoretical study of the heat cycle during arc welding (in French), in: 2-eme Congres National des Sciences, Brussels, 1935, pp. 1277–1292.
[17] D. Rosenthal, Mathematical theory of heat distribution during welding and cutting, Welding Researach Supplement (1941) 220s–234s.
[18] D. Rosenthal, R. Schmerber, Thermal study of arc welding — experimental verification of theoretical formulas, Welding Research Supplement (1938) 2–8.
[19] D. Rosenthal, The theory of moving sources of heat and its application to metal treatments, Trans. ASME 80 (1946) 849–866.
[20] H. Blok, Theoretical study of temperature rise at surfaces of actual contact under oiliness lubricating conditions, in: Proc. of the General Discussion on Lubrication and Lubricants, vol. 2, Inst. of Mech. Engrs., London, 1937, pp. 222–235.
[21] H. Blok, The dissipation of frictional heat, Appl. Sci. Res., Section A 5 (1955) 151–181.
[22] X. Tian, F.E. Kennedy Jr, Maximum and average flash temperatures in sliding contact, Trans. ASME, J. Tribology 116 (1994) 167–174.
[23] J. Bos, H. Moes, Frictional heating of tribological contacts, Trans. ASME, J. Tribology 117 (1995) 171–217.
[24] Z.B. Hou, R. Komanduri, Magnetic field assisted finishing of ceramics, Part I: thermal model, Trans. ASME, J. Tribology 120 (1998) 645–651.
[25] Z.B. Hou, R. Komanduri, General solutions for plane heat source problems in manufacturing and tribology, Part I: stationary heat sources, Part II: moving heat sources, MAE Research Report, Oklahoma State University, Stillwater, OK, 1998.
[26] M.R. Spiegel, Mathematical Handbook of Formulas and Tables, Schaum's Outline Series, McGraw-Hill, New York, 1993.
[27] E.M. Mahla, M.C. Rowland, C.A. Shook, G.E. Doan, Heat flow in arc welding, Welding Journal 20 (1941) 459.